MECHANISTIC ASPECTS OF SILYLENE AND GERMYLENE REACTIONS

MECHANISTIC ASPECTS OF THE COMPLEXATION, CHALCOGEN ABSTRACTION AND SIGMA BOND INSERTION REACTIONS BY TRANSIENT SILYLENES AND GERMYLENES IN SOLUTION

By: SVETLANA STEPANOVNA KOSTINA, B.Sc. (Honours)

A Thesis

Submitted to the School of Graduate Studies

in Partial Fulfillment of the Requirements

for the Degree Doctor of Philosophy

McMaster University

DOCTOR OF PHILOSOPHY (2014) McMaster University
(Chemistry and Chemical Biology) Hamilton, Ontario

TITLE: Mechanistic Aspects of the Complexation, Chalcogen Abstraction and Sigma Bond Insertion Reactions by Transient Silylenes and Germylenes in Solution

AUTHOR: Svetlana Stepanovna Kostina

B.Sc. (Honours, McMaster University)

SUPERVISOR: Professor William J. Leigh

NUMBER OF PAGES: xliii, 300

ABSTRACT

The complexation reactions of silylenes ($SiMe_2$, $SiPh_2$ and $SiMes_2$) and germylenes ($GeMe_2$, $GePh_2$ and $GeMes_2$) with a series of O-, S-, N- and P-donors have been studied in hexanes solution. The equilibrium constants for complexation of $SiMes_2$ and $GeMes_2$ with 7 Lewis bases were determined, and demonstrate that the silylene is more Lewis acidic than the germylene by ca. 1 kcal mol^{-1}. Diethyl ether reacted with the six tetrellylenes with equilibrium constants that decrease in the order $SiPh_2 > SiMe_2 > GePh_2 > GeMe_2 > SiMes_2 > GeMes_2$, establishing a trend in the Lewis acidities of the silylenes and germylenes. Experimental results are complemented by calculated (G4) binding enthalpies of the MMe_2-donor complexes, which were found to correlate with Drago's E and C parameters leading to the classification of $SiMe_2$ and $GeMe_2$ as borderline soft Lewis acids.

A number of sigma-bond insertion reactions by transient silylenes was examined, namely the O-H, N-H and Si-O insertion reactions with alcohols, amines and siloxanes, respectively. In all cases the reactions were found to proceed via a two step mechanism in which the first step is a reversible formation of a Lewis acid-base complex. The second step was found to be a catalytic H-migration in the reactions with alcohols and amines; the catalysis by the alcohol is at least 10^4 times faster than that by the amine. Complexes of silylenes with alkoxysilanes and siloxanes transform into the final products via a unimolecular [1,2]-silyl migration.

Chalcogen abstraction reactions by silylenes ($SiMe_2$, $SiPh_2$, $SiTmp_2$ and $SiMes_2$) and germylenes ($GeMe_2$ and $GePh_2$) from oxiranes (cyclohexene oxide (CHO) and propylene oxide (PrO)) and thiiranes (cyclohexene sulfide (CHS) and propylene sulfide (PrS)) were investigated by laser flash photolysis and steady-state photolysis methods. The results indicate that the reaction proceeds via a two step mechanism, in which the first step is a reversible complexation followed by a unimolecular decomposition of the complex to yield products of chalcogen abstraction, namely alkenes and the corresponding $R_2M{=}X$ transients (R = Me, Ph, Tmp and Mes, M = Si or Ge, X = O or S). Diphenylsilanethione was directly detected and identified on the basis of its spectra and reactivity with amines and alcohols. The O- and S- abstraction by silylenes proceed with ca. 50% efficiency; in contrast, no evidence for O-abstraction by $GeMe_2$ from CHO could be found, while propene was formed in ca. 35% yield in the reaction of $GeMe_2$ with PrS.

ACKNOWLEDGEMENTS

Throughout my time as a graduate student at McMaster University I was truly fortunate to have Willie as my supervisor, whose infuriating attention to detail drove me to finally learn the correct usage of the article “the”. I am certain by the time I was ready to graduate he developed an involuntary eye-twitch whenever he heard me knocking on his door. His endless patience, sense of humour and words of encouragement were sometimes all that kept me going.

My gratitude goes to my outstanding committee members, Drs. Vargas-Baca and Emslie, who courageously read hundreds of pages of my writing over the years and provided invaluable advice about the research and to my external committee member, Dr. Baines, who came from London to attend my Ph.D. defense.

The administrative staff of the Department of Chemistry and Chemical Biology deserves special thanks, particularly Christine Cosgrove who never passed the opportunity to greet me with a cheery “Hi, Lana!!!” every morning.

Experimental assistance was provided by many individuals, Drs. Don Hughes, Bob Berno, Dan Sorensen, Steve Kornic, Tadek Olech, Hilary Jenkins, Jim Britten, Leah Allan and Karen Neumann, to name a few.

I would like to extend my appreciation to my bright and motivated peers, Ian Duffy and Ketha Jeyakanthan, who put up with me during the production of this thesis. Ian, thank you for teaching me the proper technique of drinking wine at our supervisor’s house! Past group members, especially Adroha Bhattacharya, Dr. Farah Lollmahomed and Dr. Lawrence Huck, have made my stay here extremely enjoyable.

I can't name all the undergraduate students who worked with me over the years (because there are so many of them), but you guys know who you are.

To my closest friends, Anna and Corey (you see what I am saying?), who helped me keep my sanity over the years, Thank You. For those whose names I've forgotten to mention, please feel free to drop by and complain to me about that.

I wish to extend a thank you to my mom and dad, who are still waiting for me to stop "fooling around in the lab" and go to med school. To my sister, who took the journey through grad school with me. To Peng, my husband, who made me food.

TABLE OF CONTENTS

LIST OF FIGURES

LIST OF TABLES

LIST OF ABBREVIATIONS AND SYMBOLS

Me	methyl group, CH_3-
Et	ethyl group, CH_3CH_2-
nBu	*n*-butyl group, $CH_3CH_2CH_2CH_2$-
tBu	*tert*-butyl group, $(CH_3)_3C$-
Ph	phenyl group, C_6H_5-
Cy	cyclohexyl group, C_6H_{11}-
Mes	2,4,6-trimethylphenyl group
Dmp	2,4-dimethylphenyl group
Tmp	3,4,5-trimethylphenyl group
TMS	trimethylsilyl group, $SiMe_3$-
CHO	cyclohexene oxide
CHS	cyclohexene sulfide
PrO	propylene oxide
PrS	propylene sulfide
BuO	butylene oxide
PhO	phenyl oxirane
THF	tetrahydrofuran
THT	tetrahydrothiophene
DMB	dimethylbutadiene
D_2	tetramethylcyclodisiloxane, $(Me_2SiO)_2$
D_3	hexamethylcyclotrisiloxane, $(Me_2SiO)_3$
D_4	octamethylcyclotetrasiloxane, $(Me_2SiO)_4$
ΔG	Gibbs free energy

PA	proton affinity
ZPE	zero point energy
DSSE	divalent state stabilization energy
NMR	nuclear magnetic resonance
COSY	Correlation Spectroscopy
TOCSY	Total Correlation Spectroscopy
HSQC	Heteronuclear Single Quantum Coherence Spectroscopy
HMBC	Heteronuclear Multiple Bond Correlation
DFT	Density Functional Theory
B3LYP	Becke, 3-parameter, Lee-Yang-Parr
QCISD	Quadratic Configuration Interaction with Single and Double Excitation

LIST OF COMPOUND NUMBERS

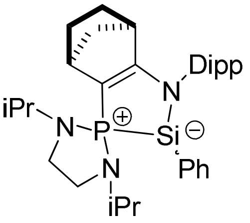

1

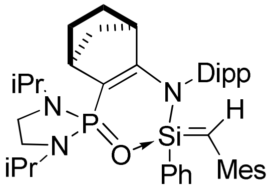

2

$(t\text{-}Bu_2Si)_3$

3

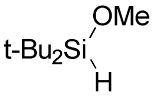

$t\text{-}Bu_2Si(OMe)H$

4

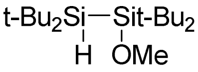

$t\text{-}Bu_2SiH\text{—}Sit\text{-}Bu_2(OMe)$

5

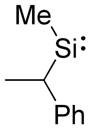

6

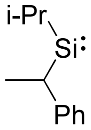

7

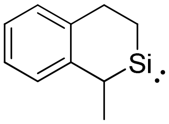

8

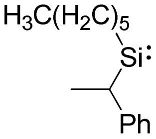

9

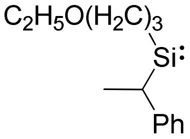

10

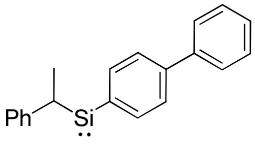

11

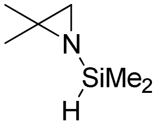

12

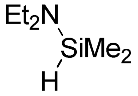

Et_2NSiMe_2H

13

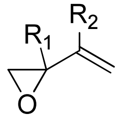

14

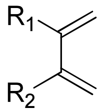

15

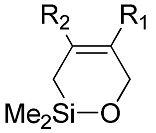

16

a. $R_1 = R_2 = H$; **b.** $R_1 = R_2 = Me$ **c.** $R_1 = H, R_2 = Me$; **d.** $R_1 = Me, R_2 = H$

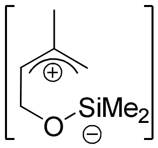

17

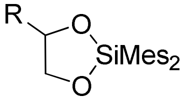

18

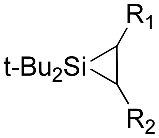

19

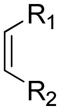

20

a. $R_1 = Me, R_2 = H$ **b.** $R_1 = R_2 = Me$

c. $R_1 = R_2 = H$

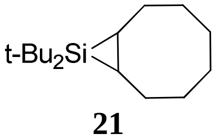

21

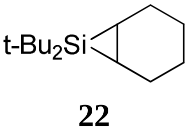

22

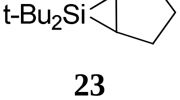

23

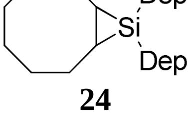

24

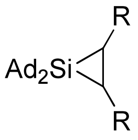

25 (**a.** R = Me **b.** R = Et)

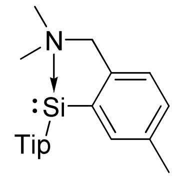

26

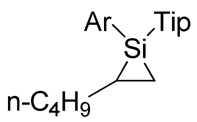

27

$RHC=CHR$

28 (**a.** R = Me, cis **b**. R = Me, trans **c**. R = H)

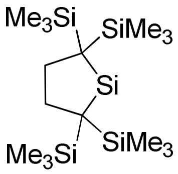

29

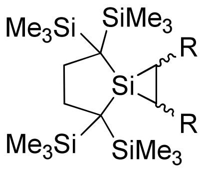

30

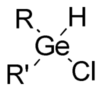

31

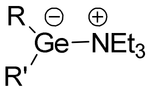

32

a. R = R' = Ph **b.** R = Ph, R' = H
c. R = Ph, R' = Me **d**. R = R' = Et

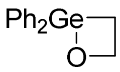

33

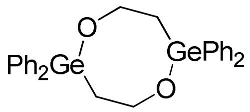

34

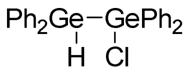

$Ph_2\underset{H}{Ge}-\underset{Cl}{Ge}Ph_2$

35

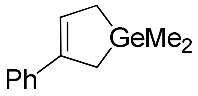

36

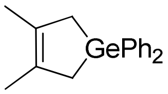

37

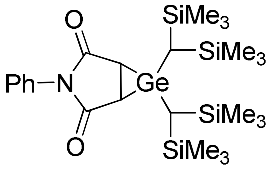

38

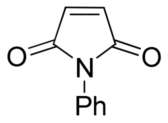

39

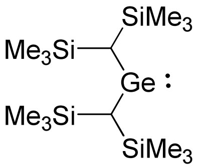

40

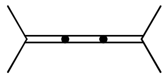

41

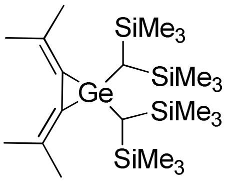

42

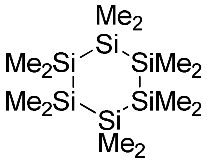

43

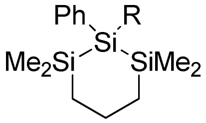

44(**a.** R = Ph, **b.** R = Me)

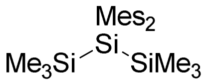

45

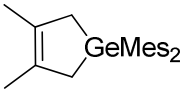

46

Ph_3SiCl

47

Me_3SiCl

48

$Ph_3Si-SiMe_3$

49

Me_2SiCl_2

50

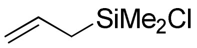

51

$H_2Cl_6Pt \cdot 6H_2O$

52

$Me_2Si(H)Cl$

53

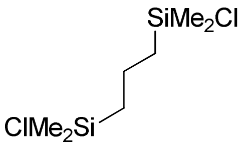

54

Ph_2SiCl_2

55

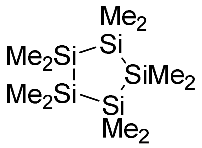

56

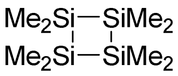

57

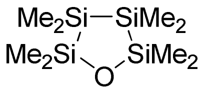

58

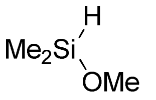

59

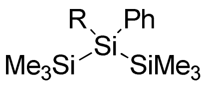

60. R = Ph
61. R = Me

$Me_3Si\text{-}SiMe_3$

62

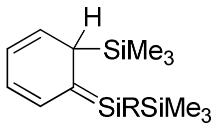

63. R = Ph
64. R = Me

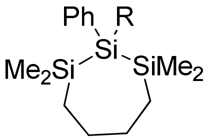

65 (a. R = Ph,
b. R = Me)

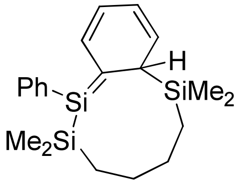

66

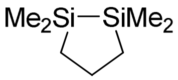

67

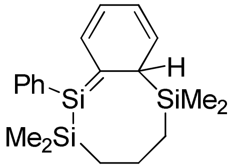

68

$Ph_2SiH(OEt)$

69

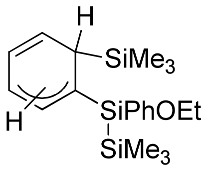

70

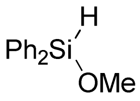

71

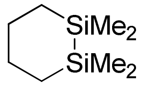

72

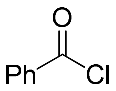

73

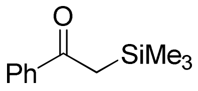

74

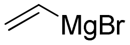

75

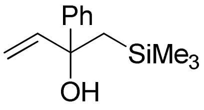

76

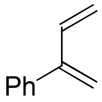

77

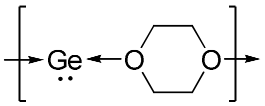

78

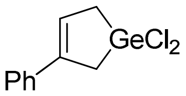

79

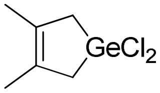

80

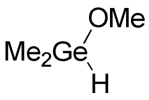

81

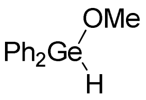

82

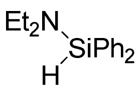

83

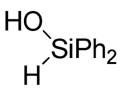

84

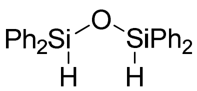

85

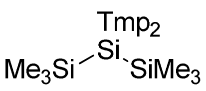

86

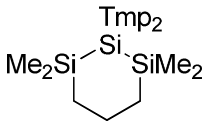
87

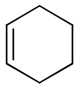
88

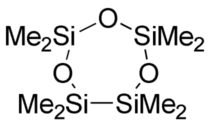
89

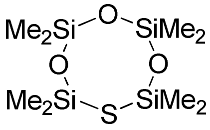
90

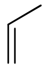
91

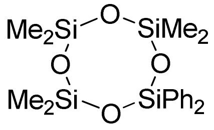
92

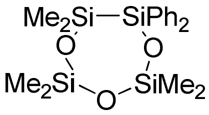
93

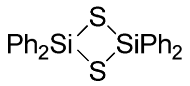
94

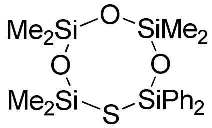
95

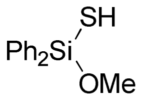
96

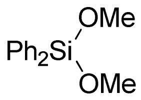
97

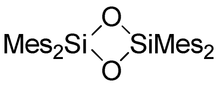
98

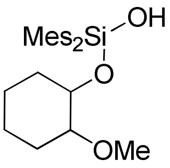
99

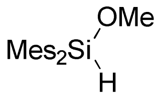
100

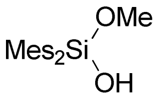
101

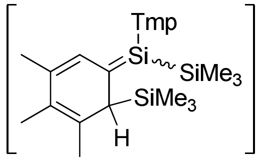
102

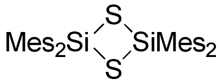
103

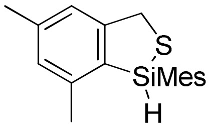
104

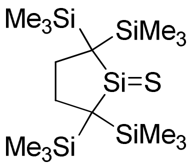
105

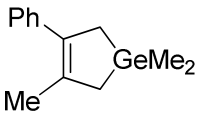
106

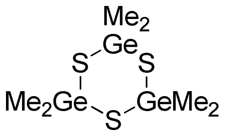
107

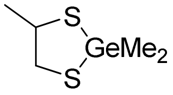
108

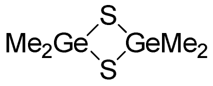
109

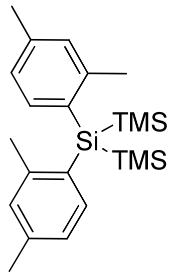
110

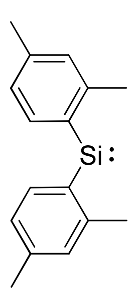

111

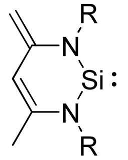

112

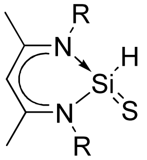

113

PREFACE

Throughout this document the results of theoretical calculations will be briefly presented to support experimental mechanistic implications. It should be noted that all calculations were carried out by my supervisor.

The flash photolysis experiments were carried out in dry hexanes (or Et_2O, where indicated). The solvents were dried by a passage through an activated alumina column immediately prior to use, while deoxygenation was carried out by bubbling of dry Ar gas at least 30 min prior to and throughout the experiments. The standard errors in rate and equilibrium constants are reported as twice the standard deviation ($\pm 2\sigma$) from the linear least-squares analysis of the data using Prism 5.0 graphing software. Kinetic simulations were performed using KinTek Explorer Pro.

The experimental section contains synthetic procedures that have previously appeared in the following articles:

Kostina, S. S.; Singh, T.; Leigh, W. J., *J. Phys. Org. Chem.* **2011,** *24*, 937

Kostina, S. S.; Leigh, W. J., *J. Am. Chem. Soc.* **2011,** *133* (12), 4377

Kostina, S. S.; Singh, T.; Leigh, W. J., *Organometallics* **2012,** *31* (9), 3755

Introductory chapters 1 and 2 contain sections that have been written as drafts for a review on the reactivity of silylenes in solution and may be published at a later time. Parts of the discussions in Chapters 4, 5 and 10 also come from the same source, along with the figures. Chapter 11 contains experimental details that are general (laser experiments and steady-state experiments) and have appeared previously in the references given above.

1. Chapter 1 – Introduction

Silylenes and germylenes are heavier group 14 counterparts of carbenes, and they are key intermediates in photochemical and thermal reactions of various organosilicon and organogermanium compounds. The latest developments in silylene and germylene chemistry have been reviewed by some of the leading workers in the field, with the main focus on their fundamental reactivity.[1-7] The burst of activity on the experimental side has been matched by theoretical interest in these compounds. One of the reasons for the increasing interest in these elusive species is the fact that the parent silylene (SiH_2) and germylene (GeH_2) are key reactive intermediates in chemical vapour deposition of solid silicon and germanium, respectively.[8] Transient silylenes are thought to be involved in the direct reaction of alkyl chlorides with silicon surface in the presence of a copper catalyst to generate chlorosilanes on an industrial scale.[9] Stable silylenes and germylenes have been used as efficient catalysts for olefin polymerization.[10-11]

Although considerable progress has been made in understanding the fundamental reactivity of these species, it is often not possible to compare the reactivity of silylenes and germylenes of homologous structure under the same experimental conditions because the reactivity with the same set of substrates has not been studied in a systematic way. The main focus of this work is to study the kinetics and thermodynamics of representative bond insertion and atom abstraction reactions of transient dialkyl- and diarylsilylenes and germylenes in solution, specifically the bond insertion reactions of silylenes with alcohols, amines, alkoxysilanes and oligosiloxanes, and the O- and S- abstraction reactions of silylenes and germylenes from oxiranes and thiiranes.

Table 1.1. Naming of some tetrel derivatives.

M	MR_2	$R_2C=MR_2$	$R_2M=MR_2$	MR_4
C	carbene	alkene	alkene	alkane
Si	silylene	silene	disilene	silane
Ge	germylene	germene	digermene	germane
Sn	stannylene	stannene	distannene	stannane
Pb	plumbylene	plumbene	diplumbene	plumbane

1.1. Nomenclature

The Group 14 elements are collectively known as the tetrels,[12] and thus the term that has been recently adapted to denote heavier carbene analogues is *tetrellylenes*; they are more commonly known as “metallylenes”, however. A list of common nomenclature of various tetrel derivatives is shown in Table 1.1. Compounds containing tetrel-carbon double bonds are known as tetrelenes or metallenes, while the prefix “di” indicates that the double bond is between two group 14 elements of the same identity.

Silylenes have been called “silenes” in the older literature,[13-14] a term which is widely accepted to refer to compounds containing Si=C double bonds. “Silanediyls” is another term that has been used more extensively,[15-20] but is now obsolete.

1.2. Divalent Group 14 Compounds

The seemingly simple formulation of a tetrellylene as MR_2 hides much of the structure and bonding information that has fascinated chemists about these species. The two non-bonding electrons can be either paired (singlet state, antiparallel spins) or unpaired (triplet state) (Fig. 1.1). In a singlet state the two electrons are constrained in the same orbital, thus the electron-electron Coulombic repulsion is significant. Stabilization in a triplet state is achieved by relief of the repulsion; however the separation of electrons comes with an energy cost. Aside from a few recent examples,[21-23] the lowest energy

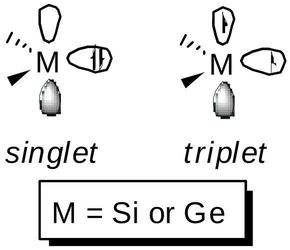

Figure 1.1. Singlet and triplet electronic states of silylenes and germylenes.

electronic state of silylenes and germylenes is generally the singlet. In contrast, the energy difference between spin states in dialkylcarbenes is small, and the multiplicity of the lower energy state can be tailored by simply changing substituents.[24] The silylenes and germylenes studied in this work are all in the singlet ground state, thus "silylene" and "germylene" will refer to "singlet silylene" and "singlet germylene", respectively. Unless substituents are present which impart kinetic or thermodynamic stability on tetrellylenes, these species are unstable and readily undergo dimerization to form the doubly-bonded dimers, disilenes and digermenes. Unlike planar alkenes, disilenes and digermenes usually adapt trans-bent geometries.[25]

One key fact that influences the chemistry of silylenes and germylenes is the increase in stabilization of the divalent state with increasing atomic number of the element. Lower group 14 elements have a more stable divalent state relative to that of carbon due to the DSSE (divalent state stabilization energy). Walsh[26] defined DSSE as the difference between the first and the second M-X bond dissociation energy (BDE) in MX_4, which is demonstrated through eq. 1.1-1.3.

$$MX_4 \rightarrow MX_3 + X \qquad \Delta H_1 \qquad (1.1)$$

$$MX_3 \rightarrow MX_2 + X \qquad \Delta H_2 \qquad (1.2)$$

$$\mathrm{DSSE}(MX_2) = \mathrm{BDE}(X_3M\text{-}X) - \mathrm{BDE}(X_2M\text{-}X) = \Delta H_1 - \Delta H_2 \qquad (1.3)$$

In the parent hydrides the following pattern emerges: for methane, the second BDE is larger than the first, while for the heavier counterparts the opposite is true.[25-26] The DSSEs of CH_2, SiH_2 and GeH_2 are -6 kcal mol^{-1}, 20 kcal mol^{-1} and 26 kcal mol^{-1}, respectively.[27] The accepted reasoning for the trend in DSSEs is that the methyl radical is planar and has stronger sp^2 hybridized bonds compared to the analogous trivalent silicon and germanium hydrides, which are pyramidal.[25]

1.3. Reactivity of Silylenes

1.3.1. Complexation With Chalcogen and Pnictogen Donors

Most of known silylene reactions involve coordination of the nucleophilic site of the donor molecule with the empty p-orbital on the silicon center to yield the corresponding Lewis acid-base adducts. The resulting complexes are typically less reactive than the non-coordinated silylenes,[28-29] thus many donor-stabilized silylene derivatives have been prepared.[30-36] Coordination to silylenes is accompanied by an increase in nucleophilicity at the silicon center[37] and may lead to intriguing reactivity of these species. For instance, silylene-phosphine adducts exhibit Wittig-like reactivity (eq. 1.4).[38-39]

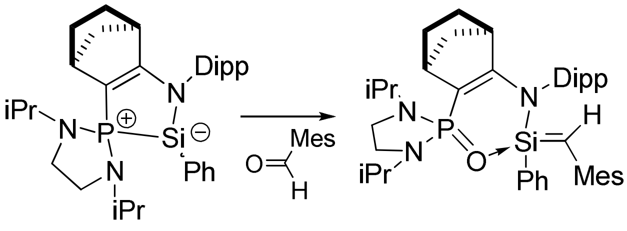

1 **2**

(1.4)

The first direct observation of silylene-donor complexes was achieved over 25 years ago by the groups of Ando[40] and West[41-42] in frozen matrixes by spectroscopic methods. Introduction of an ether, amine, sulfide or phosphine as a complexing agent induces a blue shift in the *n,p* transition of silylenes; the magnitude of the spectral shift decreases in the order $SiMes_2 > SiMe_2 \geq SiMes(t\text{-}Bu) >> SiMes(OAr)$. The oxygen-substituted silylene gives rise to the smallest spectral shift upon complexation, consistent with intramolecular stabilization of the silylene by the neighbouring oxygen atom leading to weaker interactions with other donors. With "non-reactive" substrates (where the energy barriers for further reactions past complexation are too high to proceed under typical conditions) the ultimate product of decomposition of the Lewis acid-base complexes is the formation of the corresponding disilenes, which subsequently oligomerize. The disilene was postulated to be formed by one or more of the three possible pathways shown in Scheme 1.1.[41] The first possibility involves direct dimerization of two free silylene units present at equilibrium. The complex could also dimerize with elimination of two substrate units, or the complex could combine with free silylene present at equilibrium. The authors favoured the first possibility, involving dimerization of two free silylene units, to be the dominant pathway for the formation of the disilene under the conditions of the experiments. Corriu et al.[43] demonstrated that intramolecularly coordinated amino(aryl)silylenes also react to form the corresponding disilenes in soft matrixes; the authors proposed direct dimerization of the silylene-amine complexes as a plausible route for the formation of the dimers.

Table 1.2. UV-vis absorption maxima of the Lewis acid-base complexes of transient silylenes with chalcogen and pnictogen donors in hydrocarbon solutions at 25 ^{o}C.

	SiMe$_2$	*SiPh$_2$*	*SiTmp$_2$^{f}*
THF	$310^{a,b,c}$	295, 370^b	375^d
Et$_2$O	305^a	-	-
dioxane	310^a	370^b	-
THT	335^c	-	-
Et$_3$N	$\leq 270^a$	-	-
DABCO^e	$\leq 270^a$ 285^c	-	-
pyrrolidine	290^c	-	-
N-methylpyrrolidine	285^c	-	-
CH$_3$CN	340^a	-	-
nBu$_3$P	310^c	-	-

[a] in cyclohexane, 20 ^{o}C ref. 44; [b] in hexanes, ref. 45; [c] in cyclohexane, ref. 46; [d] in hexanes, ref. 47; [e] DABCO = 1,4-diazabicyclo[2.2.2]octane; [f] Tmp = 3,4,5-trimethylphenyl

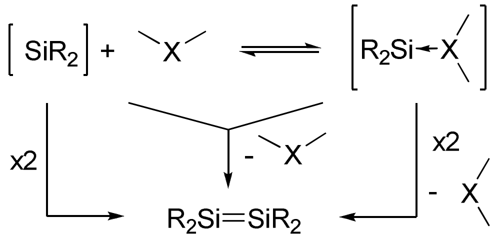

Scheme 1.1

In hydrocarbon solutions some silylene-chalcogen and silylene-pnictogen complexes have been observed with a variety of donors (Table 1.2). Although complexation with SiMe$_2$ has been investigated fairly thoroughly, there are significant deficiencies in the available data that warrant a more comprehensive study.

Table 1.3. Rate constants for the reactions of transient silylenes with chalcogen and pnictogen donors in hydrocarbon solutions at 25 °C, k_q / 10^9 M^{-1} s^{-1}.

	SiMe₂	*SiPh₂*	*SiTmp₂*[g]
THF	12.7[a] 17 ± 2[b] 10.3 ± 0.5[c]	15 ± 1[b]	8.3 ± 0.8[e]
1,4-dioxane	-	18 ± 1[b]	-
$C_2H_5O(CH_3)_2SiH$	6.2[d]	-	-
THT	10.3 ± 0.5[c]	-	-
N-methylpyrrolidine	8.0 ± 0.4[c]	-	-
pyrrolidine	9.4 ± 0.4[c]	-	-
DABCO[f]	9.7 ± 0.3[c]	-	-
nBu_3P	2.8 ± 0.1[c]	-	-

[a] in cyclohexane, error 20%, ref. 48; [b] in hexanes, ref. 45; [c] in cyclohexane, ref. 46; [d] in cyclohexane, error 15%, ref. 44; [e] in hexanes, ref. 47; [f] DABCO = 1,4-diazabicyclo[2.2.2]octane; [g] Tmp = 3,4,5-trimethylphenyl

Kinetics studies of the complexation of $SiMe_2$, $SiPh_2$, and $SiTmp_2$ (Tmp = 3,4,5-trimethylphenyl) with various donors in hydrocarbon solution indicate that the formation of the Lewis acid-base adducts is an enthalpically barrierless process, since the reactions proceed at close-to-diffusion controlled rates spanning the range of $(2.8 - 18) \times 10^9$ $M^{-1}s^{-1}$ (Table 1.3). Interestingly, none of these reactions have been investigated with $SiMes_2$, one of the most important silylenes that laid the groundwork for the solution studies. The only complete set of rate constants is known for complexation of THF with all three silylenes; the variation in the rate constants follows the trend $SiMe_2 \approx SiPh_2 > SiTmp_2$. In order to understand substituent effects on silylene reactivity and start drawing conclusions, it is desirable to study the reactivity of $SiPh_2$ with a more complete set of substrates and also explore the reactivity of $SiMes_2$ in hydrocarbon solutions.

The nature of Lewis acid-base interactions of SiH_2 with chalcogen[37, 49-52] and pnictogen[37, 49-54] hydrides has been studied extensively using ab initio and DFT theoretical calculations. The predicted stability (binding energy) of the SiH_2-donor complexes decreases in the order $NH_3 > PH_3 > H_2O > H_2S$.[37, 49] The results indicate that the interaction of silylenes with these substrates is charge-controlled, such that the stronger interactions exist with the harder base in each of the two series. This led to the classification of silylenes as “hard” Lewis acids; a similar classification has been proposed for GeH_2.[51-52] The Lewis acidity of SiH_2 has also been compared to that of GeH_2, indicating that the silylene is more Lewis acidic than the germylene.[37, 51]

1.3.2. Insertion Into the O-H Bonds of Alcohols

Insertion into the O-H bonds of alcohols and water is one of the best characterized reactions of transient silylenes.[1, 3, 55-58] In the early 1980s Weber and co-workers studied the effects of alcohol structure, solvent, and isotopic substitution on the reactions of photochemically generated $SiMe_2$ and SiMePh with EtOH, t-BuOH and H_2O by competition kinetics.[57-60] Kinetic isotope effects (KIEs), determined by competition experiments in cyclohexane, Et_2O or THF, were found to vary between 1.8 and 2.3 irrespective of solvent (Table 1.4).[60] The reaction was postulated to occur either via a reversible formation of a silylene-alcohol complex followed by a unimolecular rearrangement, or through a one-step direct reaction (eq. 1.5). The stepwise mechanism was intuitively favoured by the authors, although the concerted mechanism could not be ruled out based on the available evidence. The two-step mechanism involving the

Table 1.4. Isotopic product ratios (H/D) for the O-H insertion reactions by silylenes into alcohols, and alcohol concentrations used for the determination, [ROH]/[ROD] in M.[a]

alcohol	*$SiMe_2$*		*SiMePh*		*solvent*
	[ROH]/[ROD]	*KIE*	*[ROH]/[ROD]*	*KIE*	
EtOH/D	1.4 M/1.5 M	2.33 ± 0.02	-	-	Et_2O
	1.4 M/1.5 M	2.2 ± 0.1	-	-	THF
	1.4 M/1.5 M	2.1 ± 0.2	-	-	cyclohexane
t-BuOH/D	0.36 M/0.37 M	1.80 ± 0.07	0.9 M/0.5 M	1.8 ± 0.1	Et_2O
	-	-	0.9 M/0.5 M	2.09 ± 0.06	cyclohexane

[a] determined by competition experiments, ref. 60

formation of an acceptor-donor complex followed by 1,2 H migration is indicated by theory.[37, 49, 61-66]

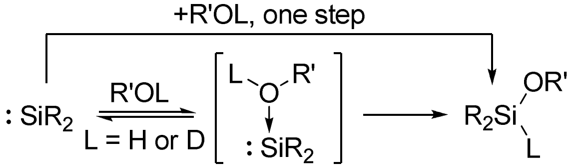

(1.5)

The O-H insertion reaction soon became established as a standard method to test silylene intermediacy.[67-72] A variety of photochemically generated silylenes (Si(t-Bu)$_2$,[67] SiMePh,[68] $SiPh_2$[69-72]) were found to insert into the O-H bond of alcohols such as MeOH, EtOH and t-BuOH in yields exceeding 80%. For instance, photolysis of the cyclotrisilane **3** in methanol yields two products in equimolar quantities – the product of O-H insertion by silylene **4**, and the product of MeOH addition to disilene, **5** (eq. 1.6). The chiral silylenes **6-11** were shown to undergo O-H insertion reactions stereoselectively, in a manner consistent with complexation occurring from the least hindered side of the silylene.[73] Reversed diastereoselectivity was observed with silylene **10**, which was ascribed to the intramolecular formation of a silylene-ether complex, forcing complexation with ROH and subsequent O-H insertion to proceed on the other face. The silylenes were generated from 254 nm photolysis of the corresponding 1,3-diphenyltrisilane precursors in the presence of either t-BuOH, n-BuOH, or 2,6-dimethylphenol.

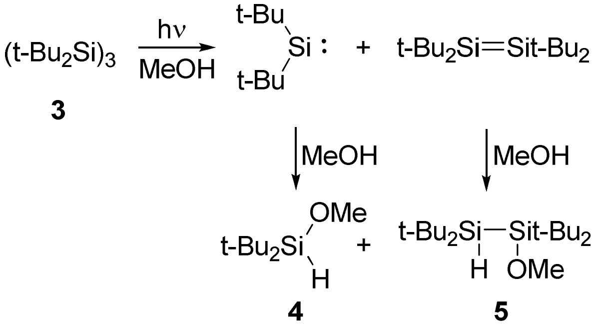

(1.6)

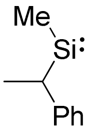

6

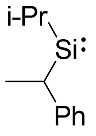

7

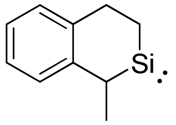

8

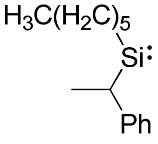

9

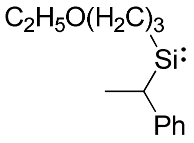

10

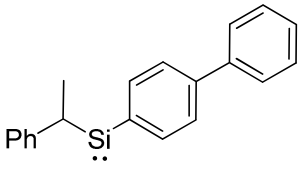

11

The first evidence for diarylsilylene-alcohol complexes was obtained by UV-vis spectroscopy in hydrocarbon matrixes at 77K by West and co-workers, who studied the reactions of $SiMes_2$, SiMes(t-Bu), and SiMes(ODip) (Dip = 2,6-diisopropylphenyl) with aliphatic alcohols.[41] The $SiMe_2$-ethanol complex was initially detected in hydrocarbon solution as a weakly absorbing, short-lived transient at low alcohol concentrations (1 – 2 mM) which was not characterized;[44] similar observations were made from the reaction of $SiPh_2$ with MeOH in the preliminary report on diphenylsilylene reactivity.[71] A possible pathway responsible for the seemingly strange behaviour of these complexes is catalysis

Table 1.5. Rate constants (10^9 M^{-1} s^{-1}) for the reactions of transient silylenes with alcohols in hydrocarbon solvents at ambient temperatures.

	$SiMe_2$	*SiMePh*	*$SiPh_2$*	*$SiTmp_2$*	*$SiMes_2$*	*SiPh(TMS)*
MeOH	18 ± 2 [a] (9.1 ± 0.5)[b]	18 ± 2 [a]	13 ± 2 [a]	10.4 ± 0.4[e]	0.82 ± 0.03 [a]	11 ± 1 [c]
EtOH	9 ± 2 [d]	-	-	-	-	-
2-butanol	10 ± 2 [d]	-	-	-	-	-
t-BuOH	10 ± 2 [d]	-	-	-	-	-

[a] In hexanes at 25 °C, ref. 71 [b] in methylcyclohexane at 20 °C; ref. 74. [c]In hexanes at 25 °C; ref. 75; [d] In cyclohexane at 23 °C; refs. 44, 48. [e] In hexanes at 25 °C; ref. 47.

by a second molecule of alcohol, which leads to the ultimate formation of the O-H insertion product. Gas phase studies of the reaction of parent silylene (SiH_2) with H_2O and MeOH by Becerra and coworkers support catalysis.[64, 66]

Absolute rate constants for the reactions of various silylenes in hydrocarbon solvents with alcohols are collected in Table 1.5. All of these have been measured by laser flash photolysis methods and extracted from the linear plots of k_{decay} vs [ROH]. The rate constants for the reactions of silylenes with MeOH follow the trend $SiMe_2$ > SiMePh > $SiPh_2$ > $SiTmp_2$ ≈ SiPhTMS >> $SiMes_2$, and are within a factor of 2 of the diffusional rate constant in hexanes in all cases except $SiMes_2$.

In Chapter 4, we investigated the reactions of transient silylenes $SiMe_2$ and $SiPh_2$ with MeOL and t-BuOL (L = H or D) in order to establish a mechanism for the O-H insertion reactions. In contrast to the previously published work, the experiments were carried out at submillimolar concentrations of alcohols, which led to the direct detection of the silylene-alcohol complexes in all cases. Evidence for catalysis by the second molecule of alcohol during the rate-determining step of the reaction was obtained through determination of the kinetic isotope effects. The experimental study was complemented by theoretical calculations, and compared to similar studies performed with $SiMes_2$.

1.3.3. Insertion Into the N-H Bonds of Amines

Early studies by Gu and Weber showed that $SiMe_2$ inserts efficiently into the N-H bonds of secondary amines such as Et_2NH and 2,2-dimethylaziridine (eq. 1.7).[59] The first spectroscopic detection of silylene-amine complexes was achieved in frozen matrixes by Ando et al,[40] who studied the reaction of $SiMes_2$ with amines; this was followed by the direct detection of a variety of silylene-amine complexes by West and co-workers also in frozen matrixes.[41] The complexation of silylenes with NH_3 has been the subject of several theoretical investigations,[37, 54, 76-77] which indicate that the SiH_2-NH_3 complex should have ca. 11 kcal/mol higher binding energy than the SiH_2-H_2O or SiH_2-H_2S complexes at the MP2/CEP-31G(2d,1p) level of theory.[37]

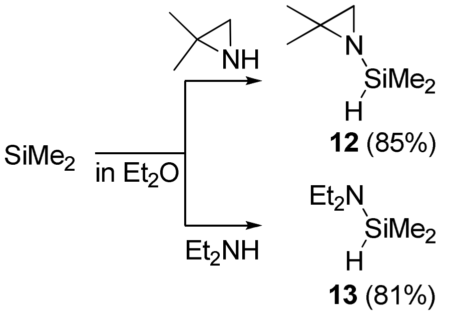

(1.7)

The kinetics of the reaction of the parent silylene SiH_2 with ammonia have been studied in the gas phase by Becerra et al.[77] The results suggest that in the gas phase at low pressure and ambient temperatures the reaction proceeds only as far as the complex, in agreement with calculations that suggest that the (unimolecular) 1,2-H migration to produce the formal N-H insertion product is too energetically unfavourable to occur under these experimental conditions.[49]

The reactions of $SiMe_2$ with secondary and tertiary amines in cyclohexane solution were investigated in cyclohexane solutions in early studies by the groups of Das and Shizuka.[44, 46] The bimolecular rate constants for complexation showed little variation with the amine structure (Table 1.5), all being very close to the diffusional rate constant. The corresponding $SiMe_2$-amine complexes could be readily detected and their spectroscopic properties are given in Table 1.2. These results contrast those for silylene-alcohol complexes, which are evidently much more difficult to detect in solution. In Chapter 5 the reactions of $SiMe_2$, $SiPh_2$ and $SiMes_2$ with n-$BuNH_2$ and Et_2NH were investigated. The corresponding Lewis acid-base complexes were detected in every case at large concentrations of the amine, indicative of a higher activation barrier for the formal N-H insertion process relative to the analogous O-H insertion reaction.

1.3.4. Insertion Into the Si-O Bonds of Siloxanes

Insertion reactions of silylenes into the Si-O bond of alkoxy- and oligosiloxanes (eq. 1.8-1.9) have been employed to test for the presence of silylenes in mechanistic studies for the last four decades.[78-84] The cyclic siloxanes hexamethylcyclotrisiloxane (D_3) and 2,2,5,5-tetramethyl-2,5-disila-1-oxacyclopentane (TMDOP) trap $SiMe_2$ in near-quantitative yields, while lower yields are obtained with SiMePh,[85] suggesting that the presence of phenyl groups on the silicon reduces the efficiency of the reaction.[80-82, 85]. Octamethylcyclotetrasiloxane (D_4) and hexamethyldisiloxane were found to be ineffective traps for $SiMe_2$, suggestive that the effectiveness of silylene trapping may be enhanced with decreasing angle about oxygen on the siloxane. Whereas the insertion of $SiMe_2$ into Si-O-Si single bonds of siloxanes is restricted to angle-strained siloxanes, the analogous insertion into Si-S bonds of disilthianes appears to be a more general reaction.[86-87]

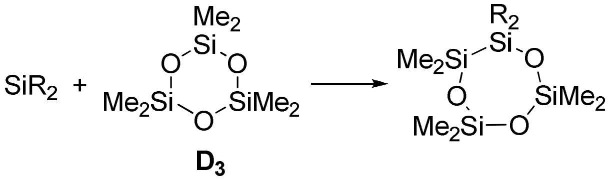

(1.8)

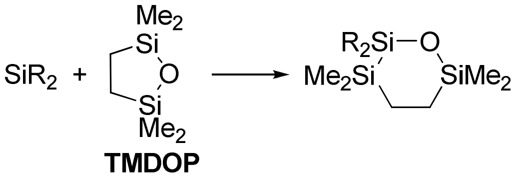

(1.9)

Dimethylsilylene, generated either thermally or photochemically, reacts readily with alkoxysilanes to give unsymmetrical alkoxydisilanes.[79, 81, 83-84] The ability of Si-OR bonds to trap silylenes is enhanced with increasing number of silane units, such that alkoxydi- and trisilanes are substantially more reactive toward silylene than alkoxymonosilanes.[45, 56-57, 84] Of some interest has been the insertion of silylenes into the Si-O bond of methoxytrimethylsilane (MeOTMS).[45, 57, 88-89] In 1990, Scaiano and co-workers made an interesting observation regarding the reaction of $SiMes_2$ with MeOTMS: although the trapping product $MeO(Mes)_2SiSiMe_3$ was isolated in high yield, time-resolved experiments showed that the silylene lifetime was unaffected by the presence of MeOTMS.[89]

Fast kinetic studies have also been carried out of the reactions of MeOTMS with $SiMe_2$ and $SiPh_2$.[45] Rate constants of 6.2×10^9 M^{-1} s^{-1} and 4.2×10^9 M^{-1} s^{-1} were reported for the reaction of MeOTMS with $SiMe_2$ and $SiPh_2$, respectively, and were assigned to the rate constants for formation of the complex (k_1 in eq. 1.10). In both cases unusual behaviour was noted: the substrate-mediated pseudo first-order decay of $SiPh_2$ was accompanied by a systematic decrease in the silylene signal intensity, while a plot of k_{decay} ($SiMe_2$) vs. [MeOTMS] displayed a downward curvature suggestive of saturation kinetics. The data are consistent with the mechanism shown in eq. 1.10, where a fast reversible complexation is followed by a slow unimolecular [1,2]-$SiMe_3$ migration.[45]

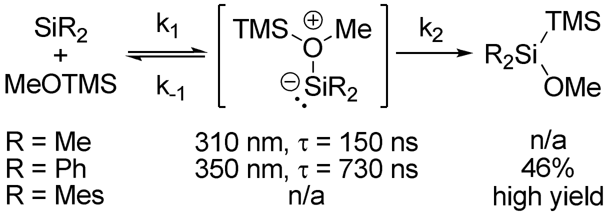

(1.10)

The $SiMe_2$- and $SiPh_2$-MeOTMS complexes have been characterized in hexane solution at 25 ^{o}C, where they exhibit UV-vis absorption maxima centered at 310 nm and 370 nm, respectively.[45] The lifetimes of the complexes were associated with the rate constant (k_2 in eq. 1.10) for the [1,2]-$SiMe_3$ migration from oxygen to silicon to form the final product. Phenyl- for methyl- substitution in the silylene results in ca. 5-fold reduction in the rate constant, such that the lifetimes of the $SiMe_2$-MeOTMS and $SiPh_2$-MeOTMS complexes are 150 ns and 730 ns, respectively. The rate constants for decay of the complexes are consistent with an activation energy of $E_a \approx 7.5$ kcal mol^{-1} for the 1,2-$SiMe_3$ migration, assuming pre-exponential factors on the order of 10^{12} s^{-1}.[45]

In Chapter 6, the reactions of $SiMe_2$ and $SiPh_2$ with MeOTMS and oligosilanes were investigated with the goals of establishing the mechanism for the Si-O insertion by silylenes. The experimental work is accompanied by kinetic simulations, which provide compelling evidence for the two-step mechanism involving reversible complexation followed by a slow unimolecular [1,2]-$SiMe_3$ migration of eq. 1.10.

1.3.5. O- and S- Abstraction Reactions From Oxiranes and Thiiranes

The reactions of $SiMe_2$ with epoxides were studied in the early 1980s by the groups of Weber[90] and Barton.[91] Tzeng and Weber demonstrated that photochemically generated $SiMe_2$ reacts with the vinyl epoxides **14a-d** to yield butadiene (**15**), the corresponding oxasilacyclohexane (**16**) and the cyclic Me_2SiO oligomers D_3 and D_4 (eq. 1.11).[90] The authors proposed a mechanism involving the initial formation of an acid-base complex, which undergoes ring opening to generate the zwitterionic intermediate **17** (Scheme 1.2). Two competing processes are then responsible for product formation - fragmentation to yield transient $Me_2Si{=}O$ and the diene, or ring-closure to form **16**.

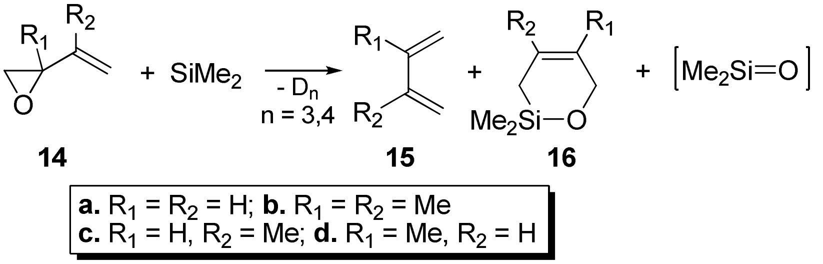

(1.11)

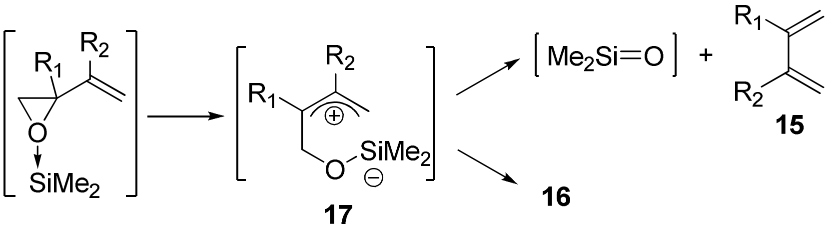

Scheme 1.2

Barton showed that thermally or photochemically generated $SiMe_2$ reacts with cyclooctene oxide to afford cyclooctene in ~75% yield along with D_3 and D_4; the corresponding silylene-oxirane complex was again proposed as an intermediate.[91-92] The inclusion of a silanone trapping agent, D_3, resulted in a cleaner reaction mixture, with D_4

being isolated as the only silanone-derived product. The sterically hindered silylene $SiMes_2$ was found to react with various epoxides (oxirane, propylene oxide (PrO), butylene oxide (BuO), phenyl oxirane (PhO) and cyclohexene oxide (CHO)) to yield products consistent with oxygen abstraction along with the corresponding alkenes in yields of 39-65%.[93] With all the oxirane derivatives except CHO, a cyclic siloxane **18** was isolated in 9-24% yield (eq. 1.12). Its formation was attributed to insertion of the initially formed dimesitylsilanone into the C-O bond of a second molecule of the starting epoxide.

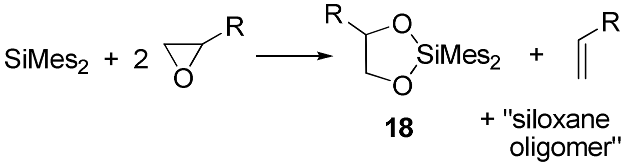

(1.12)

One kinetic study on the reaction of $SiMe_2$ with oxirane has been reported in the gas phase by Baggott et al.[94] The rate constant for this reaction was found to be pressure-dependent spanning the range of 2.0 to 2.8 x 10^9 M^{-1} s^{-1} (1-10 torr). The clean first-order decays of the silylene imply that the silylene-oxirane complex is short-lived under the experimental conditions, although it was not observed directly. Pressure dependency suggests the first step to be reversible and competitive with consequent decomposition of the complex to generate ethene.

The reactions of SiH_2 and $SiMe_2$ with oxirane and thiirane have been examined by DFT (B3LYP/6-311G(d)[95-96]) and ab initio (MP2/6-31G(d,p) and QCISD/6-31G(d,p),[97] and QCISD/6-311G(d)[95]) calculations. The results indicate that the first step of the reaction is the exothermic formation of the corresponding silylene-oxirane and silylene-thiirane complex, while the barriers for the second step are similar in both cases. The main difference between the reactions with oxirane and thiirane is the mode of decomposition of the complex: fragmentation of the silylene-thiirane complex to form silanethione leads directly to the silanethione and ethene, while the silylene-oxirane complex dissociates via the initial formation of a singlet biradical which undergoes β-cleavage to yield silanone and ethene. However, DFT calculations by M. D. Su failed to locate the biradical intermediate.[95-96]

Silanones are important intermediates in interstellar chemistry,[98] the oxidation of silicon surfaces,[99] silicon chemical vapor deposition processes,[8] polysiloxane production[100] and the combustion of silanes.[101] Most of our experimental knowledge about the properties and reactivities of silanones has been gained through low temperature IR detection of transient derivatives in argon matrices,[99, 102-106] although several groups have observed transient silanones by rotational spectroscopy,[107-108] luminescence,[109-110] and mass spectrometry in the gas phase.[111] Only one stable silanone has been synthesized by reaction of a silylene with N_2O; the highly reactive silicon-oxygen double bond in this molecule is stabilized by chelating amine ligands.[36] The main sources of information regarding the stability and reactivity of silanones are theoretical calculations, the parent silanone, $H_2Si{=}O$, having received the most attention.[112]

Molecules containing a silicon-sulfur double bond, silanethiones, are thought to be more thermodynamically stable than silanones due to a lower polarity and a higher HOMO-LUMO gap of the Si=S bond.[112-113] Stable silanethiones with sterically protecting or intramolecularly coordinating substituents have been synthesized by desulphurization of silatetrathiolanes,[114-115] reaction of silanes with CS_2[116] and by reaction of stable silylenes with elemental sulfur.[117] Transient silanethiones with small substituents have been observed in argon matrices at low temperature by IR spectroscopy.[118] Several transient silanethiones have been postulated to exist based on the results of trapping studies with D_3, ethanol, or 1,3-butadiene.[86, 119-120] Stable silanethiones have been found to react with methanol and water.[114-115]

In chapter 7, the kinetics and thermodynamics of the reactions of $SiMe_2$, $SiPh_2$, $SiTmp_2$ and $SiMes_2$ with PrO, CHO and propylene sulfide (PrS) were studied by laser flash and steady-state photolysis techniques in an attempt to elucidate the mechanism of the O- and S-abstraction. In conjunction with kinetic simulations and theoretical calculations, the results are indicative of a biradical mechanism for oxygen abstraction.

1.3.6. Reactions with Alkenes and Alkynes

The discovery of stable silacyclopropanes (siliranes) by Seyferth in the early 1970's[121-123] led to the realization that these molecules can act as transient silylene precursors.[16, 124-126] The formation of silylene decomposition products from these molecules is usually inferred from product studies which show products consistent with silylene generation. Silacyclopropane derivatives **19**(**a-c**) and **21-23** were shown to generate t-Bu_2Si either thermally (100-200 ^oC) or upon 254 nm photolysis (eq. 1.13).[16, 125-126] Thermal generation of t-Bu_2Si from the 7-silabicyclo[4.1.0]heptane derivative **22** and silver-mediated t-Bu_2Si transfer reactions have been extensively studied by Woerpel and his group.[126-150]

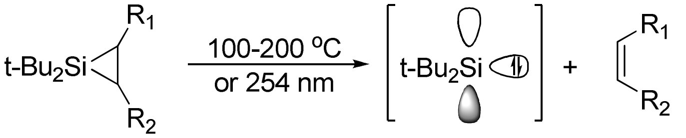

(1.13)

19

a. R_1 = Me, R_2 = H
b. R_1 = R_2 = Me
c. R_1 = R_2 = H

20

a. R_1 = Me, R_2 = H
b. R_1 = R_2 = Me
c. R_1 = R_2 = H

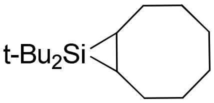

21

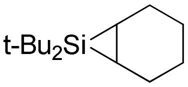

22

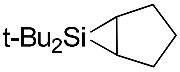

23

More recently, the novel silirane **24** was shown to generate transient bis(2,6-diethylphenyl)silylene (Dep_2Si) and cyclooctene either thermally (180 °C) or upon irradiation with a medium-pressure mercury vapour lamp.[151] Diadamantylsilylene can also be generated either photochemically or thermally from the siliranes **25a** and **25b**, and was shown to undergo [1+2] cycloaddition reactions with a variety of alkenes.[152] A stable silylene-amine complex **26** with bulky aryl substituents can be thermally generated from silirane **27**.[153]

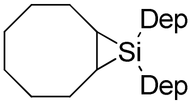

24

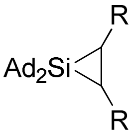

25a. R = Me
25b. R = Et

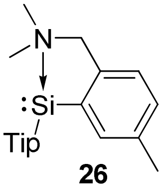

26

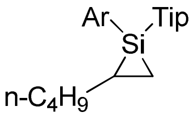

27

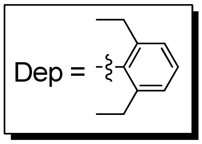

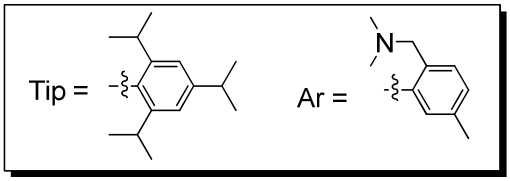

Given the importance of siliranes in silylene chemistry, the need for a direct feasible synthesis of these compounds is evident. Cycloaddition reactions of a variety of silylenes to olefins have been studied extensively,[3, 154-156] and were shown to yield either intermediary[13, 81, 157-160] or stable[125, 152, 161-165] siliranes in high yields, thus providing an efficient synthetic route to these cyclic compounds. Silylenes add to alkenes stereospecifically, which was first discovered by Tortorelli and coworkers in the reactions of $SiMe_2$ and $SiPh_2$ with cis- and trans-2-butene (eq. 1.14).[157, 166] The stereospecificity of the reactions was determined by analysis of the products of methanolysis of the initially formed siliranes. Siliranes formed from phenylmethyl-[78, 167], diphenyl-[157] and dimesitylsilylenes[168] are known to be photolabile, and thus under photochemical conditions the initially formed siliranes often undergo light-induced 1,3 silyl migration (eq. 1.15). Retention of stereochemistry was also demonstrated for the reactions of (t-Bu_3Si)(t-Pr_3Si)Si,[161] Ad_2Si (Ad = adamantyl),[152] $SiMe_2$,[81] $SiMes_2$,[164, 168] and Si(TMS)Ph[169] with various alkenes. Silylenes also add to alkynes to produce the corresponding silirenes (silacyclopropenes).[162, 170-171]

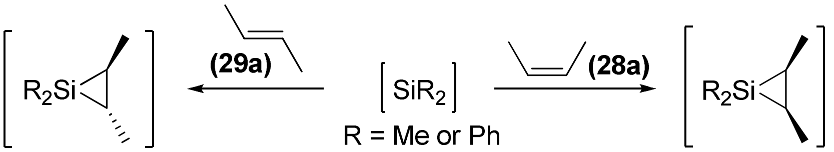

(1.14)

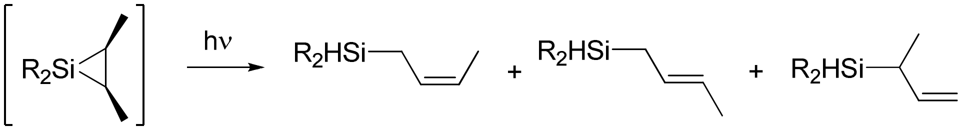

(1.15)

Kira's stable dialkylsilylene **29** was shown to undergo [1 + 2] cycloaddition reactions with alkenes and alkynes.[162] While **29** was found to add to ethene and cis-2-butene in hexane at room temperature to generate **30c** and **30a**, respectively, in quantitative yields (eq. 1.16), the analogous reaction with trans-2-butene did not give silirane under the same experimental conditions, yielding a complex product mixture instead. The results suggest that the reaction with the trans-alkene is significantly slower than that with the cis isomer, in accordance with the earlier findings of Conlin and co-workers that cycloaddition of $SiMes_2$ to cis-2-butene proceeds 25-28 times faster than that to trans-2-butene.[168] N-heterocyclic silylenes, on the other hand, have been discovered to act as efficient catalysts for polymerization of terminal alkenes and alkynes, and do not undergo the [1 + 2] cycloaddition reaction typical of other silylenes.[10]

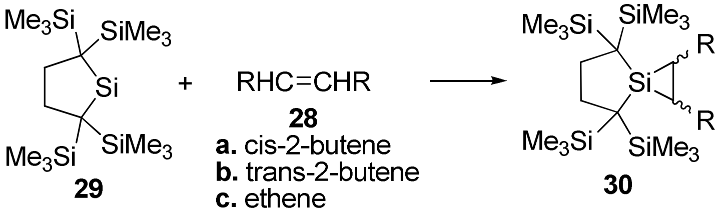

(1.16)

The rate constants for the reactions of $SiMe_2$, SiMePh, $SiPh_2$, $SiTmp_2$ and $SiMes_2$ with a series of alkenes and alkynes have been measured in hexanes or cyclohexane solutions and are summarized in Table 1.6. The values range from 2.8×10^{6} M^{-1} s^{-1} to 1.78×10^{10} M^{-1} s^{-1} and decrease in the order $SiMe_2$ > SiMePh ≈ $SiPh_2$ > $SiTmp_2$ >> $SiMes_2$. The absolute rate constant for the reaction with cyclohexene is ca. 2 times slower for $SiTmp_2$ than that for $SiPh_2$, reflecting the electronic effects on the rate determining step provided by the methyl groups on the aromatic ring. $SiMes_2$ reacts with the same substrate ca. 1500 times slower than does $SiTmp_2$ under the same experimental conditions, which can be attributed to steric interactions of the ortho-methyl groups with the alkene. A similar trend in the rate constants is observed in the reactions with the alkyne $(CH_3)_3SiC{\equiv}CSi(CH_3)_3$ (Table 1.6).

Table 1.6. Rate constants (k_1 / 10^9 M^{-1} s^{-1}) for the reactions of transient silylenes with alkenes and alkynes in hydrocarbon solvents at 25 °C.[a]

	SiMe$_2$	*SiMePh*	*SiPh$_2$*	*SiTmp$_2$*	*SiMes$_2$*
1-hexene	7.3 ± 1.4[b,c]	-	-	-	-
cyclohexene	8 ± 1[e]	-	7.9 ± 0.7[e]	4.3 ± 0.2[h]	0.0028 ± 0.0003[d]
$(CH_3)_3SiCH{=}CH_2$	5.9 ± 1.2[b,c]	-	-	-	-
$(CH_3)_3SiC{\equiv}CH$	8.0 ± 1.6[b,c]	-	-	-	-
$(CH_3)_3SiC{\equiv}CSi(CH_3)_3$	13.8 ± 0.5[e]	-	7.6 ± 0.6[e]	1.60 ± 0.09[h]	0.026 ± 0.001[h]
4,4-dimethylpentene	11.7 ± 0.5[e]	7.0 ± 0.3[g]	8.7 ± 0.4[f]	-	-
t-BuCC≡CH	17.8 ± 0.6[e]	9.5 ± 0.2[g]	9.7 ± 0.4[f] 8.3 ± 0.7[e,g]	-	-

[a] in hexanes unless noted otherwise; [b] in cyclohexane, ref. 48; [c] in cyclohexane, ref. 44; [d] in cyclohexane, ref. 89; [e] ref. 45; [f] ref. 72; [g] ref. 68; [h] ref. 47

1.4. Reactivity of Germylenes

1.4.1. Complexation with Chalcogen and Pnictogen Donors

As with silylenes, the primary driving force for the reactions involving germylenes is their high electrophilicity resulting from the empty (4)p orbital on the tetrel center. In principle singlet germylenes are amphoteric; the nucleophilicity of the lone pair can be enhanced by introduction of electron density to the empty p-orbital. Stabilization of transient germylenes by coordination with stable carbenes has been shown to lead to intriguing reactivity of these species.[172-179]

Ando's group was the first to detect not only silylene-donor complexes at low temperatures, but germylene-donor complexes as well.[180-181] The reactions of dimethyl- and diarylgermylenes with O-, S-, N- and P- donors are analogous to the reactions between silylenes and donors. Coordination of the germylenes induces blue shifts in the absorption spectra relative to "free" germylenes; annealing of the matrices leads to the prompt formation of the corresponding digermenes.

Quantum chemical calculations on the reaction of the parent tetrellylenes SiH_2, GeH_2 and SnH_2 with chalcogen and pnictogen hydrides[37] indicate that the strength of the acceptor-donor interaction decreases in the order $SiH_2 > GeH_2 > SnH_2$. This is demonstrated for SiH_2 and GeH_2 in Fig. 1.2, which shows a plot of calculated binding energies of the germylene complexes versus the corresponding values for the homologous silylene complexes. The plot shows excellent linearity over a ca. 12 kcal mol^{-1} range in binding energy; the slope of 0.8 indicates that the difference in Lewis acidities of SiH_2 and GeH_2 increase somewhat as a function of the Lewis base strength of the donor. The intercept of 0.4 kcal mol^{-1} indicates that on average, the strength of the acceptor-donor interaction for the silylene is stronger than that for the germylene by a small amount. The Lewis acid and Lewis base character of various substituted silylenes and germylenes has been the subject of more recent DFT (B3LYP/6-311+G(d,p)) calculations by Oláh and coworkers.[51] The results indicate that the interactions of silylenes and germylenes with NH_3, PH_3 and AsH_3 correlate with electrostatic potential near the empty p orbital of the donors, and the relative magnitudes of the binding energies led to the classification of both silylenes and germylenes as "hard" electrophiles. The interaction of dihalogenated

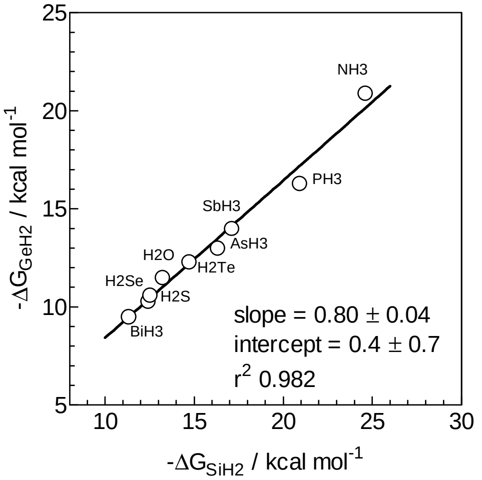

Figure 1.2. Plot of gas phase binding energies of silylene complexes ($-\Delta G_{SiH2}$ / kcal mol^{-1}) against binding energies of the corresponding germylene complexes ($-\Delta G_{GeH2}$ / kcal mol^{-1}), calculated at ab initio level. Data from ref. 37

germylenes as well as GeH_2 and $GeMe_2$ with a series of σ- and π- donors has also been investigated at the DFT level.[182] The complexation energy of the GeH_2-THF complex was found to be 6.6 kcal mol^{-1} higher (more negative) than that of the $GeMe_2$-THF complex, indicating that GeH_2 is a stronger Lewis acid than $GeMe_2$.

Several studies in our group explored the kinetics and thermodynamics of the complexation of transient germylenes with O- and N- donors; the data for the reactions of $GeMe_2$, GeMePh, $GePh_2$ and $GeMes_2$ with some amines and THF are provided in Table 1.7. The rate constants for complexation decrease with increasing substitution on the nitrogen atom. The rate constants for complexation with n-$BuNH_2$ follow the trend $GeMe_2$ ≈ GeMePh > $GePh_2$ > $GeMes_2$, and a similar trend appears to hold for complexation with Et_3N. Equilibrium constants have been measured for the reactions with THF and decrease in the order $GePh_2$ > $GeMe_2$ > $GeMes_2$ which establishes the trend in Lewis acidities of the three germylenes. The equilibrium constants for complexation of the four germylenes with n-$BuNH_2$ and for the other amines with $GeMe_2$, GeMePh and $GePh_2$ are too large to be measured under laser flash photolysis conditions.

Table 1.7. Forward rate (k_1 / 10^9 M^{-1} s^{-1}) and equilibrium constants (K_1 / M^{-1}) for complexation of transient germylenes with N- and O-donors.

	$GeMe_2$	GeMePh	$GePh_2$	$GeMes_2$
n-$BuNH_2$	13 ± 3 [a]	12 ± 1 [b]	10.1 ± 0.6 [c]	7.0 ± 0.3 [c]
Et_2NH	-	-	7.3 ± 0.9 [d]	-
Et_3N	8.7 ± 0.7 [a]	3.9 ± 0.4 [b]	2.8 ± 0.9 [d]	-
THF	11 ± 2 [e]	-	6.3 ± 0.6 [e]	
	[10,000 ± 4000]		[23,000 ± 5000]	[1.2 ± 0.2] [e]

[a] ref. 183; [b] ref. 184; [c] ref. 185; [d] ref. 186; [e] ref. 187

Chapter 3 concentrates on theoretical and experimental manifestations of complexation reactions by the transient silylenes and germylenes MMe_2, MPh_2 and $MMes_2$ (M = Si or Ge). Aided by theoretical calculations at the “chemically accurate”[188] G4 level of theory, substantial evidence has been collected allowing the classification of silylenes and germylenes as “hard” Lewis acids to be revised.

1.4.2. Insertion Into the O-H and N-H Bonds of Alcohols and Amines

As opposed to complexation with “unreactive” Lewis bases, σ bond insertion reactions of transient germylenes have been studied quite extensively. Subsequent to the early indications that germylenes insert into the O-H bonds of alcohols by the groups of Lappert and Atwood, [189] and Satge,[190] the first spectroscopic detection of the germylene-alcohol[180] and GeH_2-H_2O[191] complexes was achieved in frozen matrixes. This work was followed by a review of transient germylene chemistry by Neumann,[2] which spurred a burst of activity on the O-H and N-H insertion reactions by transient germylenes by both experimentalists and theoreticians. [63, 183-187, 192-199]

Transient germylenes were found to readily undergo O-H insertion with water and alcohols to form stable products;[192-193] the authors proposed the initial formation of a

Lewis acid-base adduct to account for the observed results. The products of N-H insertion with amines, on the other hand, are unstable and generally cannot be isolated.[185, 192, 199]

Ab initio calculations indicate that the reactions of GeH_2 and $GeMe_2$ with NH_3 and H_2O all begin with the initial formation of an acceptor-donor complex, followed by a high energy barrier for the formation of the formal X-H insertion product via a three-membered transition state.[63, 194-196] For the GeH_2-H_2O system, the barrier to the 1,2-H migration is predicted to be higher and reaction exothermicity smaller than that in the corresponding SiH_2-H_2O system, which has been attributed to a larger size of the germanium atom compared to silicon. A systematic ab initio study of the complexation of GeH_2-donor complexes has also appeared in the literature, which predicted that complexation of GeH_2 with ammonia is ca. 10 kcal mol^{-1} more favourable than that with water.[37]

The kinetics of the reactions of GeH_2 with MeOH, MeOD and D_2O were investigated in the gas phase by Alexander et al.[197] The results showed that the reactions are pressure-dependent in every case, indicative of a third-body assisted complexation reaction. Unequivocal evidence for the involvement of intermediate complexes along the reaction pathway of germylenes with alcohols and amines was obtained in a series of studies by our group.[183-187, 199] Germylene-alcohol complexes have been detected in neat MeOH solution, which led to a study focused on the reactivity of the germylene-MeOH complexes towards strong acids and bases.[198] The $GePh_2$-MeOH complex exhibit a 50 μs lifetime in neat MeOH, while the $GeMe_2$-MeOH complex decays over ca. 4 μs under similar conditions. While dimerization of the germylenes is suppressed in neat alcohol solution presumably due to catalysis, it is still a significant pathway for the disappearance of the germylenes in dilute hexanes solution (Scheme 1.3).

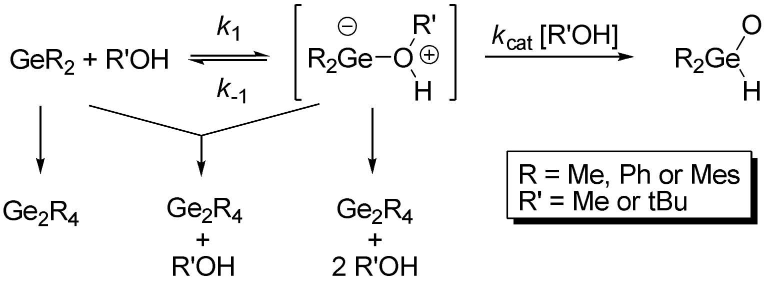

Scheme 1.3

Rate and equilibrium constants for the formation of the corresponding Lewis acid-base complexes in the reactions of germylenes with amines and alcohols are collected in Table 1.8. Reactions with alcohols were found to be reversible in all six cases, which led to the determination of equilibrium constants in the 3.7 M^{-1} – 3,300 M^{-1} range. The reaction of $GeMes_2$ with EtOH was also examined in a preliminary investigation;[200] the conclusion at the time was that this germylene does not react with EtOH on the microsecond timescale. However, those results are in fact consistent with a low equilibrium constant for complexation, in line with those later obtained[187] for the reactions of $GeMes_2$ with MeOH and t-BuOH (Table 1.8). In contrast, complexation with amines was found to proceed with equilibrium constants above the measurement limit of ca. 25,000 M^{-1}. This indicates that the binding energies of germylene-amine complexes are higher (more negative) than the corresponding alcohol complexes, consistent with earlier ab initio studies.[37] The rate constants are all within a factor of 10 from the diffusional rate in hexanes and decrease with increasing substitution on the amine.

Table 1.8. Forward rate (k_1 / 10^9 M^{-1} s^{-1}) and equilibrium constants (K_1 / M^{-1}) for complexation of transient germylenes with amines and alcohols in hexanes at 25 °C.

	k_1 / 10^9 M^{-1} s^{-1} [K_1 / M^{-1}]				
	n-$BuNH_2$	Et_2NH	Et_3N	MeOH	t-BuOH
$GeMe_2$	12 ± 3 [a]	-	8.7 ± 0.7 [a]	[900 ± 60] [c]	[340 ± 50] [c]
$GePh_2$	10.1 ± 0.6[d]	7.3 ± 0.9 [b]	2.8 ± 0.9 [e]	6 ± 1 [c] [3,300 ± 800]	5 ± 2 [c] [1,000 ± 300]
$Ge(4\text{-}MeC_6H_4)_2$	-	6.9 ± 0.8 [b]	-	-	-
$Ge(4\text{-}FC_6H_4)_2$	-	7.3 ± 0.4 [b]	-	-	-
$Ge(4\text{-}F_3CC_6H_4)_2$	-	9 ± 1 [b]	-	-	-
$GeMes_2$	7.0 ± 0.3 [d]	-	-	[15 ± 6] [c]	[3.7 ± 0.2] [c]

[a] ref. 183; [b] ref. 201; [c] ref. 187; [d] ref. 185; [e] ref. 184, 186

1.4.3. O- and S- Abstraction Reactions from Oxiranes and Thiiranes

Experimental studies of the reactions of germylenes with oxiranes and thiiranes are limited to the work of Satge and co-workers in the 1970's, who examined the reaction of these substrates with the product of a room-temperature reaction of chlorogermanes with pyridine or triethylamine (eq. 1.17), and formulated as the corresponding germylene-amine complex.[202] Diphenylgermylene generated by the aforementioned method was reported to insert into oxiranes to form the corresponding germaoxetanes followed by dimerization to form dioxagermacyclooctanes (**34**), instead of abstracting oxygen as lighter tetrelylenes have been shown to do (eq. 1.18).[203] Diethylgermylene was reported to react thermally with oxiranes and thiiranes to yield products consistent with chalcogen abstraction, the corresponding alkene and hexaethylcyclotrigermoxane.[190, 204-205] It was also shown that germanones and germathiones insert into oxiranes and thiiranes to form 5-membered rings.

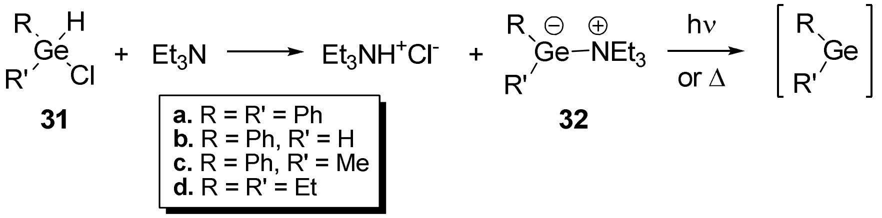

(1.17)

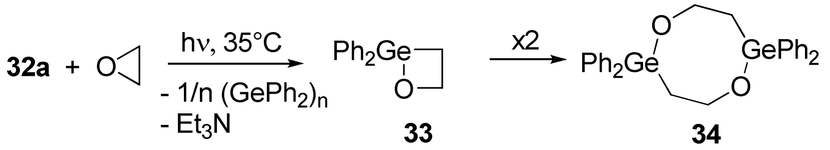

(1.18)

A report by Collins and coworkers following these studies refuted the formation of the germylene-amine complexes by this route, and suggested an alternate mechanism (eq. 1.19).[206] It was shown that a room temperature reaction of diphenylchlorogermane (**31a**) with Et_3N in fact yields 1,1,2,2-tetraphenylchlorodigermane (**35**) and not the germylene-amine complex as was previously reported. In turn, photolysis or thermolysis of the digermane results in regeneration of **31a** and formation of $GePh_2$, which subsequently oligomerizes.

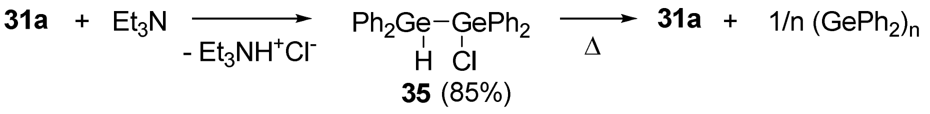

(1.19)

Transient germylenes $GeMe_2$ and $GePh_2$ are known to form Lewis acid-base complexes with a variety of donors in hexanes solution.[207] Germylene complexes with ethers and tetrahydrothiophene can be readily detected in hexane solution at 25 ^{o}C, and decay with the formation of the corresponding digermene.[198] Both the Me_2Ge-Et_3N and

Ph_2Ge-Et_3N complexes have been shown to have lifetimes on the order of several microseconds at ambient temperature in solution, which supports the conclusions of Collins and coworkers that they were not the actual germylene precursors in the French studies.

The reaction of the parent germylene (GeH_2) with oxirane was explored computationally using density functional theory.[96] These results suggest that the reaction should proceed via the initial formation of the GeH_2-oxirane complex, which undergoes concerted bond cleavage to yield germanone and ethene. The GeH_2-oxirane complex was predicted to be kinetically unstable and elude direct detection.

In Chapter 8, a study of the reactions of transient germylenes $GeMe_2$ and $GePh_2$ with cyclohexene oxide (CHO) and propylene sulfide (PrS) are presented; the germylenes were generated using photolysis of the corresponding germacyclopentene derivatives **36** and **37**. The study was carried out in order to ascertain whether (a) an acceptor-donor complex is formed along the reaction pathway; (b) the O- and/or S- abstraction takes place under conditions similar to those by silylenes; (c) dioxagermacyclooctanes of structure **34** are the likely products of oxygen abstraction; (d) the rate and equilibrium constants for complexation can be measured.

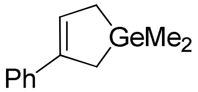

36

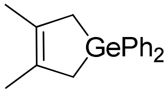

37

1.4.4. Reactions with Alkenes and Alkynes

While there are many examples of stable siliranes known (see Section 1.3.6), only three stable germiranes have been reported to date.[208-209] Two of the three known stable germiranes **38** and **42** have been synthesized by the reaction of the stable germylene **40** with either tetramethylbutatriene (**41**) or N-phenylmaleimide (**39**) (Scheme 1.4).[208] A number of stable germacyclopropenes have also been prepared, either by reaction of a germylene with an alkyne[210] or by other synthetic routes.[211]

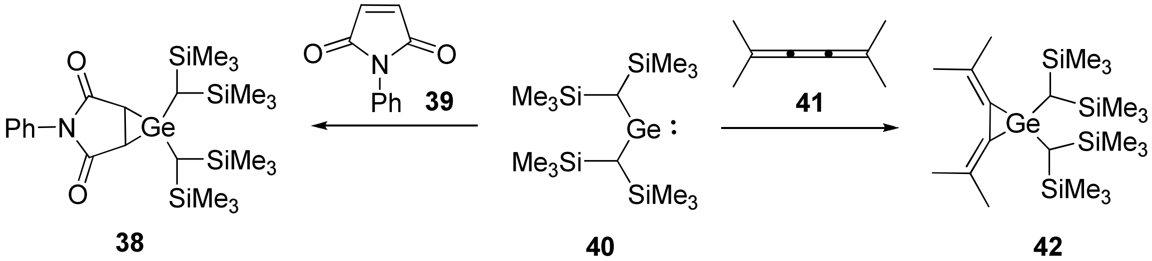

Scheme 1.4

The reactions of the parent germylene, GeH_2, with C-C unsaturated compounds have been investigated in the gas phase[212-216] and computationally.[214, 217-219] Becerra et al showed that the reaction of GeH_2 with propene occurs at approximately half the collisional rate at 298 °C, and the pressure dependence is indicative of a third-body assisted association reaction.[213-214] A small negative activation energy for the reaction suggests an involvement of an intermediate π-complex between the alkene and the germylene, in accordance with theoretical calculations of the reaction of GeH_2 with ethylene by Sakai[217], Su et al[218], Birukov et al[219] and Becerra et al.[214] Quantum chemical calculations (both DFT and G2//QCISD) indicate there are two modes of decomposition available to the initially formed π-complex: either HGe-H addition to yield ethylgermylene or 1,2-cycloaddition to yield germirane.[214] The mechanism involving the formation of ethylgermylene was supported by a large inverse kinetic isotope effect measured for the reaction of GeH_2 with ethylene-d_4.[215]

The reactions of transient germylenes $GeMe_2$ and $GePh_2$ have also been investigated in condensed phases. While the reaction of $GeMe_2$ with a series of aliphatic alkenes does not afford isolable products,[220] $GeMe_2$ reacts with two molecules of substituted styrenes to generate germacyclopentenes.[220-221] On glass surfaces, $GeMe_2$ reacts with alkenes and alkynes to form intermediary germiranes and germirenes, respectively, which could be trapped with water.[223] Several transient germiranes have been directly detected by time-resolved UV-vis spectroscopy from the reactions of $GePh_2$ with various alkenes by S. S. Chitnis (*unpublished*) and Y. Saeidi Hayeniaz,[222] and were efficiently trapped with MeOH to generate the corresponding addition products. Transient germiranes decay on microsecond timescales and are substantially more reactive than their silicon counterparts.

The reactions of diarylgermylenes with dienes was investigated by Huck and Leigh.[224] The results indicate that germiranes are the kinetic products of the reaction and are formed reversibly, while the (1 + 4) cycloaddition products are thermodynamically more stable. Saeidi Hayeniaz[222] studied the reaction of $GePh_2$ with a series of alkenes and established a rough correlation between the Gibbs free energy of the reaction and the ionization potential of the alkene, indicating that the stability of germiranes decreases with increasing substitution. The results were complemented by DFT calculations, which are in good agreement with experimental findings.

1.5. Techniques used

In order to study reaction mechanisms, two techniques were used in this thesis – *steady state photolysis* and *laser flash photolysis* experiments. The former is used to identify product structures and determine product yields, while the latter is used to directly detect and monitor reactive intermediates formed along the reaction pathway. In a steady state photolysis experiment, a mixture of a silylene or germylene precursor and a scavenger is photolyzed in an inert solvent. The intermediates are generated *in situ*, and the formation of stable products is typically followed by ^{1}H NMR spectroscopy in regular intervals. The photolysis is usually carried out to *ca*. 30% conversion of starting materials, and the resulting product mixture at the end of the photolysis is analyzed by a variety of techniques including, but not limited to, ^{1}H-^{29}Si HMBC spectroscopy (for the analysis of silicon-containing compounds), COSY spectroscopy, ^{1}H-^{13}C HSQC and HMBC spectroscopy, and GC/MS. Owing to the lower sensitivity of the 1D ^{29}Si- and ^{13}C experiments compared to the 2D ^{1}H-^{29}Si HMBC and ^{1}H-^{13}C HSQC and HMBC experiments, the 1D NMR experiments on those nuclei are usually not carried out. Although isolation of products and/or spiking of the photolysis mixtures with authentic samples are the only really rigorous way or identifying product structures, in many cases isolation is not possible due to high reactivity with water and/or oxygen and the small amounts typically available. In these cases, more specialized techniques are required to aid the characterization of products. One of these is a TOCSY experiment (Total Correlation Spectroscopy); this technique is described in detail in Section 7.2.1.

The laser flash photolysis technique is one of many time-resolved spectroscopic techniques that can be used to study physical or chemical processes that occur on picosecond, nanosecond, or microsecond timescales. In our system, a 248 nm laser pulse (~20 ns) supplies the energy necessary for the generation of transient species of interest from the photochemical precursors. The transient absorption is monitored by a xenon lamp, along the monitoring beam of which is located the sample cell and a detection system (a monochromator and a photomultiplier). The transient absorption spectra are obtained by generating absorbance-time profiles at multiple wavelengths. The *n,p* electronic transition of silylenes and germylenes studied in this work occurs in the spectral range of 450-600 nm (see Chapter 2), and thus this technique is very convenient to study the reactivity of these species.

1.6. Thesis Outline

The thesis present the results of a study of the kinetics and mechanisms of several bond insertion and atom abstraction reactions of transient dialkyl- and diarylsilylenes and -germylenes in solution, specifically the bond insertion reactions of silylenes with alcohols, amines, alkoxysilanes, and oligosiloxanes and the O- and S- abstraction reactions of silylenes and germylenes from oxiranes and thiiranes. These reactions are shown to all proceed via multi-step mechanisms involving the initial formation of a tetrellylene-substrate Lewis acid-base complex, and thus the first part of the document (Chapter 3) will describe the results of a detailed study of the kinetics and thermodynamics of the Lewis acid-base complexation reactions of silylenes and germylenes of homologous structure (MMe_2, MPh_2 and $MMes_2$, M = Si or Ge) with chalcogen and pnictogen donors. Complexation reactions with a series of ethers (Et_2O and THF), sulfides (Et_2S and THT), amines (Et_2NH and Et_3N) and trialkylphosphines (Et_3P and Cy_3P) were examined. Equilibrium constants were measured for complexation of all six tetrellylenes with Et_2O, and show that their Lewis acidities decrease in the order $SiPh_2 > SiMe_2 > GePh_2 > GeMe_2 > SiMes_2 > GeMes_2$. The equilibrium constants for the reactions of $SiMes_2$ and $GeMes_2$ with all the donors studied except Et_3P were determined, and show consistently that the silylene is more acidic than the germylene by ca. 1 pK unit. The free energies of complexation correlate roughly with the gas phase proton affinities of the donors. Calculated (G4) binding enthalpies of the complexes of MMe_2 with 17 Lewis bases correlate with Drago's E and C parameters,[225-226] in a manner consistent with the classification of $SiMe_2$ and $GeMe_2$ as borderline soft Lewis acids.

In Chapter 4 the mechanism of the reactions of dimethyl- and diphenylsilylene ($SiMe_2$ and $SiPh_2$) with alcohols (MeOL or t-BuOL, L = H or D) in hexanes solution will be discussed. The reaction was found to proceed via initial complexation followed by catalytic O-L insertion. The catalytic O-L insertion process proceeds with rate constants within a factor of 10 of the diffusion limit, while the putative unimolecular process is too slow to be detected in solution. The results are compared to the analogous reactions of dimesitylsilylene ($SiMes_2$), where the complexation step is reversible and the complex is a steady-state intermediate.

A study of the insertion reactions of $SiMe_2$, $SiPh_2$ and $SiMes_2$ into the N-H bonds of amines (n-$BuNH_2$ and Et_2NH) is described in Chapter 5. The bimolecular rate constants for complexation with amines was found to follow the trend n-$BuNH_2 > Et_2NH > Et_3N$, in the order of increasing steric bulk on the nitrogen. The complexation rate constants of silylenes with the same substrate increased in the order $SiMe_2$ > $SiPh_2$ > $SiMes_2$. The results indicate that amine catalysis is at least 10^4 times slower than the analogous process in the SiR_2-MeOH complexes.

The results of laser photolysis studies of silylene insertions into the Si-O bonds of alkoxysilanes and siloxanes (MeOTMS, D_3, D_4, TMDOP, TMS_2O and $Me_2Si(OTMS)2$) are described in Chapter 6. The results are consistent with a mechanism in which the first step is a reversible formation of a Lewis acid-base complex followed by a unimolecular [1,2]-silyl migration. The ability to detect the corresponding Lewis acid-base complexes depends on the relative magnitudes of the rate constants for the first and second step.

Chapters 7 and 8 focus on the O- and S- abstraction reactions of silylenes ($SiMe_2$, $SiPh_2$, $SiMes_2$ and $SiTmp_2$) and germylenes ($GeMe_2$ and $GePh_2$) from oxiranes (cyclohexene oxide (CHO) and propylene oxide (PrO)) and a thiirane (propylene sulfide (PrS)). The results indicate that the reaction proceeds via a two-step mechanism, involving initial complexation followed by unimolecular collapse of the complex to form the corresponding $R_2M=X$ transient compounds (R = Me, Ph, Mes or Tmp; M = Si or Ge, X = O or S). For $SiMe_2$ and $SiPh_2$ the first step is essentially irreversible ($K_{eq} > 25{,}000\ M^{-1}$), while for $SiMes_2$ the unfavourable equilibrium renders the rate constant undeterminable in the reactions with oxiranes. Intermediate complexes could be detected in all cases except in the $SiMes_2$-PrS system. Diphenylsilanethione ($Ph_2Si=S$, $\lambda_{max} = 275$ nm) was detected from the reaction of $SiPh_2$ with PrS and identified on the basis of its spectra and rate constants for reaction with n-$BuNH_2$, Et_2NH, MeOH and t-BuOH. The spectra of $SiMes_2$ in the presence of PrS did not correspond to what is expected for either the $SiMes_2$-PrS complex or $Mes_2Si{=}S$, therefore the S-abstraction reactions by $SiTmp_2$ was investigated. The results for $SiTmp_2$ were found to be analogous to those for $SiPh_2$. The O- and S-abstraction reactions by germylenes are much less efficient than those by silylenes; no evidence for O-abstraction by $GeMe_2$ could be found, while S-abstraction from PrS proceeded in ca. 35% yield. Laser photolysis studies of the behaviour of $GePh_2$ and $GeMe_2$ in the presence of CHO, PrO and PrS will also be presented.

1.7. References

1. Becerra, R.; Walsh, R., *Phys. Chem. Chem. Phys.* **2007,** *9*, 2817.

2. Neumann, W. P., *Chem. Rev.* **1991,** *91*, 311.

3. Gaspar, P. P.; West, R., In *The Chemistry of Organic Silicon Compounds*, Rappoport, Z.; Apeloig, Y., Eds. John Wiley & Sons: 1998; Vol. 2, pp 2463-2558.

4. Hargittai, M.; Schultz, G.; Hargittai, I., *Russ. Chem. Bull. Int. Ed.* **2001,** *50* (11), 1903.

5. Driess, M.; Grützmacher, H., *Angew. Chem. Int. Ed. Engl.* **1996,** *35*, 828.

6. Tokitoh, N.; Okazaki, R., *Coord. Chem. Rev.* **2000,** *210* (1), 251.

7. Hill, N. J.; West, R., *J. Organomet. Chem.* **2004,** *689*, 4165.

8. Jasinski, J. M.; Meyerson, B. S.; Scott, B. A., *Ann. Rev. Phys. Chem.* **1987,** *38,* 109.

9. Yoo, R. B.; Jung, N. I., In *Adv. Organomet. Chem.*, Academic Press: 2004; Vol. 50, pp 145-177.

10. West, R.; Moser, D.; Haaf, M. Silylene Catalysis of Olefin Polymerization. US Patent 6576729 B2, Jun. 10, 2003.

11. Dumitrescu, A.; Gornitzka, H.; Martin-Vaca, B.; Bourissou, D.; Bertrand, G.; Cazaux, J.-B. Use of Stannylenes and Germylenes as Polymerization Catalysts for Heterocycles. US Patent 7084237 B2, Aug. 1, 2006.

12. Layfield, R. A., *Organomet. Chem.* **2005,** *32*, 171.

13. Skell, P. S.; Goldstein, E. J., *J. Am. Chem. Soc.* **1964,** *86* (7), 1442.

14. John, P.; Purnell, J. H., *J. Chem. Soc., Faraday Trans. 1* **1973,** *69*, 1455.

15. Belzner, J.; Ihmels, H.; Pauletto, L., *J. Org. Chem.* **1996,** *61*, 3315.

16. Boudjouk, P.; Samaraweera, U.; Sooriyakumaran, R.; Chrusciel, J.; Anderson, K. R., *Angew. Chem. Int. Ed.* **1988,** *27* (10), 1355.

17. Weidenbruch, M.; Flintjer, B.; Pohl, S.; Saak, W., *Angew. Chem. Int. Ed.* **1989,** *28* (1), 95.

18. Belzner, J.; Ihmels, H.; Kneisel, B. O.; Herbst-Irmer, R., *Chem. Ber.* **1996,** *129* (2), 125.

19. Ando, W.; Hamada, Y.; Sekiguchi, A., *Chem. Commun.* **1983,** (17), 952.

20. Nakao, R.; Oka, K.; Dohmaru, T.; Nagata, Y.; Fukumoto, T., *Chem. Commun.* **1985,** *0* (12), 766.

21. Jiang, P.; Gaspar, P. P., *J. Am. Chem. Soc.* **2001,** *123*, 8622.

22. Sekiguchi, A.; Tanaka, T.; Ichinohe, M.; Akiyama, K.; Tero-Kubota, S., *J. Am. Chem. Soc.* **2003,** *125*, 4962.

23. Sekiguchi, A.; Tanaka, T.; Ichinohe, M.; Akiyama, K.; Gaspar, P. P., *J. Am. Chem. Soc.* **2008,** *130*, 426.

24. Tomioka, H., In *Reactive Intermediate Chemistry*, Moss, R. A.; Platz, M. S.; Maitland, J. J., Eds. John Wiley & Sons: New York, 2004; p 1071.

25. Grev, R. S., In *Adv. Organomet. Chem.*, Stone, F. G. A.; Robert, W., Eds. Academic Press: 1991; Vol. Volume 33, pp 125-170.

26. Walsh, R., *Acc. Chem. Res.* **1981,** *14* (8), 246.

27. Horner, D. A.; Grev, R. S.; Schaefer, H. F., *J. Am. Chem. Soc.* **1992,** *114* (6), 2093.

28. Belzner, J.; Ihmels, H., *Adv. Organomet. Chem.* **1999,** *43*, 1.

29. Boganov, S. E.; Faustov, V. I.; Egorov, M. P.; Nefedov, O. M., *Russ. Chem. Bull. Int. Ed.* **2004,** *53*, 960.

30. Takeda, N.; Suzuki, H.; Tokitoh, N.; Okazaki, R.; Nagase, S., *J. Am. Chem. Soc.* **1997,** *119* (6), 1456.

31. Takeda, N.; Kajiwara, T.; Suzuki, H.; Okazaki, R.; Tokitoh, N., *Chem. Eur. J.* **2003,** *9*, 3530.

32. So, C. W.; Roesky, H. W.; Gurubasavaraj, P. M.; Oswald, R. B.; Gamer, M. T.; Jones, P. G.; Blaurock, S., *J. Am. Chem. Soc.* **2007,** *129*, 12049.

33. So, C.-W.; Roesky, H. W.; Magull, J.; Oswald, R. B., *Angew. Chem. Int. Ed. Engl.* **2006,** *45* (24), 3948.

34. Ghadwal, R. S.; Roesky, H. W.; Merkel, S.; Henn, J.; Stalke, D., *Angew. Chem. Int. Ed. Engl.* **2009,** *48* (31), 5683.

35. Filippou, A. C.; Chernov, O.; Schnakenburg, G., *Angew. Chem. Int. Ed. Engl.* **2009,** *48* (31), 5687.

36. Yao, S.; Xiong, Y.; Brym, M.; Driess, M., *J. Am. Chem. Soc.* **2007,** *129*, 7268.

37. Schoeller, W. W.; Schneider, R., *Chem. Ber.* **1997,** *130* (7), 1013.

38. Gau, D.; Kato, T.; Saffon-Merceron, N.; Cossio, F. P.; Baceiredo, A., *J. Am. Chem. Soc.* **2009,** *131*, 8762.

39. Gau, D.; Rodriguez, R.; Kato, T.; Saffon-Merceron, N.; Cossio, F. P.; Baceiredo, A., *Chem. Eur. J.* **2010,** *16*, 8255.

40. Ando, W.; Sekiguchi, A.; Hagiwara, K.; Sakakibara, A.; Yoshida, H., *Organometallics* **1988,** *7*, 558.

41. Gillette, G. R.; Noren, G. H.; West, R., *Organometallics* **1989,** *8*, 487.

42. Gillette, G. R.; Noren, G. H.; West, R., *Organometallics* **1987,** *6*, 2617.

43. Corriu, R.; Lanneau, G.; Priou, C.; Soulairol, F.; Auner, N.; Probst, R.; Conlin, R.; Tan, C., *J. Organomet. Chem.* **1994,** *466* (1–2), 55.

44. Levin, G.; Das, P. K.; Bilgrien, C.; Lee, C. L., *Organometallics* **1989,** *8*, 1206.

45. Moiseev, A. G.; Leigh, W. J., *Organometallics* **2007,** *26*, 6277.

46. Yamaji, M.; Hamanishi, K.; Takahashi, T.; Shizuka, H., *J. Photochem. Photobiol. A: Chem.* **1994,** *81*, 1.

47. Bhattacharya, A., M.Sc. Thesis, McMaster University, Hamilton, ON, 2010.

48. Levin, G.; Das, P. K.; Lee, C. L., *Organometallics* **1988,** *7*, 1231.

49. Raghavachari, K.; Chandrasekhar, J.; Gordon, M. S.; Dykema, K., *J. Am. Chem. Soc.* **1984,** *106* (20), 5853.

50. Liao, H.-Y.; Yen, M.-Y., *New J. Chem.* **2008,** *32* (3), 511.

51. Olah, J.; De Proft, F.; Veszpremi, T.; Geerlings, P., *J. Phys. Chem. A* **2005,** *109*, 1608.

52. Oláh, J.; Veszprémi, T.; De Proft, F.; Geerlings, P., *J. Phys. Chem. A* **2007,** *111* (42), 10815.

53. Calhorda, M. J.; Krapp, A.; Frenking, G., *J. Phys. Chem. A* **2007,** *111* (15), 2859.

54. Conlin, R. T.; Laakso, D.; Marshall, P., *Organometallics* **1994,** *13*, 838.

55. Gaspar, P. P., In *Reactive Intermediates,* Jones, M. J.; Moss, R. A., Eds. Wiley: New York, 1985; Vol. 3, pp 333-427.

56. Tokitoh, N.; Ando, W., In *Reactive Intermediate Chemistry*, Moss, R. A.; Platz, M. S.; Jones, M. J., Eds. John Wiley & Sons, Inc: 2004; pp 651-715.

57. Steele, K. P.; Tzeng, D.; Weber, W. P., *J. Organomet. Chem.* **1982,** *231*, 291.

58. Steele, K. P.; Weber, W. P., *J. Am. Chem. Soc.* **1980,** *102* (19), 6095.

59. Gu, T.-Y. Y.; Weber, W. P., *J. Organomet. Chem.* **1980,** *184* (1), 7.

60. Steele, K. P.; Weber, W. P., *Inorg. Chem.* **1981,** *20* (4), 1302.

61. Su, S.; Gordon, M. S., *Chem. Phys. Lett.* **1993,** *204* (3-4), 306.

62. Lee, S. Y.; Boo, B. H., *J. Mol. Struct.: THEOCHEM* **1996,** *366* (1-2), 79.

63. Heaven, M. W.; Metha, G. F.; Buntine, M. A., *J. Phys. Chem. A* **2001,** *105*, 1185.

64. Becerra, R.; Cannady, J. P.; Walsh, R., *J. Phys. Chem. A* **2011,** *115* (17), 4231.

65. Becerra, R.; Cannady, J. P.; Walsh, R., *J. Phys. Chem. A* **2003,** *107* (50), 11049.

66. Becerra, R.; Goldberg, N.; Cannady, J. P.; Almond, M. J.; Ogden, J. S.; Walsh, R., *J. Am. Chem. Soc.* **2004,** *126* (21), 6816.

67. Schäfer, A.; Weidenbruch, M.; Peters, K.; von Schnering, H.-G., *Angew. Chem. Int. Ed.* **1984,** *23* (4), 302.

68. Moiseev, A. G.; Coulais, E.; Leigh, W. J., *Chem. Eur. J.* **2009,** *15* (34), 8485.

69. Kira, M.; Miyazawa, T.; Koshihara, S. Y.; Segawa, Y.; Sakurai, H., *Chem. Lett.* **1995**, 3.

70. Miyazawa, T.; Koshihara, S. Y.; Liu, C.; Sakurai, H.; Kira, M., *J. Am. Chem. Soc.* **1999,** *121*, 3651.

71. Moiseev, A. G.; Leigh, W. J., *Organometallics* **2007,** *26*, 6268.

72. Moiseev, A. G.; Leigh, W. J., *J. Am. Chem. Soc.* **2006,** *128*, 14442.

73. Sanji, T.; Fujiyama, H.; Yoshida, K.; Sakurai, H., *J. Am. Chem. Soc.* **2003,** *125*, 3216.

74. Shizuka, H.; Tanaka, H.; Tonokura, K.; Murata, K.; Hiratsuka, H.; Ohshita, J.; Ishikawa, M., *Chem. Phys. Lett.* **1988,** *143*, 225.

75. Leigh, W. J.; Moiseev, A. G.; Coulais, E.; Lollmahomed, F.; Askari, M. S., *Can. J. Chem.* **2008,** *86* (12), 1105.

76. Bharatam, P. V.; Moudgil, R.; Kaur, D., *Organometallics* **2002,** *21* (18), 3683.

77. Becerra, R.; Cannady, J. P.; Walsh, R., *Silicon Chem.* **2005,** *3*, 131.

78. Ishikawa, M.; Kumada, M., In *Adv. Organomet. Chem.*, Stone, F. G. A.; Robert, W., Eds. Academic Press: 1981; Vol. Volume 19, pp 51-95.

79. Ishikawa, M.; Kumada, M., *J. Organomet. Chem.* **1972,** *42*, 325.

80. Okinoshima, H.; Weber, W. P., *J. Organomet. Chem.* **1978,** *155*, 165.

81. Seyferth, D.; Annarelli, D. C.; Duncan, D. P., *Organometallics* **1982,** *1*, 1288.

82. Soysa, H. S. D.; Okinoshima, H.; Weber, W. P., *J. Organomet. Chem.* **1977,** *133*, C17.

83. Atwell, W. H.; Mahone, L. G.; Hayes, S. F.; Uhlmann, J. G., *J. Organomet. Chem.* **1969,** *18* (1), 69.

84. Gu, T. Y.; Weber, W. P., *J. Organomet. Chem.* **1980,** *195* (1), 29.

85. Okinoshima, H.; Weber, W. P., *J. Organomet. Chem.* **1978,** *150* (2), C25.

86. Soysa, H. S. D.; Jung, I. N.; Weber, W. P., *J. Organomet. Chem.* **1979,** *171*, 177.

87. Chihi, A.; Weber, W. P., *J. Organomet. Chem.* **1981,** *210*, 163.

88. Welsh, K. M.; Michl, J.; West, R., *J. Am. Chem. Soc.* **1988,** *110* (20), 6689.

89. Conlin, R. T.; Netto-Ferreira, J. C.; Zhang, S.; Scaiano, J. C., *Organometallics* **1990,** *9*, 1332.

90. Tzeng, D.; Weber, W. P., *J. Am. Chem. Soc.* **1980,** *102*, 1451.

91. Barton, T. J., *Pure Appl. Chem.* **1980,** *52*, 615.

92. Goure, W. F.; Barton, T. J., *J. Organomet. Chem.* **1980,** *199*, 33.

93. Ando, W.; Ikeno, M.; Hamada, Y., *Chem. Commun.* **1981**, 621.

94. Baggott, J. E.; Blitz, M. A.; Frey, H. M.; Lightfoot, P. D.; Walsh, R., *Int. J. Chem. Kinet.* **1992,** *24*, 127.

95. Su, M.-D., *J. Am. Chem. Soc.* **2002,** *124* (41), 12335.

96. Su, M.-D., *J. Phys. Chem. A.* **2002,** *106* (41), 9563.

97. Apeloig, Y.; Sklenak, S., *Can. J. Chem.* **2000,** *78*, 1496.

98. Turner, J. L.; Dalgarno, A., *Astrophys. J.* **1977,** *213*, 386.

99. Chabal, Y. T.; Raghavachari, K.; Zhang, X.; Garfunkel, E., *Phys. Rev. B.* **2002,** *66*, 161315.

100. Voronkov, M. G.; Basenko, S. V., *Journal of Organometallic Chemistry* **1995,** *500* (1-2), 325.

101. Fukutani, S.; Uodome, Y.; Kunioshi, N.; Jinno, H., *Bull. Chem. Soc. Jpn.* **1991,** *64*, 2328.

102. Arrington, C. A.; West, R.; Michl, J., *J. Am. Chem. Soc.* **1983,** *105*, 6176.

103. Khabashesku, V. N.; Kudin, K. N.; Margrave, J. L.; Fredin, L., *J. Organomet. Chem.* **2000,** *595*, 248.

104. Khabashesku, V. N.; Kerzina, Z. A.; Kudin, K. N.; Nefedov, O. M., *J. Organomet. Chem.* **1998,** *566* (1-2), 45.

105. Withnall, R.; Andrews, L., *J. Am. Chem. Soc.* **1986,** *108* (25), 8118.

106. Patyk, A.; Sander, W.; Gauss, J.; Cremer, D., *Angew. Chem. Int. Ed. Engl.* **1989,** *28* (7), 898.

107. Bailleux, S.; Bogey, M.; Demuynck, C.; Destombes, J.-L.; Walters, A., *J. Chem. Phys.* **1994,** *101*, 2729.

108. Bogey, M.; Delcroix, B.; Walters, A.; Guillemin, J.-C., *J. Mol. Spectrosc.* **1996,** *175*, 421.

109. Gole, J. L.; Dixon, D. A., *J. Phys. Chem. B.* **1997,** *101*, 8098.

110. Wolkin, M. V.; Jorne, J.; Fauchet, P. M., *Phys. Rev. Lett.* **1999,** *82* (1), 197.

111. Srinivas, R.; Böhme, D. K.; Sülzle, D.; Schwarz, H., *J. Phys. Chem.* **1991,** *95*, 9836.

112. Apeloig, Y., In *The chemistry of organic silicon compounds*, Patai, S.; Rappoport, Z., Eds. Wiley: Chichester, U. K., 1989.

113. Kudo, T.; Nagase, S., *Organometallics* **1986,** *5*, 1207.

114. Suzuki, H.; Tokitoh, N.; Okazaki, R.; Nagase, S.; Goto, M., *J. Am. Chem. Soc.* **1998,** *120*, 11096.

115. Iwamoto, T.; Sato, K.; Ishida, S.; Kabuto, C.; Kira, M., *J. Am. Chem. Soc.* **2006,** *128*, 16914.

116. Arya, P.; Boyer, J.; Carre, F.; Corriu, R.; Lanneau, G.; Lapasset, J.; Perrot, M.; Priou, C., *Angew. Chem. Int. Ed. Engl.* **1989,** *28* (8), 1016.

117. Haaf, M.; Schmiedl, A.; Schmedake, T. A.; Powell, D. R.; Millevolte, A. J.; Denk, M.; West, R., *J. Am. Chem. Soc.* **1998,** *120*, 12714.

118. Köppe, R.; Schnöckel, H., *Z. Anorg. Allg. Chem.* **1992,** *607*, 41.

119. Borisova, I.; Zemlyanskii, N.; Shestakova, A.; Khrustalev, V.; Ustynyuk, Y.; Chernyshev, e., *Russ. Chem. Bull.* **2000,** *49* (9), 1583.

120. Barton, T. J.; Chong Bok, K., Dissertation, Iowa State University, Ames, Iowa, 1990.

121. Lambert, R. L.; Seyferth, D., *J. Am. Chem. Soc.* **1972,** *94,* 9246.

122. Seyferth, D.; Annarelli, D. C., *J. Am. Chem. Soc.* **1975,** *97* (3), 2273.

123. Seyferth, D., *J. Organomet. Chem.* **1975,** *100* (1), 237.

124. Seyferth, D.; Annarelli, D. C., *J. Am. Chem. Soc.* **1975,** *9* (24), 7162.

125. Boudjouk, P.; Black, E.; Kumarathasan, R., *Organometallics* **1991,** *10* (7), 2095.

126. Driver, T. G.; Woerpel, K. A., *J. Am. Chem. Soc.* **2003,** *125* (35), 10659.

127. Palmer, W. S.; Woerpel, K. A., *Organometallics* **1997,** *16* (6), 1097.

128. Palmer, W. S.; Woerpel, K. A., *Organometallics* **1997,** *16*, 4824.

129. Franz, A. K.; Woerpel, K. A., *J. Am. Chem. Soc.* **1999,** *121* (5), 949.

130. Palmer, W. S.; Woerpel, K. A., *Organometallics* **2001,** *20,* 3691.

131. Ćiraković, J.; Driver, T. G.; Woerpel, K. A., *J. Am. Chem. Soc.* **2002,** *124* (32), 9370.

132. Driver, T. G.; Franz, A. K.; Woerpel, K. A., *J. Am. Chem. Soc.* **2002,** *124* (23), 6524.

133. Cirakovic, J.; Driver, T. G.; Woerpel, K. A., *J. Org. Chem.* **2004,** *69* (12), 4007.

134. Driver, T. G.; Woerpel, K. A., *J. Am. Chem. Soc.* **2004,** *126*, 9993.

135. Calad, S. A.; Woerpel, K. A., *J. Am. Chem. Soc.* **2005,** *127,* 2046.

136. Calad, S. A.; Woerpel, K. A., *J. Am. Chem. Soc.* **2005,** *127* (7), 2046.

137. Clark, T. B.; Woerpel, K. A., *Organometallics* **2005,** *24* (25), 6212.

138. Cleary, P. A.; Woerpel, K. A., *Org. Lett.* **2005,** *7* (24), 5531.

139. Bourque, L. E.; Cleary, P. A.; Woerpel, K. A., *J. Am. Chem. Soc.* **2007,** *129* (42), 12602.

140. Calad, S. A.; Woerpel, K. A., *Org. Lett.* **2007,** *9* (6), 1037.

141. Howard, B. E.; Woerpel, K. A., *Org. Lett.* **2007,** *9* (22), 4651.

142. Nevárez, Z.; Woerpel, K. A., *Org. Lett.* **2007,** *9* (19), 3773.

143. Bourque, L. E.; Haile, P. A.; Loy, J. M. N.; Woerpel, K. A., *Tetrahedron* **2009,** *65*, 5608.

144. Bourque, L. E.; Haile, P. A.; Woerpel, K. A., *J. Org. Chem.* **2009,** *74*, 7180.

145. Howard, B. E.; Woerpel, K. A., *Tetrahedron* **2009,** *65*, 6447.

146. Prevost, M.; Woerpel, K. A., *J. Am. Chem. Soc.* **2009,** *131*, 14182.

147. Ager, B. J.; Bourque, L. E.; Buchner, K. M.; Woerpel, K. A., *J. Org. Chem.* **2010,** *75* (16), 5729.

148. Ventocilla, C. C.; Woerpel, K. A., *J. Am. Chem. Soc.* **2011,** *133* (3), 406.

149. Greene, M. A.; Prévost, M.; Tolopilo, J.; Woerpel, K. A., *J. Am. Chem. Soc.* **2012,** *134* (30), 12482.

150. Ventocilla, C. C.; Woerpel, K. A., *J. Org. Chem.* **2012,** *77*, 3277.

151. Sato, K.; Kako, M.; Suzuki, M.; Mizorogi, N.; Tsuchiya, T.; Olmstead, M. M.; Balch, A. L.; Akasaka, T.; Nagase, S., *J. Am. Chem. Soc.* **2012,** *134*, 16033.

152. Pae, D. H.; Xiao, M.; Chiang, M. Y.; Gaspar, P. P., *J. Am. Chem. Soc.* **1991,** *113* (4), 1281.

153. Belzner, J.; Dehnert, U.; Ihmels, H.; Hübner, M.; Müller, R.; Usón, I., *Chem. Eur. J.* **1998,** *4* (5), 852.

154. Gaspar, P. P., In *Reactive Intermediates*, Jones, M. J.; Moss, R. A., Eds. Wiley: New York, 1978; Vol. 1, pp 229-277.

155. Gaspar, P. P., In *Reactive Intermediates*, Jones, M. J.; Moss, R. A., Eds. Wiley: New York, 1981; Vol. 2, pp 335-385.

156. Lee, V. Y.; Sekiguchi, A., In *Organometallic Compounds of Low-Coordinate Si, Ge, Sn and Pb*, John Wiley & Sons, Ltd: Chichester, 2010; pp 139-197.

157. Tortorelli, V. J.; Jones, M.; S., W.; Li, Z., *Organometallics* **1983,** *2* (6), 759.

158. Ishikawa, M.; Ishiguro, M.; Kumada, M., *J. Organomet. Chem.* **1973,** *49* (2), C71.

159. Ishikawa, M.; Kumada, M., *J. Organomet. Chem.* **1974,** *81*, C3.

160. Ishikawa, M.; Ohi, F.; Kumada, M., *Tetrahedron Lett.* **1975,** *16* (9), 645.

161. Jiang, P.; Trieber, D. I.; Gaspar, P. P., *Organometallics* **2003,** *22*, 2233.

162. Ishida, S.; Iwamoto, T.; Kira, M., *Heteroat. Chem.* **2011,** *22* (3/4), 432.

163. Lips, F.; Fettinger, J. C.; Mansikkamaki, A.; Tuononen, H. M.; Power, P. P., *J. Am. Chem. Soc.* **2013,** (Copyright (C) 2013 American Chemical Society (ACS). All Rights Reserved.), Ahead of Print.

164. Ando, W.; Fujita, M.; Yoshida, H.; Sekiguchi, A., *J. Am. Chem. Soc.* **1988,** *110*, 3310.

165. Saso, H.; Ando, W.; Ueno, K., *Tetrahedron* **1989,** *45* (7), 1929.

166. Tortorelli, V. J.; Jones, M., Jr., *J. Am. Chem. Soc.* **1980,** *102*, 1425.

167. Ishikawa, M.; Fuchikami, T.; Kumada, M., *J. Organomet. Chem.* **1978,** *162*, 223.

168. Zhang, S.; Wagenseller, P. E.; Conlin, R. T., *J. Am. Chem. Soc.* **1991,** *113*, 4278.

169. Ishikawa, M.; Nakagawa, K. I.; Kumada, M., *J. Organomet. Chem.* **1979,** *178*, 105.

170. Tsutsui, S.; Tanaka, H.; Kwon, E.; Matsumoto, S.; Sakamoto, K., *Organometallics* **2004,** *23* (24), 5659.

171. Suzuki, K.; Matsuo, T.; Hashizume, D.; Tamao, K., *J. Am. Chem. Soc.* **2011,** *133* (49), 19710.

172. Rupar, P. A.; Staroverov, V. N.; Baines, K. M., *Organometallics* **2010,** *29*, 4871.

173. Yao, S. L.; Xiong, Y.; Driess, M., *Chem. Commun.* **2009,** (42), 6466.

174. Arduengo, A. J.; Dias, H. V. R.; Calabrese, J. C.; Davidson, F., *Inorg. Chem.* **1993,** *32* (9), 1541.

175. Rupar, P. A.; Jennings, M. C.; Ragogna, P. J.; Baines, K. M., *Organometallics* **2007,** *26*, 4109.

176. Rupar, P. A.; Jennings, M. C.; Baines, K. M., *Organometallics* **2008,** *27* (19), 5043.

177. Ruddy, A. J.; Rupar, P. A.; Bladek, K. J.; Allan, C. J.; Avery, J. C.; Baines, K. M., *Organometallics* **2010,** *29* (6), 1362.

178. Sidiropoulos, A.; Jones, C.; Stasch, A.; Klein, S.; Frenking, G., *Angew. Chem. Int. Ed.* **2009,** *48* (51), 9701.

179. Al-Rafia, S. M. I.; Malcolm, A. C.; Liew, S. K.; Ferguson, M. J.; Rivard, E., *J. Am. Chem. Soc.* **2011,** *133*, 777.

180. Ando, W.; Itoh, H.; Tsumuraya, T., *Organometallics* **1989,** *8* (12), 2759.

181. Ando, W.; Itoh, H.; Tsumuraya, T.; Yoshida, H., *Organometallics* **1988,** *7*, 1880.

182. Broeckaert, L.; Geerlings, P.; Ruzicka, A.; Willem, R.; De Proft, F., *Organometallics* **2012,** *31* (5), 1605.

183. Leigh, W. J.; Lollmahomed, F.; Harrington, C. R., *Organometallics* **2006,** *25*, 2055.

184. Leigh, W. J.; Dumbrava, I. G.; Lollmahomed, F., *Can. J. Chem.* **2006,** *84*, 934.

185. Leigh, W. J.; Harrington, C. R.; Vargas-Baca, I., *J. Am. Chem. Soc.* **2004,** *126*, 16105.

186. Leigh, W. J.; Harrington, C. R., *J. Am. Chem. Soc.* **2005,** *127*, 5084.

187. Leigh, W. J.; Lollmahomed, F.; Harrington, C. R.; McDonald, J. M., *Organometallics* **2006,** *25*, 5424.

188. Curtiss, L. A.; Redfern, P. C.; Raghavachari, K., *J. Chem. Phys.* **2007,** *126*, 084108.

189. Lappert, M. F.; Miles, S. J.; Atwood, J. L.; Zaworotko, M. J.; Carty, A. J., *J. Organomet. Chem.* **1981,** *212*, C4.

190. Barrau, J.; Bouchaut, M.; Lavayssiere, H.; Dousse, G.; Satge, J., *J. Organomet. Chem.* **1983,** *243*, 281.

191. Withnall, R.; Andrews, L., *J. Phys. Chem.* **1990,** *94*, 2351.

192. Klein, B.; Neumann, W. P.; Weisbeck, M. P.; Wienken, S., *J. Organomet. Chem.* **1993,** *446*, 149.

193. Neumann, W. P.; Weisbeck, M. P.; Wienken, S., *Main Group Metal Chem.* **1994,** *17*, 151.

194. Heaven, M. W.; Metha, G. F.; Buntine, M. A., *Aust. J. Chem.* **2001,** *54* (3), 185.

195. Su, M.-D.; Chu, S.-Y., *J. Phys. Chem. A* **1999,** *103* (50), 11011.

196. Su, M. D.; Chu, S. Y., *J. Chin. Chem. Soc.* **2000,** *47*, 135.

197. Alexander, U. N.; King, K. D.; Lawrance, W. D., *Phys. Chem. Chem. Phys.* **2003,** *5* (8), 1557.

198. Lollmahomed, F.; Huck, L. A.; Harrington, C. R.; Chitnis, S. S.; Leigh, W. J., *Organometallics* **2009,** *28* (5), 1484.

199. Leigh, W. J.; Harrington, C. R.; Vargas-Baca, I., *J. Am. Chem. Soc.* **2006,** *128* (4), 1394.

200. Toltl, N. P.; Leigh, W. J.; Kollegger, G. M.; Stibbs, W. G.; Baines, K. M., *Organometallics* **1996,** *15* (17), 3732.

201. Huck, L. A.; Leigh, W. J., *Organometallics* **2007,** *26*, 1339.

202. Riviere, P.; Satge, J.; Castel, A., *C. R. Acad. Sci. Ser. C* **1975,** *281*, 835.

203. Castel, A.; Riviere, P.; Satge, J.; Cazes, A., *C. R. Acad. Sci. Paris Ser. C* **1978,** *287* (Serie C), 205.

204. Barrau, J.; Bouchaut, M.; Lavayssiere, H.; Dousse, G.; Satge, J., *Helv. Chim. Acta* **1979,** *62* (1), 152.

205. Barrau, J.; Rima, G.; Lavayssiere, H.; Dousse, G.; Satge, J., *J. Organomet. Chem.* **1983,** *246*, 227.

206. Collins, S.; Murakami, S.; Snow, J. T.; Masamune, S., *Tetrahedron Lett.* **1985,** *26* (10), 1281.

207. Kostina, S. S.; Singh, T.; Leigh, W. J., *Organometallics* **2012,** *31* (9), 3755.

208. Ando, W.; Ohgaki, H.; Kabe, Y., *Angew. Chem. Int. Ed. Engl.* **1994,** *33*, 659.

209. Kabe, Y.; Ohgaki, H.; Yamagaki, T.; Nakanishi, H.; Ando, W., *J. Organomet. Chem.* **2001,** *636*, 82.

210. Meiners, F.; Saak, W.; Weidenbruch, M., *Z. Anorg. Allg. Chem.* **2002,** *628*, 2821.

211. Sasamori, T.; Tokitoh, N., *Organometallics* **2006,** *25* (15), 3522.

212. Becerra, R.; Boganov, S. E.; Egorov, M. P.; Nefedov, O. M.; Walsh, R., *Chem. Phys. Lett.* **1996,** *260*, 433.

213. Becerra, R.; Walsh, R., *J. Organomet. Chem.* **2001,** *636*, 49.

214. Becerra, R.; Boganov, S. E.; Egorov, M. P.; Faustov, V. I.; Promyslov, V. M.; Nefedov, O. M.; Walsh, R., *Phys. Chem. Chem. Phys.* **2002,** *4*, 5079.

215. Becerra, R.; Walsh, R., *Phys. Chem. Chem. Phys.* **2002,** *4*, 6001.

216. Alexander, U. N.; King, K. D.; Lawrance, W. D., *Chem. Phys. Lett.* **2000,** *319*, 529.

217. Sakai, S., *Int. J. Quantum Chem.* **1998,** *70*, 291.

218. Su, M. D.; Chu, S. Y., *J. Am. Chem. Soc.* **1999,** *121*, 11478.

219. Birukov, A. A.; Faustov, V. I.; Egorov, M. P.; Nefedov, O. M., *Russ. Chem. Bull. Int. Ed.* **2005,** *54*, 2003.

220. Koecher, J.; Neumann, W. P., *Organometallics* **1985,** *4* (2), 400.

221. Shusterman, A. J.; Landrum, B. E.; Miller, R. L., *Organometallics* **1989,** *8*, 1851.

222. Saeidi Hayeniaz, Y., M.Sc. Thesis, McMaster University, Hamilton, 2012.

223. Neumann, W. P.; Sakurai, H.; Billeb, G.; Brauer, H.; Kocher, J.; Viebahn, S., *Angew. Chem. Int. Ed. Engl.* **1989,** *28* (8), 1028.

224. Huck, L. A.; Leigh, W. J., *Organometallics* **2009,** *28*, 6777.

225. Drago, R. S.; Dadmun, A. P.; Vogel, G. C., *Inorg. Chem.* **1993,** *32* (11), 2473.

226. Vogel, G. C.; Drago, R. S., *J. Chem. Ed.* **1996,** *73*, 701.

2. Chapter 2 – Synthesis and Photochemistry of Silylene and Germylene Precursors

2.1. Overview

The photochemical precursors of $SiMe_2$ (**43**), $SiPh_2$ (**44a**), $GeMe_2$ (**36**) and $GePh_2$ (**37**) have been prepared following published procedures and a brief outline of each synthesis is given in this chapter. Laser flash photolysis experiments with each of these compounds are introduced, in addition to those with the precursors of $SiMes_2$ (**45**) and $GeMes_2$ (**46**) which were already available in our group. The methods used to determine rate and equilibrium constants for simple Lewis acid-base reactions of these species are introduced.

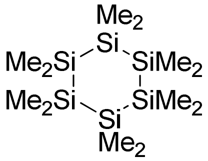

43

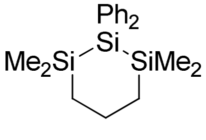

44a

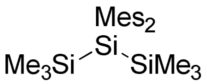

45

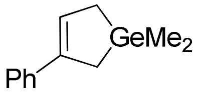

36

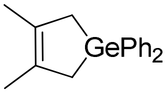

37

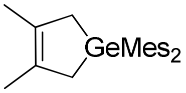

46

2.2. Synthesis of Silylene Precursors

The precursor of dimethylsilylene, dodecamethylcyclohexasilane (**43**) was prepared via published procedures involving the initial synthesis of 1,1,1-trimethyl-2,2,2-triphenyldisilane (**49**) (Scheme 2.1),[1] followed by the reaction of dichlorodimethylsilane (**50**) with lithium metal in the presence of **49** (eq. 2.1).[2] Compound **49** (87% purity by ^{1}H NMR) was isolated in 30% yield after recrystallization from ethanol. Compound **43** (23.53 g) was synthesized in 81% crude yield and purified by consecutive recrystallizations from ethanol:THF (7:1) to afford colourless plates. Recrystallizations were repeated until the purity determined by GC/MS was > 98% and a single methyl peak was evident by ^{1}H NMR; this generally required 4-7 recrystallizations. Pure **43** was characterized by ^{1}H NMR spectroscopy and GC/MS.

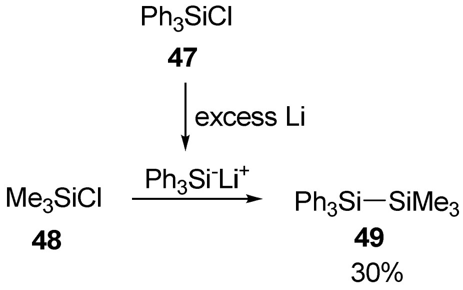

Scheme 2.1

$$\underset{\textbf{50}}{6\ Me_2SiCl_2} + 12\ Li \xrightarrow[\text{THF / 0 }^{o}\text{C}]{\textbf{49}} \underset{\substack{\textbf{43}\\ \text{81\% crude}\\ \text{48\% pure}}}{(SiMe_2)_6} + 12\ LiCl \qquad (2.1)$$

The synthesis of the photochemical precursor of $SiPh_2$, compound **44a** (m.p. = 50.4-50.8 ^{o}C),[3] begins with the synthesis of 1,3-bis(chlorodimethylsilyl)propane (**54**, eq. 2.2)[4] which is subsequently reacted with dichlorodiphenylsilane (**55**) and lithium to yield the target compound **44a** in yields ranging from 8 to 34% over several trials (eq. 2.3).[3] Purification of **44a** was carried out by silica gel chromatography with hexanes as eluent, followed by a slow recrystallization from MeOH. A purity of >98% was estimated by ^{1}H NMR and GC/MS analysis.

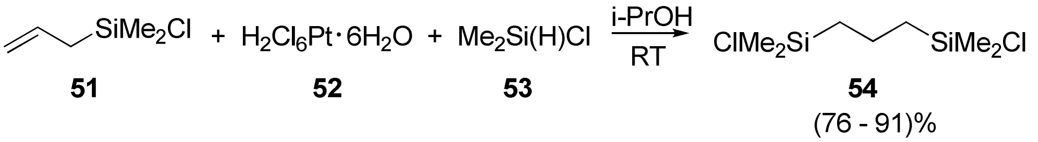

(2.2)

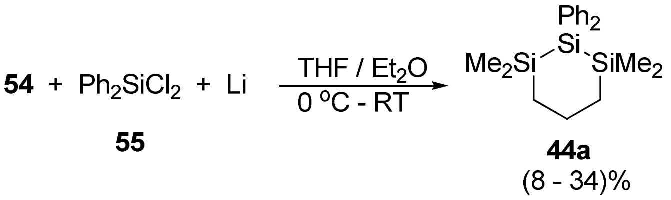

(2.3)

2.3. Photochemistry of silylene precursors

One of the best known methods for the generation of transient silylenes is by photolysis of oligo- and polysilanes.[5] The precursor usually contains at least three consecutive silane units, with one of the silicon atoms being extruded upon photolysis as the major decomposition pathway. Dodecamethylcyclohexasilane (**43**) is the most commonly used photochemical source of dimethylsilylene ($SiMe_2$). [6-17] The co-product of photolysis, (**56**), undergoes further photolysis to generate **57** and $SiMe_2$ (Scheme 2.2). Although **57** does not extrude another molecule of $SiMe_2$, it is reactive towards oxygen and is generally isolated as the corresponding siloxane **58**.[10] Dimethylsilylene generated using this method can be readily detected in frozen matrixes[11, 18] and in solution[6-9, 17] using UV/vis spectroscopy (λ_{max} = 470 nm, Fig. 2.1a), which allows for kinetic and thermodynamic studies of silylene reactions with various scavengers to be performed.

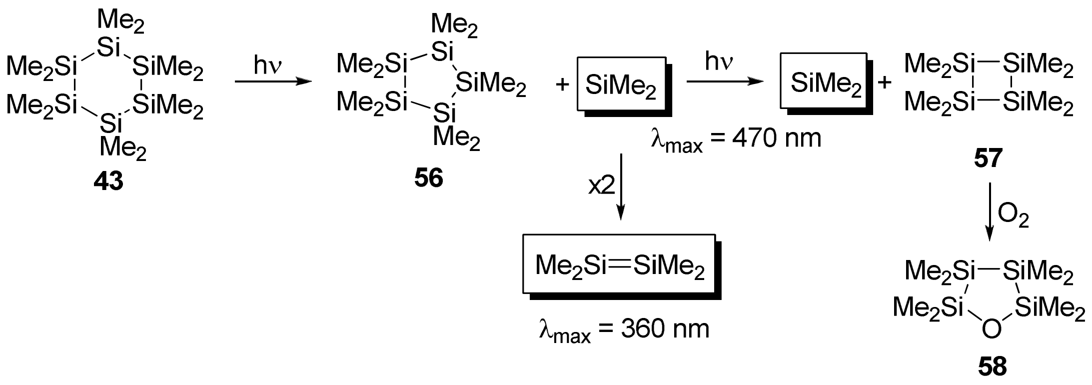

Scheme 2.2

Dimethylsilylene generated by lamp photolysis of **43** in a solution of tetrahydrofuran (THF) and methanol yields **59** (89%) (eq. 2.2).[13] The products of insertion reactions of $SiMe_2$ into O-H single bonds of alcohols were also obtained when the photolysis was carried out in ether solutions containing **43** and *tert*-butanol or ethanol in yields of >85%; the yields were determined based on the generation of two $SiMe_2$ molecules for each molecule of **43**.[13]

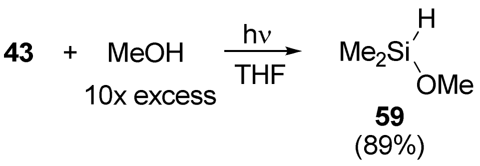

(2.2)

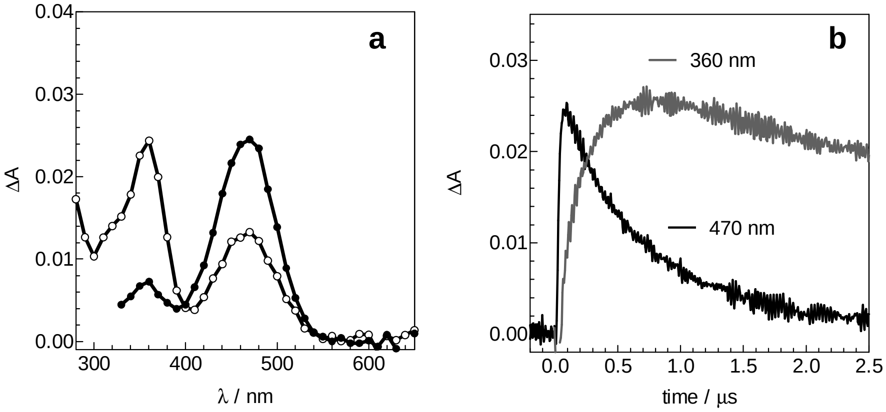

Figure 2.1. (a) Transient absorption spectra from laser flash photolysis of a deoxygenated hexanes solution of **43** at 25^{o}C, recorded 0.06-0.09 μs (●) and 0.48-0.51 μs (o) after the laser pulse. (b) Transient decay profiles recorded at 360 nm and 470 nm.

Although this reaction is clean for the generation of dimethylsilylene, much difficulty has been encountered in the direct detection of photochemically generated phenylated silylenes from oligosilanes. It is now well-known that 2-phenyl trisilanes such as **60** and **61** undergo two competitive photochemical processes – silylene extrusion (path I) and 1,3-silyl migration to yield conjugated silenes (path II) (Scheme 2.3).[19-20] Although extrusion is usually at least two times more efficient than 1,3-migration, silenes of this type were shown to absorb strongly in the 420-500 nm range[21] and thus could obscure the weak silylene absorptions. This has led to misassignment of the silene absorption bands in solution (ca. 440 nm, Fig. 2.2a) to those due to $SiPh_2$ and SiMePh.[22-25] The photorearrangement is suppressed in frozen matrixes, however, allowing the correct identification of $SiPh_2$ (λ_{max} = 495 nm) and SiPhMe (λ_{max} = 490 nm) from photolysis of **60** and **61**, respectively.[26] The problems with the spectral assignment in solution were recognized by comparison of rate constants for lifetime quenching of the 440 nm species by various silylene scavengers with those for the analogous reactions with SiMe$_2$[6-9, 17] and SiMes$_2$,[27] which showed that the reactivity this transient exhibits more closely resembles that of a silene than a silylene.[3, 21, 28-31]

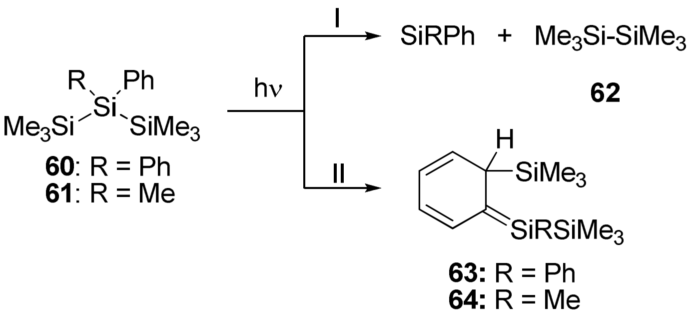

Scheme 2.3

Incorporation of the trisilane unit into a cyclic structure reduces the relative yield of the silene (path II, scheme 2.3) compared to the silylene. It was shown that cyclic trisilane **65a** produces the corresponding silene **66** in ca. 15% chemical yield upon 254 nm photolysis,[3, 32] which can be compared to a ca. 37% yield of the analogous product from photolysis of **60**.[19, 33] Although the silene is formed in significant yield and its spectrum overlaps with that of the silylene (Fig. 2.2b), SiPh$_2$ can still be directly observed in solution by flash photolysis of both **60**[33] and **65a**[32] (λ_{max}(SiPh$_2$) = 515 nm and 290 nm, $\tau \approx$ 1.2 μs). The relative yield of silene is reduced further in the 6-membered cyclic trisilane **44a**, photolysis of which yields the corresponding silene **68** in <5% yield (Scheme 2.4, Fig. 2.2c).[3] Similar results have been achieved with compounds **65b** and **44b**, which yield silylene SiMePh in higher yields relative to the 1,3-silyl migration product compared to that from compound **61**.[34]

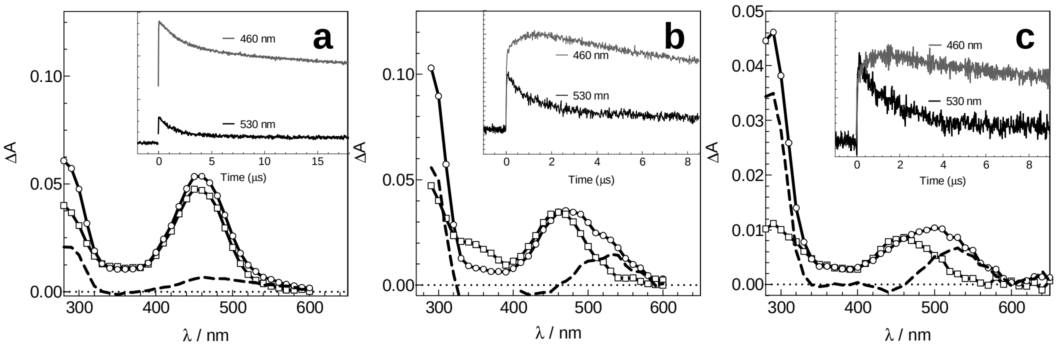

Figure 2.2. (a) Transient absorption spectra recorded 0.48-0.54 μs (o) and 2.08-2.30 μs (□) after the laser pulse, from laser flash photolysis of a hexanes solution of **60**. (b) Transient absorption spectra recorded 0.13-0.19 μs (o) and 4.24-4.32 μs (□) after the laser pulse, from laser flash photolysis of a hexanes solution of **65a**. (c) Transient absorption spectra of a deoxygenated hexanes solution of **44a** at 25°C, recorded 0.19-0.26 μs (o) and 4.24-4.35 μs (□) after the laser pulse. Also shown are the difference spectra (--, o minus □). The insets show transient decay profiles recorded at 460 nm and 530 nm.

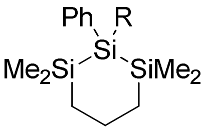

44
a. R = Ph
b. R = Me

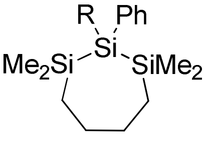

65
a. R = Ph
b. R = Me

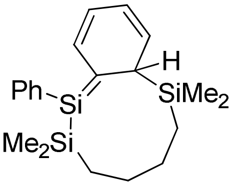

66

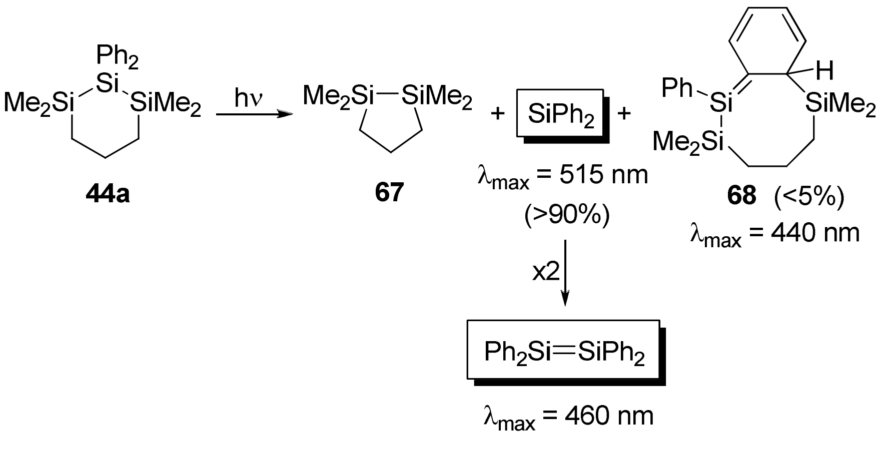

Scheme 2.4

The differences in the relative yields of silene- and silylene from the photolysis of the three trisilanes have been determined from steady-state experiments employing a hydrocarbon solution containing the trisilane (**44a**, **65a**, or **60**) and MeOH or EtOH as the trapping agent for both transient products. Thus, photolysis of **60** in the presence of ethanol (1.0 M) in hexane gave **69** (50%) and **70** (37%) (eq. 2.3), where **52** and **53** are the ethanol adducts of $SiPh_2$ and silene intermediate **46** from the photolysis of **43**, respectively.[19] In comparison, photolysis of **48a** in the presence of MeOH (0.16 M) in C_6D_{12} gave **54** and **55** in 69% and 83% yields, respectively (eq. 2.4). [32] Five minor products were also formed in 14% combined yield, whose NMR and mass spectra are consistent with adducts of MeOH and a silene intermediate (Scheme 2.5). Analogous photolysis of a cyclohexane-d_{12} solution containing **44a** and MeOH (0.21 M) resulted in a substantially higher yield of **54** (93%) accompanied by less than a 5% combined yield of minor products derived from the reaction of MeOH to **51** (eq. 2.5). [3]

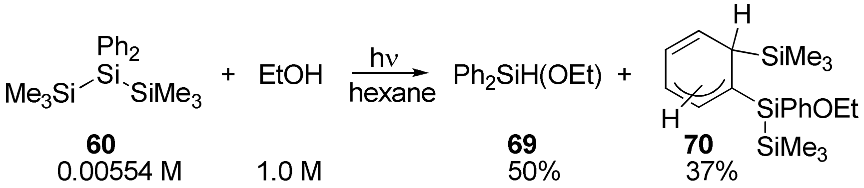

(2.3)

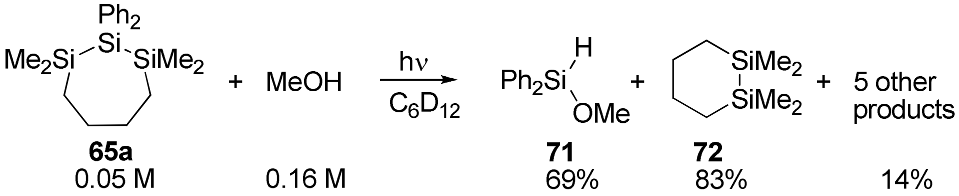

(2.4)

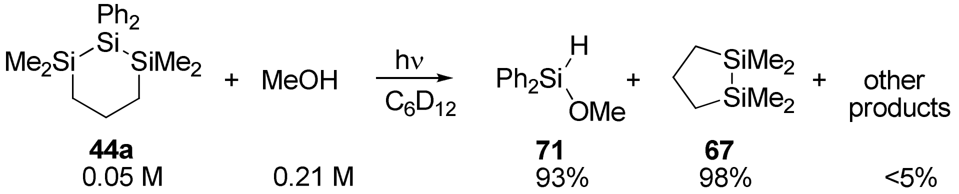

(2.5)

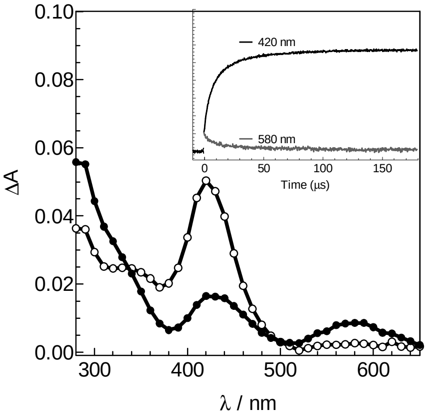

Figure 2.3. Transient absorption spectra from laser photolysis of a deoxygenated hexanes solution of **45** at 25°C, recorded 0.00-1.28 μs (●) and 27.20-28.48 μs (o) after the laser pulse. The inset shows transient decay profiles recorded at 420 nm and 580 nm

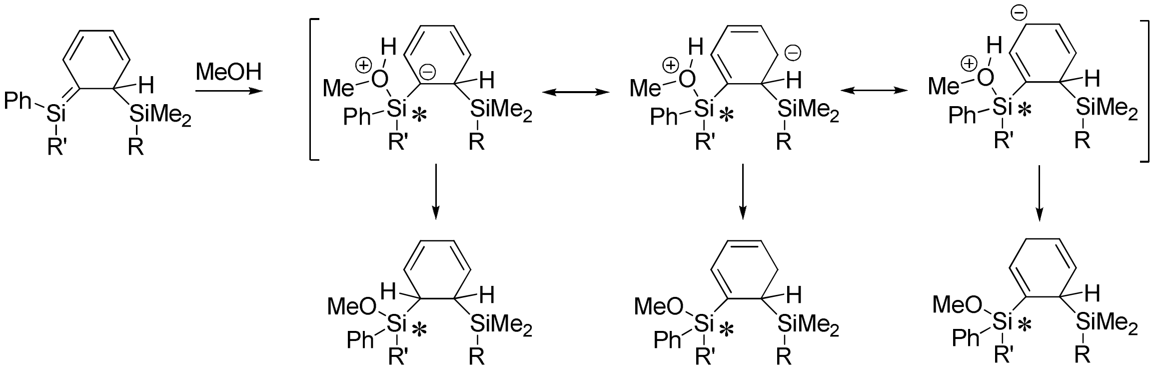

Scheme 2.5

Photochemical 1,3-migration of the $SiMe_3$ group into an ortho position is blocked in ortho substituted aryl trisilanes. Thus, compound **45** generates dimesitylsilylene ($SiMes_2$, λ_{max} = 580 nm, Fig. 2.3c) in high yield upon photolysis. The ultimate fate of $SiMes_2$ is the formation of isolable tetramesityldisilene (Si_2Mes_4) in > 95% yield (Scheme 2.6).[35-36] By time-resolved UV/vis spectroscopy, an additional transient can also be observed from **45** which exhibits an absorption spectrum centered at 440 nm that overlaps with that of tetramesityldisilene (Si_2Mes_4, λ_{max} = 420 nm).[27] This additional transient has not yet been identified.

Table 2.1. UV-vis absorption maxima (λ_{max} / nm) and second order decay rate coefficients ($2k_{dim}/\varepsilon_{max}$ / 10^7 cm^{-1} s^{-1}) of $SiMe_2$, $SiPh_2$ and $SiMes_2$ in hexanes at 25°C, unless stated otherwise.

	λ_{max} / nm	$2k_{dim}$ / ε_{max} (/ 10^7 cm^{-1} s^{-1})
$SiMe_2$	470[7]	1.7 [7, a]
$SiPh_2$	290, 515[3]	-
$SiMes_2$	290,[37] 580[27, 37]	0.9 (580 nm)[27, a]

[a] in cyclohexane

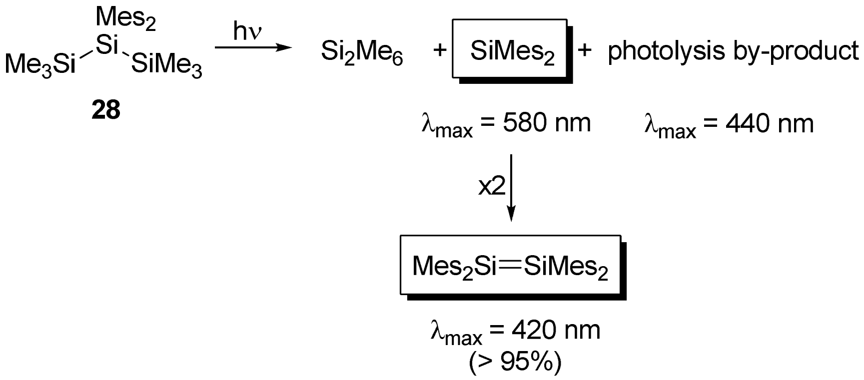

Scheme 2.6

Table 2.1 lists UV-vis absorption maxima, extinction coefficients and dimerization rate constants for $SiMe_2$, $SiPh_2$ and $SiMes_2$.

2.4. Synthesis of Germylene Precursors

The germacyclopentene derivative **36** was prepared via the 5 step route shown in eq. 2.6-2.8.[38-39]

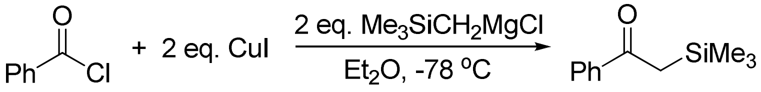 (2.6)

73 **74** (62%)

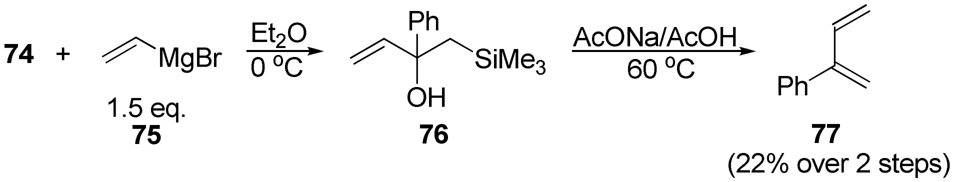

(2.7)

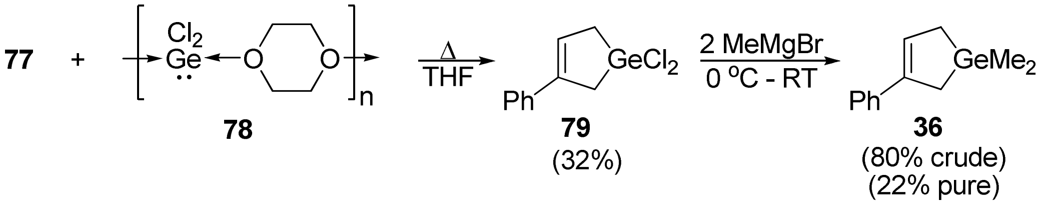

(2.8)

The sequence begins with the synthesis of compound **74**, which involves treatment of **73** with the Grignard reagent in the presence of CuI to give **74** in 62% yield (eq. 2.6).[40] Treatment of **74** with vinyl magnesium bromide generates **76**, which was used directly in the next step to form the target diene **77** in 22% yield from **74** (eq. 2.7).[41] The reaction of $GeCl_2$-dioxane **78** [42] with **77** gave **79** (32%), which was subsequently treated with 2 eq. of MeMgBr to afford **36** in 80% crude yield (eq. 2.8).[38-39] Column chromatography on silica gel using hexanes as eluent afforded **36** (22% yield) in >98% purity as determined by GC/MS.

Compound **37** was synthesized via the two step procedure shown in eq. 2.9. The compound was purified by silica gel chromatography with hexanes as eluent followed by multiple recrystallizations from hexanes to remove any traces of biphenyl.[43-44]

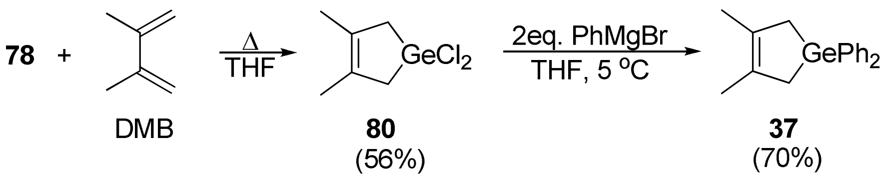

(2.9)

2.5. Photochemistry of Germylene Precursors

Far-UV photolysis of germacyclopentene derivatives has been utilized for the generation and direct detection of the transient germylenes GeH_2[45] and $GeMe_2$[43, 46] in the gas phase and hexane solution. Photolysis of a variety of other germylene precursors in hydrocarbon matrixes or in solution, however, led to inconsistencies in the kinetic and spectroscopic data assigned to $GeMe_2$[47-48] prior to the work by our group in 2004.[38-39, 49-50] For instance, photolysis of $PhMe_2GeSiMe_3$, $Me_2Ge(SePh)_2$, $Me_2Ge(GePhMe_2)_2$ or cyclo-$(GeMe_2)_n$ (n = 5 or 6) in matrixes or in solution yielded transients that were assigned to "$GeMe_2$", however the absorption maximum varies between 420 nm and 506 nm depending on the precursor.[47-48] In contrast, germacyclopentene derivatives generate a transient centered at 470 nm and 480 nm in solution and the gas phase, respectively, which displays kinetic behaviour consistent with a germylene. Germacyclopentene derivative **36** extrudes $GeMe_2$ in high chemical (90-95%) and quantum ($\Phi = 0.55 \pm 0.09$) yields according to eq. 2.10-2.11.[38-39] The phenyl group on the germacyclopentene ring provides the chromophore that is necessary for generation of the germylene by photolysis with 248 nm light; for instance, photolysis of a cyclohexane-d_{12} solution containing **36** and MeOH results in the equimolar formation of **81** and **77** (eq. 2.11).

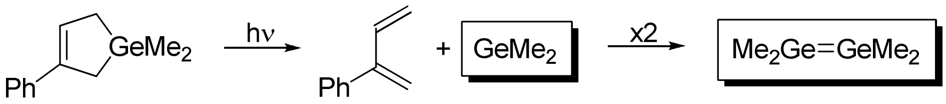

36 **77** λ_{max} = 470 nm λ_{max} = 370 nm

(2.10)

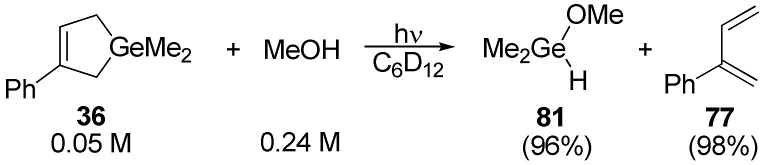

(2.11)

Photolysis of **37** was shown to generate $GePh_2$ cleanly according to eq. 2.12.[44, 50-53] The photochemical extrusion of $GePh_2$ from **37** proceeds with high chemical and quantum yields (Φ = 0.55 ± 0.08), such that when the photolysis was carried out in the presence of MeOH (0.2 M) the O-H insertion product (**82**) was obtained in ca. 86% yield (eq. 2.13).[43, 54] Germacyclopentene derivatives of type **37** have been employed for the formation of not only $GePh_2$, but also a variety of other diarylgermylenes such as $GeMes_2$ (eq. 2.14),[43, 49, 55] such that photolysis of a hydrocarbon solution containing **46** and MeOH results in the quantitative formation of the O-H insertion product.[43]

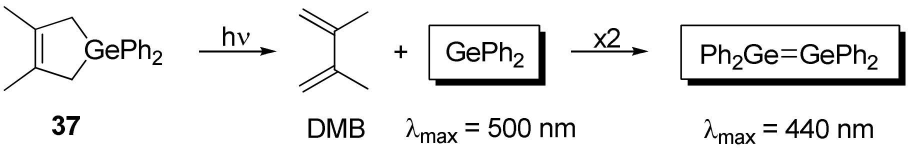

(2.12)

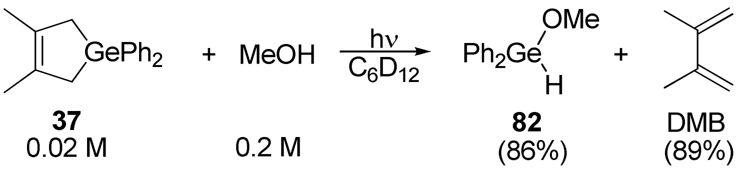

(2.13)

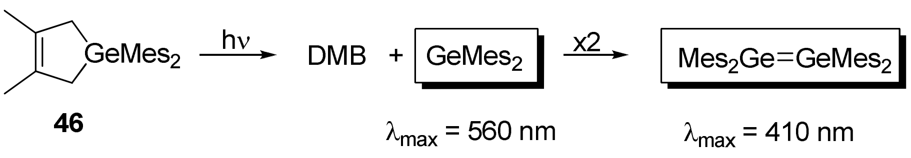

(2.14)

Fig. 2.4 shows transient absorption spectra of hexanes solutions of **36** (a), **37** (b) and **46** (c). The *n,p* electronic transitions of the germylenes ($S^0 \rightarrow S^1$) occur in the spectral range of 470-560 nm (λ_{max} $GeMe_2$ = 470 nm; $GePh_2$ = 500 nm; $GeMes_2$ = 560

Table 2.2. UV-vis absorption maxima (λ_{max} / nm) and second order decay rate coefficients ($2k_{dim}/\varepsilon_{max}$ / 10^7 cm^{-1} s^{-1}) of $GeMe_2$, $GePh_2$ and $GeMes_2$ in hexanes at 25°C.

	λ_{max} / nm	$2k_{dim}$ / ε_{max} (/ 10^7 cm^{-1} s^{-1})
$GeMe_2$	470	10 ± 2[38]
$GePh_2$	300, 500	1.8 ± 0.4[43-44, 54]
$GeMes_2$	325, 560	0.8 ± 0.4 (550 nm)[43]

nm in hexanes) (Table 2.2) and are very similar to those of the Si homologs (see Table 2.1). The primary mode of reaction of each germylene in the absence of scavengers is dimerization to yield the corresponding digermenes (Ge_2R_4, R = Me, Ph or Mes) which in each case absorb at shorter wavelengths than the germylene. The rate constants for dimerization decrease in the order k_{dim} ($GeMe_2$) > k_{dim} ($GePh_2$) > k_{dim} ($GeMes_2$) and are listed in Table 2.2, along with the extinction coefficients of each germylene at the monitoring wavelength.

The long-wavelength band in the absorption spectrum of $GePh_2$ (λ_{max} = 500 nm) overlaps significantly with that due to tetraphenyldigermene (Ge_2Ph_4, λ_{max} = 440 nm). Thus, the transient decay profiles for the germylene need to be isolated by scaled subtraction of the digermene decay profile from absorbance-time profiles recorded at the absorption maximum of the germylene.[43, 56] The resulting corrected $GePh_2$ transient decay profiles are then subjected to kinetic analysis.

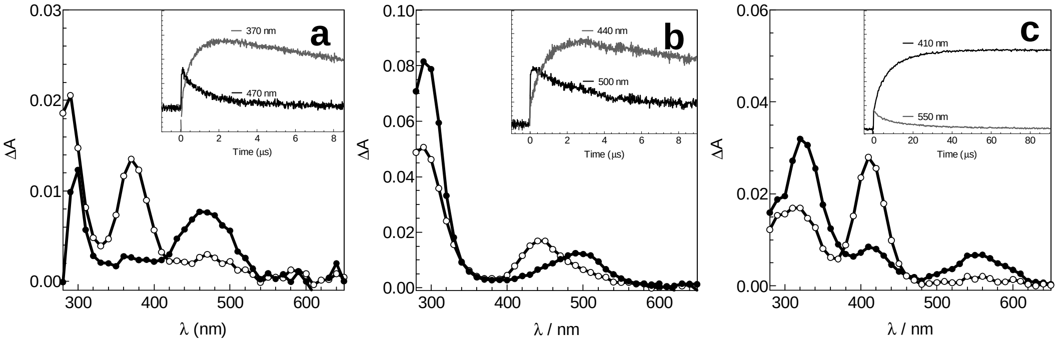

Figure 2.4. (a) Transient absorption spectra of a deoxygenated hexanes solution of **36** at 25°C, recorded 0.08-0.14 μs (●) and 1.55-1.62 μs (o) after the laser pulse. The inset shows transient decay profiles recorded at 370 nm and 470 nm. (b) Transient absorption spectra of a deoxygenated hexanes solution of **37** at 25°C, recorded 0.08-0.16 μs (●) and 3.76-3.84 μs (o) after the laser pulse. The inset shows transient decay profiles recorded at 440 nm and 500 nm. (c) Transient absorption spectra of a deoxygenated hexanes solution of **46** at 25°C, recorded 0.03-0.08 μs (●) and 17.00-18.00 μs (o) after the laser pulse. The inset shows transient decay profiles recorded at 410 nm and 550 nm

2.6. Kinetic and Thermodynamic Measurements

2.6.1. Determination of Rate and Equilibrium Constants for Reversible Reactions

In the absence of added substrates transient silylenes and germylenes decay on the microsecond time scale with the concomitant formation of longer-lived absorptions in the 360−460 nm range due to the corresponding disilenes and digermenes, respectively.[3, 38, 43] Addition of a nucleophilic scavenger (S) to the solution introduces a second reaction pathway producing R_2M-S that slows down dimerization (eq. 2.15).

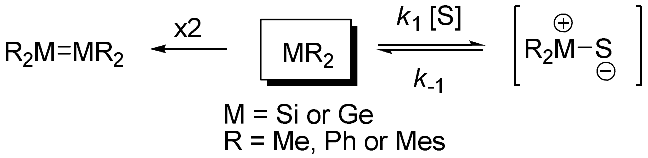

(2.15)

In the situation where R_2M-S is unreactive, the decay of the free tetrellylene proceeds in two stages – a fast pseudo first order approach to equilibrium due to the reaction with the substrate, followed by a slow second order component due to dimerization. The pseudo first order approach to equilibrium is described by eq. 2.16, where k_{decay} is the pseudo first order rate coefficient for the decay of the tetrellylene in the presence of S, k_1 is the forward rate constant for complexation with S, and k_{-1} is the dissociation rate constant for the complex. The complete exclusion of adventitious impurities is often difficult, and so the intercept of the plot of k_{decay} vs [S] gives the sum of the rate constants for the reaction with impurities (k_0) and k_{-1}.

$$k_{decay} = k_{-1} + k_1[S] \qquad (2.16)$$

The equilibrium constant for reaction with the substrate, such as complexation in this case, is defined by eq. 2.17, where k_1 and k_{-1} are the forward and reverse rate constants for complexation of the tetrellylene with the donor.

$$K_1 = \frac{k_1}{k_{-1}} = \frac{[complex]_{eq}}{[MR_2]_{eq}[S]_{eq}} \qquad (2.17)$$

The variation in the ratio of the initial and equilibrium absorbances ($\Delta A_0/\Delta A_{eq}$) with substrate concentration is proportional to the equilibrium constant K_1 according to eq. 2.18.[49]

$$\Delta A_0/\Delta A_{eq} = 1 + K_1 [S] \qquad (2.18)$$

The observed response of the absorbance-time profiles of the tetrellylene to added substrate takes one of three forms depending on the magnitude of the equilibrium constant: small ($K_1 \leq 1{,}000$ M^{-1}), medium (25,000 M^{-1} $\leq K_1 \leq$ 1,000 M^{-1}) and large ($K_1 >$ 25,000 M^{-1}); note that these limits are approximate. When the K_1 value is large, the absorbance of the tetrellylene after equilibrium has been established (ΔA_{eq}) is too small to be detected. In this situation the decay of the tetrellylene follows clean first order kinetics at any substrate concentration. The forward rate constant for reaction with the substrate is obtained by analysis of the data according to eq. 2.16.

For systems where the equilibrium constant falls in the medium regime, both the rate and equilibrium constants can be determined. The free tetrellylene decays consist of two components – a fast one due to the reaction with the substrate, and a slow one due to the dimerization reaction. The forward rate constant for reaction with the substrate is

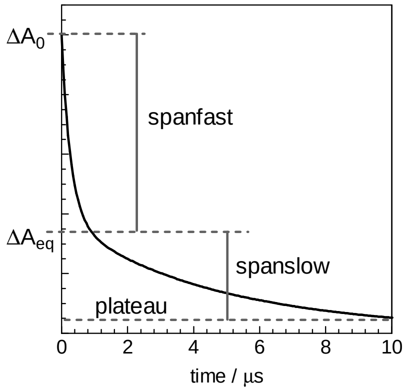

Figure 2.5. The general appearance of a two-phase transient decay profile.

obtained from the rate coefficients associated with the initial fast decay (k_{fast}), which are obtained from analysis of the two-phase decay profiles according to eq. 2.19. The *plateau*, *spanfast* and *spanslow* are labelled on a typical two phase decay profile shown in Fig. 2.5. The *plateau* is generally unrestricted; however, when the value of *plateau* given by the unrestricted analysis is negative, the analysis is repeated with *plateau* set to zero. The k_{fast} values are then plotted against [S] to obtain the value of k_1 according to eq. 2.16, where $k_{\mathrm{decay}} = k_{\mathrm{fast}}$ from the above analysis. The equilibrium constant can be estimated from the variation of the ΔA_{eq} with substrate concentration according to eq. 2.18. The ΔA_{eq} in this situation is estimated visually as the breakpoint between the fast and the slow components of the absorbance-time profile.

$$\Delta A = plateau + spanfast \cdot e^{-k_{fast} \cdot t} + spanslow \cdot e^{-k_{slow} \cdot t} \qquad (2.19)$$

In situations where K_1 falls below 1,000 M^{-1}, the approach to equilibrium cannot be resolved from the laser pulse, and the only thing that can be observed is a reduction in the apparent initial signal intensity due to the free tetrellylene as a function of substrate concentration. Generally, it would also be expected to see a gradual increase in the apparent lifetime with increasing [S] as the equilibrium concentration of free tetrellylene decreases. However, this is rarely encountered because the small increase in the lifetime is counterbalanced by the reduction in the lifetime caused by the reaction with adventitious impurities present in the solvent and/or the substrate. Typically, therefore, no apparent change in the decay characteristics of the absorbance-time profiles is observed. In these cases the rate constants for complexation cannot be determined, while the equilibrium constants can be obtained from analysis of the “initial” signal intensities according to eq. 2.18, where ΔA_{eq} is the *apparent* initial signal intensity due to the free tetrellylene.

An example of each of these three cases is shown in Fig. 2.6. The reaction of $SiPh_2$ with tricyclohexylphosphine (Cy_3P) proceeded with an equilibrium constant of $K_1 \geq$ 25,000 M^{-1} (Fig. 2.6a), where successive additions of Cy_3P resulted in a systematic shortening of the silylene lifetime as a function of substrate concentration. In comparison, $SiMes_2$ reacted with tetrahydrothiophene (THT) with an intermediate K_1 (Fig. 2.6b), where both approach to equilibrium and the subsequent dimerization were well-resolved. A situation described by a small K_1 was encountered upon addition of Et_2O to $SiMes_2$ (Fig. 1c), where only a systematic reduction in the apparent signal intensity due to $SiMes_2$ could be observed (see Chapter 3 for complete discussion).

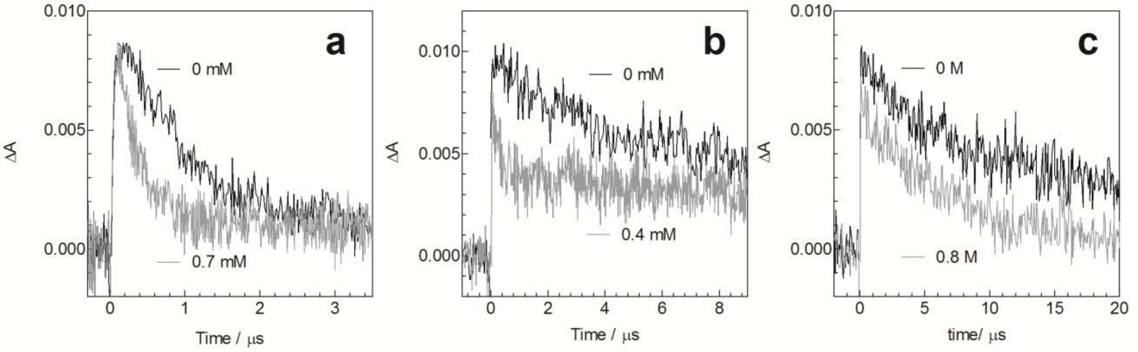

Figure 2.6. (a) Transient decay profiles of the $SiPh_2$ absorption at 530 nm, recorded by laser flash photolysis of **44a** in hexanes containing 0 mM and 0.7 mM Cy_3P; (b) transient decay profiles of the $SiMes_2$ absorption at 580 nm, recorded by laser flash photolysis of **45** in hexanes containing 0 mM and 0.4 mM THT; (c) transient decay profiles of the $SiMes_2$ absorption at 580 nm, recorded by laser flash photolysis of **45** in hexanes containing 0 M and 0.8 M Et_2O.

2.6.2. Fast Reversible Complexation Followed by a Rapid Unimolecular Reaction

One situation that is commonly encountered throughout this work is rapid unimolecular rearrangement of the initially formed complex to yield a stable product (eq. 2.20).

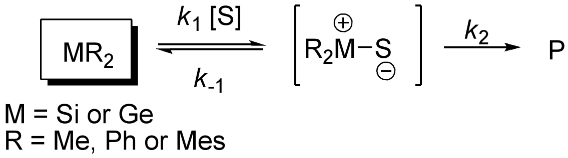

(2.20)

In instances where the total rate of production of the intermediate complex is nearly equal to the total rate of its removal, the rate of change of the concentration of the complex with time is approximately zero. In such situations the reaction can be analyzed by the steady state approximation. The expression for k_{decay} is shown in eq. 2.21.[57] According to the steady state approximation, a plot of k_{decay} vs [S] should be linear with slope of $k_2k_1/(k_{-1} + k_2)$.

$$k_{decay} = \frac{k_2 k_1 [S]}{k_{-1} + k_2} \qquad (2.21)$$

When k_2 is small, the equilibrium between [MR$_2$ + S] and [complex] can be maintained and this slowly escapes to products. If equilibrium is not attained rapidly, the kinetics are complex and kinetic simulations are required in order to obtain approximate values of k_1, k_{-1} and k_2. If the equilibrium is established very rapidly relative to the product forming step and maintained, the expression for k_{decay} is given by eq. 2.22,[57] where $K_1 = k_1/k_{-1}$ and S = substrate. In our experiments, this is generally true when the approach to equilibrium cannot be resolved from the laser pulse. In principle, the reaction can be followed by monitoring the time evolution of the product, [P], the tetrelylene, [MR_2], or the intermediate complex, [R_2M-S]. In practice it is usually the case that only the free tetrellylene can be monitored. In some instances though, both the tetrelylene and the complex can be monitored as a function of substrate concentration. This allows the values of k_2 and K_1 to be obtained by two independent methods.

$$k_{decay} = \frac{k_2 K_1[S]}{1 + K_1[S]} \qquad (2.22)$$

There are two limiting cases for k_{decay}:

K_1[S] >> 1 (saturation), when

$1 + K_1[S] \rightarrow K_1[S]$, and $k_{\text{decay}} \approx k_2$ (2.23)

and the reaction rate is zero order in [S];

K_1[S] << 1, when

$1 + K_1[S] \rightarrow 1$, and $k_{\text{decay}} \approx k_2K_1[S]$ (2.24)

and the reaction rate is first order in [S].

The steady state (eq. 2.21) and pre-equilibrium (eq. 2.22) expressions for k_{decay} are kinetically non-equivalent, and should be distinguishable experimentally. A linear plot of k_{decay} vs [S] is typically indicative of a steady state situation, while a curved plot of k_{decay} vs [S] obtained from both MR_2 *and* R_2M-S absorptions suggests a fast pre-equilibrium situation. Sometimes, however, the distinction may not be straightforward if the system is far from saturation and the plot of k_{decay} vs [S] appears to be linear. The direct detection of the intermediate complex also serves to support the mechanism – while in the steady state situation the complex does not build up to an appreciable amount to be directly detected, in the pre-equilibrium situation the complex usually can be readily observed.

2.7. Kinetic Isotope Effects

The kinetic isotope effect (KIE) is a quantitative measure of the change in reaction rate that results from isotopic substitution and is expressed as the ratio of the rate constants for reaction of two molecules labelled with different isotopes, generally the lighter one over the heavier one (eq. 2.25).[58-61] The percentage difference in mass change is great for hydrogen (H) and deuterium (D), and thus the KIE resulting from these isotopic substitutions are usually large.

$$KIE = k_{\mathrm{H}} / k_{\mathrm{D}} \qquad (2.25)$$

When the isotopic substitution is in a chemical bond that is broken or formed in the rate determining step, the change in the reaction rate can be substantial and a primary KIE is observed. The change in rate constant due to isotopic substitution at a position not directly involved in the rate determining step is known as a secondary KIE, and is intrinsically smaller than a primary KIE. However, primary KIEs are often small and thus the magnitude alone does not necessarily differentiate whether a KIE is primary or secondary.

The potential energy function for a general bond dissociation reaction in which the R-H or R-D bond is broken is shown in Fig. 2.7.[61] The potential energy surface is not altered as a result of isotopic substitution; all differences are attributable only to the change in mass which is reflected in the vibrational frequencies. The vibrational energy of a molecule R-D in the ground state (zero point energy or ZPE) is lower than that of a

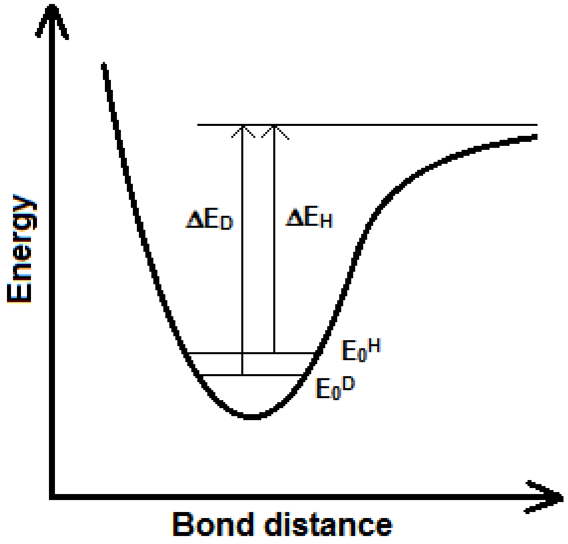

Figure 2.7. Bond dissociation curve showing the different zero-point energies of isotopic species R-H and R-D.

molecule R-H as illustrated in Fig. 2.7, thus greater activation energy is required for cleavage. The maximum lowering in energy (ΔE_0) which results from D-for-H substitution is given by eq. 2.26, where ν_0 is the classical vibrational frequency, *h* is the Planck's constant, and *m* is the reduced mass.[60]

$$\Delta E_0 = E_0^H - E_0^D = \frac{1}{2}h\left(\nu_0^H - \nu_0^H\sqrt{\frac{m_H}{m_D}}\right) = \frac{1}{2}h\nu_0^H\left(1-\sqrt{\frac{m_H}{m_D}}\right) \qquad (2.26)$$

The ratio of the rate constants for a reaction with isotopic substitution can be expressed as[60-61]

$$\frac{k_H}{k_D} = \sqrt{\frac{m_D}{m_H}} \cdot e^{-\frac{\Delta E_0}{RT}} \qquad (2.27)$$

where ΔE_0 is given by eq. 2.26. For an isotopic substitution of a heavy atom other than hydrogen the ratio of the reduced masses is close to unity, resulting in small KIEs. The maximum primary KIE that can be observed for a C-H bond dissociation process is equal to 6.5;[61] the experimentally observed values are generally lower than that, however.

The range in the observed KIE values is explained by the fact that in most cases the hydrogen atom is transferred from one atom to another, rather than freely dissociating as is implied by this simple model. The hydrogen remains partially bonded throughout the transfer process, thus requiring a more complex mathematical approximation.[61]

2.8. Determination of Screening Effects

When a large amount of a scavenger is required in order to determine K_1 for complexation of silylenes or germylenes with the substrate, the screening effects by that substrate have to be assessed. Equilibrium constant values are obtained by analysis of signal intensities; eq. 2.18 is valid only when the initial photochemical yield of the silylene or germylene does not vary with concentration of the substrate. If the substrate absorbs the incident light and the equilibrium constant is small, the value could be artificially enhanced due to light screening by the substrate. The percent of light absorbed ($\%_{A(prec)}$) by the tetrellylene precursor in the presence of a screening substrate (screen) can be calculated using eq. 2.28, where A_{248nm} (prec) is the static absorbance of the precursor at the laser wavelength in the absence of the screening agent, and A_{248nm} (screen) is the static absorbance of the screen at 248 nm. The value of the denominator can be measured either by measuring the total static absorbance of the sample in the presence of the screen, or by calculating the expected absorbance based on the concentration of added screen and knowledge of the extinction coefficient of the screen at the laser wavelength.

$$\%_{A(prec)} = \frac{A_{248nm}(prec.)}{A_{248nm}(prec.) + A_{248nm}(screen)} \qquad (2.28)$$

In order to test the validity of eq. 2.28, the screening effects on the tetrellylene signals were evaluated by examining the reaction of $GeMes_2$ with dimethylbutadiene (DMB). This reaction is expected to proceed with an equilibrium constant of $<10\ M^{-1}$, therefore no effect on the germylene signal is expected between 0-5 mM DMB except that due to the screening of the signal ($\varepsilon_{248\ nm}{}^{53} = 160 \pm 20\ M^{-1}\ cm^{-1}$).

The initial ΔA_0 of the germylene in the absence of the screening agent can be multiplied by the $\%_{A(prec)}$ factor obtained from eq. 2.28 to obtain the expected signal intensity in the presence of the screen ($\Delta A_{screen} = \Delta A_0 \times \%_{A(prec)}$). The slope of the $\Delta A_0/\Delta A_{screen}$ vs [S] plot will give the expected screening factor x_{calc}, assuming 100% screening efficiency of the screen (eq. 2.29).

$$\frac{\Delta A_0}{\Delta A_{screen}} = 1 + x_{calc}[S] \qquad (2.29)$$

Addition of DMB (0-6 mM) to a hexane solution of **46** resulted in a drop in the signal intensity of the germylene, and the resulting plot of $\Delta A_0/\Delta A_{DMB}$ ($GeMes_2$, 550 nm) vs [DMB] is shown on Fig. 2.8b. The dotted lines represent the predicted drop in the signal intensity based on eq. 2.29, while the solid line shows the experimental data. The ratio of the expected slope to the actual slope gives the correction factor of 0.75 ± 0.07 which represents 75% screening efficiency of DMB (eq. 2.30), therefore eq. 2.29 can be written as eq. 2.31 which accounts for the correction factor. The plot of the calculated transmittance (using the Beer-Lambert law) ($\%\ T_{248\ nm}$) vs [DMB] is shown in Fig. 2.8a, which indicates that the %T of the sample used for this experiment ranges between 5-25 %.

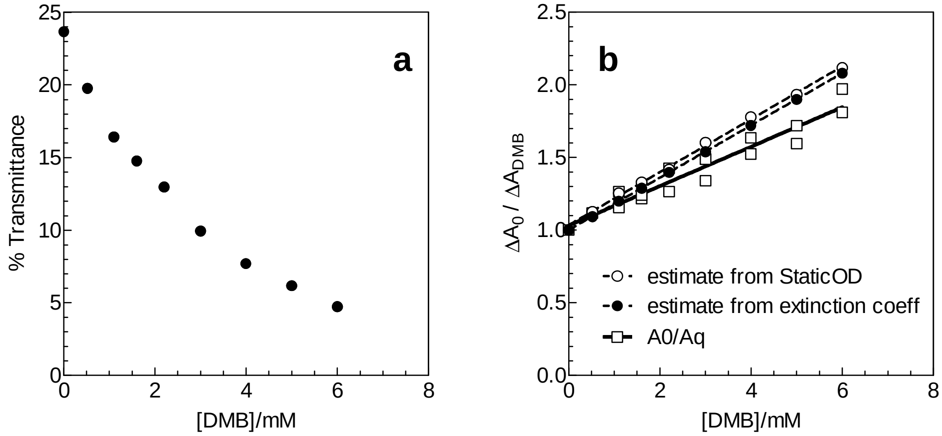

Figure 2.8. (a) Plot of %Transmittance (248 nm) vs. [DMB] for the reaction of $GeMes_2$ with DMB. (b) Plot of $\Delta A_0/\Delta A_{DMB}$ ($GeMes_2$, 550 nm) vs [DMB] for the reaction of $GeMes_2$ with DMB. The solid line is the least squares fit of the data to eq. 2.29.

$$x_{actual} = (0.75 \pm 0.07) \times x_{calc} \qquad (2.30)$$

$$\frac{\Delta A_0}{\Delta A_{screen}} = 1 + \frac{x_{actual}}{(0.75 \pm 0.07)}[S] \qquad (2.31)$$

This correction factor was used to estimate the equilibrium constant for the reactions of $SiMes_2$ and $GeMes_2$ with Et_2S ($\varepsilon_{248\ nm}$ = 14 M^{-1} cm^{-1}), where the addition of Et_2S yielded a reduction in the apparent tetrellylene signal intensity but had no effect on the decay kinetics (Ch. 3).

2.9. References

1. Matsumoto, Y.; Hayashi, T.; Ito, Y., *Tetrahedron* **1994,** *50* (2), 335.

2. Chen, S.-M.; Katti, A.; Blinka, T. A.; West, R., *Synthesis* **1985,** *6-7*, 684.

3. Moiseev, A. G.; Leigh, W. J., *Organometallics* **2007,** *26*, 6268.

4. Kumada, M.; Tamao, K.; Takubo, T.; Ishikawa, M., *J. Organomet. Chem.* **1967,** *9*, 43.

5. Ishikawa, M.; Kumada, M., In *Adv. Organomet. Chem.*, Stone, F. G. A.; Robert, W., Eds. Academic Press: 1981; Vol. Volume 19, pp 51-95.

6. Levin, G.; Das, P. K.; Bilgrien, C.; Lee, C. L., *Organometallics* **1989,** *8*, 1206.

7. Yamaji, M.; Hamanishi, K.; Takahashi, T.; Shizuka, H., *J. Photochem. Photobiol. A: Chem.* **1994,** *81*, 1.

8. Levin, G.; Das, P. K.; Lee, C. L., *Organometallics* **1988,** *7*, 1231.

9. Shizuka, H.; Tanaka, H.; Tonokura, K.; Murata, K.; Hiratsuka, H.; Ohshita, J.; Ishikawa, M., *Chem. Phys. Lett.* **1988,** *143*, 225.

10. Ishikawa, M.; Kumada, M., *J. Organomet. Chem.* **1972,** *42*, 325.

11. Drahnak, T. J.; Michl, J.; West, R., *J. Am. Chem. Soc.* **1979,** *101* (18), 5427.

12. Gu, T. Y.; Weber, W. P., *J. Organomet. Chem.* **1980,** *195* (1), 29.

13. Gu, T.-Y. Y.; Weber, W. P., *J. Organomet. Chem.* **1980,** *184* (1), 7.

14. Steele, K. P.; Weber, W. P., *J. Am. Chem. Soc.* **1980,** *102* (19), 6095.

15. Tzeng, D.; Weber, W. P., *J. Am. Chem. Soc.* **1980,** *102*, 1451.

16. Chihi, A.; Weber, W. P., *J. Organomet. Chem.* **1981,** *210*, 163.

17. Moiseev, A. G.; Leigh, W. J., *Organometallics* **2007,** *26*, 6277.

18. Gillette, G. R.; Noren, G. H.; West, R., *Organometallics* **1989,** *8*, 487.

19. Miyazawa, T.; Koshihara, S. Y.; Liu, C.; Sakurai, H.; Kira, M., *J. Am. Chem. Soc.* **1999,** *121*, 3651.

20. Becerra, R.; Walsh, R., *Dalton Trans.* **2010,** *39*, 9217.

21. Leigh, W. J.; Sluggett, G. W., *Organometallics* **1994,** *13*, 269.

22. Gaspar, P. P.; Hyun Boo, B.; Chari, S.; Ghosh, A. K.; Holten, D.; Kirmaier, C.; Konieczny, S., *Chem. Phys. Lett.* **1984,** *105* (2), 153.

23. Gaspar, P. P.; Holten, D.; Konieczny, S.; Corey, J. Y., *Acc. Chem. Res.* **1987,** *20* (9), 329.

24. Konieczny, S.; Jacobs, S. J.; Braddock Wilking, J. K.; Gaspar, P. P., *J. Organomet. Chem.* **1988,** *341*, C17.

25. Safarik, I.; Sandhu, V.; Lown, E.; Strausz, O.; Bell, T., *Res. Chem. Intermed.* **1990,** *14* (2), 105.

26. Michalczyk, M. J.; Fink, M. J.; De Young, D. J.; Carlson, C. W.; Welsh, K. M.; West, R., *Silicon, Germanium, Tin and Lead Compounds* **1986,** *9*, 75.

27. Conlin, R. T.; Netto-Ferreira, J. C.; Zhang, S.; Scaiano, J. C., *Organometallics* **1990,** *9*, 1332.

28. Gaspar, P. P., In *Reactive Intermediates*, Jones, M. J.; Moss, R. A., Eds. Wiley: New York, 1978; Vol. 1, pp 229-277.

29. Gaspar, P. P., In *Reactive Intermediates*, Jones, M. J.; Moss, R. A., Eds. Wiley: New York, 1981; Vol. 2, pp 335-385.

30. Gaspar, P. P., In *Reactive Intermediates*, Jones, M. J.; Moss, R. A., Eds. Wiley: New York, 1985; Vol. 3, pp 333-427.

31. Leigh, W. J.; Sluggett, G. W., *J. Am. Chem. Soc.* **1992,** *114*, 1195.

32. Moiseev, A. G.; Leigh, W. J., *J. Am. Chem. Soc.* **2006,** *128*, 14442.

33. Leigh, W. J.; Moiseev, A. G.; Coulais, E.; Lollmahomed, F.; Askari, M. S., *Can. J. Chem.* **2008,** *86* (12), 1105.

34. Moiseev, A. G.; Coulais, E.; Leigh, W. J., *Chem. Eur. J.* **2009,** *15* (34), 8485.

35. Fink, M. J.; DeYoung, D. J.; West, R.; Michl, J., *J. Am. Chem. Soc.* **1983,** *105* (4), 1070.

36. Fink, M. J.; Michalczyk, M. J.; Haller, K. J.; West, R.; Michl, J., *Organometallics* **1984,** *3*, 793.

37. Leigh, W. J.; Kostina, S. S.; Bhattacharya, A.; Moiseev, A. G., *Organometallics* **2010,** *29* (3), 662.

38. Leigh, W. J.; Lollmahomed, F.; Harrington, C. R., *Organometallics* **2006,** *25*, 2055.

39. Lollmahomed, F., Ph.D. Thesis, McMaster University, Hamilton, 2009.

40. Yamamoto, Y.; Ohdoi, K.; Nakatani, M.; Akiba, K., *Chem. Lett.* **1984,** *1984*, 1967.

41. Brown, P. A.; Bonnert, R. V.; Jenkins, P. R.; Lawrence, N. J.; Selim, M. R., *J. Chem. Soc., Perkin Trans. I* **1991,** *1991*, 1893.

42. Kolesnikov, S. P.; Rogozhin, I. S.; Nefedov, O. M., *Izv. Akad. Nauk. SSSR, Ser. Khim.* **1974**, 2297.

43. Leigh, W. J.; Harrington, C. R.; Vargas-Baca, I., *J. Am. Chem. Soc.* **2004,** *126*, 16105.

44. Huck, L. A., Ph.D. Thesis, McMaster University, Hamilton, 2010.

45. Becerra, R.; Boganov, S. E.; Egorov, M. P.; Faustov, V. I.; Nefedov, O. M.; Walsh, R., *J. Am. Chem. Soc.* **1998,** *120*, 12657.

46. Becerra, R.; Boganov, S. E.; Egorov, M. P.; Lee, V. Y.; Nefedov, O. M.; Walsh, R., *Chem. Phys. Lett.* **1996,** *250*, 111.

47. Boganov, S. E.; Egorov, M. P.; Faustov, V. I.; Nefedov, O. M., In *The Chemistry of Organic Germanium, Tin and Lead Compounds*, Rappoport, Z., Ed. John Wiley & Sons, Ltd: 2002; Vol. 2, pp 749-841.

48. Neumann, W. P., *Chem. Rev.* **1991,** *91*, 311.

49. Leigh, W. J.; Lollmahomed, F.; Harrington, C. R.; McDonald, J. M., *Organometallics* **2006,** *25*, 5424.

50. Lollmahomed, F.; Huck, L. A.; Harrington, C. R.; Chitnis, S. S.; Leigh, W. J., *Organometallics* **2009,** *28* (5), 1484.

51. Bobbitt, K. L.; Lei, D.; Maloney, V. M.; Parker, B. S.; Raible, J. M.; Gaspar, P. P. In *Proceedings of the VIIth International Conference on the Organometallic and Coordination Chemistry of Germanium, Tin and Lead*, Riga, 1993; Lukevics, E.; Ignatovich, L., Eds. Latvian Institute of Organic Synthesis: Riga, 1992; pp 41-53.

52. Huck, L. A.; Leigh, W. J., *Organometallics* **2007,** *26*, 1339.

53. Huck, L. A.; Leigh, W. J., *Organometallics* **2009,** *28*, 6777.

54. Leigh, W. J.; Harrington, C. R.; Vargas-Baca, I., *J. Am. Chem. Soc.* **2006,** *128* (4), 1394.

55. Toltl, N. P.; Leigh, W. J.; Kollegger, G. M.; Stibbs, W. G.; Baines, K. M., *Organometallics* **1996,** *15* (17), 3732.

56. Leigh, W. J.; Harrington, C. R., *J. Am. Chem. Soc.* **2005,** *127*, 5084.

57. Wright, M. R., *An Introduction to Chemical Kinetics*. John Wiley & Sons Ltd.: Chichester, England, 2004.

58. Espenson, J. H., *Chemical Kinetics and Reaction Mechanisms*. McGraw-Hill, Inc.: New York, 1995.

59. Connors, K. A., *Chemical Kinetics: The Study of Reaction Rates in Solution*. Wiley-VCH: 1990; p 496.

60. Upadhyay, S. K., *Chemical Kinetics and Reaction Dynamics*. Springer with Anamaya: 2006; p 256.

61. Lowry, T. H.; Richardson, K. S., *Mechanism and Theory in Organic Chemistry*. 3rd ed.; Harper and Row: New York, 1987.

3. Chapter 3 – Kinetic and thermodynamic studies of the Lewis acid-base complexation of silylenes and germylenes with chalcogen and pnictogen donors

3.1. Overview

The chapter describes the results of a detailed study of the kinetics and thermodynamics of the Lewis acid-base complexation reactions of silylenes and germylenes of homologous structure (MMe_2, MPh_2 and $MMes_2$, M = Si or Ge) with chalcogen and pnictogen donors. Complexation reactions with a series of ethers (Et_2O and tetrahydrofuran), sulfides (Et_2S and tetrahydrothiophene), amines (Et_2NH and Et_3N) and trialkylphosphines (Et_3P and tricyclohexylphosphine) were examined. Equilibrium constants for complexation were measured for all six tetrellylenes with Et_2O, and show that Lewis acidities decrease in the order $SiPh_2 > SiMe_2 > GePh_2 > GeMe_2 >> SiMes_2 > GeMes_2$. The equilibrium constants for the reactions of $SiMes_2$ and $GeMes_2$ with all donors except Et_3P were determined, the silylene being consistently more acidic than the germylene by ca. 1 pK unit. The free energies of complexation roughly follow the trend expected from proton affinities. Calculated (G4) binding enthalpies of the complexes of MMe_2 with 17 Lewis bases correlate with Drago’s E and C parameters, which indicate that silylenes and germylenes can in fact be classified as borderline soft Lewis acids, and not hard Lewis acids as previously thought.

The three silylenes and three germylenes studied in this work were generated by laser photolysis of compounds **36**, **37,** and **43 - 46**.[1-6] The species are formed promptly with the laser pulse and decay with approximate second-order kinetics with the concomitant formation of longer-lived UV-vis absorptions due to the corresponding disilenes or digermenes.

3.2. Transient spectroscopy

3.2.1. Complexation with O- and S- donors

Addition of millimolar concentrations of Et_2O to hexanes solutions of **43**, **36** or **37** led to closely analogous results – the signals due to $SiMe_2$, $GeMe_2$ or $GePh_2$ diminished in intensity, while the lifetimes of the tetrellylenes remained unaffected. This behaviour is consistent with a reversible reaction with an equilibrium constant in the < 1,500 M^{-1} regime. Analysis of the data according to eq. 3.1 (where ΔA_0 and ΔA_{eq} are the initial and equilibrium absorbances of tetrellylene, respectively, S is the substrate, and K_1 is the equilibrium constant) resulted in linear plots of $\Delta A_0/\Delta A_{eq}$ vs $[Et_2O]$ in all cases. Equilibrium constants of 1260 ± 50 M^{-1}, 110 ± 10 M^{-1} and 160 ± 10 M^{-1} were extracted by linear least-squares analysis of plots of $\Delta A_0/\Delta A_{eq}$ vs $[Et_2O]$ for $SiMe_2$, $GeMe_2$ and $GePh_2$, respectively (Fig. 3.1a and b). Addition of submillimolar concentrations of Et_2O to a hexanes solution of **44a** resulted in a bimodal decay due to the silylene, consistent with K_1 in the intermediate range. The plots of k_{decay} ($SiPh_2$) vs $[Et_2O]$ and $\Delta A_0/\Delta A_{eq}$ vs $[Et_2O]$ exhibited good linearity (Fig. 3.1a and c). The data were analyzed using eq. 3.2 to obtain a k_1 value of $(15 \pm 4) \times 10^9$ M^{-1} s^{-1}, and using eq. 3.1 to obtain a K_1 value of 7,100 ± 600 M^{-1} s^{-1}. Transient absorption spectra of the $SiPh_2$-Et_2O and $GePh_2$-Et_2O complexes are shown in Fig. 3.2; in both cases the spectra are similar to those of the corresponding THF complexes.[3, 7]

$$\Delta A_0/\Delta A_{eq} = 1 + K_1[S] \qquad (3.1)$$

$$k_{decay} = k_{-1} + k_1[S] \qquad (3.2)$$

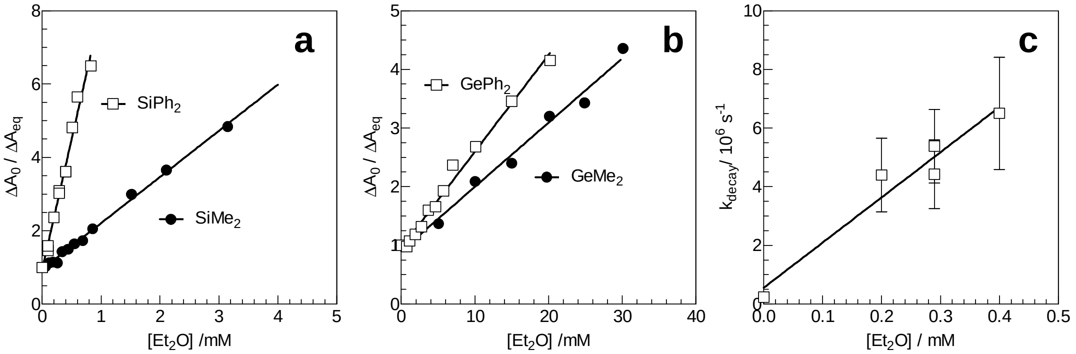

Figure 3.1. Plots of $\Delta A_0 / \Delta A_{eq}$ vs [Et_2O] for MR_2 (R = Me (●), Ph (□)), where (a) M = Si, (b) M = Ge. (c) Plot of the pseudo-first-order decay coefficient (k_{decay}) of the $SiPh_2$ absorption vs [Et_2O].

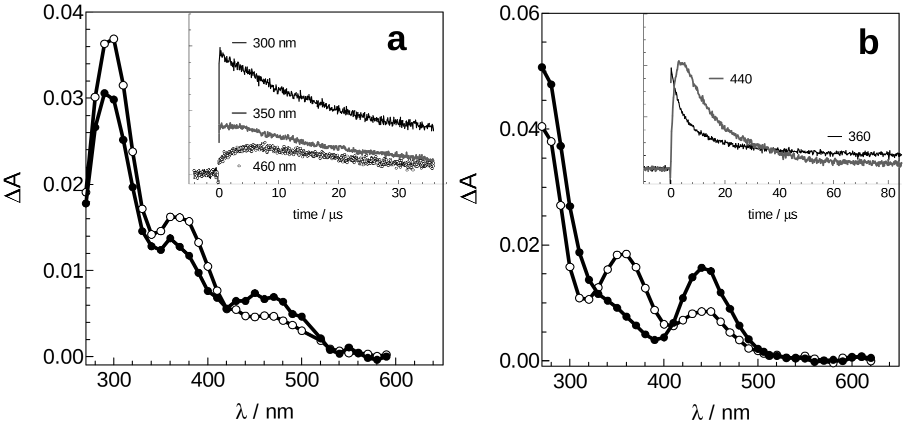

Figure 3.2. Transient absorption spectra of hexanes solutions containing 0.1 M Et_2O and (a) **44a**, recorded 0.64-1.28 μs (o) and 5.92-6.72 μs (●) after the laser pulse (the inset shows transient decay profiles recorded at 300, 350 and 460 nm) (b) **37**, recorded 0.16-0.80 μs (o) and 8.32-9.28 (●) after the laser pulse (the inset shows transient decay profiles recorded at 360 and 440 nm).

An analogous experiment involving $SiMes_2$ generated from **45** resulted in no noticeable change in either the decay rate or the intensity of the signals due to the silylene in the presence of millimolar concentrations of Et_2O, which indicates the equilibrium constant is too low to be measured using the usual method. Addition of a solution of **45** in diethyl ether to an optically matched solution of **45** in hexanes in molar increments resulted in a drop in the intensity of the signals due to the silylene. A plot of $\Delta A_0/\Delta A_{eq}$ vs $[Et_2O]$ was linear and is shown in Fig. 3.3a. An equilibrium constant of 0.9 ± 0.1 M^{-1} was extracted for the reaction with Et_2O, which is *ca*. 2.5 times lower than that for the reaction with THF (K_1 = 2.4 M^{-1}).[8] A weak signal due to free $SiMes_2$ was also observed in neat Et_2O solution, which decayed with concomitant formation of Si_2Mes_4 on a similar timescale as was previously observed in hexanes solution (Fig. 3.3b). In order to obtain the equilibrium constant for the complexation of $GeMes_2$ with Et_2O, an optically matched solution of **46** in Et_2O was added in portions to a solution of **46** in hexanes, in a similar fashion as was done in the reaction with $SiMes_2$. This experiment yielded an equilibrium constant of 0.09 ± 0.01 M^{-1}, and free $GeMes_2$ could be detected easily even in neat ethereal solution (Fig. 3.3c). A new weak absorption band centered below 290 nm was also detected which underlies the absorption due to $GeMes_2$ (Fig. 3.3c). In comparison, a previously reported transient absorption spectra of the $GeMes_2$-THF complex shows two bands centered at < 280 nm (strong) and ca. 390 nm (weak).[7] Due to such unfavourable equilibrium, however, we are unable to detect the long-wavelength band of the $GeMes_2$-Et_2O complex, and the assignment of the short wavelength band to the complex should be accepted with caution.

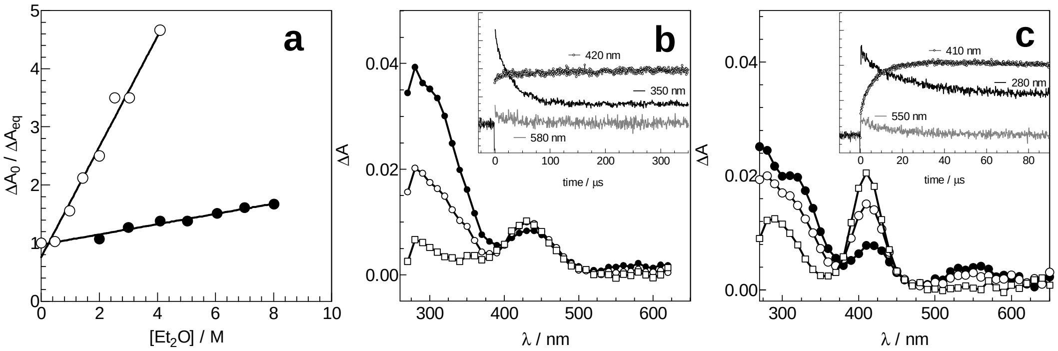

Figure 3.3. (a) Plots of ΔA_0 / ΔA_{eq} vs [Et_2O] for $SiMes_2$ (o) and $GeMes_2$ (●). (b) Transient absorption spectra from laser flash photolysis of a solution of $SiMes_2$ precursor **45** in neat Et_2O, recorded 1.9-4.5 μs (●), 23.7-27.5 μs (o), and 215.7-218.9 μs (□) after the laser pulse; the inset shows transient decay profiles recorded at 350 nm, 420 nm and 580 nm. (c) Transient absorption spectra from laser flash photolysis of a solution of $GeMes_2$ precursor **46** in neat Et_2O, recorded 0.8-1.4 μs (●), 5.9-6.7 μs (o), and 69.9-70.7 μs (□) after the laser pulse; the inset shows transient decay profiles recorded at 280 nm, 410 nm and 550 nm.

Addition of submillimolar concentrations of Et_2S to $SiMe_2$, $GeMe_2$, $SiPh_2$ or $GePh_2$ led to closely analogous results – the lifetime of the tetrellylene shortened and the transient decay profiles decayed with pseudo first order kinetics consistent with equilibrium constants of $K_1 \geq 25{,}000$ M^{-1}. Plots of k_{decay} vs [Et_2S] were linear in each case, the slopes of which yielded rate constants within a factor of two of the diffusional rate constant in hexanes (Fig. 3.4a-b, Table 3.2). The decay of the tetrellylenes led to the formation of the MR_2-Et_2S complexes which decayed with mixed order kinetics with concomitant formation of the corresponding dimers.

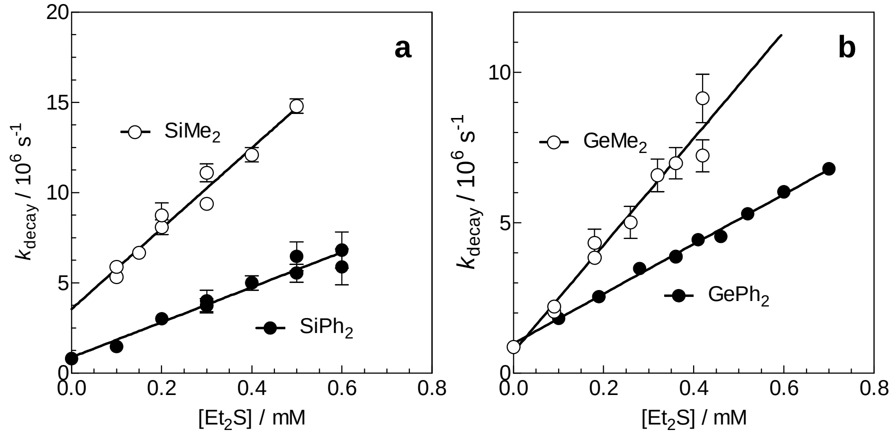

Figure 3.4. Plots of the pseudo-first-order decay coefficients (k_{decay}) *versus* [Et$_2$S] for (a) SiMe$_2$ (o) and SiPh$_2$ (●) and, (b) GeMe$_2$ (o) and GePh$_2$ (●).

Table 3.1. Forward rate (k_1) and equilibrium constants (K_1) for complexation of transient silylenes and germylenes with O-donors in hexanes at 25 ^{o}C.

	k_1 / 10^9 $M^{-1}s^{-1}$ [K_1 / M^{-1}]	
Donor	Et$_2$O	THF
SiMe$_2$	[a] [1,260 ± 50]	17 ± 2 [b, c]
SiPh$_2$	15 ± 4 [7,100 ± 600]	15 ± 1 [b, c]
SiMes$_2$	[a] [0.9 ± 0.1]	[a] [2.4 ± 0.4]
GeMe$_2$	[a] [110 ± 10]	11 ± 2 [d] [10,000 ± 4,000]
GePh$_2$	[a] [160 ± 10]	6.3 ± 0.6 [d] [23,000 ± 5,000]
GeMes$_2$	[a] [~0.06]	[a, d] [1.1 ± 0.2]

a. k_1 indeterminable ($\geq 0.002K_1$ $M^{-1}s^{-1}$); *b*. K_1 > 25,000 M^{-1}; *c*. Ref. 3; *d*. Ref. 7.

Addition of Et_2S in millimolar concentrations to solutions of the $SiMes_2$ or $GeMes_2$ precursors resulted in a systematic drop in the apparent intensity of the tetrellylene signal with increasing substrate concentration. Plots of $\Delta A_0/\Delta A_{eq}$ vs $[Et_2S]$ were linear in both cases and are characterized by slopes of 97 ± 4 M^{-1} and 75 ± 3 M^{-1} for $SiMes_2$ and $GeMes_2$, respectively (Fig. 3.5a). Diethylsulfide (Et_2S) screens the incident light at 248 nm ($\varepsilon_{248\ nm}$ = 14 M^{-1} cm^{-1}), and so its contribution to the reduction in the apparent signal intensity of tetrellylene signals has to be accounted for. Assuming that the screening efficiency of Et_2S is equal to that of DMB (0.75) (see Chapter 2.8), the equilibrium constants for the reactions of $SiMes_2$ and $GeMes_2$ with Et_2S can be calculated. The $A_{248\ nm}$ (screen) at each concentration of Et_2S was calculated according to eq. 3.3 using the Beer-Lambert law and the extinction coefficient of Et_2S at 248 nm. The reduction of the apparent intensity of the $MMes_2$ signal expected due to screening by Et_2S was calculated at each concentration and subtracted from the signal intensity before addition of the substrate. The ratio of the signal intensity due to screening to the actual signal intensity observed in the experiment was plotted as a function of $[Et_2S]$ to yield the linear plot shown in Fig. 3.5b. The corrected K_1 values are listed in Table 3.2 (K_1 ($SiMes_2 + Et_2S$) = 54 ± 3 M^{-1} and K_1 ($GeMes_2 + Et_2S$) = 40 ± 4 M^{-1}).

$$\%_{A(prec)} = \frac{A_{248nm}(prec.)}{A_{248nm}(prec.) + A_{248nm}(screen)} \qquad (3.3)$$

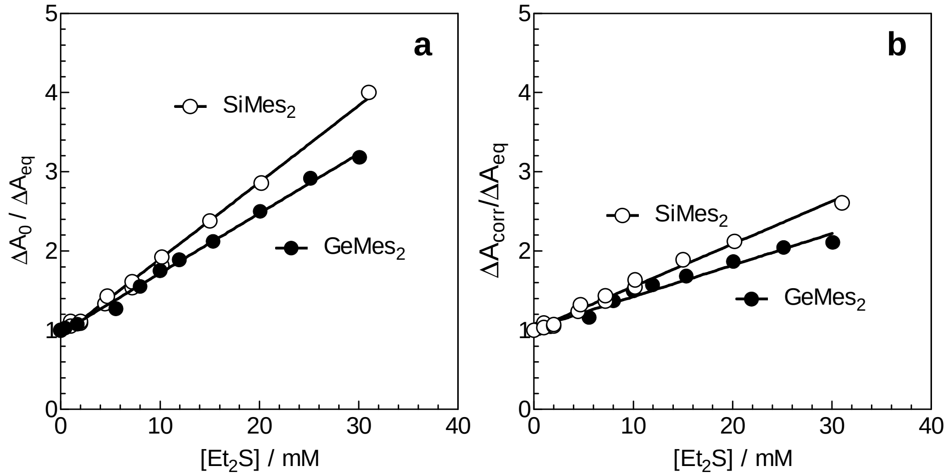

Figure 3.5. Plots of $\Delta A_0/\Delta A_{eq}$ *versus* [Et_2S] for $SiMes_2$ (o) and GeMes (●) absorptions; (a) obtained from raw data; (b) corrected for screening effects by Et_2S (see text).

Figure 3.6 shows transient absorption spectra and representative absorbance-time profiles obtained with hexanes solutions of the six silylene and germylene precursors containing Et_2S. In each case, the spectra of the MR_2-Et_2S complexes closely resemble those of O-donors, and are nearly identical to those of the MR_2-THT complexes (*vide infra*). The spectra of the SiR_2-Et_2S complexes are blue-shifted relative to those of the homologous GeR_2-Et_2S complexes by ca. 20 nm.

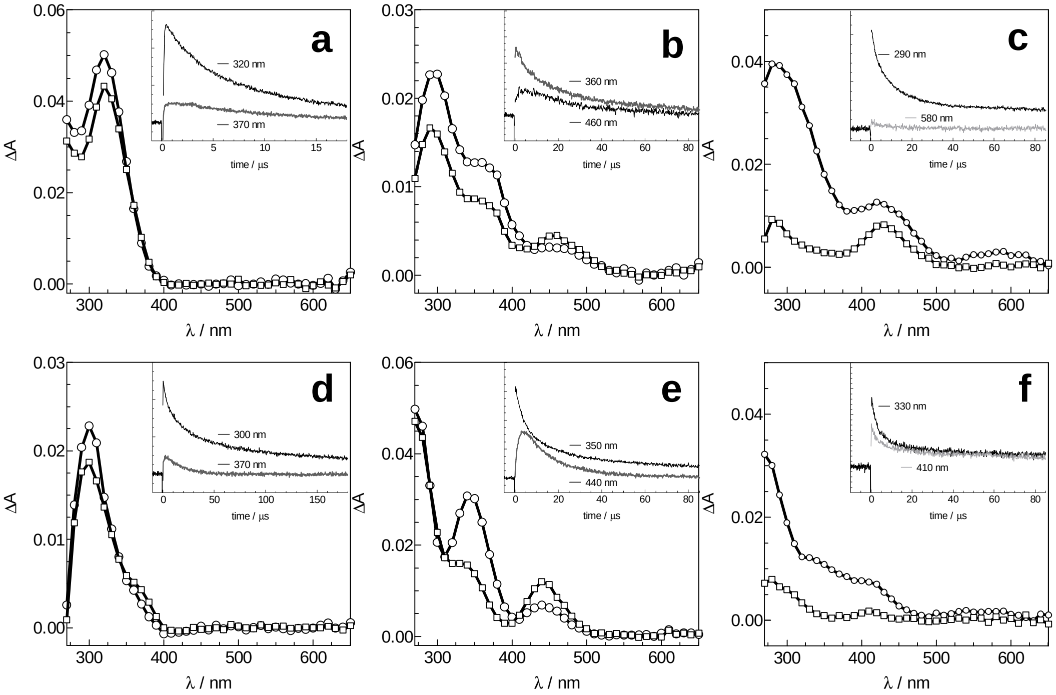

Figure 3.6. Transient absorption spectra of a deoxygenated hexanes solution of (a) **43** containing 4.5 mM Et_2S recorded 0.26-0.38 μs (o) and 1.50-1.63 μs (□) after the laser pulse; (b) **44a** containing 4.5 mM Et_2S recorded 0.32-0.96 μs (o) and 5.92-6.72 μs (□) after the laser pulse; (c) **45** containing 20 mM Et_2S recorded 0.48-1.12 μs (o) and 69.92-70.72 μs (□) after the laser pulse. (d) **36** containing 5 mM Et_2S recorded 0.00-1.60 μs (o) and 3.84-5.44 μs (□) after the laser pulse; (e) **37** containing 4.5 mM Et_2S recorded 0.16-0.96 μs (o) and 9.12-9.92 μs (□) after the laser pulse; (f) **46** containing 30 mM Et_2S recorded 0.16-0.96 μs (o) and 85.92-86.72 μs (□) after the laser pulse. The insets in each of the figures show transient absorbance vs. time profiles recorded at representative wavelengths in the spectra.

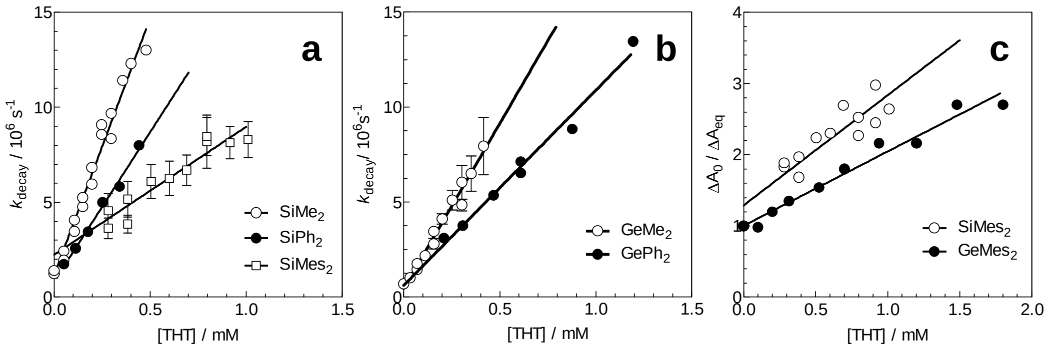

Figure 3.7. Plots of the pseudo-first-order decay coefficients (k_{decay}) *versus* [THT] for (a) SiMe$_2$ (o), SiPh$_2$ (●) and SiMes$_2$ (□), (b) GeMe$_2$ (o) and GePh$_2$ (●). (c) Plots of $\Delta A_0/\Delta A_{eq}$ *versus* [THT] for SiMes$_2$ (o) and GeMes$_2$ (●).

Tetrahydrothiophene (THT) reacted with SiMe$_2$, SiPh$_2$, GeMe$_2$ and GePh$_2$ with similar rate constants to those with Et$_2$S (Table 3.2). The plots of k_{decay} vs [THT] were linear in each case and are shown in Fig. 3.7a-b. The transient decay profiles of SiMes$_2$ and GeMes$_2$ responded to increasing [THT] in a manner consistent with higher equilibrium constants than those for the reactions of these tetrellylenes with Et$_2$S. Upon addition of THT the decay traces due to SiMes$_2$ became bimodal, exhibiting a fast decay component followed by a slow-decaying residual level. This characteristic corresponds to an equilibrium constant in the medium range, where both the rate and equilibrium constants can be determined (see Chapter 2). The rate constant was extracted from the slope of the plot of k_{decay} vs [THT], which is shown in Fig. 3.7a. The apparent absorptions due to GeMes$_2$ became increasingly weaker as a function of THT concentration, thus representing a small K_1 situation. The plots of $\Delta A_0/\Delta A_{eq}$ vs [THT] were linear in both cases (Fig. 3.7c), the slopes corresponding to equilibrium constants of 1000 M^{-1} and 1500 M^{-1} for GeMes$_2$ and SiMes$_2$, respectively (Table 3.2).

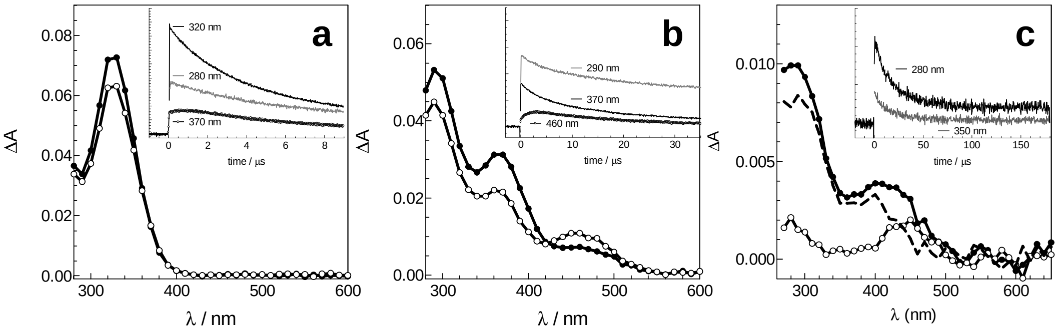

Figure 3.8. (a) Transient absorption spectra from laser flash photolysis of a hexane solution of **43** containing 5.3 mM THT, recorded 0.26-0.32 (●) and 0.88-0.94 µs (o) after the laser pulse; (b) transient absorption spectra from laser flash photolysis of a hexane solution of **44a** containing 5.3 mM THT, recorded 0.26-0.51 µs (●) and 4.16-4.42 µs (o) after the laser pulse; (c) transient absorption spectra from laser flash photolysis of a hexane solution of **45** containing 52 mM THT, recorded 2.24-3.52 (●) and 107.84-109.12 µs (o) after the laser pulse; the dashed line is the difference spectrum calculated by subtracting (o) from (●). The inset in each of the figures shows transient absorbance vs. time profiles recorded at representative wavelengths in the spectra.

Figure 3.8 shows transient absorption spectra of the silylene-THT complexes, while Figure 3.9 shows those of the germylene-THT complexes. In each case, the spectra are nearly identical to those of the corresponding Et_2S complexes.

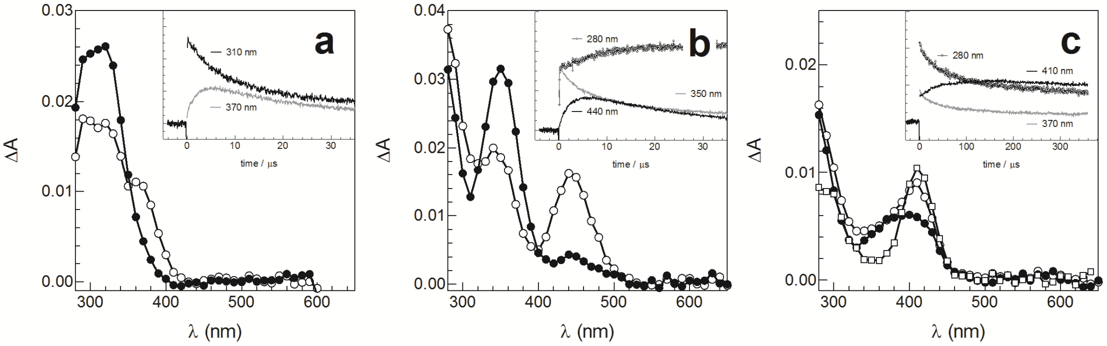

Figure 3.9. (a) Transient absorption spectra from laser flash photolysis of a hexane solution of **36** containing 5 mM THT, recorded 0.19-0.45 (●) and 5.25-5.50 μs (o) after the laser pulse; (b) transient absorption spectra from laser flash photolysis of a hexane solution of **37** containing 5.5 mM THT, recorded 0.19-0.45 μs (●) and 6.34-6.46 μs (o) after the laser pulse; (c) transient absorption spectra from laser flash photolysis of a hexane solution of **46** containing 5.4 mM THT, recorded 1.3-4.5 μs (●), 23.7-26.9 μs (o), and 279.7-282.9 μs (□) after the laser pulse. The inset in each of the figures shows transient absorbance vs. time profiles recorded at representative wavelengths in the spectra.

Table 3.2. Forward rate (k_1) and equilibrium constants (K_1) for complexation of transient silylenes and germylenes with S-donors in hexanes at 25 ^{o}C.

	k_1 / 10^9 $M^{-1}s^{-1}$ [K_1 / M^{-1}]	
Donor	Et_2S	THT
$SiMe_2$	22 ± 3 [a]	21 ± 2 [a, b]
$SiPh_2$	10 ± 1 [a]	15 ± 2 [a, b]
$SiMes_2$	[c] [54 ± 3]	7 ± 2 [$1{,}500 \pm 100$]
$GeMe_2$	18 ± 2 [a]	17 ± 2 [a]
$GePh_2$	8.3 ± 0.4 [a]	10 ± 2 [a]
$GeMes_2$	[c] [40 ± 4]	[c] [$1{,}000 \pm 100$]

a. $K_1 > 25{,}000$ M^{-1}; *b*. Ref. 9; *c*. k_1 indeterminable ($\geq 0.002K_1$ $M^{-1}s^{-1}$).

3.2.2. Complexation with N- and P- donors

Addition of triethylphosphine (Et_3P) in small increments to hexanes solutions of **36**, **37**, or **43 -46** yielded results consistent in each case with large K_1 – the signals due to SiR_2 or GeR_2 reduced to first order kinetics, the lifetimes shortened at higher [Et_3P], and new absorption bands formed in the regions characteristic of the acceptor-donor adducts which decayed with mixed order kinetics. Although the decay of the adducts should yield the formation of ditetrellylenes, in the reactions involving silylenes the disilenes were not

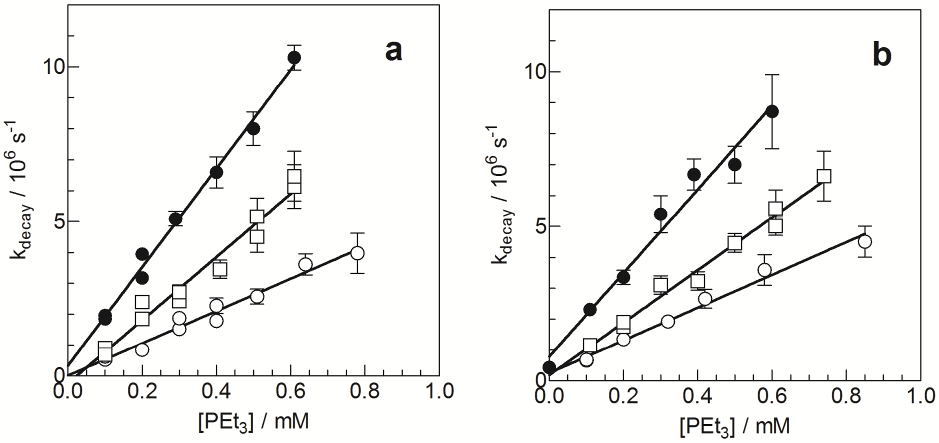

Figure 3.10. Plots of the pseudo-first-order decay coefficients (k_{decay}) of the MR_2 absorptions (R = Me (●), Ph (□), Mes (o)) vs [PEt_3], where (a) M = Si, (b) M = Ge.

always observed. This may be due to the presence of trace impurities in the solvent that react with the complexes or with dimers. Plots of k_{decay} (MR_2) vs. [Et_3P] were linear in each case and exhibited slopes in the range of (5 - 16) × 10^9 M^{-1} s^{-1} (Figure 3.10, Table 3.3). Quenching of the tetrellylenes with tricyclohexylphosphine (Cy_3P) was found to be characterized by bimolecular rate constants *ca*. 2 times lower than those with Et_3P; the plots of k_{decay} vs [Cy_3P] are shown in Fig. 3.11. Behaviour consistent with large equilibrium constants for the reactions with MMe_2 and MPh_2 was observed, while with the more sterically hindered tetrellylenes, $MMes_2$, equilibrium constants of 18,000 M^{-1} ($SiMes_2$) and 1,500 M^{-1} ($GeMes_2$) were measured. Transient absorption spectra of the tetrellylene-Et_3P complexes closely resemble those of the homologous tetrellylene-Cy_3P complexes, and are shown in Fig. 3.12-3.15.

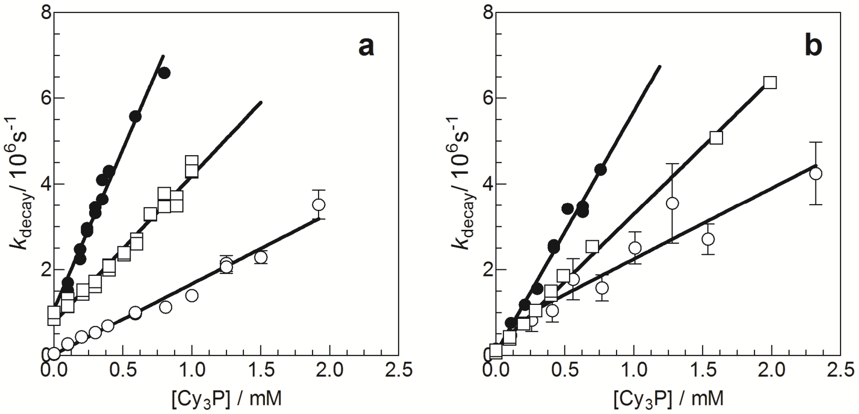

Figure 3.11. Plots of the pseudo-first-order decay coefficients (k_{decay}) of the MR_2 absorptions (R = Me (●), Ph (□), Mes (o)) vs [Cy_3P], where (a) M = Si, (b) M = Ge.

Table 3.3. Forward rate (k_1) and equilibrium constants (K_1) for complexation of transient silylenes and germylenes with P-donors in hexanes at 25 °C.

	k_1 / 10^9 $M^{-1}s^{-1}$ [K_1 / M^{-1}]	
Donor	Et_3P	Cy_3P
$SiMe_2$	16 ± 1 [a]	7.5 ± 0.6 [a]
$SiPh_2$	10 ± 1 [a]	3.4 ± 0.2 [a]
$SiMes_2$	5.2 ± 0.6 [a]	1.7 ± 0.1 [18,000 ± 4,000]
$GeMe_2$	14 ± 2 [a]	5.6 ± 0.5 [a]
$GePh_2$	8.5 ± 0.8 [a]	3.1 ± 0.1 [a]
$GeMes_2$	5.3 ± 0.6 [a]	1.7 ± 0.5 [1500 ± 700]

a. $K_{eq} > 25,000\ M^{-1}$

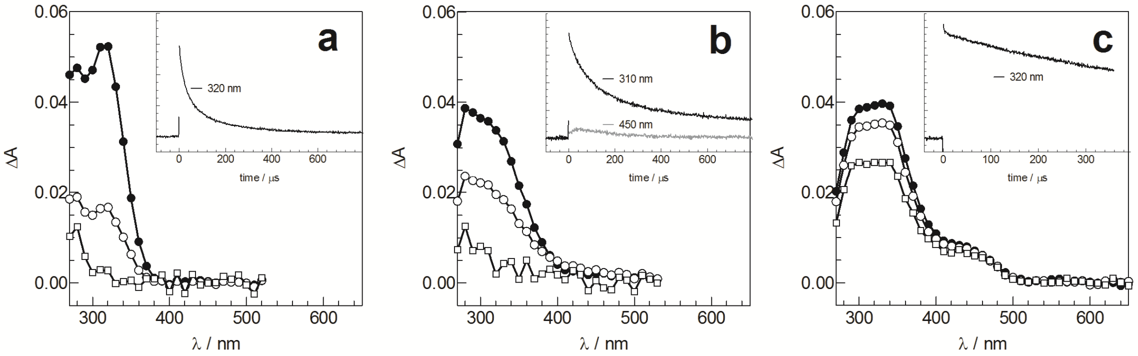

Figure 3.12. (a) Transient absorption spectra from laser flash photolysis of a hexane solution of **43** containing 5.6 mM Et_3P, recorded 0-8 µs (●), 83.2-91.2 µs (o), and 699.2-707.2 µs (□) after the laser pulse; (b) transient absorption spectra from laser flash photolysis of a hexane solution of **44a** containing 5.6 mM Et_3P, recorded 0-8 µs (●), 83.2-91.2 µs (o), and 699.2-707.2 µs (□) after the laser pulse; (c) transient absorption spectra from laser flash photolysis of a hexane solution of **45** containing 3.5 mM Et_3P, recorded 1.9-5.1 µs (●), 55.7-58.9 µs (o), and 279.7-282.9 µs (□) after the laser pulse. The inset in each of the figures shows transient absorbance vs. time profiles recorded at representative wavelengths in the spectra.

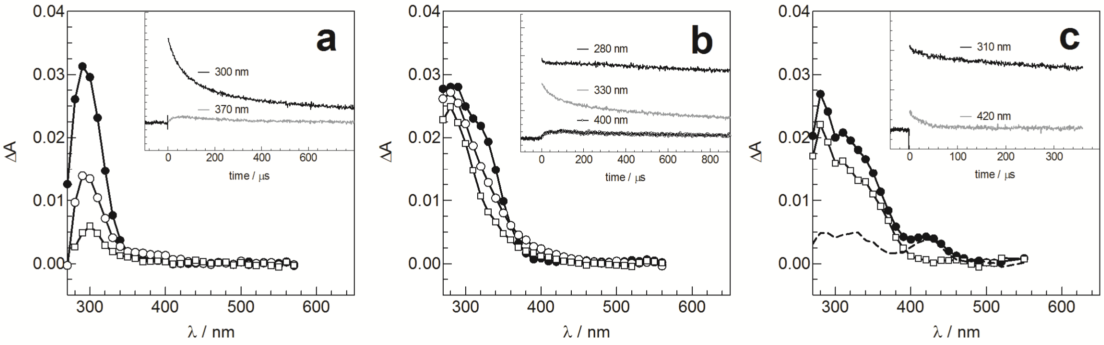

Figure 3.13. (a) Transient absorption spectra from laser flash photolysis of a hexane solution of **36** containing 4.7 mM Et$_3$P, recorded 0-6.4 μs (●), 139.2-147.2 μs (o), and 699.2-707.2 μs (□) after the laser pulse; (b) transient absorption spectra from laser flash photolysis of a hexane solution of **37** containing 4.8 mM Et$_3$P, recorded 4.8-12.8 μs (●), 139.2-147.2 μs (o), and 699.2-707.2 μs (□) after the laser pulse; (c) transient absorption spectra from laser flash photolysis of a hexane solution of **46** containing 4.8 mM Et$_3$P, recorded 1.9-5.1 μs (●) and 279.7-282.9 μs (□) after the laser pulse, dotted line shows the difference spectrum between (●) and (□). The inset in each of the figures shows transient absorbance vs. time profiles recorded at representative wavelengths in the spectra.

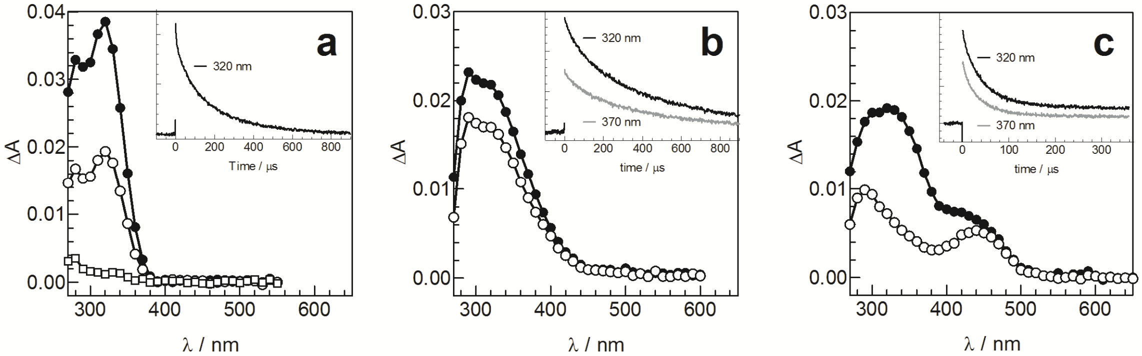

Figure 3.14. (a) Transient absorption spectra from laser flash photolysis of a hexane solution of **43** containing 3.76 mM Cy$_3$P, recorded 4.8-12.8 μs (●), 91.2-99.2 μs (o), and 699.2-707.2 μs (□) after the laser pulse; (b) transient absorption spectra from laser flash photolysis of a hexane solution of **44a** containing 2.0 mM Cy$_3$P, recorded 59.2-65.6 μs (●) and 139.2-147.2 μs (o) after the laser pulse; (c) transient absorption spectra from laser flash photolysis of a hexane solution of **45** containing 2.75 mM Cy$_3$P, recorded 10.9-13.4 μs (●) and 87.7-90.9 μs (o) after the laser pulse. The inset in each of the figures shows transient absorbance vs. time profiles recorded at representative wavelengths in the spectra.

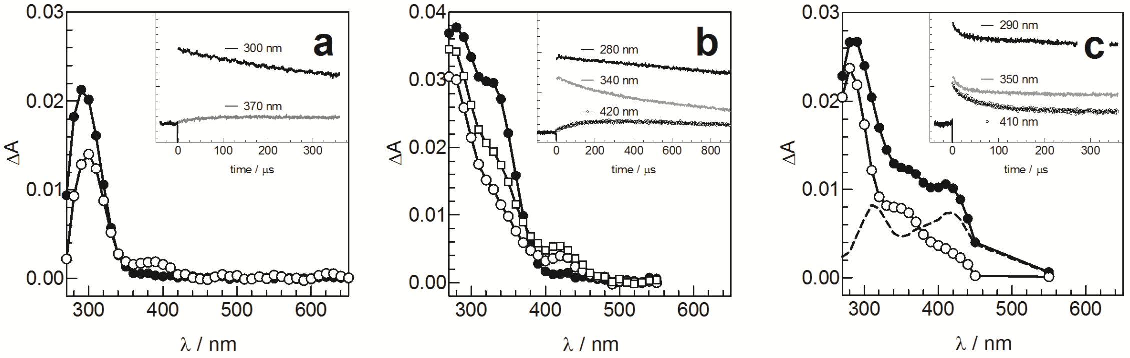

Figure 3.15. (a) Transient absorption spectra from laser flash photolysis of a hexane solution of **36** containing 1.36 mM Cy_3P, recorded 0-3.2 μs (●) and 279.7-282.9 μs (o) after the laser pulse; (b) transient absorption spectra from laser flash photolysis of a hexane solution of **37** containing 3.6 mM Cy_3P, recorded 11.2-17.6 μs (●), 379.2-388.8 μs (o), and 859.2-867.2 μs (□) after the laser pulse; (c) transient absorption spectra from laser flash photolysis of a hexane solution of **46** containing 2.3 mM Cy_3P, recorded 0-2.6 μs (●) and 279.7-282.9 μs (o) after the laser pulse, dotted line shows the difference spectrum between (●) and (o). The inset in each of the figures shows transient absorbance vs. time profiles recorded at representative wavelengths in the spectra.

Experimental details of the study of the reactions of transient silylenes $SiMe_2$, $SiPh_2$ and $SiMes_2$ with amines are described in Chapter 5; the values of the rate and equilibrium constants obtained therein are summarized in Table 3.4. Some reactions of germylenes with the same set of amines have been investigated previously (see Chapter 1, Table 1.7, also Table 3.4), therefore only new results are described here, namely, $GeMe_2$ with Et_2NH, $GeMes_2$ with Et_2NH, and $GeMes_2$ with Et_3N. The latter experiment was also used to determine the screening effects by Et_3N at concentrations below 1.5 mM, which was used to aid the determination of equilibrium constant for the reaction of $SiMes_2$ with Et_3N (see Chapter 5).

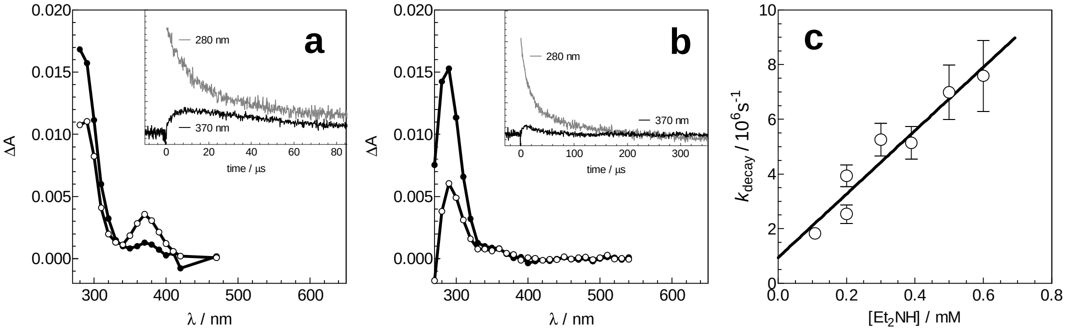

Figure 3.16. Transient absorption spectra from laser flash photolysis of a hexane solution of $GeMe_2$ precursor **36** containing (a) 0.6 mM Et_2NH, recorded 0.64-1.28 µs (●) and 9.12-10.08 µs (o) after the laser pulse; (b) 5.3 mM Et_2NH, recorded 1.92-4.48 µs (●) and 36.48-40.32 µs (o) after the laser pulse; the insets show the transient decay profiles recorded at 280 nm and 370 nm. (c) Plot of the pseudo-first-order decay coefficients (k_{decay}) *versus* [Et_2NH] for $GeMe_2$ absorptions.

$GeMe_2$ was quenched by Et_2NH in a manner consistent with a large equilibrium constant. The germylene decayed to yield the $GeMe_2$-Et_2NH complex, the absorption spectra of which was similar to those exhibited by other $GeMe_2$-amine complexes.[4] Transient absorption spectra obtained from a hexane solution of **36** containing 0.6 mM and 5.3 mM Et_2NH are shown in Fig. 3.16 a and b, respectively. The ultimate product of the decay of the complex is the corresponding digermene, which can be detected at both concentrations of the amine; at higher amine concentrations adventitious impurities in the amine sample may contribute to the weaker absorptions. The rate constant for complexation ($k_1 = (12 \pm 3) \times 10^9$ M^{-1} s^{-1}) was determined from the plot of k_{decay} vs [Et_2NH], which displayed good linearity (Fig. 3.16c).

The bulkier germylene $GeMes_2$ reacts with Et_2NH and Et_3N in a manner consistent with low equilibrium constants – the lifetime of the germylene is unaffected upon addition of the amines, but the apparent intensity of the germylene signals is diminished. The plot of $\Delta A_0/\Delta A_{eq}$ vs $[Et_2NH]$ exhibited excellent linearity and afforded $K_1 = 510 \pm 20$ M^{-1} (Fig. 3.17a). Transient absorption spectra in the presence of 20 mM Et_2NH indicate the presence of a new strongly absorbing transient species assignable to the $GeMes_2$-donor complex (Fig. 3.17b). Measurement of the equilibrium constant for complexation with Et_3N is not possible due to secondary photolysis of the amine. This complication limits the amount of Et_3N that can be added to the precursor solution to 1.3 mM, at which concentration the $GeMes_2$ signal intensity is 90% of its value in the absence of the amine. This affords an upper limit of 100 M^{-1} for the equilibrium constant in this case. Transient absorption spectra recorded with a hexanes solution of **46** in the presence of 1.3 mM Et_3N does not show any new transient absorption bands other than those due to the germylene and the amine photolysis product.

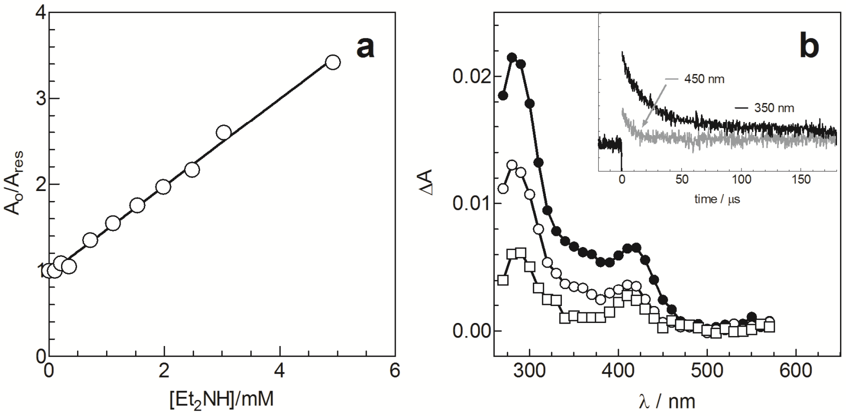

Figure 3.17. (a) Plot of ΔA_0 / ΔA_{eq} vs $[Et_2NH]$ for the $GeMes_2$ absorption monitored at 550 nm, (b) transient absorption spectra from laser flash photolysis of a hexane solution of **46** containing 20 mM Et_2NH, recorded 0.96-2.56 µs (●), 18.24-19.84 µs (o), and 139.84-141.44 µs (□) after the laser pulse; the inset shows transient decay profiles recorded at 350 nm and 450 nm.

Table 3.4. Forward rate (k_1) and equilibrium constants (K_1) for complexation of transient silylenes and germylenes with N-donors in hexanes at 25 °C.

	k_1 / 10^9 $M^{-1}s^{-1}$ [K_1 / M^{-1}]		
Donor	$nBuNH_2$	Et_2NH	Et_3N
$SiMe_2$	17 ± 2 ^{a}	16 ± 3 ^{a}	9.8 ± 0.8 ^{a}
$SiPh_2$	11 ± 3 ^{a}	8.3 ± 0.7 ^{a}	3.9 ± 0.4 ^{a}
$SiMes_2$	10 ± 3 ^{a}	3.5 ± 0.5 [4,700 ± 700]	^{b} [130 ± 60]
$GeMe_2$	12 ± 3 $^{a, c}$	12 ± 3 ^{a}	8.7 ± 0.7 $^{a, c}$
$GePh_2$	10.1 ± 0.6 $^{a, d}$	7.3 ± 0.9 $^{a, e}$	2.8 ± 0.9 $^{a, f}$
$GeMes_2$	7.0 ± 0.3 $^{a, d}$	^{b} [510 ± 20]	^{b} [≤ 100]

a. K_{eq} > 25,000 M^{-1}; *b*. k_1 indeterminable; *c*. ref. 4; *d*. ref. 6; *e*. ref. 5; *f*. ref. 10

3.3. Discussion

Table 3.5 lists the absolute rate and equilibrium constants for the 28 tetrellylene-donor systems studied in this work and earlier by other workers. The equilibrium constants for complexation of $SiMe_2$ with Et_2O and THF are in good agreement with those measured by Walsh and co-workers in the gas phase for the $SiMe_2$-Me_2O system ($K_1 \approx 3{,}600$ M^{-1}) and the $SiMe_2$-THF system ($K_1 \approx 30{,}000$ M^{-1}).[11,12]

The equilibrium constants for the six tetrellylene + Et_2O pairs span a range of about 5 orders of magnitude, corresponding to a range in binding free energies of -3.4 to +3.3 kcal mol^{-1} (standard state: gas phase, 1 atm at 25 ^oC, Table 3.6). The trend in Lewis acidities follows the order $MPh_2 > MMe_2 >> MMes_2$ for both the silylenes and germylenes. Phenyl substituents provide larger σ- and π- withdrawing effects compared to methyl, leading to enhanced Lewis acidity. The differences in the binding energies of silylenes and germylenes with the O-donors indicate 1.4-2.2 kcal mol^{-1} more favourable complexation with the silylene, consistent with theoretical predications for other tetrellylene-O-donor systems.[14-17] Mesityl groups provide substantially greater steric hindrance than methyl and phenyl substituents, which significantly destabilizes the Lewis acid-base complexes with $SiMes_2$ and $GeMes_2$. Thus, mesityl for phenyl substitution results in reductions in binding free energies of ca. 5 kcal mol^{-1} in the Et_2O complexes. Steric interactions provided by the Lewis base influence the differences in the equilibrium constants for complexation in the germylene series, leading to a trend in the K_1^{GePh2} / K_1^{GeMes2} ratio of THF >> Et_2O > MeOH (Table 3.5). A similar trend is expected to develop for the silylene series as well; however the actual equilibrium constants for

Table 3.5. Forward Rate (k_1) and Equilibrium Constants (K_1) for Complexation of Transient Silylenes and Germylenes with Chalcogen and Pnictogen Donors in Hexanes at 25 °C.

	k_1 / 10^9 $M^{-1}s^{-1}$ [K_1 / M^{-1}]					
Donor	$SiMe_2$	$SiPh_2$	$SiMes_2$	$GeMes_2$	$GePh_2$	$GeMe_2$
MeOH	15 ± 1 [a,b]	18 ± 2 [a,b]	1.0 ± 0.1 [a,b]	[c, d] [15 ± 6]	6 ± 1 [c] [3,300 ± 800]	[c, d] [900 ± 60]
Et_2O	[d] [1,260 ± 50]	15 ± 4 [7,100 ± 600]	[d] [0.9 ± 0.1]	[d] [~0.06]	[d] [160 ± 10]	[d] [110 ± 10]
THF	17 ± 2 [e, f]	15 ± 1 [e, f]	[d] [2.4 ± 0.4]	[c, d] [1.1 ± 0.2]	6.3 ± 0.6 [c] [23,000 ± 5,000]	11 ± 2 [c] [10,000 ± 4,000]
THT	21 ± 2 [e, g]	15 ± 2 [e, g]	7 ± 2 [1,500 ± 100]	[d] [1,000 ± 100]	10 ± 2 [e]	17 ± 2 [e]
Et_2S	22 ± 3 [e]	10 ± 1 [e]	[d] [54 ± 3]	[d] [40 ± 4]	8.3 ± 0.4 [e]	18 ± 2 [e]
$BuNH_2$	17 ± 2 [e, h]	11 ± 3 [e, h]	10 ± 3 [e, h]	7.0 ± 0.3 [e, i]	10.1 ± 0.6 [e, i]	12 ± 3 [e, j]
Et_2NH	16 ± 3 [e, h]	8.3 ± 0.7 [e, h]	3.5 ± 0.5 [e, h] [4,700 ± 700]	[d] [510 ± 20]	7.3 ± 0.9 [e, k]	12 ± 3 [e]
Et_3N	9.8 ± 0.8 [e h]	3.9 ± 0.4 [e, h]	[d, h] [130 ± 60]	[d] [≤ 100]	2.8 ± 0.9 [e, k]	8.7 ± 0.7 [e, j]
Et_3P	16 ± 1 [e]	10 ± 1 [e]	5.2 ± 0.6 [e]	5.3 ± 0.6 [e]	8.5 ± 0.8	14 ± 2
Cy_3P	7.5 ± 0.6 [e]	3.4 ± 0.2 [e]	1.7 ± 0.1 [18,000 ± 4,000]	1.7 ± 0.5 [1500 ± 700]	3.1 ± 0.1 [e]	5.6 ± 0.5 [e]

a. Ref. 1; *b*. K_1 indeterminable; *c*. Ref. 7; *d*. k_1 indeterminable ($\geq 0.002K_1$ $M^{-1}s^{-1}$); *e*. $K_1 >$ 25,000 M^{-1}; *f*. Ref. 3; *g*. Ref. 9; *h*. Ref. 13*; i*. Ref. 6*; j*. Ref. 4; *k*. Ref. 10.

complexation with MeOH and THF could not be measured for all three silylenes; those for complexation of $SiMe_2$ and $SiPh_2$ with THF are too large to measure, while those for complexation with MeOH are inaccessible because of the high reactivity of the complexes toward catalytic H-transfer (see Chapter 4).[1] In contrast, germylene-MeOH complexes can be detected even in neat alcohol solution, owing to higher activation barriers for proton transfer.[18] The equilibrium constants for complexation of $SiMe_2$ and $SiPh_2$ with THF are above the measurement limit ($K_1 \geq 25{,}000$ M^{-1}), estimates of $K_1 \approx 10^5$ and 10^6 M^{-1} s^{-1}, respectively, can be derived for the complexation of the two silylenes with THF based on the trends observed in the germylene data. The value for $SiMes_2$ is in good agreement with the value determined by Baggott et al for the reaction of $SiMe_2$ with THF in the gas phase ($K_1 \approx 30{,}000$ M^{-1}).[11,12] Similarly, values of $K_1 \approx 10^4$, 1.5×10^5, and 150 M^{-1} can be estimated for complexation of $SiMe_2$, $SiPh_2$ and $SiMes_2$ with MeOH, respectively, in hexanes at 25 ^oC.

Significant steric effects of the mesityl groups impede the complexation reactions of $SiMes_2$ and $GeMes_2$, leading to measurable values of K_1 for all $MMes_2$-donor systems except those with Et_3P and $nBuNH_2$, which are larger than the measurable limit (Table 3.6). In every case $SiMes_2$ forms the more stable complex with a given donor than $GeMes_2$, as illustrated by the plot of the binding free energies of the germylene complexes versus those for the corresponding silylene complexes in Fig. 3.18. The plot reveals a good linear correlation with a slope of 0.9 ± 0.1, indicating the difference in Lewis acidities of $SiMes_2$ and $GeMes_2$ is essentially independent of the Lewis base

Table 3.6. Standard Gibbs free energy values (standard state: gas phase at 1 atm, 25 °C) for the Lewis acid-base complexes of silylenes and germylenes chalcogen and pnictogen donors in hexanes at 25 °C (in kcal mol^{-1}).

	ΔG^0 / kcal mol^{-1}					
	$SiMe_2$	$SiPh_2$	$SiMes_2$	$GeMes_2$	$GePh_2$	$GeMe_2$
MeOH	[a]	[a]	[a]	+0.3 ± 0.3	-2.9 ± 0.2	-2.1 ± 0.1
Et_2O	-2.3 ± 0.1	-3.4 ± 0.1	+2.0 ± 0.1	+3.3 ± 0.4	-1.1 ± 0.1	-0.9 ± 0.1
THF	-4.2 ± 0.1[b]	[c]	+1.4 ± 0.1	+1.8 ± 0.1	-4.0 ± 0.1	-3.5 ± 0.3
THT	[c]	[c]	-2.4 ± 0.1	-2.2 ± 0.1	[c]	[c]
Et_2S	[c]	[c]	-0.5 ± 0.1	-0.3 ± 0.1	[c]	[c]
$BuNH_2$	[c]	[c]	[c]	[c]	[c]	[c]
Et_2NH	[c]	[c]	-3.3 ± 0.1	-1.8 ± 0.1	[c]	[c]
Et_3N	[c]	[c]	-1.0 ± 0.4	≥ -0.8	[c]	[c]
Et_3P	[c]	[c]	[c]	[c]	[c]	[c]
Cy_3P	[c]	[c]	-4.1 ± 0.1	-2.8 ± 0.2	[c]	[c]

[a] K_1 indeterminable; [b] Gas phase, see ref. 12; [c] upper limit is -6.0 kcal mol^{-1}.

strength of the donor. The intercept gives the average difference in the binding energies of $SiMes_2$ and $GeMes_2$ with the same donor, which is 0.7 ± 0.3 kcal mol^{-1} more negative for the silylene.

In contrast to the previous classification of silylenes and germylenes as hard Lewis acids, our results show that complexation with softer bases of the third row donors (phosphines and sulfides) is significantly stronger than that with the second-row homologues (amines and ethers, respectively).

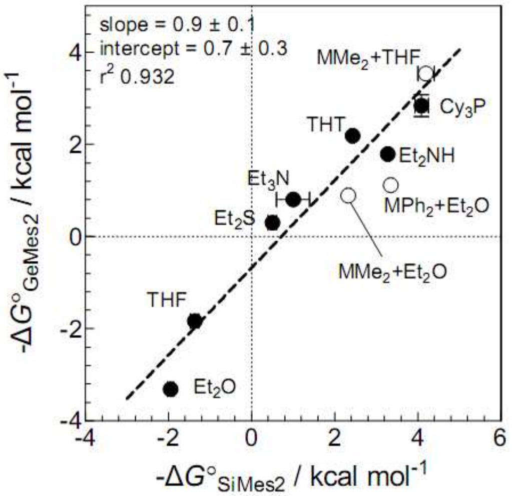

Figure 3.18. Plot of experimental free energies of complexation of $GeMes_2$ vs those of $SiMes_2$ with the same donor in hexanes at 25 °C (●); the dashed line is the least-squares fit of the seven data points. The points for the MPh_2-Et_2O, MMe_2-Et_2O and MMe_2-THF systems are also included in the plot (o) (reference state: gas phase, 1 atm and 25 °C)

The standard free energies of complexation of $SiMe_2$ and $GeMe_2$ with a series of 17 chalcogen and pnictogen donors were calculated using the G4[19] method.[8] The calculated binding free energies of the MMe_2-Et_2O, MMe_2-THF and $SiMe_2$-Me_2O complexes match the experimentally determined values to within 1 kcal mol^{-1}, and predict the same order of stability of the $SiMe_2$-O-donor and $GeMe_2$-O-donor complexes as was determined experimentally. The ordering of the calculated ΔG values for $SiMe_2$ and $GeMe_2$ with chalcogen and pnictogen hydrides was found to be $H_2S < H_2O < PH_3 < NH_3$, analogous to that predicted previously for SiH_2[14, 20] and GeH_2[14]. Calculations by Su and Chu at the B3LYP/6-311G(d) and MP2/6-311G(d) levels of theory appear to overestimate the binding energy for the $GeMe_2$-H_2O complex, and thus predicted different ordering.[21]

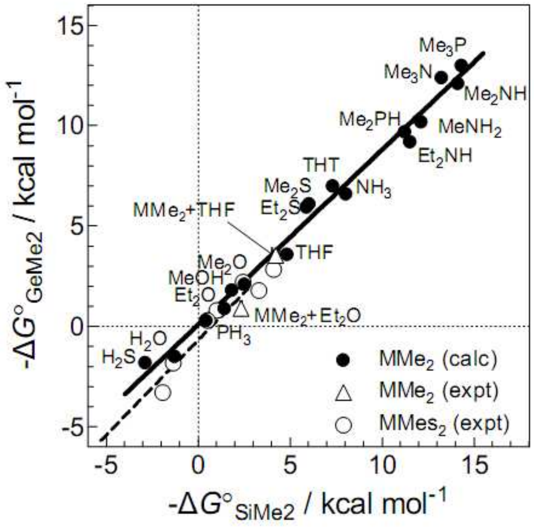

Figure 3.19. Plot of calculated (G4) binding free energies of $GeMe_2$-donor complexes vs those of the corresponding $SiMe_2$-donor complexes (●). The experimental data points for the MMe_2-O-donor (Δ) and $MMes_2$-donor (o) Lewis pairs (see Fig. 3.18) are also included in the figure (standard state gas phase, 1 atm, and 25 ^{o}C). Ref. 8

Figure 3.19 shows a plot of the calculated ΔG values for the 17 $GeMe_2$-donor complexes versus those of the corresponding $SiMe_2$-donor complexes. The experimentally determined values are also included for comparison to demonstrate the level of agreement between the predicted trends and those obtained experimentally. The slope of the plot (0.87 ± 0.03) is in very good agreement with that of the experimental plot for the $MMes_2$ systems, and thus predicts a similar difference in the Lewis acidities of $SiMe_2$ and $GeMe_2$ as was found experimentally for the $MMes_2$ analogs. The calculated variation in Lewis acidities of the MH_2 systems is slightly larger, as given by a slope of 0.80 ± 0.04 (see Chapter 1, section 1.5.1).[14]

The experimental binding energies of the $SiMes_2$ and $GeMes_2$ complexes do not show a significant correlation with the gas phase proton affinity (PA) of the donors,[22-23] as shown in Fig. 3.20. The calculated (G4) binding energies of the MMe_2-donor complexes display a rough correlation with the PA values of the donors, predicting an

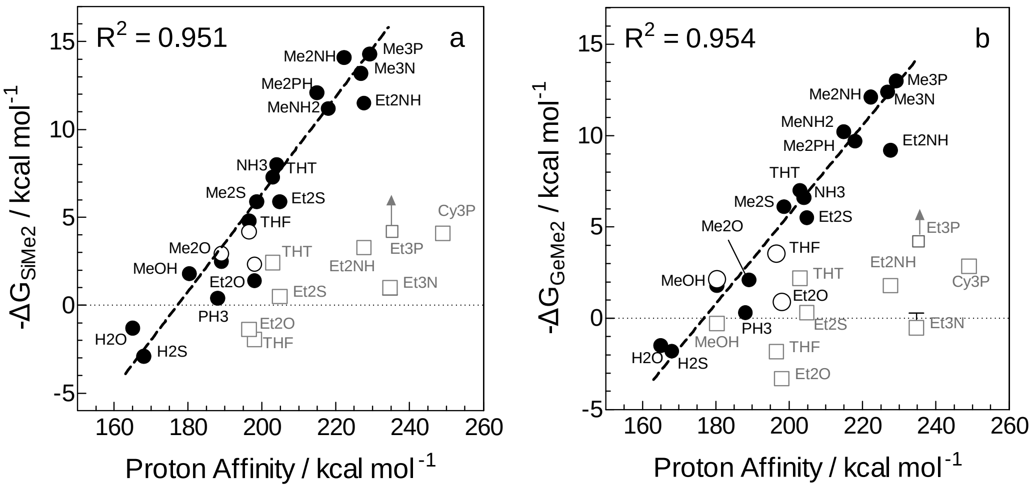

Figure 3.20. Plots of calculated (G4; ●) and experimental (hexanes; △) standard free energies of complexation of chalcogen and pnictogen donors with (a) SiMe$_2$ and (b) GeMe$_2$ vs the (experimental) proton affinities of the donors. The experimental values for the SiMes$_2$− and GeMes$_2$−donor complexes (□; hexanes) are also shown in the plots; upward-pointing arrows indicate that only lower limits of the binding energies could be determined. The reference state is the gas phase at 1 atm and 25 °C in all cases.

increase in the binding energy with increasing PA value. A similar trend is observed with the MMes$_2$ data. Analogous correlations are obtained with the donor gas basicities (GB);[22] however we employ PA because this is the only measure of gas-phase basicity that is available for Cy$_3$P.[23]

The plots of Fig. 3.20 predict nearly equal binding energies for the complexes of SiMe$_2$ with Me$_2$NH, Me$_3$N and Me$_3$P; the same is true for the corresponding GeMe$_2$ complexes. This can be attributed in part to destabilization of the complexes with increasing steric bulk on the amine. Steric interactions in the complexes with phosphines are minimal, owing to longer M-P bonds relative to M-N bonds.

The calculated binding enthalpies of the complexes were found to correlate well with empirical E_B and C_B constants for the donors as defined by Drago and co-workers.[24-25] The "*E* and *C* model" gives a double-scale enthalpy equation (eq. 3.4) which predicts the enthalpy of adduct formation for the acid-base pair ($-\Delta H$) either in the gas phase or in poorly-solvating media.[26-28] The empirically determined covalent (*C*) and electrostatic (*E*) parameters for each acid (A) and base (B) are defined as the susceptibility of A or B to form either covalent bonds (*C*) or electrostatic bonds (*E*). Depending on which term dominates, the interaction can be either *charge-controlled* (*E* dominates) or *frontier-controlled* (*C* dominates).

$$-\Delta H = E_A E_B + C_A C_B \qquad (3.4)$$

The database is referenced to C_A and E_A values of I_2 which were set at 2.0 and 0.5, respectively, while the C_B and E_B values of DMA ($CH_3C(O)N(CH_3)_2$) were set to 3.92 and 2.35, respectively.[26] The model does not account for steric destabilization or stabilization from π-backbonding that may be present in the adducts, and thus the predicted binding enthalpies of systems in which such factors play a role deviate from the true values.[26-28] The relative softness or hardness of a given Lewis acid or base is reflected in the magnitude of the *C*/*E* ratio. If the *C*/*E* ratio is comparatively large the species is classified as soft, while species classified as hard are characterized by a relatively small *C*/*E* ratio.

The least-squares fits of the calculated binding enthalpies to eq. 3.4 are shown in Fig. 3.21; the binding enthalpies of the MMe_2-Me_3N Lewis pairs clearly deviate from the

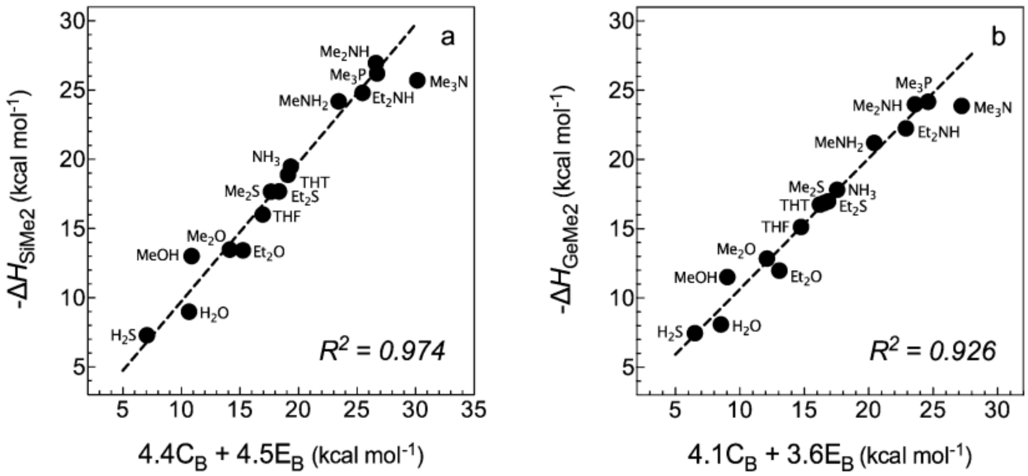

Figure 3.21. Plots of calculated (G4) gas-phase binding enthalpies of (a) $SiMe_2$ and (b) $GeMe_2$ with chalcogen and pnictogen donors, vs the two-parameter functions defined by least-squares fitting of the data to eq 3.4.

correlations due to steric interactions and were thus excluded from the fits. The corresponding PMe_3 complexes obey the correlations, however, indicating that steric interactions are not significant in these cases, while π-backbonding is not applicable for our systems. The calculated structures of the amine and phosphine complexes indicate that bonds to phosphorous are longer than those to nitrogen, which is likely responsible for the differences in steric factors. The values of C_A and E_A for $SiMe_2$ obtained from the correlation are 4.4 ± 0.2 (kcal $mol^{-1})^{1/2}$ and 4.5 ± 0.4 (kcal $mol^{-1})^{1/2}$, respectively, while those for $GeMe_2$ are 4.1 ± 0.3 (kcal $mol^{-1})^{1/2}$ and 3.6 ± 0.6 (kcal $mol^{-1})^{1/2}$, respectively. The roughly equal C_A and E_A values suggest that $SiMe_2$ and $GeMe_2$ are of *borderline* softness, significantly softer and more acidic than, for example, BMe_3 (E_A = 2.90; C_A = 3.60).[24-25]

The transient absorption spectra of the tetrellylene-donor complexes are summarized in Table 3.7. The spectra of the $MMes_2$-Et_2O and $MMes_2$-THF complexes were obtained in 4-5 M substrate or neat substrate as solvent, while the rest were recorded as dilute hexane solutions. The UV-vis spectrum of each of the silylene-donor complexes is quite similar to that of the corresponding germylene-donor complex. In the ether systems (Et_2O and THF) the SiR_2-O-donor complex absorbs at a slightly longer wavelength than the corresponding GeR_2-O-donor complex; the same is true for the S-donor complexes (THT and Et_2S). The magnitude of the spectral shift does not correlate with the relative magnitude of the binding energies, since the germylene complexes are more weakly bound than the analogous silylene complexes. Tetrellylene-chalcogen complexes consistently absorb at longer wavelength than the corresponding tetrellylene-pnictogen complexes, which could be a reflection of the differences in the binding energies. There does not appear to be a systematic variation in λ_{max} with the donor atoms within the same group, and the direction and magnitude of the spectral shift varies irregularly among the tetrellylene systems.

The rate constants for complexation of the six tetrellylenes with nearly all the donors were measured in hexanes solutions, with the exception of a handful of cases (Table 3.5). The values are within a factor of 20 from the diffusional rate ($k_{diff} \approx 2.3 \times 10^{10}$ M^{-1} s^{-1} at 25 ^{o}C in hexanes), indicative of an enthalpically barrierless process for complexation. The data show a modest decrease in the rate constant with increasing steric bulk on the tetrel center, such that in general the trend in the rate constants is k_{MMe2} >

Table 3.7. UV-vis absorption maxima (λ_{max}) of the Lewis acid-base complexes of transient silylenes and germylenes with chalcogen and pnictogen donors in hexanes at 25 °C.[a]

	λ_{max} / nm					
Donor	$SiMe_2$	$SiPh_2$	$SiMes_2$	$GeMes_2$	$GePh_2$	$GeMe_2$
none	465	300, 515	290, 580	325, 550	300, 500	470
Et_2O	305 [b]	300, 375	310	(≤ 280) [c, d]	360	300
THF	310 [e]	295, 370 [e]	310, 380(sh) [c]	285, 380 [f]	360 [f]	310 [f]
THT	325 [g]	300, 370 [g]	300, 400(sh)	270, 400(sh)	350	320
Et_2S	320	300, 370	<280, 400(sh)	<270, 400(sh)	350	300
Et_2NH	280 [h]	300 [h]	320 [h]	280, 340, 430	320 [i]	280
Et_3N	270 [h]	310 [h]	290 [h]	[l]	340 [i]	290 [j]
Et_3P	310	315	320	280, 310	330	290
Cy_3P [k]	320	320	340	310	340	280

a. This work unless otherwise noted; *b*. Cyclohexane, 20 °C, ref 29; *c*. In the neat substrate as solvent; *d*. Only the short wavelength band was observed; *e*. Ref. 3; *f*. Ref. 7; *g*. Ref. 9; *h*. Ref. 13; *i*. Ref. 10; *j*. Ref. 4 *k*. Cyclohexane solution. *l*. Complex not detected

$k_{MPh2} > k_{MMes2}$. However, the reactions of the O-donors proceed with both dimethyl and diphenyl systems with nearly equal rate constants, and a factor of ca. 2 rate inhibition is observed upon Ge-for-Si substitution. This difference is absent in all the other donor systems, perhaps reflecting a greater steric demand on the complexation process associated with the shorter bonds to oxygen than those to N, S and P in the corresponding adducts.

3.4. Conclusions

As a result of the work presented here, the general knowledge of the complexation properties of silylenes and germylenes has been expanded substantially. The results indicate that there is no systematic variation in the UV-vis spectra of the adducts with the donor atoms within the same group. The rate constants for complexation are within a factor of 20 of the diffusional rate constant in hexanes at 25 ^{o}C and vary only modestly with tetrellylene or donor structure. Equilibrium constants for complexation of $SiMes_2$ and $GeMes_2$ with two ethers, two sulfides, two amines and a phosphine were determined, along with those for complexation of MMe_2 and MPh_2 with Et_2O. The results reveal that silylenes are more Lewis acidic than the homologous germylenes by ca. 1 pK unit, independent of substitution on either the tetrellylene or the donor over a range of ca. 7 kcal mol^{-1} in binding free energy. The Lewis acidities of silylenes and germylenes decrease in the order $MPh_2 > MMe_2 >> MMes_2$, stemming from σ- and π-electron withdrawing effects of the phenyl group compared to methyl, and steric destabilization of the adducts by mesityl groups. The correlations of the calculated binding enthalpies with Drago's basicity scale led to the re-classification of silylenes and germylenes as *borderline* soft Lewis acids, not *hard* Lewis acids as previously thought.[15] This is demonstrated by binding energies of the complexes, which are strongest for phosphine systems and weakest for O-donor systems, with those for N- and S- donors in the middle.

3.5. References

1. Leigh, W. J.; Kostina, S. S.; Bhattacharya, A.; Moiseev, A. G., *Organometallics* **2010,** *29* (3), 662.

2. Moiseev, A. G.; Leigh, W. J., *Organometallics* **2007,** *26*, 6268.

3. Moiseev, A. G.; Leigh, W. J., *Organometallics* **2007,** *26*, 6277.

4. Leigh, W. J.; Lollmahomed, F.; Harrington, C. R., *Organometallics* **2006,** *25*, 2055.

5. Huck, L. A.; Leigh, W. J., *Organometallics* **2007,** *26*, 1339.

6. Leigh, W. J.; Harrington, C. R.; Vargas-Baca, I., *J. Am. Chem. Soc.* **2004,** *126*, 16105.

7. Leigh, W. J.; Lollmahomed, F.; Harrington, C. R.; McDonald, J. M., *Organometallics* **2006,** *25*, 5424.

8. Kostina, S. S.; Singh, T.; Leigh, W. J., *Organometallics* **2012,** *31* (9), 3755.

9. Kostina, S. S.; Leigh, W. J., *J. Am. Chem. Soc.* **2011,** *133* (12), 4377.

10. Leigh, W. J.; Harrington, C. R., *J. Am. Chem. Soc.* **2005,** *127*, 5084.

11. Baggott, J. E.; Blitz, M. A.; Frey, H. M.; Lightfoot, P. D.; Walsh, R., *Int. J. Chem. Kinet.* **1992,** *24*, 127.

12. The original estimates of the equilibrium constants by Baggott et al [ref. 11] for the reactions of $SiMe_2$ with Me_2O and THF in the gas phase were 400 and 12,000 atm^{-1}, respectively. Re-analysis of the data of Fig. 6 in ref. 11 according to eq. 3.1 yields estimates of 145 and 1200 atm^{-1}, respectively. These estimates correspond to ΔG values of -2.94 and -4.19 kcal mol^{-1}, respectively, in good agreement with the experimental value for the $SiMe_2$-Et_2O system studied in this work. We thank Professor Walsh for a helpful discussion which led to the determination of these values from ref. 11.

13. Kostina, S. S.; Singh, T.; Leigh, W. J., *J. Phys. Org. Chem.* **2011,** *24*, 937.

14. Schoeller, W. W.; Schneider, R., *Chem. Ber.* **1997,** *130* (7), 1013.

15. Olah, J.; De Proft, F.; Veszpremi, T.; Geerlings, P., *J. Phys. Chem. A* **2005,** *109*, 1608.

16. Heaven, M. W.; Metha, G. F.; Buntine, M. A., *J. Phys. Chem. A* **2001,** *105*, 1185.

17. Su, M.-D., *Chem. Eur. J.* **2004,** *10* (23), 6073.

18. Lollmahomed, F.; Huck, L. A.; Harrington, C. R.; Chitnis, S. S.; Leigh, W. J., *Organometallics* **2009,** *28* (5), 1484.

19. Curtiss, L. A.; Redfern, P. C.; Raghavachari, K., *J. Chem. Phys.* **2007,** *126*, 084108.

20. Raghavachari, K.; Chandrasekhar, J.; Gordon, M. S.; Dykema, K., *J. Am. Chem. Soc.* **1984,** *106* (20), 5853.

21. Su, M.-D.; Chu, S.-Y., *J. Phys. Chem. A* **1999,** *103* (50), 11011.

22. Hunter, E. P. L.; Lias, S. G., *J. Phys. Chem. Ref. Data* **1998,** *27* (3), 413.

23. Liu, M.; Yang, I.; Buckley, B.; Lee, J. K., *Org. Lett.* **2010,** *12* (21), 4764.

24. Drago, R. S.; Dadmun, A. P.; Vogel, G. C., *Inorg. Chem.* **1993,** *32* (11), 2473.

25. Drago, R. S.; Joerg, S., *J. Am. Chem. Soc.* **1996,** *118* (11), 2654.

26. Vogel, G. C.; Drago, R. S., *J. Chem. Ed.* **1996,** *73*, 701.

27. Drago, R. S.; Vogel, G. C.; Needham, T. E., *J. Am. Chem. Soc.* **1975,** *93*, 6014.

28. Drago, R. S., *Coord. Chem. Rev.* **1980,** *33*, 251.

29. Levin, G.; Das, P. K.; Bilgrien, C.; Lee, C. L., *Organometallics* **1989,** *8*, 1206.

4. Chapter 4 – Silylene insertion into the O-H bonds of alcohols

4.1. Overview

The mechanism of the reactions of dimethyl- and diphenylsilylene ($SiMe_2$ and $SiPh_2$) with alcohols (MeOL or t-BuOL, L = H or D) in hexanes solution have been studied. The data are consistent with a mechanism involving initial complexation to form the corresponding silylene-alcohol complex, followed by catalytic H(D)-transfer from O to Si. Rate constants for the first step are close to the diffusional rate constant in hexanes in all cases, while the equilibrium constants could not be measured owing to the fast secondary reaction of the complexes. The catalytic H(D)-migration proceeds with rate constants within a factor of 10 of the diffusion limit, while the putative unimolecular process is too slow to be measured in solution. Kinetic isotope effects for the catalytic H(D)-transfer process are in the 2.5 to 1 range in all cases except the $SiPh_2$-t-BuOL complex, where it is much larger (k_{HH}/k_{DD} = 11 ± 2). This value is consistent with a mechanism for catalysis involving a double proton transfer. As in our previous studies, $SiMe_2$ and $SiPh_2$ were generated photochemically from precursors **43** and **44a**, respectively.

4.2. Reactions of $SiMe_2$ with alcohols (MeOH, MeOD, t-BuOH, t-BuOD)

Addition of submillimolar concentrations of MeOL to a hexane solution of **43** as either the protiated or O-deuterated isotopomers (L = H or D) caused the decay of the silylene to become pseudo first order and the formation of the corresponding disilene to be suppressed. A new transient species was detected in the range characteristic of $SiMe_2$-O-donor complexes (300 – 310 nm, see Chapter 3), whose absorbance increased with increasing alcohol concentration, accompanied by a decrease in the lifetime until they became too short-lived to be detected. The species is assigned to the $SiMe_2$-MeOL complex. The absorptions were superimposed on a long-lived component centered at 290 nm whose contribution diminished with increasing alcohol concentration; this is most likely due to an oligomerization product of Si_2Me_4, whose yield is reduced as the reaction with alcohol outcompetes the dimerization process. The complex exhibited lifetimes that were longer than those of the free silylene under the same conditions. The plots of k_{decay} vs [MeOL] for the silylene *and* for the complexes were linear in both cases, and are shown in Fig. 4.1. Analysis of the data according to eq. 4.1 yielded rate constants in the range of $(1.5 - 2.1) \times 10^{10}$ M^{-1} s^{-1} (Table 4.1). The rate constants for quenching of the silylene by MeOH and MeOD are in good agreement with the previously reported values in cyclohexane. [1-4] The kinetic isotope effects (KIE) on both the first and the second step of the reaction (eq. 4.2) with MeOL are unity.

$$k_{decay} = k_{-1} + k_1[\mathrm{ROL}] \qquad (4.1)$$

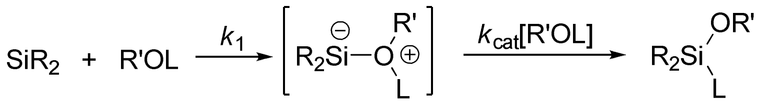

(4.2)

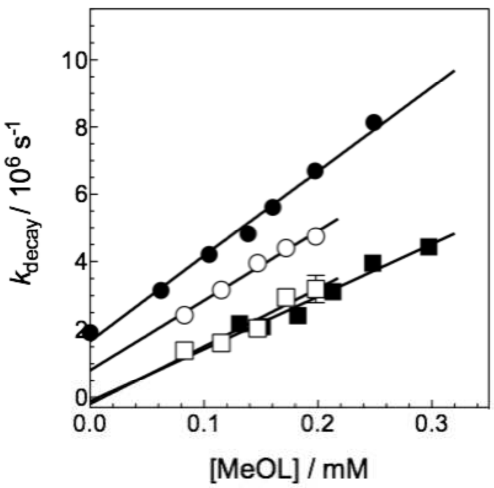

Figure 4.1. Plots of the pseudo-first order rate coefficients (k_{decay}) for the decay of free $SiMe_2$ (λ_{max} = 465 nm; L = H (●) and D (○)), and of the $SiMe_2$-MeOL complex (monitored at 310 nm; L = H (■) and D (□)), *vs*. [MeOL]. The solid lines are the linear least squares fits of the data to equation 4.1.

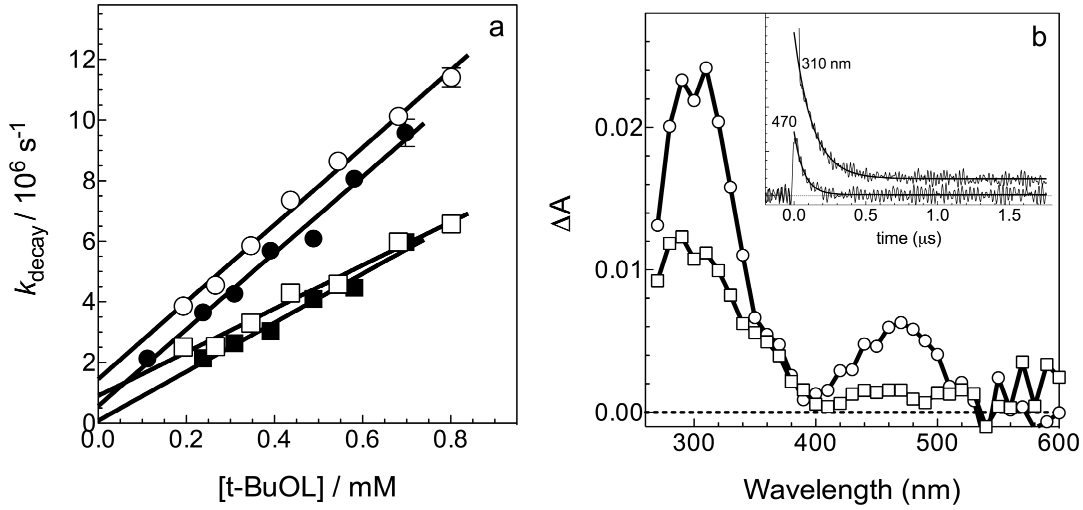

Figure 4.2. (a) Plots of the pseudo-first order decay rate coefficients (k_{decay}) vs. [*t*-BuOL], of free $SiMe_2$ (λ_{max} = 465 nm; L = H (●) and D (○)) and of the $SiMe_2$-*t*-BuOL complex (λ_{max} = 300 nm; L = H (■) and D (□)). (b) Transient absorption spectra from a deoxygenated solution of **43** in anhydrous hexanes containing 1.16 mM *t*-BuOD, recorded 16-26 ns (○) and 138-150 ns (□) after the laser pulse; the insets show transient decay traces recorded at monitoring wavelengths of 310 and 470 nm.

Figure 4.2a shows the plots of k_{decay} vs [t-BuOL] obtained from analogous experiments performed employing t-BuOL as the substrate; transient absorption spectra recorded in the presence of 1.16 mM t-BuOD are shown in Fig. 4.2b; the absorption band at λ_{max} = 300 nm is assigned to the $SiMe_2$-t-BuOD complex. As in the MeOL experiments, the lifetimes of the complexes are longer than the lifetimes of free $SiMe_2$ under the same conditions. Analysis of the plots of Fig. 4.2a according to eq. 4.1 affords rate constants of ca. 1.4×10^{10} M^{-1} s^{-1} for the complexation step independent of isotopic substitution on the alcohol, while those for the subsequent reaction by the $SiMe_2$-t-BuOL complexes are 8.1×10^9 and 7.2×10^9 M^{-1} s^{-1} for L = H and D, respectively. As in the reactions of this silylene with MeOL, the KIEs are approximately unity for both first and the second step of the reaction.

4.3. Reactions of $SiPh_2$ with alcohols (MeOH, MeOD, t-BuOH, t-BuOD)

The decay rate of $SiPh_2$ accelerated in the presence of either MeOL or t-BuOL, dimerization was suppressed and a new species was detectable in the range characteristic of $SiPh_2$-O-donor complexes (λ_{max} ~ 360 nm, see Chapter 3). The formation of the complexes occured on similar timescales as the decay of the silylene, and the signals increased in maximum intensity as a function of alcohol concentration. As with the $SiMe_2$-ROL systems, the lifetimes of the complexes increased with increasing alcohol concentration, and at each concentration was longer than that of the free silylene. Figure 4.3 shows the plots of k_{decay} vs [ROL] corresponding to the silylene absorptions, while those corresponding to the absorptions of the $SiPh_2$-ROL complexes are shown in Fig. 4.4.

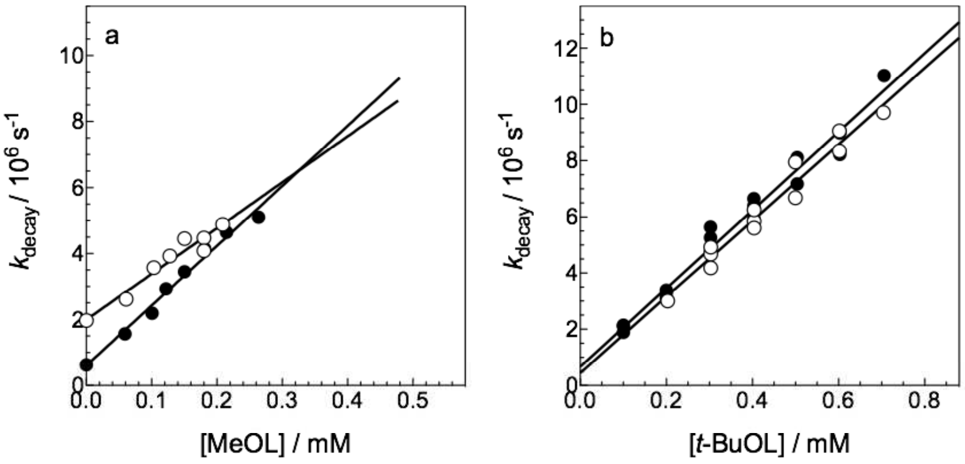

Figure 4.3. Plots of the pseudo-first order decay rate coefficients (k_{decay}) of $SiPh_2$ *vs*. [ROL] (L = H (●) or D (○)) for (a) R = Me and (b) R = *t*-Bu, in hexanes at 25 °C. The solid lines are the best linear least squares fits of the data to equation 4.1. The data were obtained in the same experiments as those represented in Figure 4.4.

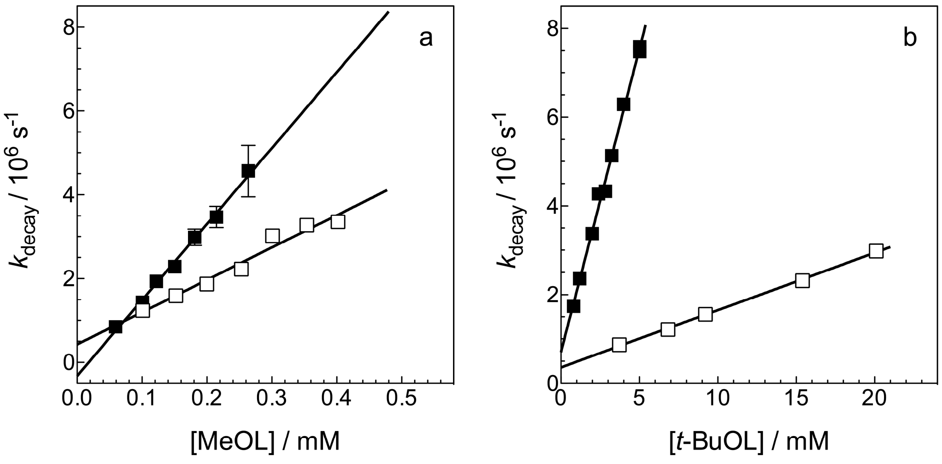

Figure 4.4. Plots of the pseudo-first order decay rate constants (k_{decay}) of the $SiPh_2$-ROL complexes (L = H (■) or D (□)) *vs*. [ROL] for (a) R = Me and (b) R = *t*-Bu, in hexanes at 25 °C. The solid lines are the best linear least squares fits of the data to equation 4.1.

Table 4.1. Absolute rate constants (in units of 10^9 $M^{-1}s^{-1}$) for reaction of $SiMe_2$ and $SiPh_2$ with alcohols in deoxygenated hexanes at 25 °C (k_1), and for quenching of the transient absorptions due to the corresponding silylene-ROL complexes by ROL (k_{cat}).[a]

	$SiMe_2$		*$SiPh_2$*	
ROL	k_1[b] / 10^9 $M^{-1}s^{-1}$	k_{cat}[c] / 10^9 $M^{-1}s^{-1}$	k_1[d] / 10^9 $M^{-1}s^{-1}$	k_{cat}[e] / 10^9 $M^{-1}s^{-1}$
MeOH	21 ± 3	15 ± 3	18 ± 2	18 ± 1
MeOD	20 ± 3	17 ± 5	14 ± 2	8.6 ± 1.2
t-BuOH	14 ± 2	8.1 ± 1.2	14 ± 1	1.4 ± 0.1
t-BuOD	13 ± 1	7.2 ± 0.9	11 ± 1	0.13 ± 0.02

[a] Rate constants are the mean of two independent measurements in each case, while errors are listed as the standard deviation of the average value. [b] monitored at 470 nm. [c] monitored at 310 nm. [d] monitored at 520-530 nm. [e] monitored at 350 nm.

The data are consistent with the reaction proceeding by a two step mechanism shown in eq. 4.2. The rate constants for complexation of $SiPh_2$ with MeOL and t-BuOL obtained by analysis of the data of Fig. 4.3 according to eq. 4.1, are listed in Table 4.1 along with those for $SiMe_2$. The rate constants for complexation span the range of 1.1×10^{10} to 1.8×10^{10} M^{-1} s^{-1} and are marginally smaller for the t-BuOL systems than for the MeOL systems. All eight reactions studied here proceed with rate constants within a factor of 2 of the diffusional limit in hexanes. The lifetimes of the $SiPh_2$-ROL complexes are significantly less responsive to alcohol concentration than the corresponding $SiMe_2$-ROL complexes, with the $SiPh_2$-ROD complexes reacting significantly slower than the corresponding $SiPh_2$-ROH complexes. Thus, KIE values of 2.1 ± 0.3 and 11 ± 2 were determined for the reactions of $SiPh_2$-MeOL complex with MeOL and $SiPh_2$-t-BuOL complex with t-BuOL, respectively. Owing to the much lower reactivity of the $SiPh_2$-t-BuOD complex towards t-BuOD, the complex was detectable even in the presence of 50 mM t-BuOD, as is shown in Fig. 2b of ref. 5.

4.4. Discussion

Absolute rate constants for the reactions of photochemically generated $SiMe_2$ and $SiPh_2$ with MeOL and t-BuOL were measured by laser flash photolysis methods, and are all within a factor of 2 of the diffusional limit in hexanes. There is no measurable kinetic isotope effect on the rate constants for the reaction, as expected for a simple complexation process as the first step. The data can be compared to the reaction of $SiMes_2$ with the same set of substrates (Table 4.2), where the rate constants for complexation are at least a factor of 10 slower than those for the analogous $SiMe_2$ and $SiPh_2$ systems.[5] The difference in reactivity presumably reflects the steric factors associated with the more bulky mesityl group. Indeed, the plots k_{decay} vs [ROL] for this silylene exhibit upward curvature, consistent with reversible complexation in the first step.[5]

The Lewis acid-base complexes of $SiMe_2$ and $SiPh_2$ with the alcohols were directly detected in each case. They exhibit absorption bands centered in the ranges characteristic of $SiMe_2$- and $SiPh_2$-O-donor complexes ($SiMe_2$-ORR', $\lambda_{max} \approx 310$ nm; $SiPh_2$-ORR', $\lambda_{max} \approx 360$ nm). The complexes are observable only within limited ranges of alcohol concentration, their lifetimes decreasing with increasing alcohol concentration. The behaviour is consistent with catalytic H-transfer within the complex, where the catalysis is provided by a second molecule of the alcohol (eq. 4.2); catalytic rate constants (k_{cat}) were determined from the variation in the decay rate constants of the complexes with ROH(D) concentration and are listed in Table 4.1. Significant kinetic isotope effects on k_{cat} were found for the reactions of $SiPh_2$ with MeOH(D) and t-BuOH(D). The largest KIE was measured for t-BuOH(D) ($k_H/k_D = 11 \pm 2$); the value is of a magnitude consistent with a mechanism involving two protons in flight in the transition state (eq. 4.3). The unimolecular H-transfer process within the complex proceeds too slowly for a rate constant (k_2) to be measured in any of the cases studied, and only an upper limit (of $k_2 \leq 10^6$ s^{-1}) could be estimated for the rate constant in the case of the $SiPh_2$-*t*-BuOH complex from the intercept of the plot of k_{decay} vs [t-BuOH].

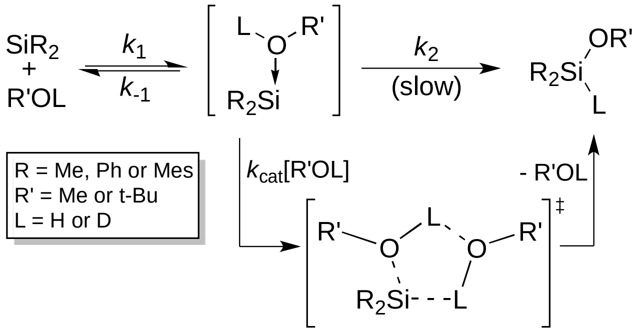

(4.3)

In the more sterically hindered system, $SiMes_2$, the data are indicative of the $SiMes_2$-alcohol complexes acting as steady-state intermediates which could not be directly observed. A non-linear dependence of k_{decay} ($SiMes_2$) on [ROL] (Fig. 4.5) is indicative of lower equilibrium constants for the complexation step compared to those with $SiMe_2$ and $SiPh_2$. The steady-state situation renders both the K_1 and k_{cat} indeterminable; however, ratios of k_{cat}/k_{-1} were obtained from the analysis of the data according to eq. 4.4 and are listed in Table 4.2. Based on the trends established in Chapter 3, equilibrium constants for complexation of $SiMe_2$, $SiPh_2$ and $SiMes_2$ with MeOH can be estimated to be $K_1 \approx 10^4$, 1.5×10^5, and 150 M^{-1}, respectively (see Chapter 3 for discussion). However, in the reactions of less hindered silylenes with alcohols reversibility in the first step cannot be detected due to a much larger K_1 than with $SiMes_2$.

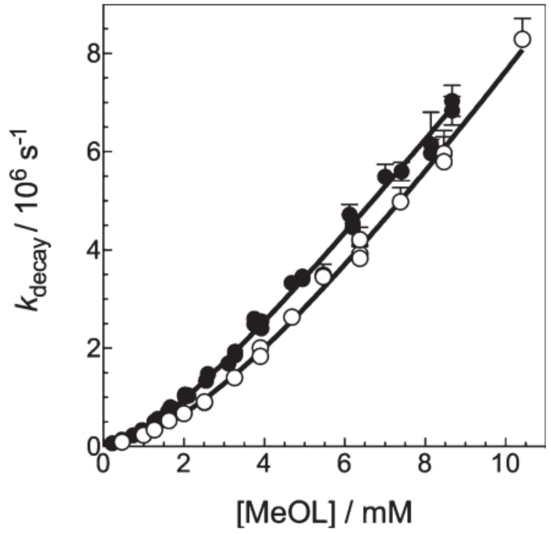

Figure 4.5. Plots of the pseudo-first-order rate constants for the decay of $SiMes_2$ vs [MeOL] (L = H, (●) or D (o)) in hexanes at 25 C. The solid lines are the nonlinear least-squares fits of the data to eq 4.4. Reproduced from ref. [5]

Table 4.2. Kinetic data for the reaction of $SiMes_2$ with alcohols in deoxygenated hexanes at 25 °C.[a]

ROL	k_1 / 10^9 $M^{-1}s^{-1}$	(k_{cat}/k_{-1}) / M^{-1}
MeOH	1.01 ± 0.09	550 ± 150
MeOD	1.26 ± 0.25	220 ± 100
t-BuOH	0.136 ± 0.005	36 ± 7
t-BuOD	0.136 ± 0.009	64 ± 5

[a] From ref. 5

$$k_{decay} = k_1\left(\frac{k_{cat}}{k_{-1}}\right)[ROL]^2 / \left(1 + \left(\frac{k_{cat}}{k_{-1}}\right)[ROL]\right) \qquad (4.4)$$

The calculated standard free energy surfaces for the reactions of two molecules of methanol with SiH_2[6] and $SiMe_2$,[7] are shown in Figure 4.6, illustrating the similarities and differences between the reaction profiles for $SiMe_2$ and the parent silylene. Interestingly, the only notable difference between the two systems is in the initial complexation step, due to the substantially lower Lewis acidity of the substituted silylene compared to the parent. The overall reaction barriers are quite similar, the catalytic H-transfer pathways winning out over the non-catalyzed pathways by a quite substantial margin in both cases.

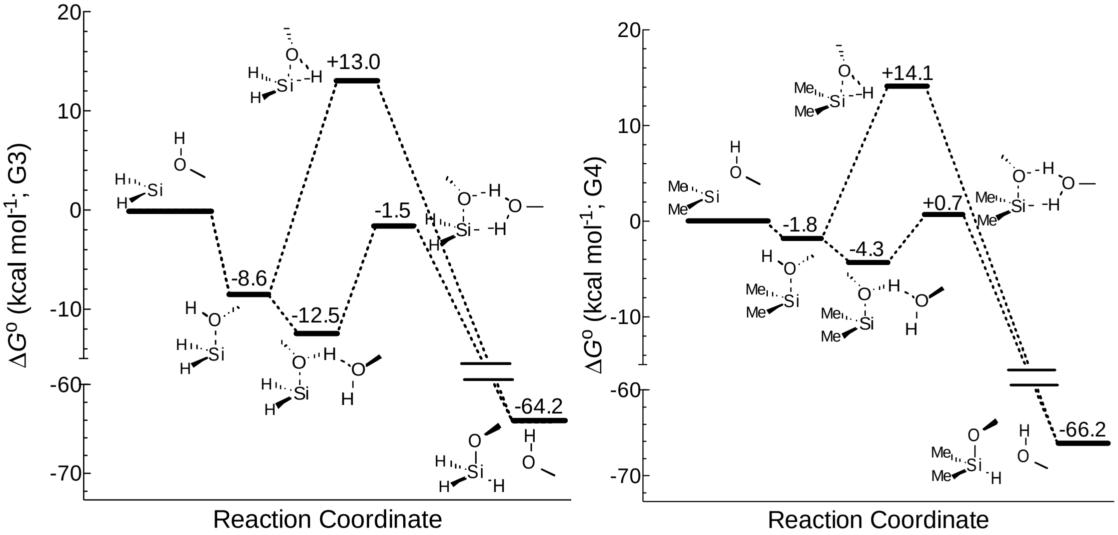

Figure 4.6. Standard free energy surfaces for the O-H insertion reactions of SiH_2 and $SiMe_2$ with MeOH, calculated at the G3 and G4 levels of theory, respectively (298.15 K, kcal mol^{-1}).$^{6-7}$

4.5. Conclusion

The O-H insertion reactions of $SiMe_2$ and $SiPh_2$ with MeOL and t-BuOL (L = H or D) have been investigated by laser flash photolysis. The data are consistent with a mechanism involving the initial formation of the corresponding silylene-alcohol complex, followed by catalytic H-migration from the oxygen to the silicon center to yield the final product; the catalyst in the second step is a second molecule of the substrate. Rate constants for complexation are invariably fast in all cases, slowing down significantly only in the more sterically hindered systems ($SiMes_2$). Unimolecular H migration with the complexes is too slow to be measured under our conditions. A remarkably large deuterium KIE was measured for the t-BuOH catalyzed proton transfer in the $SiPh_2$-t-BuOH complex (k_H/k_D = 11 ± 2), consistent with a concerted double proton transfer involving a 5-membered transition state.

4.6. References

1. Levin, G.; Das, P. K.; Bilgrien, C.; Lee, C. L., *Organometallics* **1989,** *8*, 1206.

2. Levin, G.; Das, P. K.; Lee, C. L., *Organometallics* **1988,** *7*, 1231.

3. Shizuka, H.; Tanaka, H.; Tonokura, K.; Murata, K.; Hiratsuka, H.; Ohshita, J.; Ishikawa, M., *Chem. Phys. Lett.* **1988,** *143*, 225.

4. Moiseev, A. G.; Leigh, W. J., *Organometallics* **2007,** *26*, 6277.

5. Leigh, W. J.; Kostina, S. S.; Bhattacharya, A.; Moiseev, A. G., *Organometallics* **2010,** *29* (3), 662.

6. Becerra, R.; Cannady, J. P.; Walsh, R., *J. Phys. Chem. A* **2011,** *115* (17), 4231.

7. Kostina, S. S.; Singh, T.; Leigh, W. J., *J. Phys. Org. Chem.* **2011,** *24*, 937.

5. Chapter 5 – Silylene insertion into the N-H bonds of amines

5.1. Overview

The formal N-H insertion reactions of $SiMe_2$, $SiPh_2$ and $SiMes_2$ with the amines n-$BuNH_2$, Et_2NH and Et_3N have been investigated using steady-state and laser flash photolysis experiments. The results indicate that the first step is the formation of Lewis acid-base complexes with rate constants in the range of $10^9 – 2 \times 10^{10}$ M^{-1} s^{-1} in hexanes at 25 ^oC. The rate constants decrease with increasing steric bulk on nitrogen, opposite to the trend expected based on gas phase basicities. The complexes are proposed to undergo catalyzed H transfer by a second molecule of amine, with catalytic rate constants on the order of 10^6 M^{-1} s^{-1} or less. Catalysis proceeds at least four orders of magnitude more slowly than the corresponding catalytic reaction of silylene-alcohol complexes.

The silylenes $SiMe_2$, $SiPh_2$ and $SiMes_2$ were generated using photochemical precursors **43**, **44a** and **45**, respectively.

5.2. Results

5.2.1. Product studies

Photolysis of deoxygenated solutions of the $SiMe_2$ precursor **43** in neat *tert*-butylamine, Et_2NH, or 2,2-dimethylaziridine at 5°C was shown to yield the corresponding silanamines resulting from the formal N-H insertion of $SiMe_2$ in yields of ~85%.[1] We investigated the course of the reaction of $SiPh_2$ with Et_2NH in dilute cyclohexane-d_{12}, since this reaction has not been previously characterized. This section of the document focuses on the identification and characterization of products formed from the photolysis of **44a** in cyclohexane-d_{12} containing Et_2NH.

Photolysis of a cyclohexane-d_{12} solution of **44a** (0.05 M) containing Et_2NH (0.05 M) and 1,4-dioxane (0.01 M, internal standard), with the course of the reaction being monitored by ^1H NMR spectroscopy, resulted in the formation of disilane **67** in (103 ± 4)% yield relative to consumed **44a**. Silanamine **83**, the expected product of N-H insertion of $SiPh_2$ with Et_2NH, was formed as the major product ((95 ± 3)% relative to consumed Et_2NH) (eq. 5.1). Relative to consumed **44a**, however, the yield was only about 40%, indicating that a significant portion of the silylene generated participates in other reactions. Concentration vs time plots (see Fig. 5.1) revealed a distinct induction period of roughly 5 min during which the concentration of Et_2NH does not change and **83** does not form. Closer inspection of the ^1H NMR spectra recorded within the first 5 min of photolysis revealed that diphenylsilanol **84** was formed initially (tentatively identified based on its ^1H NMR and ^1H-^{29}Si HMBC), reaching a maximum yield at about 8 minutes,

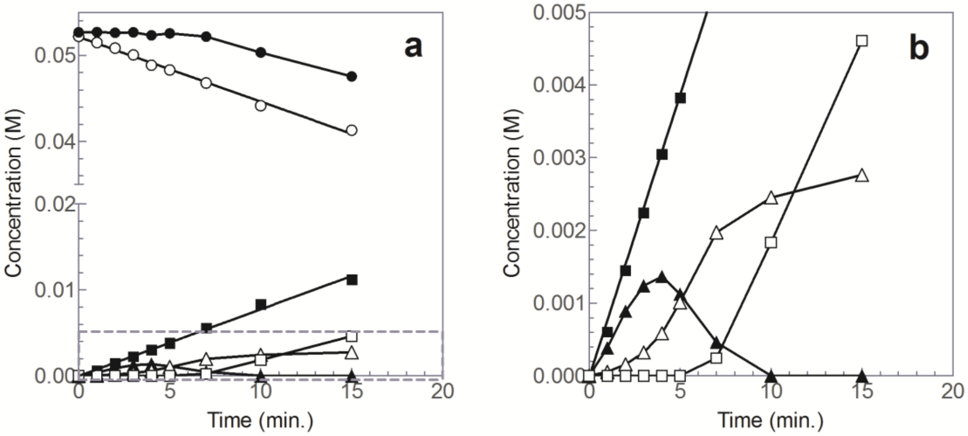

Figure 5.1. (a) Concentration vs. time plots for 254 nm irradiation of deoxygenated solutions of **44a** (0.05 M) in C_6D_{12} containing Et_2NH (0.05 M), H_2O (ca. 0.002 M) and 1,4-dioxane (0.01 M). The linear portions of the plot were analyzed by linear least squares and are characterized by the following slopes: **44a** (o) = -0.00075 ± 0.00004, **67** (■) = 0.00078 ± 0.00004, **83** (□) = 0.00055 ± 0.00001, Et_2NH (●) = -0.00058 ± 0.00002, **84** (▲), **85** (Δ). (b) expansion of (a) between 0 and 0.005 M.

after which it was consumed to afford disiloxane **85**. At the point when **84** is almost completely consumed, **83** starts to form and Et_2NH begins to disappear (Fig. 5.1). Disiloxane **85** was identified based on its characteristic ^{29}Si NMR shift at δ -19.2 ppm ($^1J_{Si\text{-}H}$ = 219.6 Hz).[2-3] ^{1}H NMR spectra of the photolysis mixture at various times in the experiment are shown in Fig. 5.2.

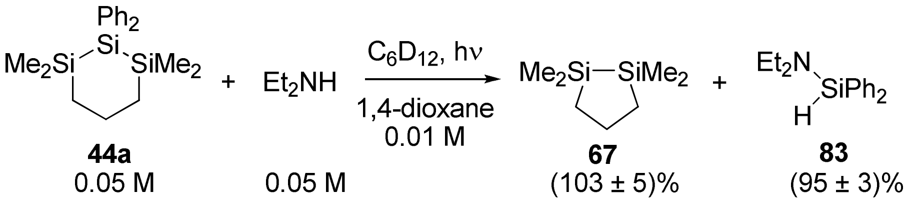

(5.1)

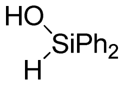

84

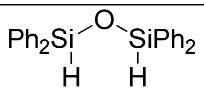

85

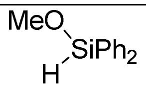

71

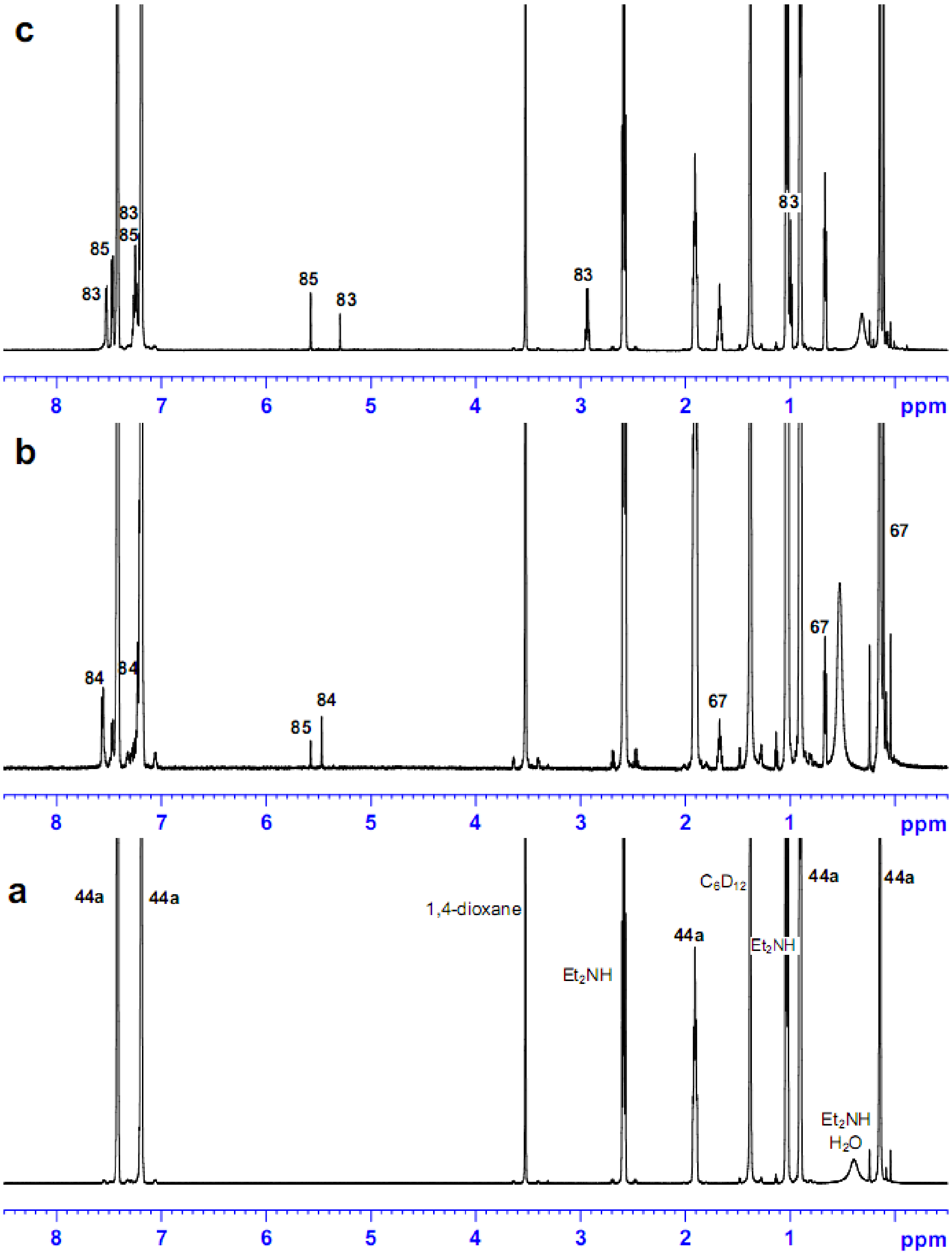

Figure 5.2. 600 MHz ^{1}H NMR spectra of a solution of 0.05 M **44a**, 0.05 M Et$_2$NH, 0.005 M H_2O and 0.01 M 1,4-dioxane in C_6D_{12}, after a) 0 min of photolysis; b) 3 min of photolysis; c) 15 min of photolysis

The reaction responsible for the formation of **84** and **85** is that of $SiPh_2$ with water. The estimated concentration of water present at the beginning of the experiment (see Fig. 5.2a) is about 2 mM. The results indicate that the formation of products with water is much more efficient than that with the amine, even when the amine is present in great excess. In order to investigate whether the silanol is formed by reaction of the silylene-amine complex with water or if the silanamine reacts with water to yield the silanol, the following control experiment was conducted.

Addition of 0.01 M MeOH to the above photolyzate resulted in complete conversion of **83** to methoxydiphenylsilane (**71**) and regeneration of Et_2NH in less than 5 min at room temperature.

Based on the results of the above experiment, it is not possible to tell whether the silanol is formed via a fast reaction of the $SiPh_2$-Et_2NH complex with water, or via the longer-timescale pathway involving the reaction of silanamine with water to form the silanol.

5.2.2. Kinetic measurements

Addition of sub-millimolar concentrations of n-BuNH$_2$, Et$_2$NH, Et$_2$ND, or Et$_3$N to hexanes solutions of **43** resulted in a reduction of the lifetime of the silylene and suppression of the formation of the disilene. Plots of the pseudo-first order decay coefficients (k_{decay}) of SiMe$_2$ vs [amine] according to eq. 5.2 were linear in each case (Fig. 5.3a-b). The rate constants are within a factor of two of the diffusional rate in hexane (k_{diff} = 2.3 × 10^{10} M^{-1} s^{-1}),[4] and those for Et$_2$NH are roughly two times lower than the published values for the reaction of SiMe$_2$ with N-methylpyrrolidine and pyrrolidine in cyclohexane.[5] The differences are consistent with the lower viscosity of hexane relative to that of cyclohexane.[6] Analogous results were obtained in experiments with **44a;** the silylene lifetime was decreased and silylene dimerization was quenched (see the plots of k_{decay} vs [S] in Fig. 5.3c-d), both to an increasing extent with increasing amine concentration. The second-order rate constants for reaction of SiPh$_2$ with these substrates (Table 5.1) are approximately a factor of 2 lower than those for SiMe$_2$, in general agreement with the trends observed for other substrates.[7] For both silylenes, the rate constants appear to correlate with the steric bulk at nitrogen, opposite to the trends expected based on amine gas phase basicities.[8] Deuterium substitution of the N-H proton in diethylamine had no effect on the rate constant for either silylene, consistent with Lewis acid-base complexation being the rate-determining step for silylene decay. The rate constants for reactions of the two silylenes with the four amines that were studied are listed in Table 5.1.

$$k_{decay} = k_0 + k_1[S] \qquad (5.2)$$

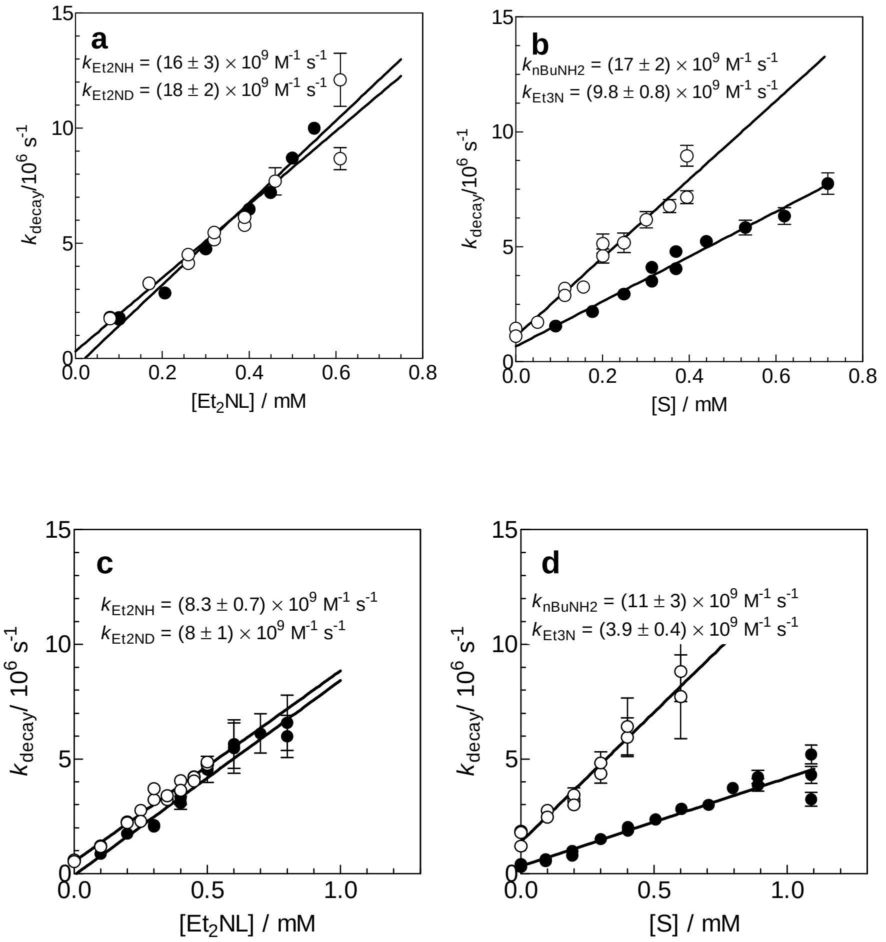

Figure 5.3. Plots of the first order decay rate coefficients (k_{decay}) vs. [S] of (a) $SiMe_2$ with S = Et_2NL, where L = H (o) and L = D (•); (b) $SiMe_2$ with S = n-$BuNH_2$ (o) and Et_3N (•); (c) $SiPh_2$ with S = Et_2NH (o) and Et_2ND (•); (d) $SiPh_2$ with S = n-$BuNH_2$ (o) and Et_3N (•) in hexanes at 25 °C. The solid lines are the linear least squares fits of the data to eq. 5.2. $SiMe_2$ and $SiPh_2$ were monitored at 470 nm and 530 nm, respectively.

Transient absorption spectra recorded for **43** in the presence of sufficiently high concentrations of amine to reduce the silylene lifetime to undetectable levels are shown in

Fig 5.4 for the three amines. The spectra show new long-lived transient absorptions centered at $\lambda_{max} \approx 290$ nm in each case. In the case of Et_3N these new absorptions overlap with those due to a shorter-lived transient resulting from the direct photolysis of the amine ($\lambda_{max} < 290$ nm, $\tau \approx 2$ μs);[9-10] unlike the others, this amine absorbs appreciably at the excitation wavelength ($\varepsilon_{248\ nm} = 103 \pm 4\ M^{-1}\ cm^{-1}$). The long-lived transients are assigned to the corresponding silylene-amine complexes; their spectra are in excellent agreement with previously reported spectra of the complexes of $SiMe_2$ with other amines in cyclohexane at 20°C[5] and in hydrocarbon matrixes at 77 K.[11] The transient absorption spectra of the $SiPh_2$-amine complexes are also very similar to each other, exhibiting absorption bands with apparent maxima at $\lambda_{max} \approx 300$ nm and a shoulder absorption at ca. 360 nm (Fig. 5.5). The absorption spectrum of the $SiPh_2$-Et_3N complex was also superimposed on an intense short-lived absorption band resulting from triethylamine photolysis, as was also observed with $SiMe_2$.

With the typical laser intensities used in these experiments (~ 98 – 102 mJ), the SiR_2-amine complexes decayed with second order kinetics, and the second order rate coefficients ($2k/\varepsilon$) decrease with increasing substitution on the amine (Table 5.1). The $2k/\varepsilon$ values measured for the $SiMe_2$-Et_2NH and –Et_2ND complexes were the same within experimental error, suggesting that proton transfer is not involved in the second-order decay pathway of the complexes. A possible mechanism to account for the second-order decay of the complexes is dimerization to the corresponding disilene, which subsequently reacts with the amine and is thus a steady-state intermediate in the overall process.

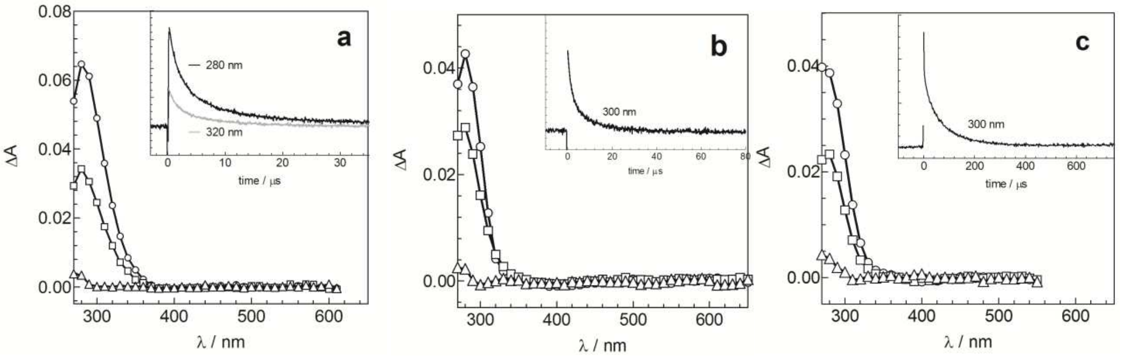

Figure 5.4. (a) Transient absorption spectra recorded 0.38-0.70 μs (o), 2.37-2.69 μs (□) and 34.37-34.69 μs (Δ) after the laser pulse, from laser flash photolysis of a deoxygenated hexane solution of $SiMe_2$ precursor **43** in the presence of 19.5 mM $n\text{-}BuNH_2$. The inset shows transient decay traces recorded at 280 nm and 320 nm. (b) Transient absorption spectra recorded 0.48-1.28 μs (o), 2.72-3.52 μs (□) and 69.92-70.72 μs (Δ) after the laser pulse, by laser flash photolysis of a deoxygenated hexane solution of **43** in the presence of 20 mM Et_2NH. The inset shows a transient decay trace recorded at 300 nm. (c) Transient absorption spectra recorded 19-27 μs (o), 59-67 μs (□) and 539-547 μs (Δ) after the laser pulse, by laser flash photolysis of a deoxygenated hexane solution of **43** in the presence of 1.5 mM Et_3N. The inset shows a transient decay trace recorded at 300 nm.

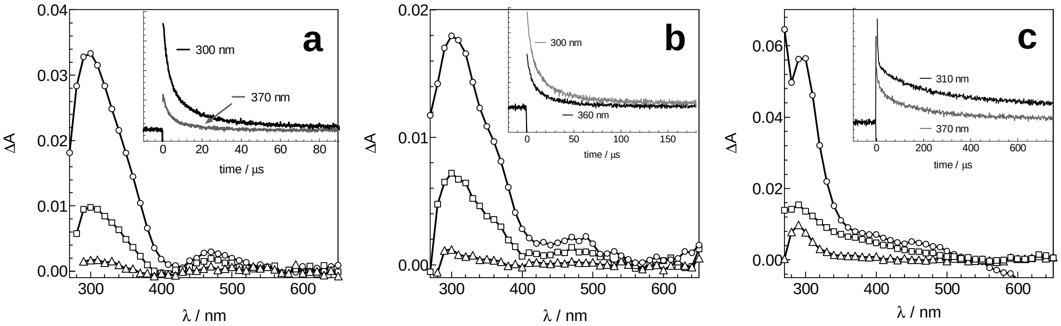

Figure 5.5. (a) Transient absorption spectra recorded 0.64-1.28 µs (o), 9.12-10.08 µs (□) and 53.92-54.72 µs (Δ) after the laser pulse, by laser flash photolysis of a deoxygenated hexane solution of $SiPh_2$ precursor **44a** in the presence of 4.77 mM n-$BuNH_2$. The inset shows transient decay traces recorded at 300 nm and 370 nm. (b) Transient absorption spectra recorded 0.96-2.24 µs (o), 11.84-13.44 µs (□) and 107.84-109.44 µs (Δ) after the laser pulse, by laser flash photolysis of a deoxygenated hexane solution of **44a** in the presence of 4.95 mM Et_2NH. The inset shows transient decay traces recorded at 300 nm and 360 nm. (c) Transient absorption spectra recorded 3.2-9.6 µs (o), 59.2-67.2 µs (□) and 699.2-707.2 µs (Δ) after the laser pulse, by laser flash photolysis of a deoxygenated hexane solution of **44a** in the presence of 1.5 mM Et_3N. The inset shows transient decay traces recorded at 310 nm and 370 nm. (*Experiments performed by T. Singh*).

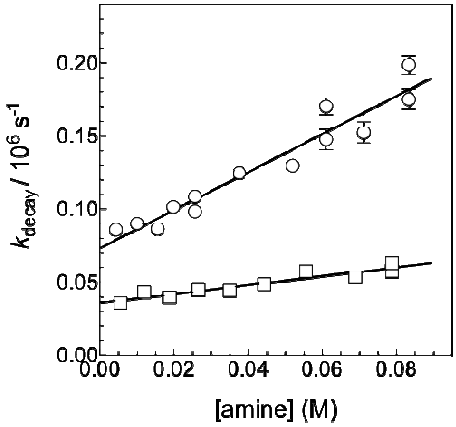

Figure 5.6. Plots of the pseudo-first order rate coefficients for decay (k_{decay}) of the $SiMe_2$-n-$BuNH_2$ (○) and $SiMe_2$-Et_2NH (□) complexes *versus* [amine] in hexanes at 25 °C.

Table 5.1. Absolute rate constants (k_1 / 10^9 M^{-1} s^{-1}) for the complexation of $SiMe_2$ and $SiPh_2$ with amines, second-order decay rate coefficients for the silylene-amine complexes ($2k/\varepsilon$), and estimated upper limits of the catalytic rate constants for N-H insertion (k_{cat} / 10^6 M^{-1} s^{-1}) measured for $SiMe_2$-amine complexes, in hexanes at 25 °C.

		n-$BuNH_2$	Et_2NH	Et_2ND	Et_3N
$SiMe_2$	k_1 / 10^9 M^{-1} s^{-1}	17 ± 2	16 ± 3	18 ± 2	9.8 ± 0.8
	$(2k/\varepsilon_{max})$ / 10^6 cm s^{-1}	13 ± 3 (280 nm)	7.4 ± 0.2 (290 nm)	8.1 ± 0.4 (290 nm)	0.60 ± 0.01 (290 nm)
	k_{cat} / 10^6 M^{-1} s^{-1}	1.3 ± 0.2	0.30 ± 0.08	-	-
$SiPh_2$[a]	k_1 / 10^9 M^{-1} s^{-1}	11 ± 3	8.3 ± 0.7	8 ± 1	3.9 ± 0.4
	$(2k/\varepsilon_{370nm})$ / 10^6 cm s^{-1}	14 ± 2	8.3 ± 0.4	11 ± 5	1.21 ± 0.04

[a] experiments with $SiPh_2$ were performed by T. Singh

In the case of the primary and secondary amines, a reduction in excitation laser intensity caused the $SiMe_2$-amine complexes to decay with predominant first order kinetics. The lifetimes of the complexes displayed a modest dependence on amine concentration, as shown in Fig. 5.6. Apparent rate constants of ca. 3.0×10^5 and 1.3×10^6 M^{-1} s^{-1} were obtained from least squares analysis of the plots of k_{decay} vs [amine] (Table 5.1). These should be considered upper limits because it is difficult to rule out contribution from adventitious impurities in the amine samples. Analogous experiments with the $SiPh_2$-amine complexes resulted in no variation in the lifetimes with increasing amine concentration.

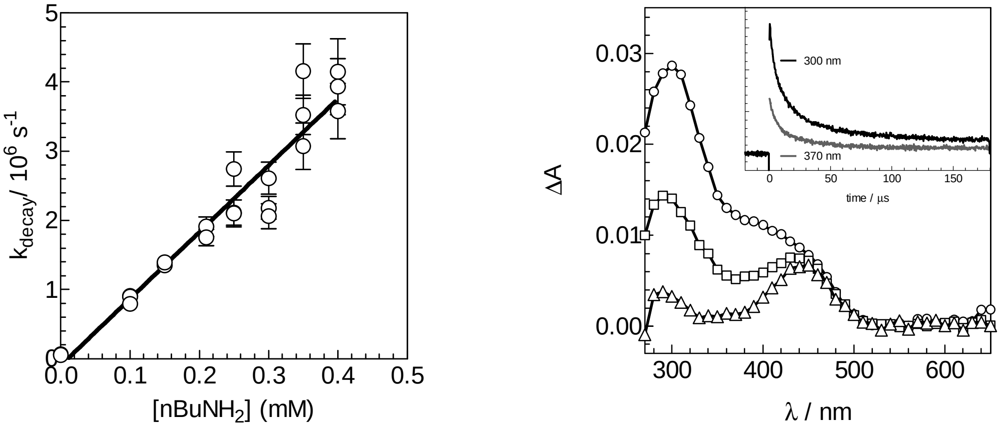

Figure 5.7. (a) Plot of the first order rate coefficient for decay (k_{decay}) of $SiMes_2$ vs. [n-BuNH$_2$]; the slope corresponds to k_1 = (1 ± 0.3) × 10^{10} M^{-1} s^{-1}; (b) Transient absorption spectra recorded 0.96-2.24 μs (○), 11.84-13.44 μs (□), and 171.84-173.44 μs (Δ) after the laser pulse, by laser flash photolysis of deoxygenated hexanes solution of **45** containing 4.8 mM n-BuNH$_2$; the inset shows transient decay profiles recorded at 310 and 370 nm.

Addition of n-BuNH$_2$ to a hexanes solution of $SiMes_2$ precursor **45** resulted in a reduction of the silylene lifetime and suppression of tetramesityldisilene formation. A plot of k_{decay} vs [n-BuNH$_2$] was linear (Fig 5.7a), affording a second order rate constant k_1 = (1.0 ± 0.3) x 10^{10} M^{-1} s^{-1} from the slope. In the presence of 4.8 mM n-BuNH$_2$ the silylene lifetime is reduced to <50 ns, and a new band with an apparent maximum at 300 nm and a shoulder absorption at ~370 nm is present (Fig 5.7b). This is similar to previously reported spectra of $SiMes_2$ in the presence of aliphatic amines in low temperature matrices, and thus the spectrum can be assigned to the $SiMes_2$–n-BuNH$_2$ complex.[12]

Addition of submillimolar concentrations of Et_2NH to a hexanes solution of **45** resulted in a bimodal decay of the silylene, consisting of a fast initial decay and a much slower decaying residual absorption. The initial decay accelerated with increasing concentration of amine, while the intensity of the residual absorption diminished. Such behaviour is consistent with a reversible reaction characterized by an equilibrium constant in the "intermediate" range (see Chapter 2), in which case the equilibrium constant can be obtained by analysis of the data according to eq. 5.3 (Fig. 5.8a). The plot of k_{decay} (initial) vs [Et_2NH] was linear (Fig. 5.8b) with a slope of $k_1 = (3.4 \pm 0.3) \times 10^9$ M^{-1} s^{-1}. In the presence of 4.7 mM Et_2NH the silylene lifetime is decreased to <50 ns, Si_2Mes_4 formation is suppressed, and a new species is formed that exhibits an apparent absorption band centered at 300 nm (Fig. 5.9a). The species decays over ca. 200 μs with mixed order kinetics and is assigned to the $SiMes_2$-Et_2NH complex. Analogous experiments employing Et_3N were limited to maximum amine concentrations of 1.5 mM to minimize direct photolysis of the amine. A modest decrease in the initial signal intensity at 580 nm with increasing [amine] was observed, while the lifetime of the signal was unaffected. A plot of $\Delta A_0/\Delta A_{eq}$ vs [S] was linear (Fig. 5.9b), and afforded a slope of 130 ± 60 M^{-1}.

Since Et_3N absorbs at the excitation wavelength, it is important to establish if screening effects influence the silylene signal intensity. It has been previously established that silylenes are more Lewis acidic than germylenes by ca. 1 kcal/mol (see Chapter 3 and ref. [13]), which leads to the expectation that the addition of Et_3N to $GeMes_2$ over the 0 – 1.5 mM concentration range of the amine should have no effect on the germylene signal

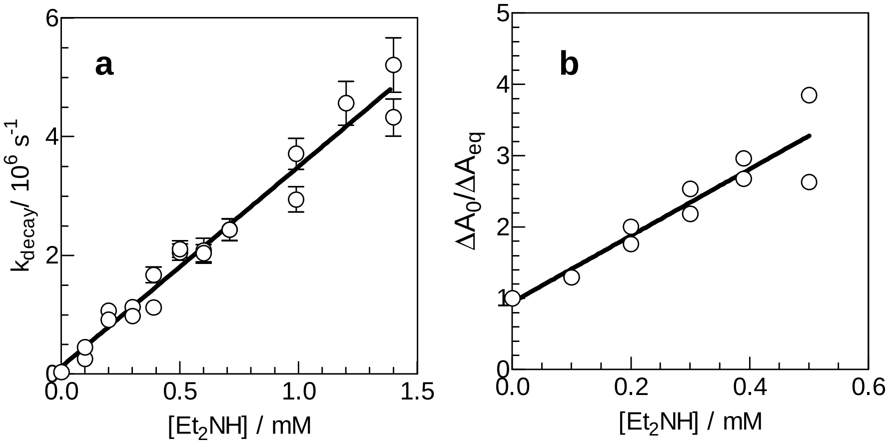

Figure 5.8. Plots of (a) k_{decay} vs [Et_2NH] and (b) ($\Delta A_0/\Delta A_{eq}$) vs [Et_2NH], for the reaction of $SiMes_2$ (monitored at 580 nm) with Et_2NH in deoxygenated hexanes at 25 ^oC. The solid lines are the linear least-squares fits of the data to eqs 5.2 and 5.3, respectively. (a) $k_1 = (3.5 \pm 0.5) \times 10^9$ M^{-1} s^{-1}; (b) $K_1 = (6 \pm 2) \times 10^3$ M^{-1}. (*Experiments performed by T. Singh*).

---

intensity other than that due to screening. In fact, addition of up to 1.5 mM [Et_3N] to $GeMes_2$ resulted in no measurable reduction in the apparent signal intensities of the germylene (see Chapter 3). This result suggest that screening effects of Et_3N are negligible within this concentration range of the amine, and thus do not affect the determination of the equilibrium constant for the reaction of $SiMes_2$ with Et_3N.

$$\Delta A_0/\Delta A_{eq} = 1 + K_1[S] \qquad (5.3)$$

Table 5.2. Absolute rate constants (k_1, in units of 10^9 M^{-1} s^{-1}) and equilibrium constants (K_1, in units of M^{-1}) for quenching of $SiMe_2$, $SiPh_2$ and $SiMes_2$ by n-butyl amine (n-$BuNH_2$), diethylamine ($Et_2NH(D)$), and triethylamine (Et_3N) in hexanes at 25 ± 1 °C.

	$SiMe_2$	$SiPh_2$	$SiMes_2$	
Substrate	k_1 / 10^9 $M^{-1}s^{-1}$	k_1 / 10^9 $M^{-1}s^{-1}$	k_1 / 10^9 $M^{-1}s^{-1}$	K_1 / M^{-1}
n-$BuNH_2$	17 ± 2	11 ± 3	10 ± 3	> 25,000
Et_2NH	16 ± 3	8.3 ± 0.7	3.4 ± 0.3	4,700 ± 700
Et_2ND	18 ± 2	8 ± 1	[a]	[a]
Et_3N	9.8 ± 0.8	3.9 ± 0.4	[b]	130 ± 60

[a] not measured; [b] no change in silylene lifetime observed over the 0-1.5 mM concentration range in added amine

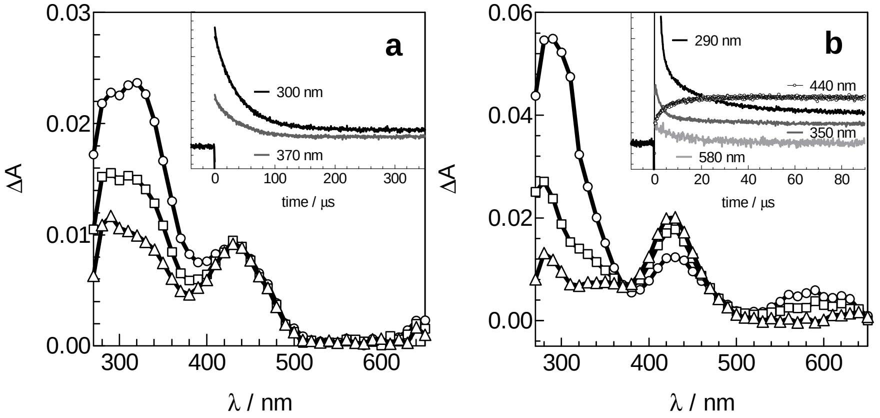

Figure 5.9. (a) Transient absorption spectra recorded 4.48-7.04 μs (○), 23.68-27.52 μs (□), and 42.88-46.08 μs (Δ) after the laser pulse, by laser flash photolysis of a deoxygenated hexanes solution of **45** containing 4.7 mM Et_2NH at 25 °C; the inset shows transient decay profiles recorded at 300 and 370 nm. (b) Transient absorption spectra recorded 2.56-3.36 μs (○), 9.12-10.08 μs (□), and 85.92-86.72 μs (Δ) after the laser pulse, by laser flash photolysis of a deoxygenated hexanes solution of **45** containing 1.5 mM Et_3N at 25 °C; the inset shows transient decay profiles recorded at 290, 350, 440 and 580 nm. (*Experiments performed by T. Singh*).

5.3. Discussion

In this study, the reactions of transient silylenes $SiMe_2$, $SiPh_2$ and $SiMes_2$ with n-butylamine (n-$BuNH_2$), diethylamine (Et_2NH) and triethylamine (Et_3N) in hydrocarbon solvents were investigated by means of laser flash photolysis and steady state photolysis methods with the goals of comparing these reactions to the analogous reactions of these species with alcohols. Product studies indicate that $SiPh_2$, analogous to $SiMe_2$,[14] reacts with Et_2NH to form the silanamine in near quantitative yield, provided hydroxylic substrates are not present in solution. The results also show that the reaction with water is substantially more efficient than that with the amine, although it is not possible to determine how the hydrolysis product is formed – whether via the direct reaction of the $SiPh_2$-Et_2NH complex with water, or on a longer timescale involving hydrolysis of the silanamine after it is formed.

The kinetics of the reactions of $SiMe_2$, $SiPh_2$ and $SiMes_2$ with n-$BuNH_2$, $Et_2NH(D)$ and Et_3N were investigated in hexanes solution, the results of which are summarized in Tables 5.1 and 5.2.[15] $SiMe_2$ reacts with primary and secondary amines with rate constants close to the diffusional rate constant in hexanes at 25 ^oC ($k_{diff} = 2.1 \times 10^{10}$ M^{-1} s^{-1})[6] and are in line with the previously reported values for the reaction of $SiMe_2$ with pyrrolidine and *N*-methylpyrrolidine in cyclohexane at 20 ^oC[5] given the difference in viscosity of the two solvents.[6] The rate constants for the reactions of $SiMe_2$ with n-$BuNH_2$ and Et_2NH correspond to a free energy barrier for complexation on the order of 3.5 kcal mol^{-1} or less in both cases. A small decrease in the rate constant is observed for the reaction of this silylene with Et_3N, which may reflect a small steric barrier for complexation induced by the three substituents on the amine. The rapidity with which $SiPh_2$ reacts with the three amines decreases with increasing steric bulk on the amine, such that the rate constants for complexation follow the trend n-$BuNH_2$ > Et_2NH > Et_3N. This trend is opposite to that expected based on the gas phase basicities of the three amines.[8] The absence of a kinetic isotope effect for the reactions of $SiMe_2$ and $SiPh_2$ with Et_2NH is expected for a simple complexation process. The equilibrium constants for complexation of $SiMe_2$ and $SiPh_2$ with Et_2NH, and of all three silylenes with n-$BuNH_2$, are evidently too large to be measured under our experimental conditions (i.e. $K_1 > 2.5 \times 10^4$ M^{-1}).

Steric factors introduced by the bulky substituents on silicon in the $SiMes_2$ systems clearly dominate the situation, which is reflected in the decreased stability of the Lewis acid-base complexes with increasing substitution on the amine. An equilibrium constant of $K_1 = (4.7 \pm 0.7) \times 10^3$ M^{-1} was determined for the formation of the $SiMes_2$-Et_2NH complex (hexanes, 25 °C), while that for the formation of the $SiMes_2$-Et_3N complex is $K_1 = 130 \pm 60$ M^{-1}. These values correspond to binding free energies of $\Delta G_{Et2NH} = -(5.0 \pm 0.1)$ kcal mol^{-1} and $\Delta G_{Et3N} = -(2.9 \pm 0.4)$ kcal mol^{-1}, where the reference state is a 1 M solution in hexanes at 25 ^oC. The equilibrium constant for the reaction of $SiMes_2$ with n-$BuNH_2$ is above our measurement limit ($K_1 \geq 25{,}000$ M^{-1}), giving an upper limit for the binding energy of ca. -6 kcal mol^{-1}. The correlations of the binding energies of the $SiMes_2$ complexes with the (experimental) gas bacisity and proton affinity values of the donors are illustrated in Fig. 5.10a and Fig. 5.10b, respectively. The correlations are in both cases excellent, but the slopes are negative and trends are opposite to those predicted for the

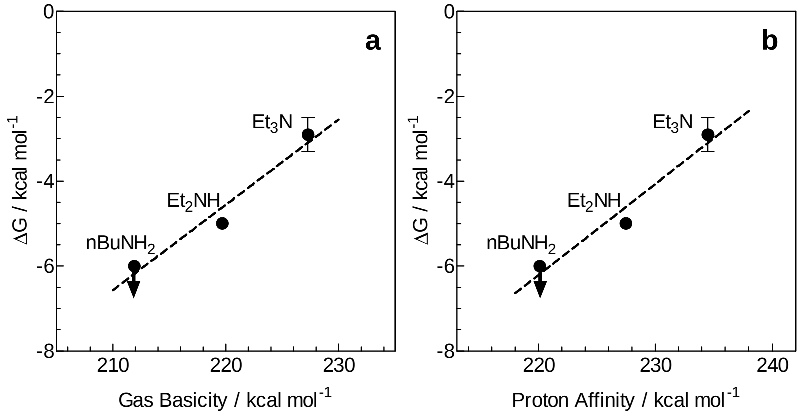

Figure 5.10. Plots of experimental standard free energy values of complexation of $SiMes_2$ with the three amines vs (a) gas basicity[8] and (b) proton affinity[8] of the donors. The reference state is a 1 M solution in hexanes at 25 °C.

---

analogous $SiMe_2$ systems at the G4 level of theory.[13] This is due to a high degree of steric destabilization of the $SiMes_2$-amine complexes as a function of increasing substitution on the amine (see Chapter 3 and ref. [13]).

In contrast to the reactions with alcohols, the Lewis acid-base complexes of $SiMe_2$ and $SiPh_2$ with primary and tertiary amines exhibit lifetimes of several tens of microseconds at ambient temperatures in solution, and are largely unresponsive to changes in amine concentration. Nevertheless, calculations suggest that formation of the N-H insertion product from the complex most likely requires catalysis by a second molecule of amine, as is the case in the reactions with alcohols. The calculated barrier for unimolecular H-migration in the $SiMe_2$-$MeNH_2$ complex is $\Delta G^{\ddagger} = 17.1$ kcal mol^{-1} relative to the free reactants, while the predicted value for the corresponding process in the $SiMe_2$-MeOH complex is $\Delta G^{\ddagger} = 14.1$ kcal mol^{-1} at the G4 level of theory. These free energy barriers correspond to a rate constant for a unimolecular H-migration of about 1 s^{-1} or smaller; such a slow process is not expected to proceed at all under the conditions of our experiments unless another pathway with a lower barrier is available. The barriers of 14-17 kcal mol^{-1} are too high to compete with other processes such as dimerization of the silylene.

The calculated (G4) standard free energy surfaces for the reactions of $SiMe_2$ with one and two molecules of $MeNH_2$ in the gas phase are shown in Fig. 5.11, while the corresponding processes with MeOH are shown in Fig. 5.12.[15] The calculations demonstrate that as in the reaction with alcohols, the preferred mechanism for N-H insertion involves two molecules of the substrate, one acting as a nucleophile in the initial step of the reaction and the other acting as a catalyst for the H-migration process that converts the intermediate complex to the final product. The calculations also indicate that the reaction barrier for the catalyzed pathway in N-H insertion is significantly higher ($\Delta\Delta G_{cat}^{\ddagger} \approx 13.2$ kcal mol^{-1}) than the corresponding one in O-H insertion. The differences in the activation energies could be due to a lower acidity of the N-H protons compared to the O-H protons in the corresponding silylene-donor complexes.

Upper limits of $k_{cat} < 10^5$-10^6 M^{-1} s^{-1} were estimated for the catalytic rate constants for H-transfer in the complexes of $SiMe_2$ with n-$BuNH_2$ and Et_2NH in hexanes, indicating the process occurs at least four orders of magnitude more slowly than the corresponding process in silylene-alcohol complexes under similar conditions (see Chapter 4).[16] These rate constants correspond to free energy barriers of ca. $\Delta G^{\ddagger} \approx 9$ kcal mol^{-1} relative to the

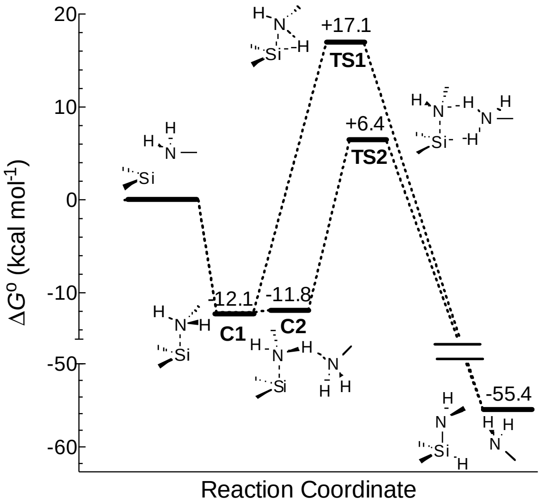

Figure 5.11. Standard free energy surfaces for the N-H insertion reaction of $SiMe_2$ with $MeNH_2$ calculated at the G4 level of theory (298.15 K, kcal mol^{-1}).[15]

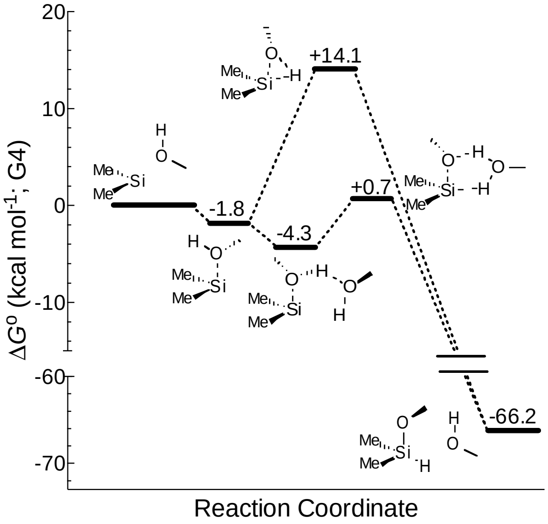

Figure 5.12. Standard free energy surface for the O-H insertion reaction of $SiMe_2$ with MeOH, calculated at the G4 levels of theory (298.15 K, kcal mol^{-1}).[15]

bimolecular complex, which is considerably lower than the calculated barrier of $\Delta G^{\ddagger} \approx$ 18.5 kcal mol^{-1}. Based on these large differences it is most likely that the experimentally measured k_{cat} values are overestimated by a significant amount, since slow rates of reaction allow the opportunity for adventitious impurities to play a role.

5.4. Conclusion

The reaction of the transient silylenes $SiMe_2$, $SiPh_2$, and $SiMes_2$ with primary, secondary and tertiary amines proceeds via the formation of long-lived Lewis acid-base complexes which were detected and characterized by UV-vis spectroscopy in each case. The rate constants for complexation are close to the diffusional limit in hexanes and show modest variations with amine structure. The complexation of the sterically bulky silylene, $SiMes_2$, with Et_2NH and Et_3N proceeds reversibly and provided the first equilibrium constants for a silylene reaction to be reported in solution.[15] According to theory, the second step of the reaction to generate the corresponding silanamines proceeds via catalytic H-migration involving a second molecule of amine. The experimentally determined upper limit for the catalytic rate constants are in the 10^5-10^6 M^{-1} s^{-1} range. Thus, the catalysis of the N-H transfer is at least four orders of magnitude slower than that exhibited by the $SiMe_2$-MeOH system under similar conditions.

5.5. References

1. Gu, T.-Y. Y.; Weber, W. P., *J. Organomet. Chem.* **1980,** *184*, 7.

2. Matarasso-Tchiroukhine, E., *Chem. Commun.* **1990**, 681.

3. Gadek, A.; Szymanska-Buzar, T., *Polyhedron* **2006,** *25*, 1441.

4. Espenson, J. H., *Chemical Kinetics and Reaction Mechanisms*. McGraw-Hill, Inc.: New York, 1995.

5. Yamaji, M.; Hamanishi, K.; Takahashi, T.; Shizuka, H., *J. Photochem. Photobiol. A: Chem.* **1994,** *81*, 1.

6. Murov, S. L.; Carmichael, I.; Hug, G. L., *Handbook of photochemistry*. Dekker: New York, 1993.

7. Moiseev, A. G.; Leigh, W. J., *Organometallics* **2007,** *26*, 6277.

8. Hunter, E. P. L.; Lias, S. G., *J. Phys. Chem. Ref. Data* **1998,** *27* (3), 413.

9. Leigh, W. J.; Harrington, C. R., *J. Am. Chem. Soc.* **2005,** *127*, 5084.

10. Leigh, W. J.; Lollmahomed, F.; Harrington, C. R., *Organometallics* **2006,** *25*, 2055.

11. Gillette, G. R.; Noren, G. H.; West, R., *Organometallics* **1989,** *8*, 487.

12. Ando, W.; Sekiguchi, A.; Hagiwara, K.; Sakakibara, A.; Yoshida, H., *Organometallics* **1988,** *7*, 558.

13. Kostina, S. S.; Singh, T.; Leigh, W. J., *Organometallics* **2012,** *31* (9), 3755.

14. Gu, T.-Y. Y.; Weber, W. P., *J. Organomet. Chem.* **1980,** *184* (1), 7.

15. Kostina, S. S.; Singh, T.; Leigh, W. J., *J. Phys. Org. Chem.* **2011,** *24*, 937.

16. Leigh, W. J.; Kostina, S. S.; Bhattacharya, A.; Moiseev, A. G., *Organometallics* **2010,** *29* (3), 662.

6. Chapter 6 – Silylene insertion into the Si-O bonds of siloxanes

6.1. Overview

The kinetics of the reactions of $SiMe_2$ and $SiPh_2$ with methoxytrimethylsilane (MeOTMS), the cyclic siloxanes 2,2,5,5-tetramethyl-2,5-disila-1-oxacyclopentane (TMDOP), hexamethylcyclotrisiloxane (D_3) and octamethylcyclotetrasiloxane (D_4), and the acyclic siloxanes hexamethyldisiloxane (TMS_2O) and octamethyltrisiloxane ($Me_2Si(OTMS)_2$) were investigated by laser flash photolysis. The results are consistent with a mechanism involving the *reversible* formation of a Lewis acid-base adduct, which undergoes unimolecular rearrangement to yield the formal Si-O insertion products (eq. 6.1). The observed kinetic behaviour varies with the relative magnitudes of the rate constants for complexation and the subsequent insertion step.

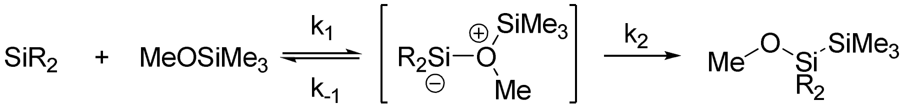

(6.1)

In laser photolysis experiments involving SiR_2 (R = Me or Ph) with MeOTMS and $SiPh_2$ with TMDOP, the Lewis acid-base complexes could be directly observed and their decay kinetics measured as a function of substrate concentration, while the absorption bands of the anticipated $SiMe_2$-TMDOP complex are obscured by fluorescence. In the reactions of both silylenes with D_3 and D_4 the complexes cannot be detected, presumably because they are steady-state intermediates. Nevertheless, the two-step mechanism is supported by the measured activation energy of 0 ± 2 kJ/mol for the reaction of $SiMe_2$ with D_3. Both silylenes were found to be unreactive toward the acyclic siloxanes TMS_2O and $Me_2Si(OTMS)_2$.

6.2. Kinetic measurements

6.2.1. The reactions of SiR_2 with MeOTMS

Addition of submillimolar concentrations of MeOTMS to a hexanes solution of **43** resulted in shortening of the lifetime of $SiMe_2$ (λ_{max} = 470 nm) and suppression of silylene dimerization. This was accompanied by the appearance of a new transient absorption centered at λ_{max} = 310 nm, whose lifetime also shortened with increasing concentration of MeOTMS. Based on the kinetic behaviour of this transient (*vide infra*), and its UV-vis spectrum, it is assigned to the $SiMe_2$-MeOTMS complex. When the absorptions due to the silylene and the $SiMe_2$-MeOTMS complex were monitored at full laser power (~100 mJ), the decay profiles at both wavelengths were bimodal – a fast initial decay overlapped on a slowly decaying residual absorbance (Fig 6.1a-b). At 470 nm the decays could not be fit acceptably to first order kinetics. Nevertheless, a plot of (approximate) first order decay rate coefficients vs [MeOTMS] was constructed and is shown in Fig 6.1c. The k_{decay} approaches a plateau region asymptotically, consistent with saturation kinetics. The plot of k_{decay} ($SiMe_2$) vs [MeOTMS] is in reasonable agreement with the previously published data.[1] The $SiMe_2$-MeOTMS complex also decayed with bimodal kinetics; a fast initial decay was superimposed on a slowly decaying residual absorption. At short timescales appropriate to observe the initial fast decay the traces did not fit to a two-phase decay, and so the decays were fit to a single exponential. The resulting plot of k_{decay} (310 nm) vs [MeOTMS] is shown in Fig 6.1c.

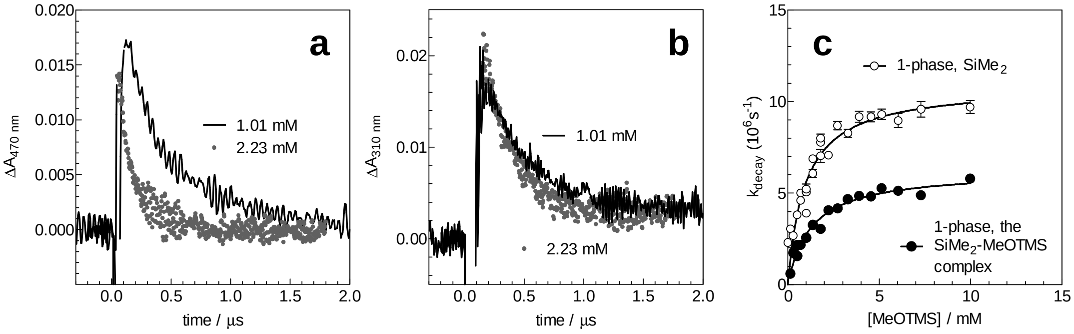

Figure 6.1. Transient decay profiles recorded at (a) 470 nm, and (b) 310 nm, for the reaction of $SiMe_2$ with MeOTMS as a function of substrate concentration. (c) Plots of the pseudo-first order decay rate coefficients (k_{decay}) for $SiMe_2$ (o) and the $SiMe_2$-MeOTMS complex (●) vs. [MeOTMS] in hexanes solution at 25 °C. The solid lines are the least squares analysis of the data to eq. 6.3

There are two factors that can cause the decay of the silylene to become bimodal: 1. the initial fast decay is the second order decay due to dimerization of the silylene, while the longer-lived component is due to the reaction of $SiMe_2$ with the substrate; 2. the initial fast decay is a rapid approach to equilibrium with the initially formed Lewis acid-base adduct, while the slow component is the rate coefficient after equilibrium has been established. In order to distinguish between the two possibilities, the laser power was reduced to 43% of its usual power by introduction of a neutral density filter between the laser beam and the sample cell. If the fast component of the silylene is due to dimerization, then the reduction of the initial silylene concentration resulting from the lower laser power should result in a partial or complete disappearance of the second order component. If the second possibility is true, however, the reduction of the laser power should result only in the reduction of the initial intensity of the silylene signal with no effect on its decay kinetics.

Addition of submillimolar concentrations of MeOTMS to $SiMe_2$, produced by laser flash photolysis of a hexane solution of **43** with laser power reduced to 43%, resulted in clean *first order* decay of the silylene absorbance-time profiles. The intensity of the initial transient absorbance due to the silylene diminished with increasing [MeOTMS] up to ca. 5 mM, above which the silylene absorption could no longer be detected (Fig 6.2a). The decay profiles of the $SiMe_2$-MeOTMS complex were monitored at 320 nm as a function of MeOTMS concentration in this experiment. At this wavelength the contribution from sample fluorescence is smaller than at 310 nm, thus more points from the absorbance vs time profiles can be used in the kinetic fits. With reduced laser power the decay profiles due to the $SiMe_2$-MeOTMS complex also fit well to first order kinetics, and the weaker long-lived overlapping component was no longer detectable (Fig 6.2b).

Plots of k_{decay} vs [MeOTMS] measured at 320 nm and 470 nm at the reduced laser intensity are shown in Fig. 6.2b. Both plots display a downward curvature consistent with saturation kinetics. The lifetime of the silylene was somewhat shorter than the lifetime of the $SiMe_2$-MeOTMS complex at each concentration, which is apparent in the k_{decay} vs [MeOTMS] plots of Fig. 6.2c. The experiment was repeated 3 times, and it was apparent that the level of the plateau of the plot for $SiMe_2$ depends on the starting lifetime of the silylene – a shorter starting lifetime yields a higher plateau of the curve. The slope of the initial portion of the curve for $SiMe_2$ was independent of the starting silylene lifetime, while the plot for the $SiMe_2$-MeOTMS complex could be consistently reproduced regardless of the starting silylene lifetime in the absence of MeOTMS. The lifetime of the $SiMe_2$-MeOTMS complex was also monitored in the presence of 0.005 – 0.18 M MeOTMS, where the silylene can no longer be detected. It was found that the decay rate constant of the complex reaches a maximum value of $(6.0 \pm 0.5) \times 10^6$ s^{-1} at ca. 0.02 M and is constant at concentrations above that value. Transient absorption spectra obtained at the highest concentration of the substrate (0.18 M MeOTMS, Fig. 6.3a) show that at this concentration the only species detectable is the $SiMe_2$-MeOTMS complex (λ_{max} = 310 nm). This spectrum is in good agreement with that previously reported.[1]

The mechanism that can explain the observed results is one involving reversible formation of a Lewis acid-base adduct followed by a unimolecular insertion (eq. 6.2).

$$\mathrm{SiR_2} + \mathrm{S} \underset{k_{-1}}{\overset{k_1}{\rightleftharpoons}} [\mathrm{cmpx}] \xrightarrow{k_2} \mathrm{P} \qquad (6.2)$$

The expression for k_{decay} for the mechanism in eq. 6.2 is given by eq. 6.3, where $K_1 = k_1/k_{-1}$ and S = substrate; it holds true when a fast pre-equilibrium is established and *the second step is rate-determining*.[2] The reaction can be followed in terms of the product, [P], the silylene, [SiR_2], or the complex, [cmpx]. Often it is most convenient to monitor the silylene; in our reaction of interest, however, both the silylene and the complex can be monitored as a function of substrate concentration to obtain the values of k_{decay}.

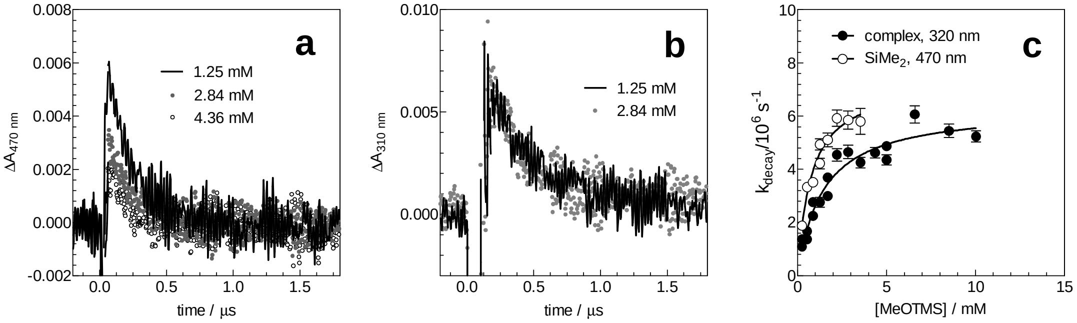

Figure 6.2. Transient decay profiles recorded at (a) 470 nm, and (b) 310 nm, for the reaction of $SiMe_2$ with MeOTMS as a function of substrate concentration at 43% maximum laser intensity. (c) Plots of the pseudo-first order decay rate coefficients (k_{decay}) for $SiMe_2$ (o) and the $SiMe_2$-MeOTMS complex (●) vs. [MeOTMS] in hexanes solution at 25 °C. The solid lines are the non-linear least squares fits of the data to (●) eq. 6.3 and (o) eq. 6.4

$$k_{decay} = \frac{k_2 K_1 [S]}{1 + K_1 [S]} \qquad (6.3)$$

There are two limiting cases for k_{decay}:

the [S] is very large (saturation), when

$1 + K_1[S] \rightarrow K[S]$, and $k_{decay} \approx k_2$ (6.4)

and the reaction rate is zero order in [S];

the [S] is small, when

$1 + K_1[S] \rightarrow 1$, and $k_{decay} \approx k_2 K[S]$ (6.5)

and the reaction rate is first order in [S].

Following the reaction by monitoring the silylene poses an additional problem: according to eq. 6.3 the y-intercept should be zero, while in the actual experiment the plot of k_{decay} ($SiMe_2$) vs [MeOTMS] never intersects the origin. The lifetime of the silylene in the absence of added substrate depends on the presence of adventitious impurities such as water. To account for the reaction with impurities, an additional term has to be introduced, k_0 (eq. 6.6). Rearrangement of eq. 6.6 yields eq. 6.7, which can now be used to obtain a plot of ($k_{\mathrm{decay}} - k_0$) vs [MeOTMS] from the silylene absorptions (Fig 6.3b). This plot overlaps nearly perfectly with that for the $SiMe_2$-MeOTMS complex, and in both cases the k_{decay} value approaches the plateau region asymptotically.

$$k_{decay} = \frac{k_2 K_1[S]}{1 + K_1[S]} + k_0 \qquad (6.6)$$

$$k_{decay}^{corr} = k_{decay} - k_0 = \frac{k_2 K_1[S]}{1 + K_1[S]} \qquad (6.7)$$

Analogous experiments probing the reaction of $SiPh_2$ (generated from **44a**) with MeOTMS were performed, and yielded results that appeared to be quite different from those previously reported.[1] The addition of 0 – 3.5 mM MeOTMS to a hexanes solution of **44a** resulted in a bimodal decay of the silylene – a fast initial component was only observable at MeOTMS concentrations below 1.0 mM (Fig 6.4a). The long-lived components of the absorbance-time profiles decayed with second order kinetics and are thus excluded from the k_{decay} vs [MeOTMS] plot (Fig 6.4b).

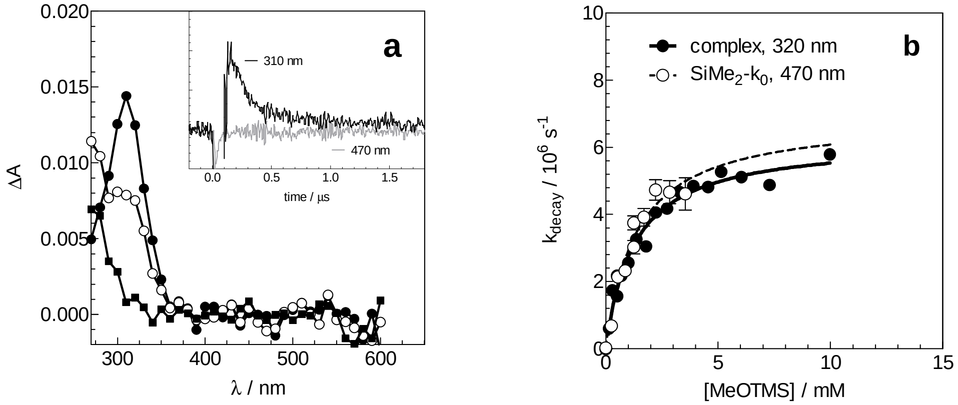

Figure 6.3. (a) Transient absorption spectra of a deoxygenated hexanes solution of **43** at 25^{o}C containing 0.18 M MeOTMS, recorded 0.21-0.25 μs (●), 0.31-0.34 μs (o) and 1.72-1.75 μs (■) after the laser pulse. The insets show transient decay profiles recorded at 310 nm and 470 nm. (b) Plots of k_{decay} (320 nm) vs [MeOTMS] (●) and ($k_{\mathrm{decay}} - k_0$) (470 nm) vs [MeOTMS] (o), from the reaction of $SiMe_2$ with MeOTMS. The solid and dashed lines are the non-linear least squares fits of the data to eq. 6.3 and eq. 6.7, respectively.

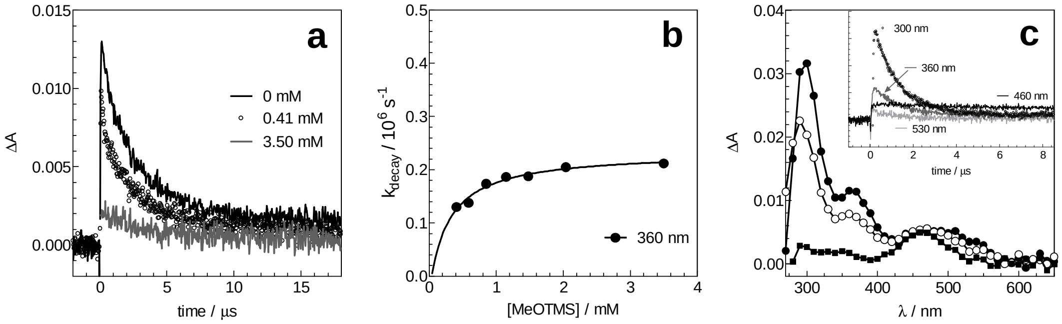

Figure 6.4. (a) Transient decay profiles recorded at 530 nm for the reaction of $SiPh_2$ with MeOTMS as a function of substrate concentration. (b) Plot of the pseudo-first order decay rate coefficient (k_{decay}) of the $SiPh_2$-MeOTMS complex (●) vs. [MeOTMS] in hexanes solution at 25 ^{o}C. The solid line is the non-linear least squares fit of the data to eq. 6.3; (c) Transient absorption spectra of a deoxygenated hexanes solution of **44a** at 25 ^{0}C containing 2 mM MeOTMS, recorded 0.19-0.26 μs (●), 0.75-0.85 μs (o) and 5.39-5.47 μs (■) after the laser pulse. The insets show transient decay profiles recorded at 300 nm, 360 nm, 460 nm, and 530 nm.

Transient absorption spectra of a hexanes solution of **44a** containing 2.0 mM MeOTMS are shown in Fig 6.4c and demonstrate the presence of a new transient centered at 360 nm (τ = 1.2 ± 0.1 μs), which has been previously assigned to the $SiPh_2$-MeOTMS complex.[1] The spectra also show the presence of two additional bands centered at 300 nm (τ = 1.13 ± 0.03 μs) and 515 nm (τ = 1.0 ± 0.2 μs), which decay with pseudo first order kinetics. Diphenylsilylene ($SiPh_2$) has two absorption bands, at 290 nm and 515 nm[3], while the $SiPh_2$-MeOTMS complex also has two absorption bands – at 300 nm and 360 nm (in the preliminary publication[1] only the long-wavelength absorption band was reported for the complex, but our more recent work[3] demonstrates that *all* $SiPh_2$-*O*-donor complexes exhibit two absorption bands). Therefore, the band at 515 nm is due to the silylene, the band at 360 nm is due to the complex, and the 300 nm band consists of contributions from the short-wavelength bands in the spectra of $SiPh_2$ and the $SiPh_2$-MeOTMS complex.

The reaction was also followed in terms of the $SiPh_2$-MeOTMS complex as a function of MeOTMS concentration (monitoring wavelength is 360 nm); a plot of k_{decay} vs [MeOTMS] is shown in Fig 6.4b. The k_{decay} value approaches a plateau value of ca. 0.2×10^6 s^{-1}, below the lifetime of the silylene; the values of k_2 and K_1 obtained from the analysis of the data to eq. 6.3 are listed in Table 6.1. The value for K_1 (4,000 ± 4,000 M^{-1}) determined from this analysis has a low degree of accuracy, because the low concentration portion of the plot in Fig 6.4b is poorly defined. Unfortunately this cannot be improved upon because at concentrations of MeOTMS below 0.4 mM the absorption due to the $SiPh_2$-MeOTMS complex are too weak to obtain a value of k_{decay}.

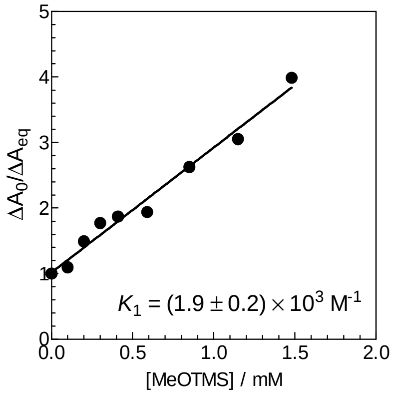

Figure 6.5. Plot of $\Delta A_0/\Delta A_{eq}$ vs [MeOTMS] for the reaction of $SiPh_2$ with MeOTMS. The solid line is the linear least-squares fit of the data to eq. 6.8.

Table 6.1. The values of K_1 (M^{-1}) and k_2 (10^6 s^{-1}) for the reactions of $SiMe_2$ and $SiPh_2$ with MeOTMS, obtained from analysis of the experimental plots of k_{decay} (the SiR_2-MeOTMS complex) vs [MeOTMS] of Figs. 6.3b and 6.4b using eq. 6.3.

	k_2 / 10^6 s^{-1}	K_1 / M^{-1}
$SiMe_2$	6.2 ± 0.4	800 ± 200
$SiPh_2$	0.3 ± 0.1^a	4000 ± 4000^a
		1900 ± 200^b

[a] errors are reported as the standard error from non-linear least squares analysis of eq. 6.3; [b] obtained from the analysis of the silylene data to eq. 6.8

In section 2.5, a different method of determining the equilibrium constants was described, for a reaction involving the formation of a "non-reactive" silylene-substrate complex. In this case, the long-lived component of the silylene decay is due to dimerization of the free silylene (in equilibrium with the complex), and the value of K_1 can be measured with reasonable precision from a plot of $\Delta A_0/\Delta A_{eq}$ vs [S] according to eq. 6.8, where S is the substrate, ΔA_0 is the initial absorbance of the silylene and ΔA_{eq} is the absorbance of the silylene at equilibrium.[3]

$$\frac{\Delta A_0}{\Delta A_{eq}} = 1 + K_1[S] \tag{6.8}$$

In the situation where a reactive complex is formed, the long-lived component of the silylene decay after equilibrium has been established is governed by the lifetime of the complex. If the approach to equilibrium is detectable then it becomes very difficult to estimate the absorption of the silylene at equilibrium, and thus the analysis of the data according to eq. 6.8 is not applicable in such situations. In the reaction of $SiPh_2$ with MeOTMS, however, the rearrangement reaction of the $SiPh_2$-MeOTMS complex is quite slow and thus the equilibrium concentration of $SiPh_2$ can be reasonably obtained. A plot of $\Delta A_0/\Delta A_{eq}$ vs [MeOTMS] is shown in Fig. 6.5 and displays a good linear correlation. The slope of the line gives a value for the equilibrium constant of $K_1 = 1900 \pm 200$ M^{-1} (Table 6.1).

In the preliminary report of the $SiPh_2$ + MeOTMS system,[1] the rate constant for complexation was reported to be 4.2×10^9 M^{-1} s^{-1}, while the loss in the signal intensity of the silylene was also observed with increasing MeOTMS concentration. The difference between the present results and the reported ones might be attributed to the rigour with which MeOTMS was purified for the flash photolysis experiments. In the present work, MeOTMS was purified by overnight reflux over sodium to remove MeOH in the sample followed by simple distillation immediately prior to the experiment. The purity of the samples was checked by ^1H NMR spectroscopy, and was >99.5% in all cases. The details of the purification procedure in the preliminary publication were not recorded.[1] Another contribution to the difference in the results might arise from silylene dimerization, if the initial silylene concentration in the previous experiments was substantially higher than in the experiments completed in this work.

Most procedures to prepare methoxytrimethylsilane involve MeOH as the starting material. For instance, a commercial sample of MeOTMS from Aldrich typically contains a small amount (<5 %) of MeOH. To investigate the effect of MeOH impurity on the kinetic measurements, MeOTMS was used as received from the supplier without any purification for a control experiment. The ^{1}H NMR spectrum of the sample showed it to contain ca. 1.6 mol% MeOH (0.12 M). In the 0-2 mM concentration range of MeOTMS (0 - 0.3 mM MeOH) no effect on the lifetime of the $SiPh_2$ was observed; thus, the presence of a small amount of MeOH impurity does not explain the published results.

6.2.2. The Reactions of $SiMe_2$ and $SiPh_2$ with 2,2,5,5-tetramethyl-2,5-disila-1-oxacyclopentane (TMDOP)

Addition of submillimolar amounts of TMDOP to a hexanes solution of **43** resulted in systematic reductions in the $SiMe_2$ lifetime and suppression of the formation of the disilene. This was accompanied by modest losses in the initial signal strength of the silylene signals, though not more than expected due to the limits of time resolution of the laser flash photolysis system. Values of k_{decay} of $SiMe_2$ were measured as a function of TMDOP concentration; the plot of k_{decay} (470 nm) vs [TMDOP] is shown in Fig. 6.6a. Analysis of the plot of Fig 6.6a according to eq. 6.7 affords values of $K_1 = (700 \pm 200)$ M^{-1} and $k_2 = (2.1 \pm 0.2) \times 10^{7}$ s^{-1} (Table 6.2).

The analysis of the silylene data suggests the complex has a lifetime of only ca. 50 ns, which is at the very edge of our detection limits. Indeed, we have been unable to detect a transient absorbing in the 290-330 nm range with solutions containing 0.5-5.5 mM TMDOP. Fig. 6.6b shows transient absorption spectra measured with a hexane solution of **43** containing 0.5 mM TMDOP. At concentrations of TMDOP below 0.5 mM the absorptions of the expected $SiMe_2$-TMDOP complex are too weak to be detected under the conditions of our experiments.

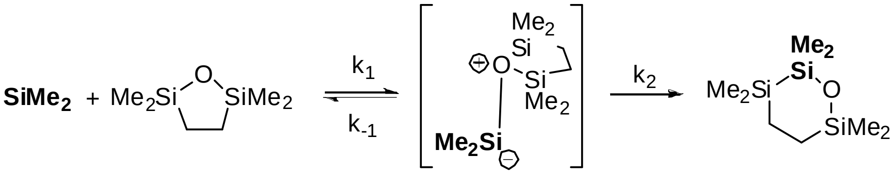

(6.9)

Analogous experiments with $SiPh_2$ precursor **44a** afforded silylene decay profiles that did not fit well to first order decay kinetics, however approximate analysis to first order decay kinetics yielded a linear plot of k_{decay} (530 nm) vs [TMDOP] with a slope of $(1.4 \pm 0.1) \times 10^9$ M^{-1} s^{-1} (Fig. 6.6c). Transient absorption spectra recorded in the presence of 3 mM TMDOP show the presence of a new band centered at 360 nm, which decays with first order kinetics and can be assigned to the $SiPh_2$-TMDOP complex based on the similarities with the spectra of the $SiPh_2$-MeOTMS complex (Fig. 6.6d). A more intense short wavelength band is also present in the spectra; however it is distorted due to strong sample fluorescence. The complex was monitored at 360 nm as a function of TMDOP concentration, and the resulting plot of k_{decay} (360 nm) vs [TMDOP] is shown in Fig. 6.6c. The plot was analyzed according to eq. 6.3 to obtain values of k_2 and K_1 of $(4.2 \pm 0.2) \times 10^6$ s^{-1} and 600 ± 200 M^{-1}, respectively. The data are summarized in Table 6.2.

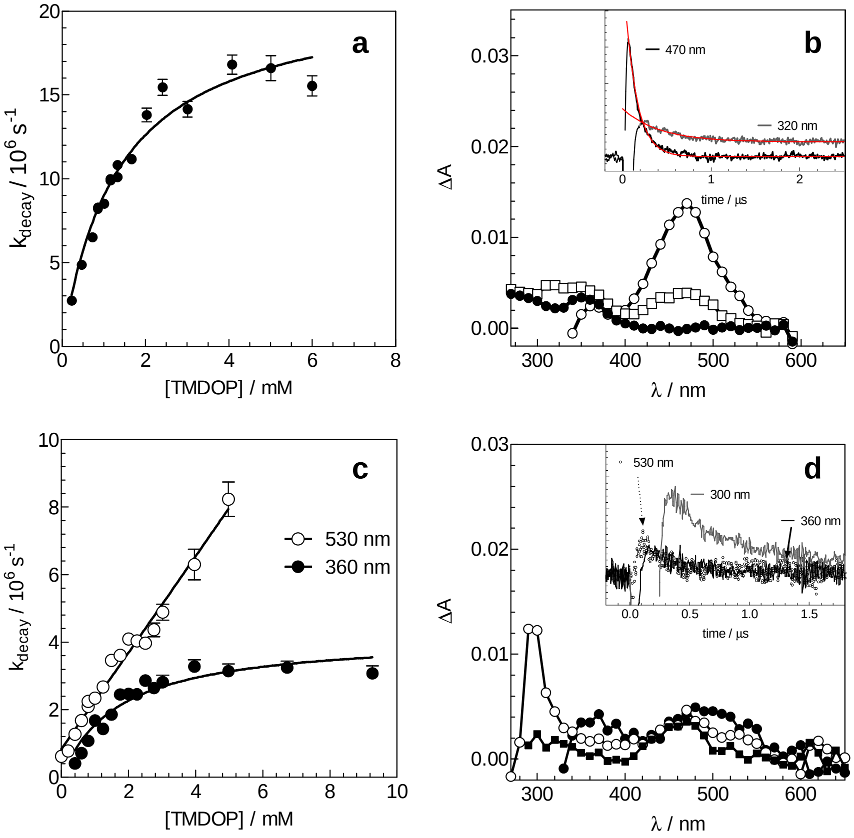

Figure 6.6. (a) Plot of the pseudo-first order decay rate coefficients (k_{decay}) of SiMe$_2$ vs. [TMDOP]. (b) Transient absorption spectra of a deoxygenated hexanes solution of **43** containing 0.5 mM TMDOP recorded at 25 ^{o}C 0.08-0.11 μs (o), 0.24-0.27 μs (□) and 2.16-2.19 μs (●) after the laser pulse. (c) Plot of the pseudo-first order decay rate coefficients (k_{decay}) of SiPh$_2$ (o) and the SiPh$_2$-TMDOP complex (●) vs. [TMDOP] in hexanes solution at 25 ^{o}C. (d) Transient absorption spectra of a hexanes solution of **44a** in the presence of 3 mM TMDOP, recorded 0.17-0.18 μs (●), 0.34-0.36 μs (o) and 1.40-1.41 μs (□) after the laser pulse. The insets show transient decay profiles recorded at selected wavelengths in the spectra.

Table 6.2. The values of K_1 (M^{-1}) and k_2 (10^6 s^{-1}) for the reactions of $SiMe_2$ and $SiPh_2$ with TMDOP, obtained from the analysis of the experimental plots of k_{decay} vs [TMDOP] using either eq. 6.3 or eq. 6.6 where appropriate (see text).

	slope from the plot of k_{decay} ($SiPh_2$) vs [TMDOP]	k_2 / 10^6 s^{-1}	K_1 / M^{-1}
$SiMe_2$	-	21 ± 2	700 ± 200
$SiPh_2$	1.4 ± 0.1	4.2 ± 0.2	600 ± 200

6.2.3. Reactions of $SiMe_2$ and $SiPh_2$ with D_3, D_4 and linear siloxanes

Addition of D_3 to a solution of **43** in dry deoxygenated hexanes resulted in a systematic decrease in the lifetime of the silylene and suppression of the growth of the disilene. A plot of the first order decay rate coefficient k_{decay} ($SiMe_2$) vs [D_3] afforded a linear plot, as shown in Fig (6.7a). Analogous results were obtained when D_3 was added to a hexanes solution of **44a**. Linear least squares analysis of these plots yielded slopes of $(1.2 \pm 0.2) \times 10^9$ M^{-1} s^{-1} and $(1.0 \pm 0.3)\times10^8$ M^{-1} s^{-1} for $SiMe_2$ and $SiPh_2$, respectively (Fig. 6.6). Similar experiments employing octamethylcyclotetrasiloxane (D_4) as substrate showed that molar quantities of the substrate had to be added in order to elicit an observable reduction in the silylene lifetime (*experiments with D_4 were performed by R. Valdizon*). The plots of k_{decay} vs [D_4] were linear and afforded slopes of $k_Q = (5.7 \pm 0.2) \times 10^6$ M^{-1} s^{-1} and $k_Q = (2.0 \pm 0.1) \times 10^6$ M^{-1} s^{-1} for the reactions with $SiMe_2$ and $SiPh_2$, respectively. With rate constants of this magnitude the presence of adventitious impurities like water presents a problem, thus these values should be considered upper limits to the actual rate constants. Transient absorption spectra recorded in the presence of a large concentration of either D_3 (20 mM) or D_4 (0.2 M) with either silylene showed no

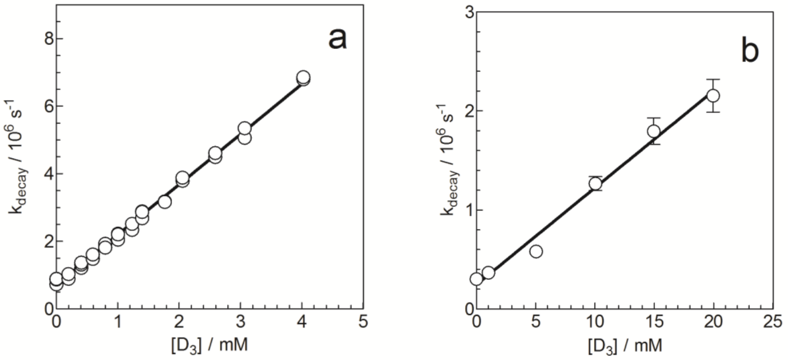

Figure 6.7. Plots of the pseudo first order decay rate constants (k_{decay}) for (a) $SiMe_2$ and (b) $SiPh_2$ vs [D_3] in hexane solution at 25 ^oC. The solid lines are the linear least-squares fit of the data to eq. 6.7.

evidence for the presence of any transient absorptions in the spectral region characteristic of silylene-O-donor complexes.

Rate constants for the reaction of $SiMe_2$ with D_3 were also determined at 5 different temperatures over the 5 - 55 ^oC temperature range by R. Valdizon (Table 6.4) and are incorporated in the Arrhenius and Eyring plots of Fig. 6.8; the corresponding activation parameters are collected in Table 6.5. The activation energy determined was zero within experimental error.

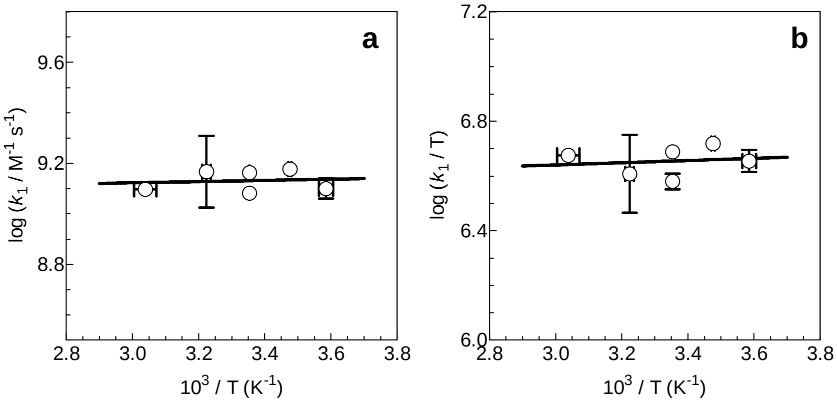

Figure 6.8. (a) Arrhenius and (b) Eyring plot for the reaction of $SiMe_2$ with D_3 in dry, deoxygenated hexanes over the range of 6-56 °C. (*experiments performed by R. Valdizon*)

Table 6.3. Rate constants for the reaction of $SiMe_2$ and $SiPh_2$ with D_3 and D_4 in deoxygenated hexanes at 25 °C.

reaction	k_Q / 10^9 M^{-1} s^{-1}
$SiMe_2 + D_3$	1.2 ± 0.2
$SiPh_2 + D_3$	0.10 ± 0.03
$SiMe_2 + D_4$	0.0057 ± 0.0002
$SiPh_2 + D_4$	0.0020 ± 0.0001

Table 6.4. Rate constants for the reaction of $SiMe_2$ with D_3 in deoxygenated hexanes over the temperature range of 6-56 °C.

T / °C	k_1 / 10^9 M^{-1} s^{-1}
6 ± 2	1.26 ± 0.05
14.5 ± 0.4	1.50 ± 0.03
25.7 ± 0.2	1.45 ± 0.02
25[a]	1.2 ± 0.2
37 ± 1	1.47 ± 0.02
56 ± 4	1.25 ± 0.03

[a] error in the temperature was not measured

Table 6.5. Activation and thermodynamic parameters for the reaction of $SiMe_2$ with D3.[a]

Parameter	value
E_a / kcal mol^{-1}	0.1 ± 0.5
log (A / M^{-1} s^{-1})	9.1 ± 0.4
$\Delta G^{\ddagger}_{298\ K}$ / kcal mol^{-1}	1.7 ± 0.5
$\Delta H^{\ddagger}$ / kcal mol^{-1}	-0.7 ± 0.5
$\Delta S^{\ddagger}_{298\ K}$ / cal $K^{-1}\cdot mol^{-1}$	-8 ± 3

[a] determined by R. Valdizon

The results are consistent with the mechanism of eq. 6.10, where the silylene reacts with D_3 via the reversible formation of an intermediate silylene-D_3 complex, which undergoes unimolecular rearrangement to yield the product of the Si-O bond insertion reaction. Given that the plots of k_{decay} vs $[D_3]$ are linear for both silylenes and that the SiR_2-D_3 complexes do not build up to detectable concentrations, the pre-equilibrium expression of eq. 6.7 is not applicable. The steady state approximation yields the expression for k_{decay} shown in eq. 6.11,[2] where a plot of k_{decay} vs [S] gives a straight line with a slope of $k_1k_2 / (k_{-1} + k_2)$, which is the overall rate constant for the reaction. The rate constants for the reactions of $SiMe_2$ and $SiPh_2$ with D_3 and D_4 are listed in Table 6.3.

$$\mathrm{SiR_2} + \mathrm{S} \underset{k_{-1}}{\overset{k_1}{\rightleftharpoons}} [\mathrm{cmpx}] \xrightarrow{k_2} \mathrm{P} \qquad (6.10)$$

$$k_{decay} = \frac{k_1 k_2 [S]}{k_{-1} + k_2} \qquad (6.11)$$

The effects of the addition of acyclic siloxanes $Me_2Si(OTMS)_2$ or TMS_2O on the silylene kinetics were also investigated by R. Valdizon. It was found that these substrates have no effect on the silylene lifetime, and free $SiMe_2$ and $SiPh_2$ and their corresponding dimers remain detectable even in the presence of molar concentrations of substrate. A modest drop in the intensity of the signal due to the silylene could be observed with both substrates, which yielded an estimate for the equilibrium constants for these reactions of ca. 2 M^{-1} using eq. 6.8. Because molar concentrations of each substrate were required to observe the drop in the intensity, dilution effects could account for a maximum of 16% artificial enhancement of the equilibrium constant. Transient absorption spectra of hexanes solution of either **43** or **44a** containing 0.3 – 1.5 M of TMS_2O or $Me_2Si(OTMS)_2$

show no evidence for the formation of silylene-siloxane complexes, which would be expected to exhibit spectra similar to those of other O-donor complexes.

6.3. Kinetic Simulations

In order to investigate the validity of our of the kinetic results for the various systems studied in this section, kinetic simulations were performed for a two-step reaction involving an initial reversible complexation followed by a unimolecular transformation to form a stable product, all in competition with dimerization of one of the reactants. The input mechanism had three steps: dimerization of silylene (Si) to form disilene (Si=Si, eq. 6.12), complexation with a donor (D) to form a complex (SiD, eq. 6.13), and unimolecular formation of a stable product (P, eq. 6.14).

$$\mathrm{Si + Si} \xrightarrow{k_{dim}} \mathrm{Si{=}Si} \qquad (6.12)$$

$$\mathrm{Si + D} \underset{k_{-1}}{\overset{k_1}{\rightleftharpoons}} \mathrm{SiD} \qquad (6.13)$$

$$\mathrm{SiD} \xrightarrow{k_2} \mathrm{P} \qquad (6.14)$$

The input rate constant for dimerization (k_{dim}) was kept constant at 2×10^{10} M^{-1} s^{-1}, because $SiMe_2$ undergoes dimerization at the diffusion-controlled rate.[4] Starting concentrations of Si were set at 10 μM to match the experimental conditions. Concentration vs time plots for both Si and SiD were simulated as a function of donor concentration, and imported into Prism 5.0 for least squares analyses. The simulated data were treated with a similar procedure as was used to treat the actual experimental data from the laser flash photolysis experiments: the decays were fit to a single exponential, excluding the portion at reaction times less than 50 ns; the excluded time window roughly corresponds to the sum of the laser pulse width and the recovery time from fluorescence. The resulting decay traces for Si consisted of two phases. However, because the experimental data do not allow differentiation between one phase and two phase decay kinetics due to the low signal-to-noise ratio, the simulated data were analyzed to a one-phase exponential fit as was done with the experimental data (eg. Fig. 6.9a). For the simulated SiD decay traces the growth portions of the kinetic traces were excluded from the analysis, and the resulting decay profiles were analysed as single exponential decays (eq. 6.15) to obtain values of k_{decay} (SiD) as a function of substrate concentration (eg. Fig. 6.9b). An example of the resulting k_{decay} vs [D] plot is shown in Fig. 6.9c, the input values of the rate coefficients are listed in Table 6.6 entry 4.

$$[Si] = [Si]_0 \cdot e^{-k_{decay}t} \qquad (6.15)$$

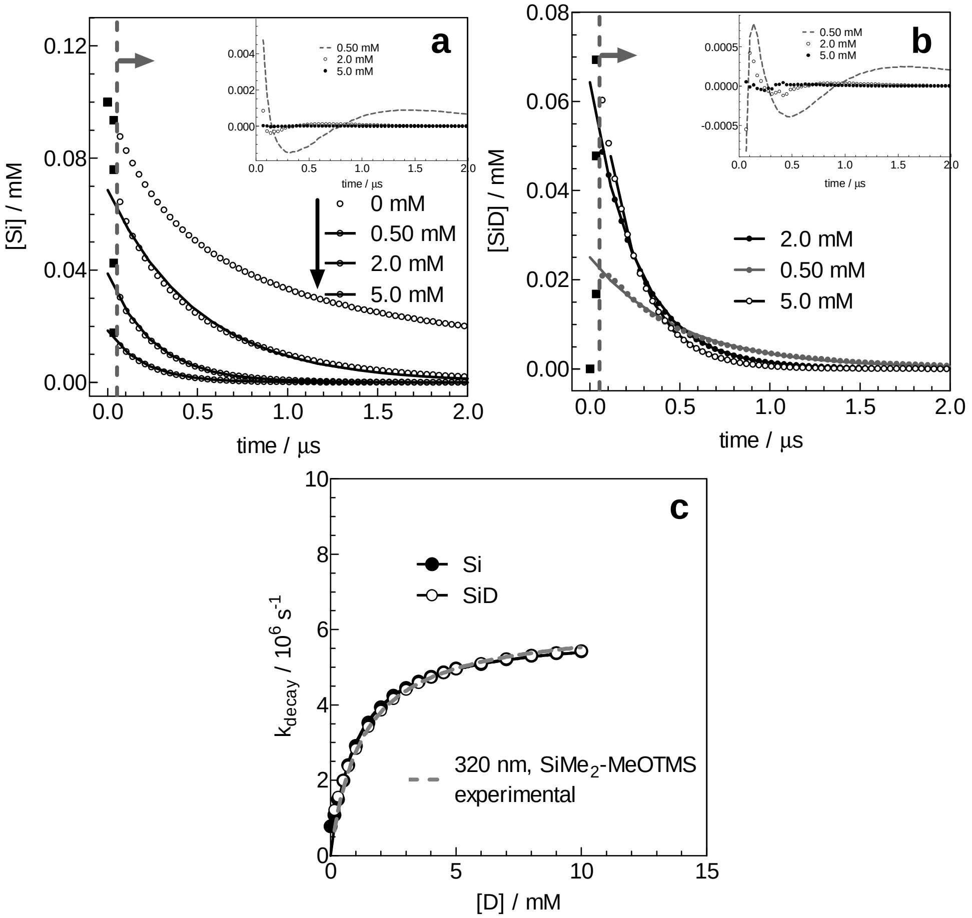

Figure 6.9. Results of kinetic simulations performed for a general reaction of silylene Si with donor D with a complexation rate constant of k_1 = 1.7×10^{10} M^{-1} s^{-1}, equilibrium constant K_1 = 1000 M^{-1}, and k_2 = 6 × 10^6 M^{-1} s^{-1}; (a) concentration vs time plots for Si as a function of D concentration, solid lines are the non-linear least squares fits of the data to first order decay kinetics (eq. 6.15), the inset shows the residual plots of the fits; (b) concentration vs time plots for SiD as a function of D concentration, solid lines are the non-linear least squares analysis of the data to first order decay kinetics, the inset shows the residual plot of the fit; (c) Plots of k_{decay} vs [D] for Si (●) and SiD (o) from the simulated concentration-time profiles, dotted gray line is the fit of experimental data of Fig. 6.3b to eq. 6.3 (Table 6.6, entry 4)

Table 6.6. The results of the kinetic simulations for the reaction of $SiMe_2$ with MeOTMS. The output values were obtained by analyzing the resulting k_{decay} vs [D] plots using eq. 6.3.

#	input values			output values			
	k_1 /10^9 $M^{-1}s^{-1}$	K_1 / M^{-1}	k_2 / 10^6 s^{-1}	K_1 / M^{-1} Si	K_1 / M^{-1} SiD	k_2 / 10^6 s^{-1} Si	k_2 / 10^6 s^{-1} SiD
1	1	1000	6	7 ± 2	74 ± 1	110 ± 30	7.64 ± 0.08
2	5	1000	6	500 ± 200	470 ± 50	7.6 ± 0.7	6.2 ± 0.1
3	5	300	6	190 ± 10	203 ± 4	5.8 ± 0.1	5.70 ± 0.03
4	17	1000	6	1020 ± 90	990 ± 60	5.9 ± 0.1	5.94 ± 0.09
5	17	300	6	220 ± 8	235 ± 1	5.48 ± 0.07	5.50 ± 0.01

6.3.1. $SiMe_2$ + MeOTMS

The rate constant for product formation (k_2) was set to 6×10^6 s^{-1}, the value that was measured experimentally (Fig. 6.3, Table 6.1). Since the experimental value of the forward rate constant k_1 cannot be determined for the reaction of $SiMe_2$ with MeOTMS, the simulated input value of k_1 was varied in the range of (1 - 17) × 10^9 M^{-1} s^{-1}, while the ratio of k_1/k_{-1} was set at either 300 M^{-1} or 1000 M^{-1}. The resulting output K_1 and k_2 values are listed in Table 6.6.

The plots of k_{decay} (SiD) vs [D] and k_{decay} (Si) vs [D] of the simulated data are shown in Fig. 6.10 for entries 1, 2, 3, and 5, while those for entry 4 are shown in Fig. 6.9c. Entries 1, 2 and 4 illustrate the effect of changes in the bimolecular rate constant k_1 on the plots of k_{decay} vs [D]. When $k_1 = 1 \times 10^9$ M^{-1} s^{-1} (Fig. 6.10a) the plot of k_{decay} vs [D] obtained from the silylene concentration-time data is linear, while that from the SiD displays a subtle curvature; both plots deviate significantly from the experimental data. Increasing k_1 to 5×10^9 M^{-1} s^{-1} (Fig. 6.10b) yields plots of k_{decay} vs [D] that are in much better agreement with the experimental data, while entry 4 yields plots that are

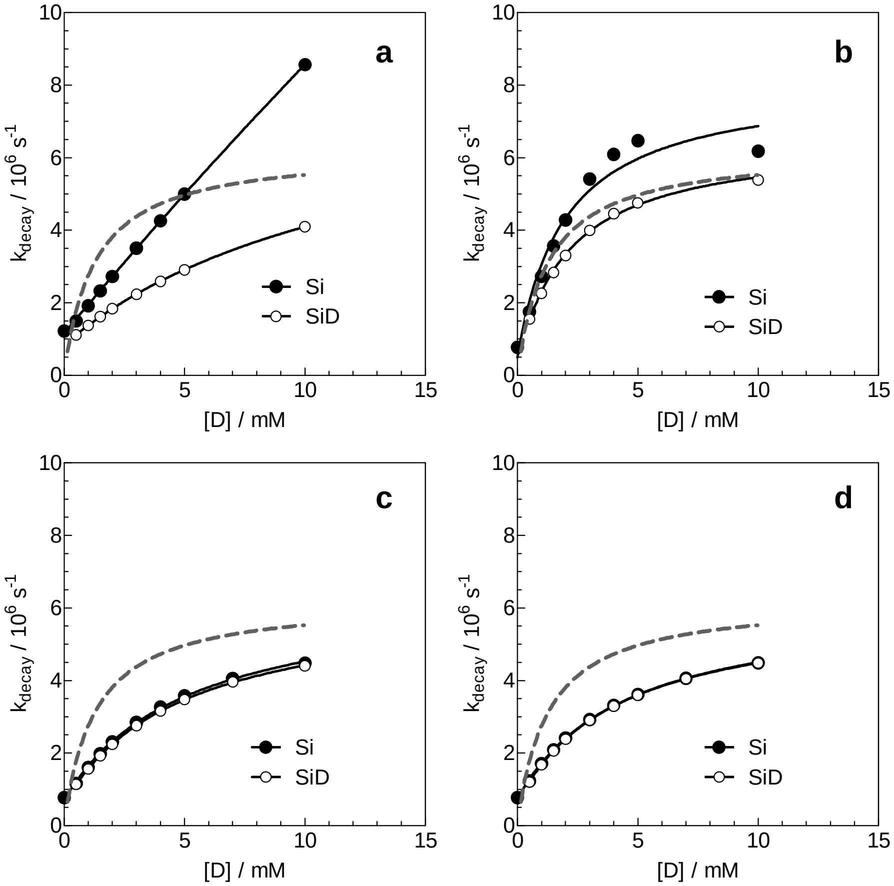

Figure 6.10. Plots of k_{decay} vs [D] for the input values of k_1, K_1 and k_2 listed in Table 6.6. (a) entry 1; (b) entry 2; (c) entry 3; (d) entry 5. The dotted lines are the fit of the experimental data of Fig 6.3b to eq. 6.3 shown for comparison; solid lines are the fits of the simulated data to eq. 6.3.

---

indistinguishable from the experimental ones. The variation in these results arises from the change in the contribution of the fast component of the two-phase decay of the silylene to the overall one phase kinetic fit. If the approach to equilibrium is complete within 50 ns, that portion of the concentration vs time profile is excluded from the kinetic analysis and thus does not contribute to the overall one phase decay analysis (entry 4).

However, when k_1 is smaller the approach to equilibrium is not complete after 50 ns, and the pre-equilibrium assumption breaks down. In these cases (entries 1 and 2), the pre-equilibrium approximation of eq. 6.3 cannot be used to extract the values of K_1 and k_2. The reduction of the input value for K_1 value to 300 M^{-1} resulted in a decrease in the initial slope of the linear portion of the plots of k_{decay} vs [D] (Fig 6.10c-d), as expected from the relationship for k_{decay} in eq. 6.3. In both cases (Table 6.6, entries 3 and 5) the pre-equilibrium assumption is applicable, since the equilibrium concentration is reached faster by the silylene when K_1 value is reduced.

The simulated data of Table 6.6 were also analysed according to eq. 6.8 in order to test whether the equilibrium constant can be determined accurately from the apparent initial silylene signal intensities. The plots of $\Delta A_0/\Delta A_{eq}$ vs [D] displayed an upward curvature in each case (Fig 6.11), however they were analysed with linear regression to determine if a rough estimate of equilibrium constant can be extracted using this method. For $k_1 = (5\text{-}17)\times10^9$ M^{-1} s^{-1}, there is a good agreement between K_1 value determined by the two methods; however, both methods underestimate the K_1 value by 35-50% compared to its “true” (i.e. input) value. Closest agreement between input and output values for k_2 and K_1 values was obtained for $k_1 = 1.7 \times 10^{10}$ M^{-1} s^{-1} and $K_1 = 1000$ M^{-1}.

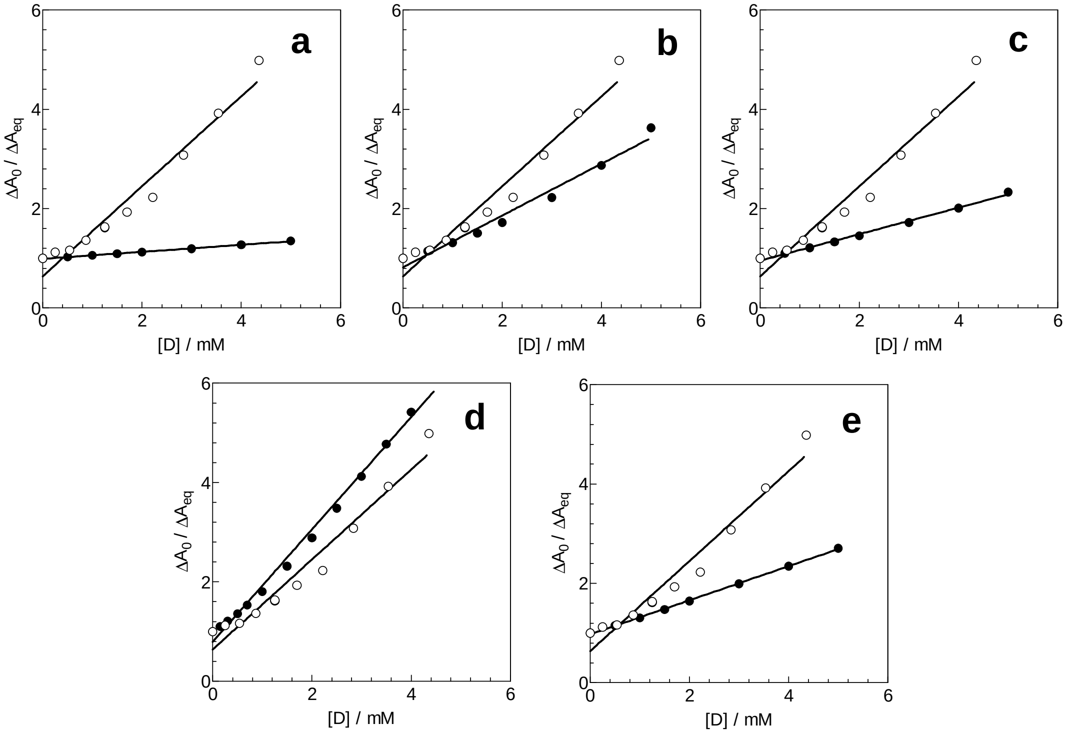

Figure 6.11. Plots of $\Delta A/\Delta A_{eq}$ determined from (●) simulated Si data obtained from the simulated input rate constant values listed in Table 6.6 (a) entry 1, (b) entry 2, (c) entry 3, (d) entry 4, (e) entry 5. (o) Obtained from experimental data for $SiMe_2$ from the reaction of $SiMe_2$ with MeOTMS. Solid lines are the least squares analysis of the data to eq. 6.8.

Impurity Quenching. The effect of impurity quenching of the silylene was also investigated using kinetic simulations. Another equation was added to the reaction scheme (eq. 6.16), which accounts for the presence of an adventitious impurity in the solvent that reacts competitively with the silylene. The input value for the rate constant for this reaction was 2×10^{10} M^{-1} s^{-1}, close to the rate constant for diffusion in hexanes at 25 ^{o}C.

$$\text{Si} + \text{impurity} \xrightarrow{k_3} \text{P}_2 \qquad (6.16)$$

The concentration of impurity was varied between 0-0.3 mM, and it was shown that the plot of k_{decay} vs [D] of the simulated silylene data using eq. 6.7 is identical to that obtained from the complex using eq. 6.3. Therefore, the experimental data can indeed be analysed using eq. 6.7 for the silylene decay traces.

The effect of the presence of 1% MeOH in the MeOTMS sample was also investigated using eq. 6.16. While the concentration of MeOTMS was varied between 0-10 mM, the impurity (MeOH in this case) concentration was adjusted as well in order to maintain the 0.01 concentration ratio relative to MeOTMS. In this case, the effect on the resulting plots of k_{decay} vs [MeOTMS] for the silylene and the complex was minimal. This result indicates that the presence of ca. 1% MeOH impurity in the MeOTMS sample used for the experiment should have no effect on the observed decay kinetics of the silylene or the complex. Therefore, either a much higher MeOH concentration is responsible for the discrepancy between the experimental results obtained in this work and the published data, or significantly higher $SiMe_2$ concentrations were used and dimerization of silylene would cause problems in data interpretation.

6.3.2. $SiPh_2$ + TMDOP

Three standard equations were used as before, eq. 6.12-6.14. The input k_{dim} value was kept constant at 2×10^{10} M^{-1} s^{-1}, while the values of k_1 were varied between 1.4×10^9 M^{-1} s^{-1} and 4×10^9 M^{-1} s^{-1}. The dissociation rate constant, k_{-1}, was adjusted as required to yield K_1 values of 600, 1300 or 1500 M^{-1}. The rate constant for the unimolecular

Table 6.7. The results of the kinetic simulations for the reaction of $SiPh_2$ with TMDOP. The bimolecular rate constant values for complexation, k_1, for the output values were obtained by linear least-squares analysis of the linear portion of the k_{decay} (Si) vs [D] simulated plot.

	input values			output values		
	k_1 /10^9 $M^{-1}s^{-1}$	K_1 / M^{-1}	k_2 / 10^6 s^{-1}	slope /10^9 $M^{-1}s^{-1}$	K_1 / M^{-1}	k_2 / 10^6 s^{-1}
a	1.4	600	4.2	0.62 ± 0.01	100 ± 10	5.6 ± 0.3
b	1.4	600	3.2	0.55 ± 0.01	120 ± 10	4.0 ± 0.2
c	3	600	3.2	0.44 ± 0.01	230 ± 20	2.70 ± 0.07
d	3	600	4.2	0.61 ± 0.02	220 ± 20	3.9 ± 0.1
e	3	1000	4.2	1.00 ± 0.02	340 ± 40	4.3 ± 0.1
f	3	1300	4.2	1.32 ± 0.02	400 ± 50	4.5 ± 0.1
g	3	1500	4.2	1.39 ± 0.03	430 ± 50	4.6 ± 0.1
h	3.5	1500	4.2	1.41 ± 0.04	520 ± 70	4.5 ± 0.1
i	4	1500	4.2	1.44 ± 0.04	610 ± 80	4.4 ± 0.1

rearrangement, k_2, was varied between 3.2×10^6 s^{-1} and 4.2×10^6 s^{-1} for the $K_1 = 600$ M^{-1} and $k_1 = 1.4$ or 3×10^9 runs, but otherwise kept constant at 4.2×10^6 s^{-1}. The complete set of simulations carried out is shown in Table 6.7 along with output values obtained after workup and analysis of the simulated data.

The simulated Si and SiD data were treated in the same way as described earlier. In each of these cases, the k_{decay} (Si) vs [D] and k_{decay} (SiD) vs [D] plots were plotted on the same graph, as shown in Fig 6.12. The plots extracted from the simulated silylene decay profiles are linear over the 0-5 mM concentration range in [D], but at higher substrate concentrations a downward curvature was observed in some cases and those points were excluded from the analysis. The slopes of the linear portions of the plots were determined by linear least squares analysis and are listed in Table 6.7. The plots extracted from the decay profiles of the SiD complexes displayed downward curvature in each case (Fig. 6.12). These data were fitted to eq. 6.3 to obtain the output values of k_2 and K_1 listed in Table 6.7.

The closest agreement between the simulated and experimental data is observed for trials *f-i* in Table 6.7. Therefore, the actual complexation rate constant k_1 for the reaction of $SiPh_2$ with TMDOP can be estimated to be $k_1 = (3.5\pm0.5)\times10^9$ M^{-1} s^{-1}, the equilibrium constant is in the 1400 ± 100 M^{-1} range, while $k_2 = 4.2 \times 10^6$ s^{-1}. These values are included in Table 6.8.

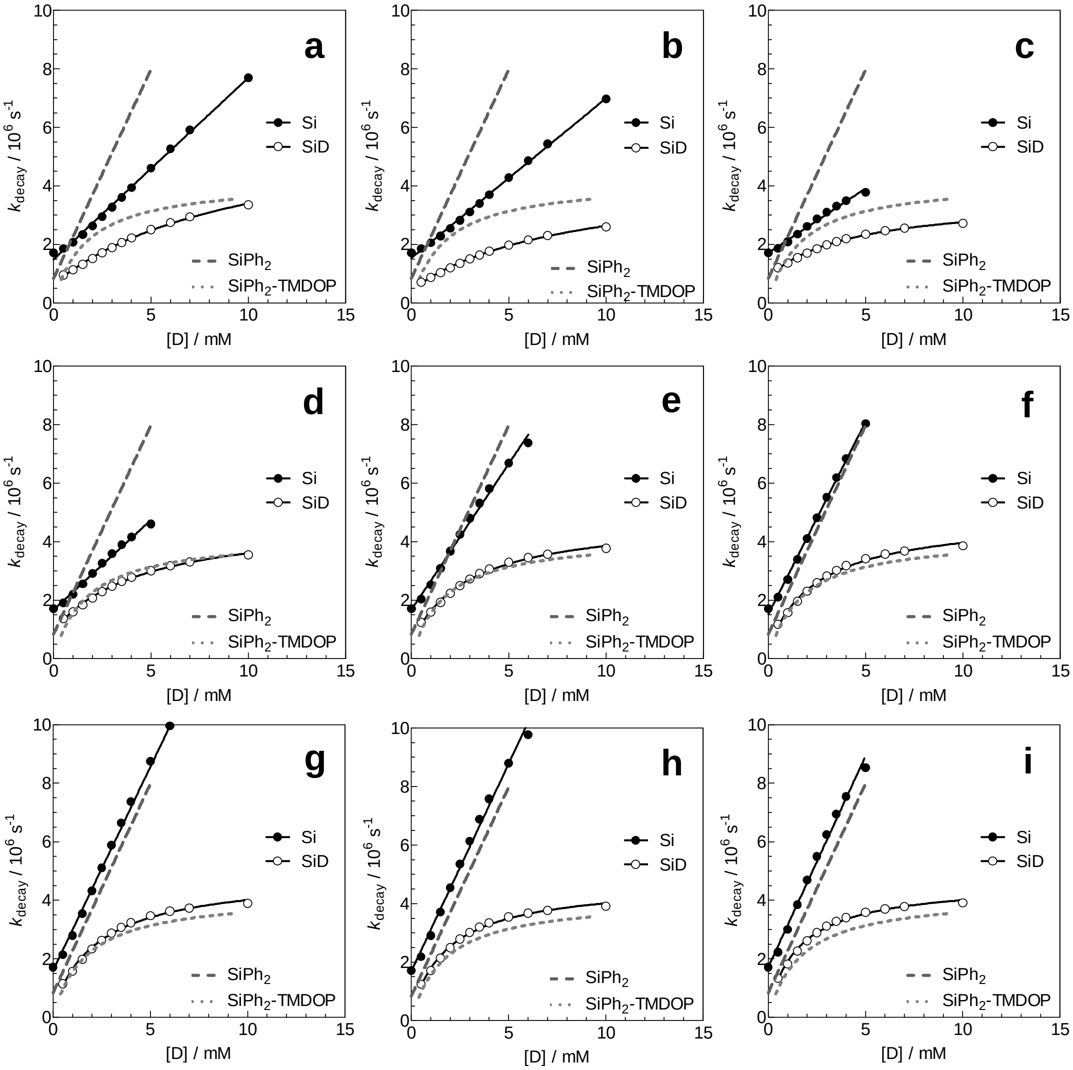

Figure 6.12. Simulated plots of k_{decay} vs [D] for the input rate constant values listed in Table 6.7 (trials *a*-*i*). The dotted lines are the experimental data obtained from the reaction of $SiPh_2$ with TMDOP (Section 6.2.2).

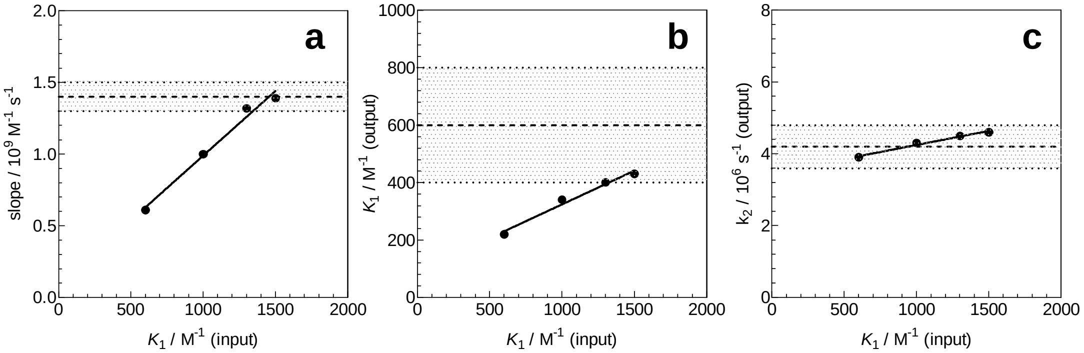

Figure 6.13. Graphical representation of the kinetic simulations of Table 6.7 *d-g*. (a) Plot of the output slope values of the k_{decay} (SiR_2) vs [D] plots vs input K_1 value; (b) plot of the output K_1 value vs input K_1 value; (c) plot of the output k_2 value vs input K_1 value. The solid lines are linear least squares analysis of the data, the gray areas are the experimentally obtained values with errors.

To explore the effect of the input K_1 value on the actual slope of the plot of k_{decay} (Si) vs [D], and K_1 and k_2 values, the plots of input K_1 versus each of the output variables were constructed from trials *d-g* of Table 6.7 and are shown in Fig. 6.13. The results indicate that input K_1 values below 1300 M^{-1} underestimate the actual output slope and the output K_1 value, while the output k_2 value is not affected to an appreciable extent. Therefore, the most reliable experimentally measurable value is the rate constant for unimolecular rearrangement, k_2, while the estimations of k_1 and K_1 require complex kinetic simulations in order to aid in the interpretation of the experimental estimates.

6.4. Discussion

The results indicate that the insertion of silylenes into the Si-O bond of MeOTMS occurs in two steps – initial reversible complexation followed by unimolecular rearrangement of the complex to form the final reaction product (eq. 6.17).

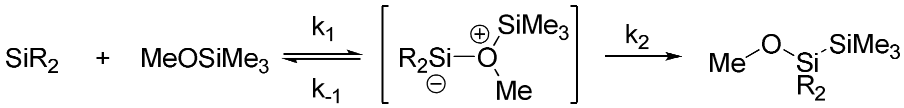

(6.17)

For the $SiMe_2$+MeOTMS system the equilibrium constants for complexation can be obtained by analyzing the plots of (k_{decay} – k_0) ($SiMe_2$) vs [MeOTMS] and k_{decay} ($SiMe_2$-MeOTMS complex) vs [MeOTMS] according to eq 6.7 and 6.3, respectively. For the reaction of $SiMe_2$ with MeOTMS, the K_1 values obtained from the two plots are the same within experimental error (Table 6.1). A lower limit value for the rate constant for complexation (k_1) was estimated to be $k_1 \geq 1\times10^{10}$ M^{-1} s^{-1} using kinetic simulations. The first-order rate constant for the decomposition of the complex is most accurately obtained from the plot of k_{decay} ($SiMe_2$-MeOTMS complex) vs [MeOTMS], since the $SiMe_2$-MeOTMS complex can be detected at much higher substrate concentrations where the silylene signal is undetectable.

The analogous reaction of $SiPh_2$ with MeOTMS presumably occurs by the same mechanism, however in this case k_2 is ca. 20x smaller than that of the $SiMe_2$-MeOTMS complex. This change in the k_2 value, in combination with adventitious impurities in the hexane solvent, results in the plot of k_{decay} ($SiPh_2$) vs [MeOTMS] being different from the plot of k_{decay} ($SiPh_2$-MeOTMS complex) vs [MeOTMS] – the silylene lifetime is

Table 6.8. Forward rate (k_1), equilibrium (K_1) and unimolecular insertion rate constants (k_2) for the reactions of $SiMe_2$ and $SiPh_2$ with MeOTMS and TMDOP. (Hexanes, 25 °C)[a]

Silylene	Donor	k_1 / 10^9 M^{-1} s^{-1}	K_1 / M^{-1}	k_2 / 10^6 s^{-1}
$SiMe_2$	MeOTMS	> 10[b]	800 ± 200[d]	6.2 ± 0.4[d]
	TMDOP	> 10[b]	700 ± 200[c]	21 ± 2[c]
$SiPh_2$	MeOTMS	> 5[b]	1900 ± 200[e]	0.3 ± 0.1[d]
	TMDOP	3.5 ± 0.5[b]	1400 ± 100[b]	4.2 ± 0.6[d]

[a] Errors are quoted as twice the standard error from linear or non-linear least-squares analysis of the data to eq 6.3, 6.7-6.8. [b] Estimated from kinetic simulations. [c] Values obtained from least-squares fit of the silylene data to eq. 6.7. [d] Values obtained from least-squares fit of the silylene-donor complex data to eq. 6.3. [e] Values obtained from the analysis of the data to eq. 6.8.

unaffected by the presence of MeOTMS, while its "initial" absorbance value consistently diminishes with increasing concentration. In this case the plot of k_{decay} ($SiPh_2$-MeOTMS complex) vs [MeOTMS] exhibits downward curvature, however the initial curved portion of the plot consists of only two data points including the zero-intercept (Fig 6.4b). This portion of the plot is defined by the value of the equilibrium constant, K_1. Since the data in this region are very limited, the K_1 value in this case is more accurately obtained from the loss of the signal intensity of the silylene as a function of substrate concentration from the least-squares analysis of the data to eq. 6.8. As is shown in Table 6.1, the K_1 values from these two analyses are a factor or two different from each other, however the data obtained from eq. 6.7 is highly inaccurate as is reflected in an unreasonably large error (vide supra).

The reaction of silylenes with the cyclic siloxane TMDOP likely proceeds via the same two-step mechanism as the reaction with MeOTMS; however the change in the relative magnitudes of the rate constants results in very different observations for these two reactions. The putative $SiMe_2$-TMDOP complex could not be detected because its k_2 value is relatively large, and hence at the concentrations where it might be detected it is too short-lived to be resolved from the strong sample fluorescence in the range where it is expected to absorb. The complexation rate constant, k_1, cannot be measured in this case but a lower limit of $k_1 \geq 1 \times 10^{10}$ M^{-1} s^{-1} could be estimated using kinetic simulations, similar to that for the reaction of $SiMe_2$ with MeOTMS. With the $SiPh_2$ + TMDOP system, behaviour consistent with saturation kinetics was observed in the plot of k_{decay} vs [TMDOP] from the $SiPh_2$-TMDOP complex decay profiles, while a linear plot was obtained from the silylene decay profiles. In this case the simulations show that the k_2 value can be reliably obtained from the experimental data, but k_1 and K_1 values have to be estimated by simulation. The simulations show that the differences in the results observed in the two experiments is due to a ca. three-fold reduction in the k_1 value in the reaction involving $SiPh_2$ compared to that with $SiMe_2$ (Table 6.8). A similar difference in the bimolecular rate constants was previously observed for the reactions of $SiMe_2$ and $SiPh_2$ with Et_2NH and Et_3N which runs counter to notion that $SiPh_2$ is a stronger Lewis acid than $SiMe_2$.[3] In the reactions with amines steric factors have an appreciable effect on the bimolecular rate constants. Calculation at the G4 level of theory indicate that Si-O and Si-N bond lengths are quite similar to each other in the $SiMe_2$-Et_2O and $SiMe_2$-Et_2NH complexes, thus comparable trends in the rate constants would be expected for the reactions with TMDOP.

The Gibbs free energy values for complexation can be obtained from the equilibrium constants for the reactions of $SiMe_2$ and $SiPh_2$ with MeOTMS, TMDOP and Et_2O and are shown in Table 6.10. It is well known that siloxanes are weaker Lewis bases than ethers (Table 6.9).[5-7] A notable difference between ethers, alkoxysilanes and silyl

Table 6.9. The relative basicities of ethers, alkoxysilanes and siloxanes from the phenol O-H stretching frequency and pyrrole N-H stretching frequency upon hydrogen bond formation with various compounds.[a]

Compound	phenol $\Delta\nu_{OH}$	pyrrole $\Delta\nu_{NH}$
Et_2O	282	149
MeOTMS	271	163
TMS_2O	169	75
$Me_2Si(OTMS)_2$	142	58
D_3	166	79
D_4	144	54

[a] Ref. 7

ethers is the widening of the bond angle about oxygen upon replacement of an alkyl group with a silyl group, which is accompanied by a reduction in the Si-O bond length.[5] Although mixing of oxygen lone pairs and 3d orbitals on silicon was thought to contribute to the angle widening and in turn to lower basicity,[7] this explanation has since been abandoned.[6] Ab initio calculations indicate that the silyl groups have relatively low lying π^* orbitals which can participate in mixing with a non-bonding MO on oxygen, and as a result the HOMO is less localized on oxygen and more on silicon.[5] Steric repulsions associated with silyl groups are substantially higher than those of alkyl groups, which also contribute to angle widening and in turn to lower basicity. The variation in ΔG values for $SiMe_2$ complexation reactions illustrates very subtle differences in the stability of the Lewis acid-base complexes among the three O-donors. The values for $SiPh_2$ complexation, however, clearly demonstrate that Et_2O is the strongest Lewis base. Linear siloxanes and D_4 are the weakest Lewis bases (Table 6.9), and thus do not display any reactivity towards the two silylenes.

The Lewis acidity of $SiPh_2$ is higher than that of $SiMe_2$, which is demonstrated by the more energetically favourable formation of the $SiPh_2$-Et_2O complex by ca. 1 kcal mol^{-1} compared to the formation of the $SiMe_2$-Et_2O complex. This difference in Lewis acidities of the two silylenes is also reflected in the ΔG values for complexation with the siloxanes studied in this work, however to a much smaller extent.

The rate constants for unimolecular rearrangement of the silylene-donor complexes appear to be highly dependent on ring strain. As shown in Table 6.8, the SiR_2-TMDOP complexes are much more reactive than the corresponding SiR_2-MeOTMS complexes with the same silylene. These differences can be attributed to the relief of the ring strain in TMDOP upon ring expansion, which accompanies SiR_2 insertion into the ring. Ring strain is not associated with MeOTMS, thus the Lewis acid-base complexes involving this donor are substantially longer lived.

The Lewis acid-base complexes could not be detected directly in the experiments involving D_3 as substrate, and while the plots of k_{decay} (SiR_2) vs [D] were linear in both cases. The near-zero activation energy for the reaction of $SiMe_2$ with D_3 is consistent with a two-step reaction mechanism in which the first step is reversible and is followed by a unimolecular second step. The complex is presumably formed as a steady-state intermediate and thus it cannot be directly observed. The acyclic siloxanes TMS_2O and $Me_2Si(OTMS)_2$ and the marginally-strained cyclic compound D_4 show little or no reactivity with silylenes.

Table 6.10. The equilibrium constants (in M^{-1}) and experimental Gibbs Free energies (reference state, gas phase, 1 atm, 25°C) for Lewis acid-base complexation of $SiMe_2$ and $SiPh_2$ with MeOTMS, TMDOP and Et_2O in hexanes at 25 °C (in kcal mol^{-1}).

silylene	substrate	K_1 / M^{-1}	ΔG / kcal mol^{-1}
$SiMe_2$	MeOTMS	800 ± 200	-2.1 ± 0.2
	TMDOP	700 ± 200	-2.0 ± 0.2
	Et_2O^a	1260 ± 50	-2.3 ± 0.1
$SiPh_2$	MeOTMS	1900 ± 200	-2.57 ± 0.06
	TMDOP	1400 ± 100	-2.39 ± 0.04
	Et_2O^a	7100 ± 600	-3.4 ± 0.1

[a] Ref. 3

6.5. Conclusions

The Si-O insertion reactions of $SiMe_2$ and $SiPh_2$ with MeOTMS, TMDOP, and D_3 occur via a two-step mechanism involving the initial reversible formation of a Lewis acid-base complex, followed by unimolecular rearrangement to yield the formal Si-O insertion product. Depending on the magnitudes of the rate constants of each step the observed kinetic behaviour is different for each system. The bimolecular rate constants for formation of the SiR_2-D complexes could not be obtained experimentally, but could be estimated with the aid of kinetic simulations. Equilibrium constants for complexation of $SiMe_2$ and $SiPh_2$ with MeOTMS and TMDOP could be obtained, and are consistent with the differences in the Lewis acidities of the silylenes and the Lewis basicities of the substrates. The SiR_2-D_3 complexes could not be detected directly in our experiments, presumably because the complexes are formed as steady-state intermediates. This is supported by the finding of a near-zero activation energy for the reaction of $SiMe_2$ with D_3, as determined from the temperature-dependent studies.

6.6. References

1. Moiseev, A. G.; Leigh, W. J., *Organometallics* **2007,** *26*, 6277.

2. Wright, M. R., *An Introduction to Chemical Kinetics*. John Wiley & Sons Ltd.: Chichester, England, 2004.

3. Kostina, S. S.; Singh, T.; Leigh, W. J., *Organometallics* **2012,** *31* (9), 3755.

4. Yamaji, M.; Hamanishi, K.; Takahashi, T.; Shizuka, H., *J. Photochem. Photobiol. A: Chem.* **1994,** *81*, 1.

5. Shambayati, S.; Schreiber, S. L.; Blake, J. F.; Wierschke, S. G.; Jorgensen, W. L., *J. Am. Chem. Soc.* **1990,** *112* (2), 697.

6. Passmore, J.; Rautiainen, J. M., *Eur. J. Inorg. Chem.* **2012,** *2012* (36), 6002.

7. West, R.; Whatley, L. S.; Lake, K. J., *J. Am. Chem. Soc.* **1961,** *83* (4), 761.

7. Chapter 7 – O- and S- abstraction reactions by transient silylenes

7.1. Overview

The reaction of the transient silylenes $SiMe_2$, $SiPh_2$, $SiTmp_2$ and $SiMes_2$ with cyclohexene oxide (CHO), propylene oxide (PrO), propylene sulfide (PrS) and cyclohexene sulfide (CHS) in hydrocarbon solvents proceeds in a manner consistent with the formation of the corresponding intermediary silanones and silanethiones, respectively. Dimethyl- and diphenylsilanone insert into an Si-O bond of hexamethylcyclotrisiloxane (D_3) to yield the cyclic tetramer (D_4), while dimesitylsilanone (Mes_2SiO) reacts with one molecule of CHO and one of MeOH to generate a novel compound **99**. On the other hand, diphenylsilanethione could be trapped efficiently with methanol to yield **96**.

The results of laser flash photolysis experiments are indicative of a multistep mechanism for the reaction, involving the initial formation of donor-acceptor complexes. The complexes were detected in all cases with the exception of the $SiTmp_2$-thiirane and the $SiMes_2$-thiirane systems. The second step of the reaction is unimolecular decomposition of the complexes to yield the corresponding silanones or silanethiones. The SiR_2-PrO complexes (R = Me, Ph, Tmp, or Mes) exhibit lifetimes of ca. 300 ns in all cases without significant variation with silylene substituents. The corresponding SiR_2-CHO complexes are shorter-lived than those with PrO, providing support for a biradical mechanism for the dissociation of the silylene-oxirane complexes. The silylene-thiirane complexes decay with significantly faster decay rate constants; the $SiMe_2$-PrS complex decays within the excitation laser pulse ($\tau \leq 25$ ns), while the $SiPh_2$-PrS complex exhibits $\tau = 48 \pm 3$ ns and decays to generate a long-lived transient product with UV spectrum centered at $\lambda_{max} \approx 275$ nm. A similar product was detected with the $SiTmp_2$-PrS system. These transients were assigned to the corresponding silanethiones on the basis of their second order decay kinetics, and in the case of the $SiPh_2$-PrS system on the reactivity of the species with methanol, *tert*-butanol, acetic acid, and *n*-butylamine. The rate constants for these bimolecular reactions fall in the range of 1.4×10^8 to 3.2×10^9 M^{-1} s^{-1}.

As in our previous studies, the four silylenes were generated by photolysis of the corresponding oligosilane derivatives, **43**, **44a**, **45**, **60**, **86** and **87**.

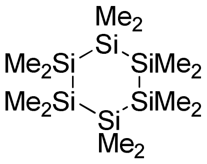

43

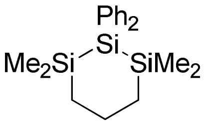

44a

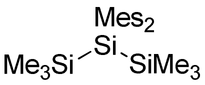

45

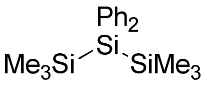

60

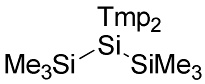

86

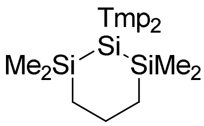

87

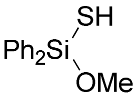

96

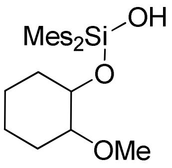

99

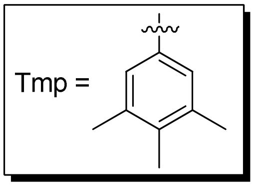

7.2. Results

7.2.1. Product studies

7.2.1.1. Reaction of $SiMe_2$ with oxiranes and thiiranes

Photolysis of **43** in the presence of CHO (0.2 M) afforded pentamethylcyclopentasilane (**56**),[1] octamethylcyclotetrasilane (**57**),[1] and cyclohexene (**88**) as the major products, along with small amounts of D_3, 1,1,3,3,5,5,7,7-octamethylcyclotetrasiloxane (D_4), and numerous other minor products that were not identified (eq. 7.1). The product mixture was monitored throughout the experiment by ^1H NMR spectroscopy and GC/MS. The two oligosiloxanes were present in an approximate ratio of D_3:D_4 ~ 4.3:1 (by GC/MS; uncalibrated) after 15 minutes photolysis time, which decreased to *ca.* 3:1 upon doubling the irradiation time. Concentration vs. time plots constructed for CHO and **88** from the NMR integrals (Figure 7.1, 7.2) indicated that the alkene was formed in 49% yield relative to consumed CHO during the early stages of the photolysis (0-2% conversion of CHO), but decreased upon continued irradiation. Photolysis of **43** in hexanes containing added D_3 (0.2 M) in addition to CHO (0.2 M) resulted in a considerably cleaner product mixture, which consisted mainly of **56**, **57**, **88**, D_4, and compound **89**. GC/MS analysis of the photolysate indicated compound **89** and D_4 to be present in a ratio of **89**:D_4 ≈ 1:2.2 after 15 minutes of photolysis. Compound **89** results from insertion of dimethylsilylene into an Si-O bond of D_3.[2] The present results are consistent with those reported by Goure and Barton for the photolysis of **43** in the presence of cyclooctene oxide, where most of the minor unidentified products formed in the absence of D_3 were no longer formed when D_3 was introduced.[2]

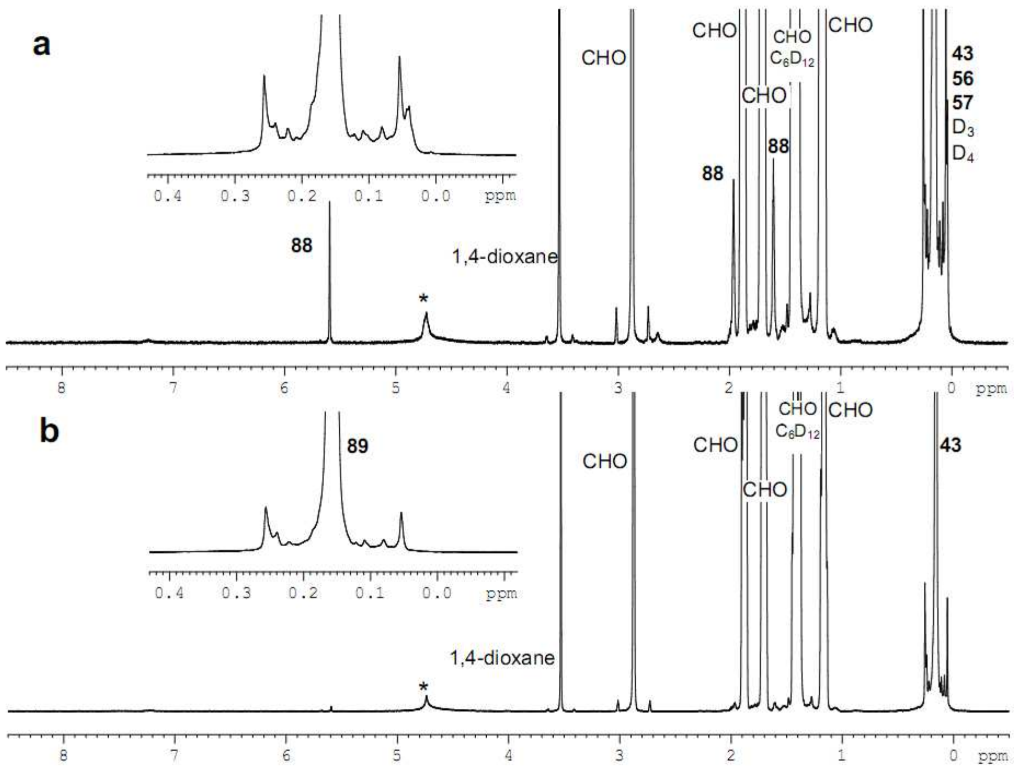

Figure 7.1. 600 MHz ^{1}H NMR spectra of a solution of 0.05 M **43** and 0.2 M CHO in C_6D_{12}, a) after 8 min of photolysis; b) before photolysis.

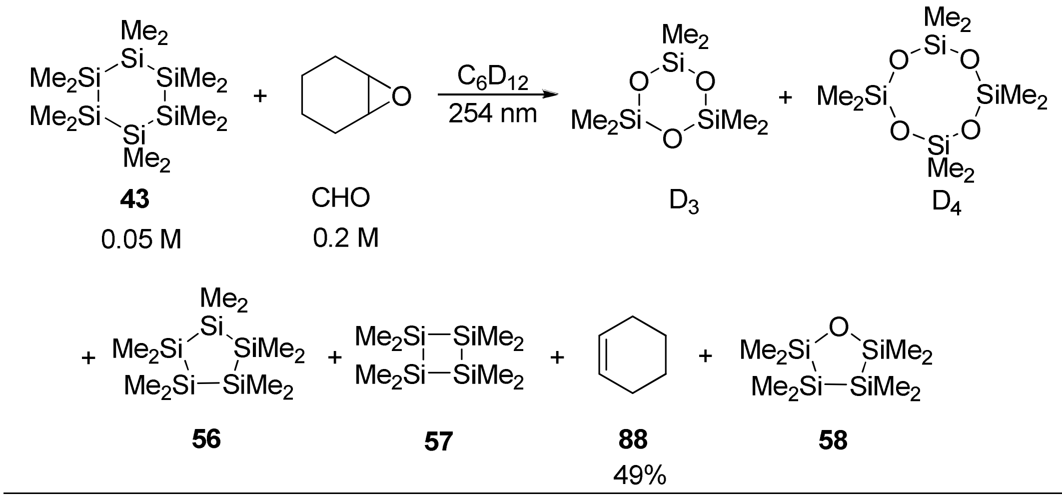

(7.1)

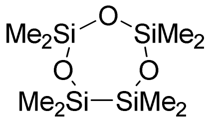

89

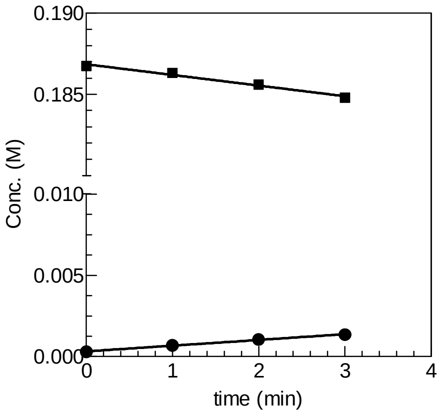

Figure 7.2. Concentration vs time plots for 254 nm irradiation of a deoxygenated solution of **43** (0.05 M) in C_6D_{12} containing CHO (0.2 M). The solid lines are the least squares fits of the data, the slopes of which are CHO (■), -0.00065 ± 0.00006; **7** (●), 0.00035 ± 0.00001.

A C_6D_{12} solution containing **43** (0.05 M), PrS (0.1 M), D_3 (0.2 M), Si_2Me_6 (0.01 M) and 1,4-dioxane (0.01 M) was photolyzed with two 254 nm lamps for 15 min in 1-2 min intervals to afford products **56**, **57**, **89-91** (see eq. 7.2), according to ^{1}H NMR, ^{29}Si NMR and GC/MS analysis of the photolysis mixture. Compound **57** was identified based on its characteristic ^{29}Si NMR shift at -27.6 ppm.[3] Compound **90** was identified on the basis of its mass spectra and ^{29}Si NMR chemical shifts which were similar to those previously reported.[4] This product is formed by insertion of dimethylsilanethione into an Si-O bond of D_3. The yields of **90** and **91** were determined relative to consumed PrS from the concentration vs time plots shown in Fig. 7.4, while the yield of **89** was estimated based on the ratio of peak areas due to **89** and **90**.

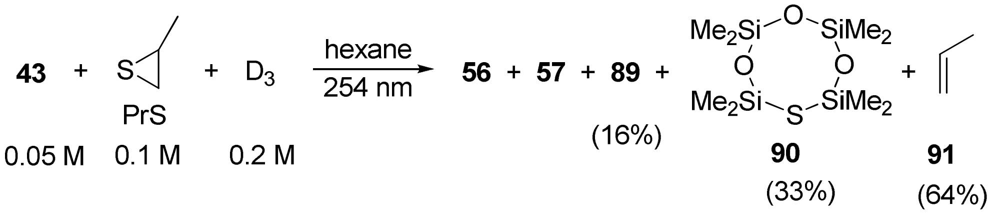

(7.2)

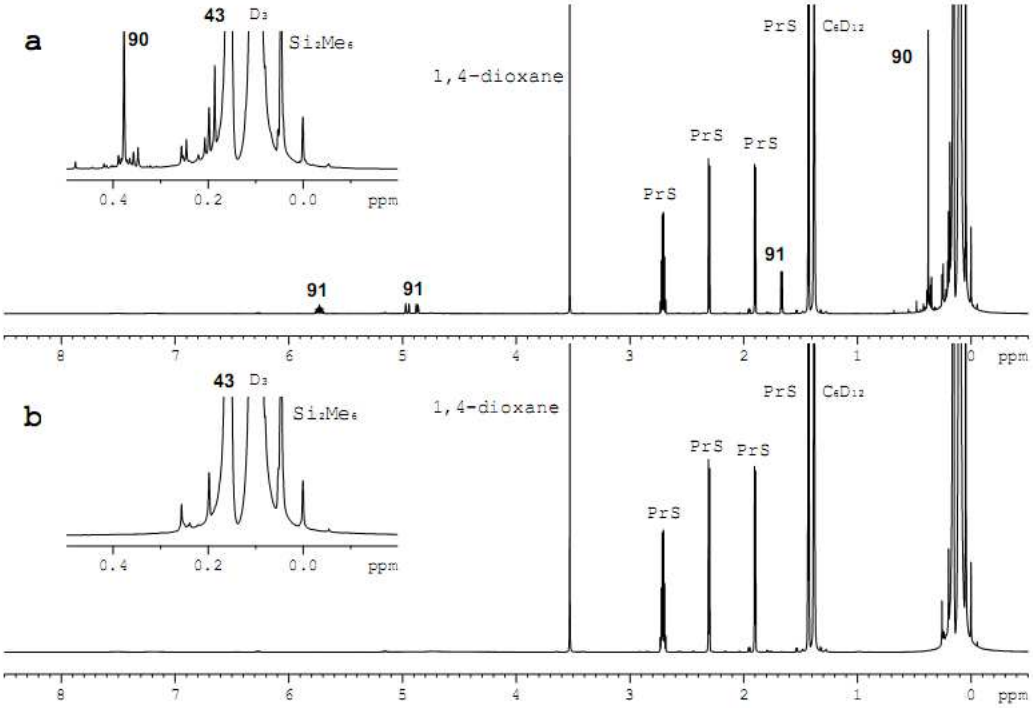

Figure 7.3. 600 MHz ^{1}H NMR spectra of a solution of 0.05 M **43**, 0.1 M PrS, 0.2 M D_3 0.01 M 1,4-dioxane and 0.01 M Si_2Me_6 in C_6D_{12}, at a) 15.5 min of photolysis; b) 0 min of photolysis.

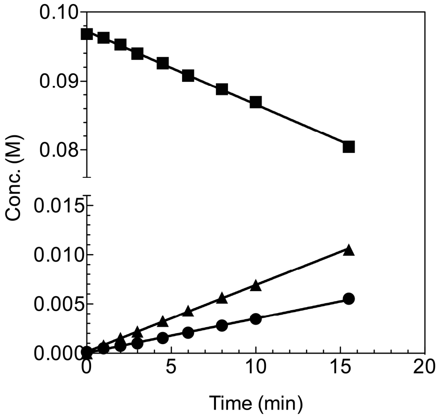

Figure 7.4. Concentration vs time plots for 254 nm irradiation of a deoxygenated solution of **43** (0.05 M) in C_6D_{12} containing D_3 (0.2 M) and PrS (0.10 M). The solid lines are the least squares fits of the data, the slopes of which are PrS (■), -0.00106 ± 0.00002; **90** (●), 0.000348 ± 0.000006; **91** (▲), 0.000676 ± 0.000007.

7.2.1.2. Reaction of $SiPh_2$ with oxiranes and thiiranes

A solution of **44a** (0.05 M), PrO (0.2 M) and D_3 (0.2 M) in C_6D_{12} was photolyzed with two 254 nm lamps for 10.5 min (18 ± 2% conversion based on **44a**), monitoring the course of the photolysis by ^{1}H NMR spectroscopy in intervals of 1 min (eq. 7.3, Fig. 7.5-7.6) and using the integral of the entire phenyl region as the internal standard. The concentration vs time plots revealed that PrO was consumed in over 350% "yield" relative to consumed **44a**, suggestive of oxirane polymerization (see Section 7.2.1.3). Product **92** was identified by GC/MS [5] and ^{1}H - ^{29}Si HMBC NMR spectroscopy;[5] the latter showed that the compound exhibits a doublet at δ7.57 ppm, which was used to quantify the yield. Product **93** was detected in trace amounts by GC/MS and was tentatively assigned on the basis of its mass spectrum. This product is that expected from the insertion of diphenylsilylene into D_3, as has been reported for $SiMe_2$ in the presence of this substrate.[2] Support for this structural assignment was obtained by photolysing a 0.05 M hexane solution of **60** containing 0.2 M D_3, which showed the same compound to be formed as the major $SiPh_2$-containing product. The compound underwent slow decomposition upon exposure to atmospheric moisture over the course of several days and was not isolated.

Conducting the photolysis in the absence of D_3 resulted in the formation of propene (**91**, 51 ± 2%) and **67** (92 ± 3%) as the major products. The progress of the photolysis was accompanied by a significant broadening of the phenyl region of the NMR spectrum, possibly due to polymerization. Oligomerization of the oxirane was also evident from the

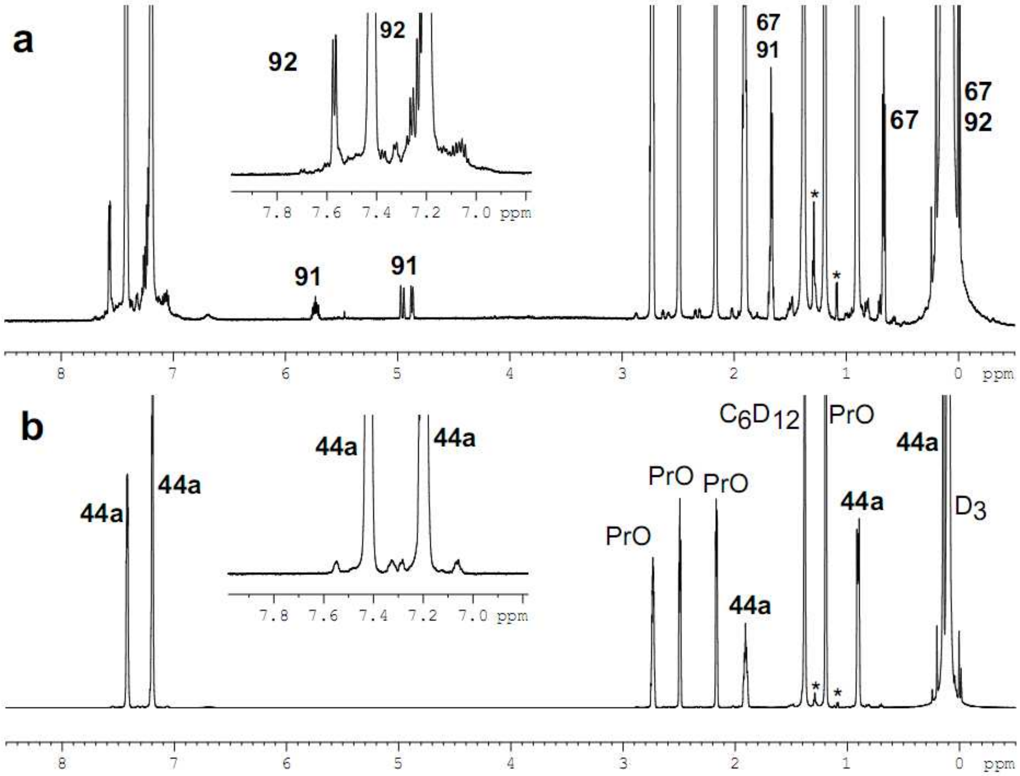

Figure 7.5. 600 MHz ^{1}H NMR spectra of a solution of 0.05 M **44a**, 0.15 M PrO, 0.2 M D_3 in C_6D_{12}, after a) 8 min of photolysis; b) 0 min of photolysis. * - unreactive impurity in the sample

---

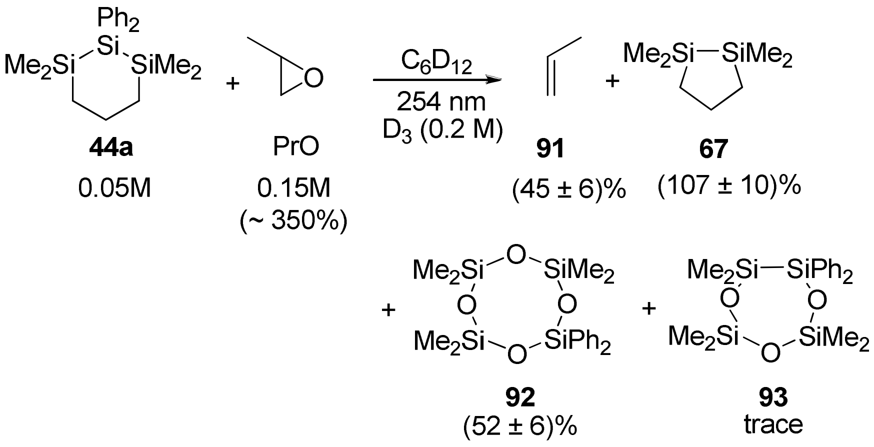

(7.3)

concentration vs time plots, which indicate that PrO was consumed in ca. 210% yield relative to consumed **44a**.

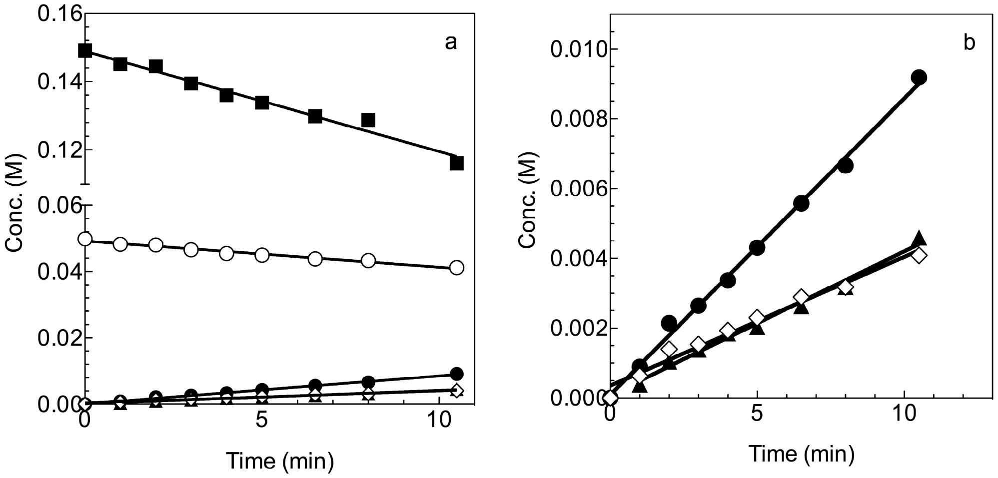

Figure 7.6. Concentration vs time plots for 254 nm irradiation of a deoxygenated solution of **44a** (0.05 M) in C_6D_{12} containing D_3 (0.2 M) and PrO (0.15 M). The solid lines are the least squared fit of the data, and are characterized by the following slopes: PrO (■), -0.0029 ± 0.0002; **44a** (○), -0.00079 ± 0.00005; **67** (●), 0.00085 ± 0.00002; **92** (▲), 0.00041 ± 0.00002; **91** (◊), 0.00037 ± 0.00002.

Photolysis of **44a** (0.05M) in the presence of PrS (0.1 M) under similar conditions ((15.1 ± 0.6)% conversion based on **44a**) afforded **91**, **67** and **94** as the major products (eq.7.4, Fig. 7.7, 7.8a). The photolysis was monitored by ^{1}H NMR and ^{1}H - ^{29}Si HMBC spectroscopy throughout and the integral of the entire phenyl region was used as the internal standard. Product **94** was identified by spiking the photolysis mixture with an authentic sample, which showed that the peak at δ 7.73 ppm belonged to the product and it was used to quantify the yield. PrS was consumed in ca. 93% relative to consumed **44a**. A similar mixture of products was obtained when the photolysis was repeated in the presence of D_3 (0.2 M) to attempt trapping of the intermediary $Ph_2Si{=}S$ with D_3 (Fig. 7.8b). GC/MS analysis of the photolysate indicated that the expected product of this reaction, **95**, was not formed.

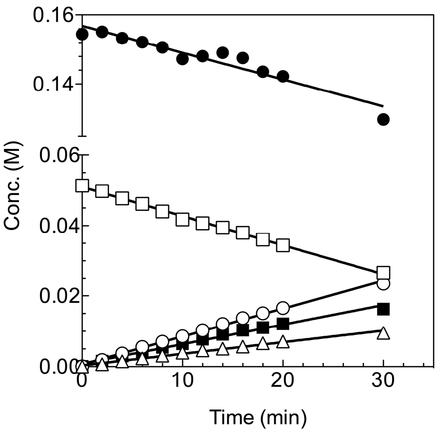

Figure 7.7. Concentration vs. time plots from steady state photolysis of **44a** (0.05 M) in deoxygenated C_6D_{12} containing PrS (0.165 M) and D_3 (0.2 M) as determined by ^{1}H NMR spectroscopy. The solid lines are the least squares fits of the data, and are characterized by the following slopes: PrS (●), -0.00077 ± 0.00007; **44a** (□), -0.00083 ± 0.00002; **67** (O), 0.00079 ± 0.00001; **91** (■), 0.00055 ± 0.00002; **94** (Δ), 0.00033 ± 0.00001.

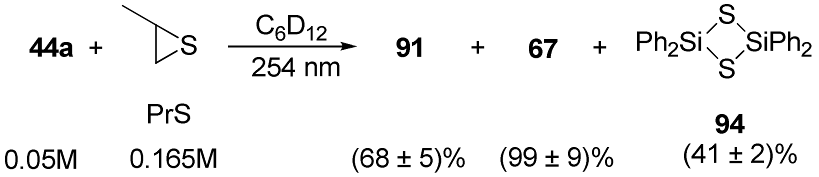

(7.4)

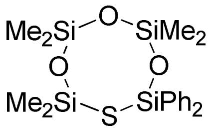

95

Sommer and McLick attempted to isolate product **95** from the reaction of diphenylsilanethione with D_3, but found that the product decomposes at high reaction temperature (611 ^{o}C) into dimethylsilanethione and the corresponding cyclic siloxane. [6] We attempted to synthesize it by refluxing $(Ph_2SiS)_3$ in 1:1 toluene/D_3 for several hours, but no insertion product was formed and the starting material crystallized out of the reaction mixture upon cooling. Reflux of $(Ph_2SiS)_3$ in neat D_3 also did not yield **95**. Although dimethylsilanethione was found to easily insert into an Si-O bond of D_3, this is clearly not the case with the bulkier silanethione.

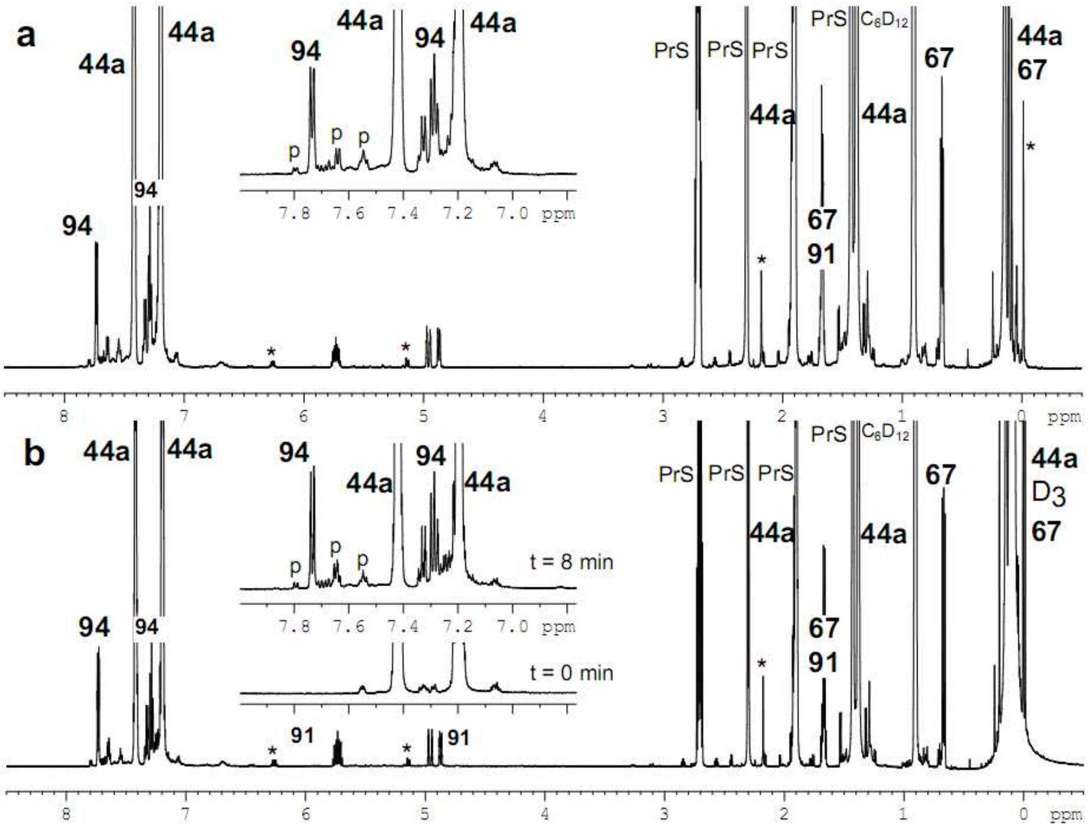

Figure 7.8. (a) 600 MHz ^{1}H NMR spectra of a solution of **44a** (0.05 M) and PrS (0.2 M) in C_6D_{12}, after 8 min of photolysis; (b) 600 MHz ^{1}H NMR spectra of a solution of 0.05 M **44a**, 0.2 M PrS and 0.2 M D_3 in C_6D_{12}, after 8 min of photolysis, the inset shows the phenyl region at the beginning of photolysis for comparison. * - unreactive impurity in the sample, p – unidentified product

In an attempt to trap the silanethione with MeOH, a known substrate for stable silanethiones,[7-8] a solution of **44a** (0.05 M), PrS (0.078 M) and MeOH (0.005 M) in C_6D_{12} was photolyzed, monitoring the course of the photolysis by ^{1}H NMR spectroscopy and using the integral of the entire phenyl region as the internal standard. Two methoxyl-containing products were formed upon photolysis, as evidenced by the ^{1}H NMR analysis (eq. 7.5, Fig. 7.9-7.10). Propene (**91**) and **67** were identified by comparison with the reported spectra, while **71** was identified by spiking the solution with an authentic sample.[9-11] The thiirane was consumed in ca. 320% yield relative to consumed **44a** in this experiment, indicative of oligomerization. The major methoxyl-containing product was identified as **96** based on its NMR and mass spectral data. Upon standing in the dark at -20 °C for several days, the peaks assigned to **96** and MeOH in the photolysis mixture disappeared and product **97** was formed. The presence of **97** was confirmed by spiking with an authentic sample. Multiple attempts to prepare an authentic sample of **96** failed. Several organoalkoxysilthianes have been prepared by treatment of the corresponding organoalkoxychlorosilanes with H_2S in the presence of NEt_3,[12] however in our hands this procedure did not yield the desired product. Heating $(Ph_2SiS)_3$ in boiling toluene in the presence of MeOH (3 eq.) yielded dimethoxydiphenylsilane (**97**), the double insertion product, instead of compound **96** (eq. 7.6). Heating $(Ph_2SiS)_3$ in the presence of a smaller amount of MeOH did not yield any appreciable quantity of product.

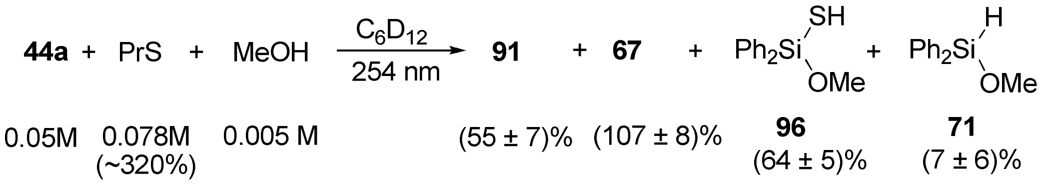

(7.5)

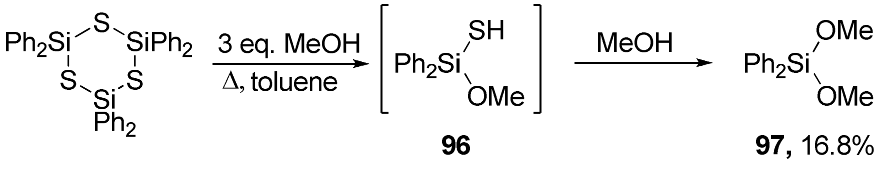

(7.6)

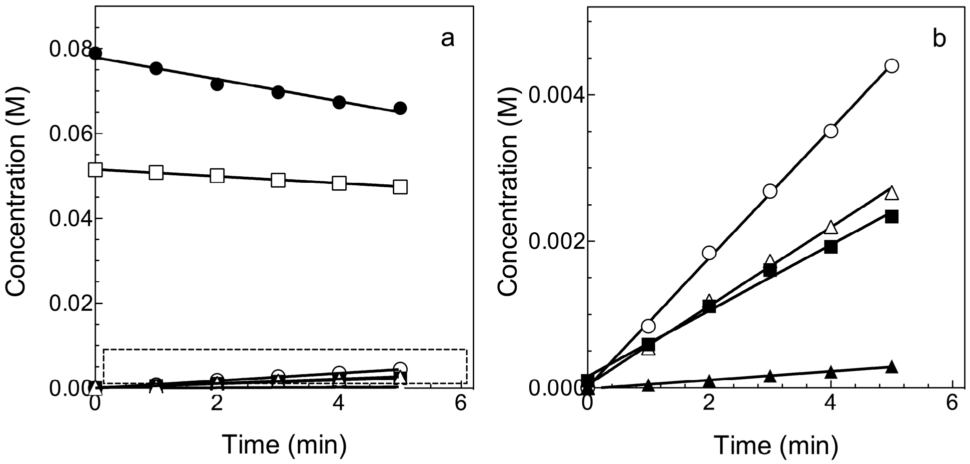

Figure 7.9. Concentration vs. time plots for 254 nm irradiation of deoxygenated solutions of **44a** (0.05 M) in C_6D_{12} containing PrS (0.08 M) and MeOH (0.005 M). The solid lines are the least squared fit of the data, and are characterized by the following slopes: PrS (●), -0.0026 ± 0.0002; **44a** (□), -0.00082 ± 0.00002; **67** (○), 0.00088 ± 0.00001; **91** (■), 0.00045 ± 0.00002; **92** (△), 0.00054 ± 0.00002; **71** (▲), 0.000059 ± 0.000002. Figure (b) shows a blow-up of the plots for the products.

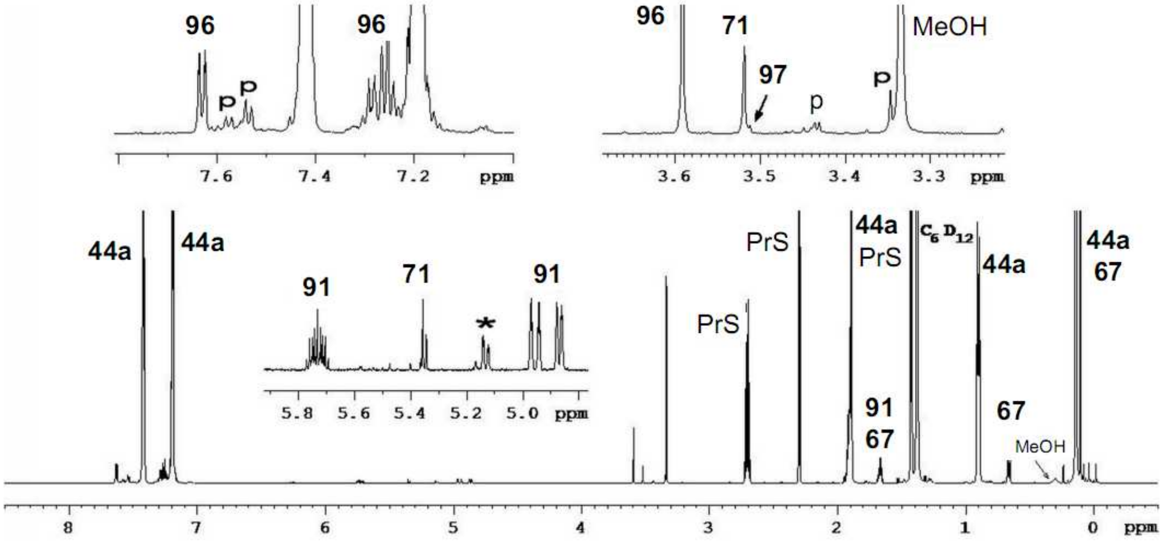

Figure 7.10. 600 MHz ^{1}H NMR spectrum of a solution of **44a** (0.05M), PrS (0.08 M) and MeOH (0.005 M) in C_6D_{12} after 5 min of photolysis followed by 4 hrs standing at room temperature in the dark. * - unreactive impurity; p – unidentified product

7.2.1.3. $SiMes_2$ with oxiranes and thiiranes

A preliminary steady-state experiment was carried out with a C_6D_{12} solution containing $SiMes_2TMS_2$ (**45**, 0.042 M), CHO (0.14 M) and dioxane as the internal integration standard (0.0008 M). The irradiation was carried out to ca. 12% conversion of starting material. Cyclohexene (**88**) was formed in 85% yield relative to consumed **45**; however the yield of the Si_2Me_6 poses a significant problem as it appears to be greater than 100%. The yield of cyclohexene also appears problematic, as it is significantly higher than that obtained in the reaction of $SiPh_2$ with CHO (ca. 50% relative to consumed **44a**).[13] During the course of other experiments it was discovered that the cause of these problems could be due to the internal standard used – when the experiment was repeated using TMS_2CH_2 instead of dioxane as internal standard, the yields of the disilane co-product were consistently ca. 70% regardless of which silylene scavenger was used. This yield is more realistic, since the formation of $SiMes_2$ from **45** is not quantitative –the precursor also participates in photo-induced rearrangements which do not result in silylene extrusion. If 1,4-dioxane is participating in the reaction, i.e. it is being consumed by the silylene, the outcome would be an artificial enhancement of product yields relative to consumed trisilane. Our results are consistent with this postulate.

The results of the three photolysis experiments with C_6D_{12} solutions containing **45**, CHO and TMS_2CH_2 or dioxane as internal standard are summarized in eq. 7.7. The experiment employing dioxane is clearly problematic among the three experiments, and thus can be disregarded. The major product of the photolysis, **88**, is formed in ca. 40% yield in both cases, while Si_2Me_6 is formed in ca. 70% yield. Concentration vs. time plots indicate that CHO is being consumed in amounts well exceeding 100% - when 0.14 M CHO was used, 190% depletion of the oxirane was observed with respect to **45** (Fig 7.11), while an increase in CHO concentration to 0.83 M resulted in a 10-fold more rapid consumption of the oxirane (Fig. 7.12). The ^{1}H NMR spectra reveal significant broadening of the baseline indicative of polymer formation. The MALDI spectrum of the reaction mixture indicates that there are a variety of oligomers present after 74% conversion of **45** (Fig. 7.13). Considering that the extinction coefficient of CHO at the excitation wavelength is ε = 0.0021 M cm^{-1}, the oxirane polymerization from direct photochemical excitation can be ruled out. In fact, our results are consistent with the silylene acting as an oxirane polymerization catalyst; we did not attempt to determine the exact structures of the polymers.

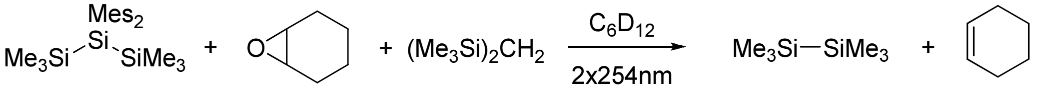

(7.7)

45			**62**	**88**
0.05 M 74% conv.	0.83 M 1800 ± 300%	0.009 M	65 ± 4%	40 ± 3%
0.05 M 80% conv.	0.14 M 190 ± 20%	0.02 M	71 ± 5%	43 ± 3%
0.042 M 12% conv.	0.14 M 300 ± 30%	0.0008 M (dioxane)	109 ± 5%	85 ± 4%

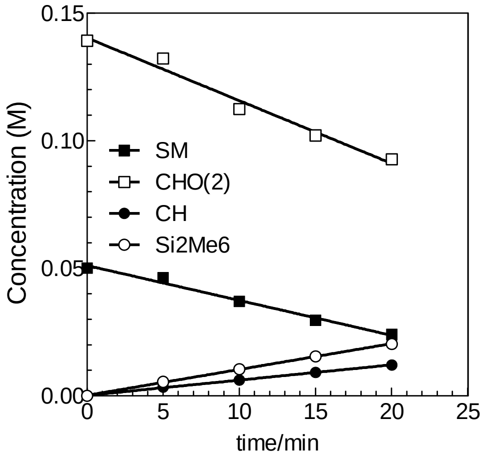

Figure 7.11. Concentration vs. time plots for 254 nm irradiation of a deoxygenated solution of **45** (0.05 M) in C_6D_{12} containing CHO (0.14 M) and TMS_2CH_2 (0.02 M). The solid lines are the least squares fits of the data, the slopes of which are CHO (□) = -0.0025 ± 0.0002; **45** (■) = -0.00137±0.00009; Si_2Me_6 (o) = 0.00101 ±0.00001; **88** (●) = 0.00060 ±0.00001

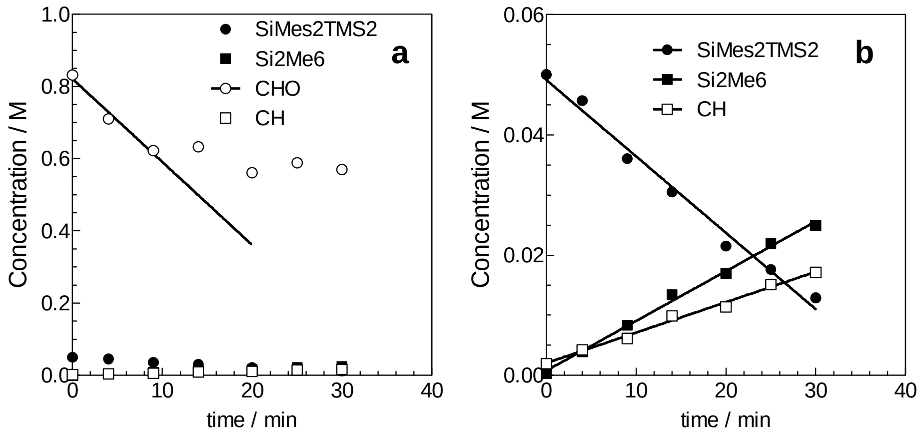

Figure 7.12. Concentration vs. time plots for 254 nm irradiation of a deoxygenated solution of **45** (0.05 M) in C_6D_{12} containing CHO (0.83 M) and TMS_2CH_2 (0.009 M). The solid lines are the least squares fits of the data, the slopes of which are CHO (o) = -0.023 ± 0.004; **45** (●) = -0.00127±0.00006; Si_2Me_6 (■) = 0.00083 ±0.00002; **88** (□) = 0.00051 ±0.00002

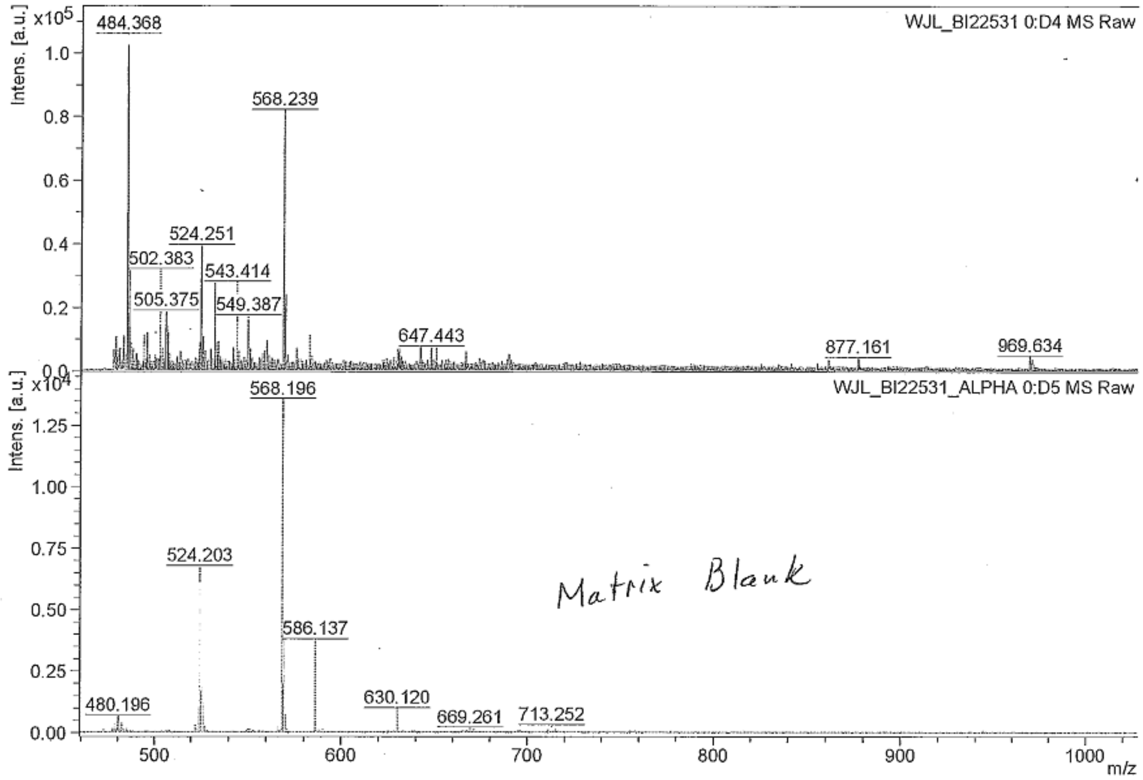

Figure 7.13. MALDI spectrum of the solution of Fig. 7.12 after 30 min of irradiation.

Since **88** was formed in ca. 40% yield in each experiment employing CHO, one important question that we set out to answer is as follows: does oxygen abstraction take place, and if it does, what is the product of the reaction? An initial guess would be that dimesitylsilanone, if formed, should undergo head-to-tail dimerization to generate the corresponding tetramesitylcyclodisiloxane **98** (eq. 7.8), which is a known compound.[14-17] However, the ^{1}H-^{29}Si HMBC and GCMS analysis of the photolysate indicated that **98** is *not* formed upon the reaction of $SiMes_2$ with CHO – there were no resonances in the – (22 ± 5) ppm region of the ^{29}Si NMR spectrum expected for **98**,[17] and the M+ peak of 564 was not found in the GC/MS chromatogram.

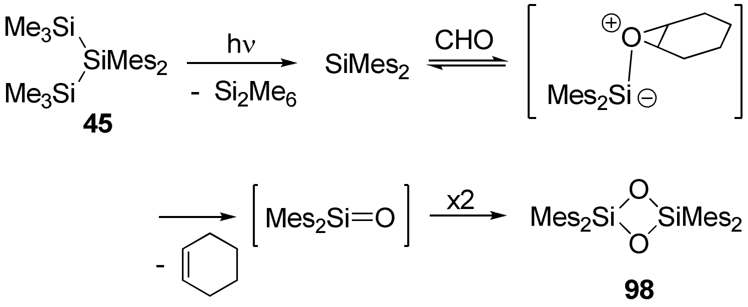

(7.8)

We also attempted to trap the transient silanone with MeOH (0.01 M). Irradiation of a C_6D_{12} solution containing **45** (0.05 M), CHO (0.35 M), MeOH (0.01 M) and TMS_2CH_2 (0.009 M) to 13% consumption of **45** resulted in the formation of one major product and two minor Si-containing products. The presence of large amounts of volatile components interfered with product identification, thus the sample was subjected to high vacuum to afford the ^1H NMR spectrum shown in Fig. 7.14b (the spectrum of the original mixture is shown in Fig. 7.14a for comparison). The spectrum features very broad absorptions in the 1-3 ppm range, which comprise the mesityl region and CHO oligomers.

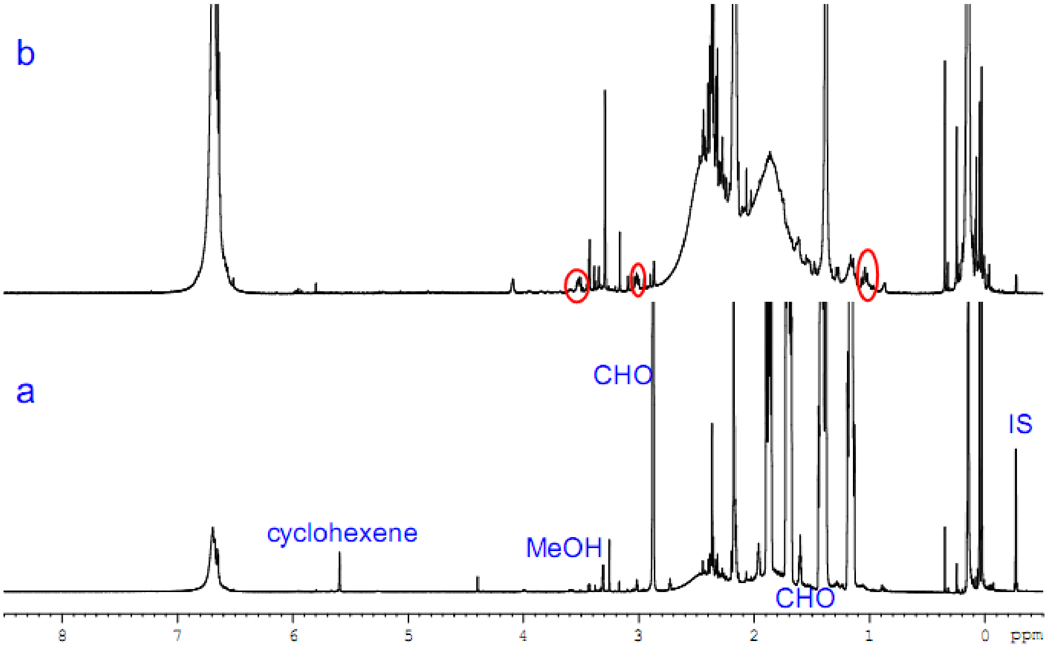

Figure 7.14. ^{1}H NMR spectra of a C_6D_{12} solution containing **45** (0.05 M), CHO (0.35 M), MeOH (0.01 M) and TMS_2CH_2 (0.009 M), recorded (a) after 30 min of irradiation, (b) after removal of volatile components from (a). The major Si-containing product is circled.

A non-invasive technique that can be used to isolate the ^{1}H NMR spectrum of the product is a TOCSY spectrum. TOCSY (Total Correlation Spectroscopy) generates correlations between all protons that are part of the same spin system. The extent of the correlations can be shortened by reducing the allowed mixing time; thus with 120 ms mixing time, the entire spin system is observed (Fig. 7.15a) while with 30 ms mixing time (Fig 7.15b) only vicinal and geminal correlations are observed (the same as in the usual COSY experiment). Because the intensity of the observed peak depends on the mixing time, integration of the TOCSY spectrum is inaccurate.

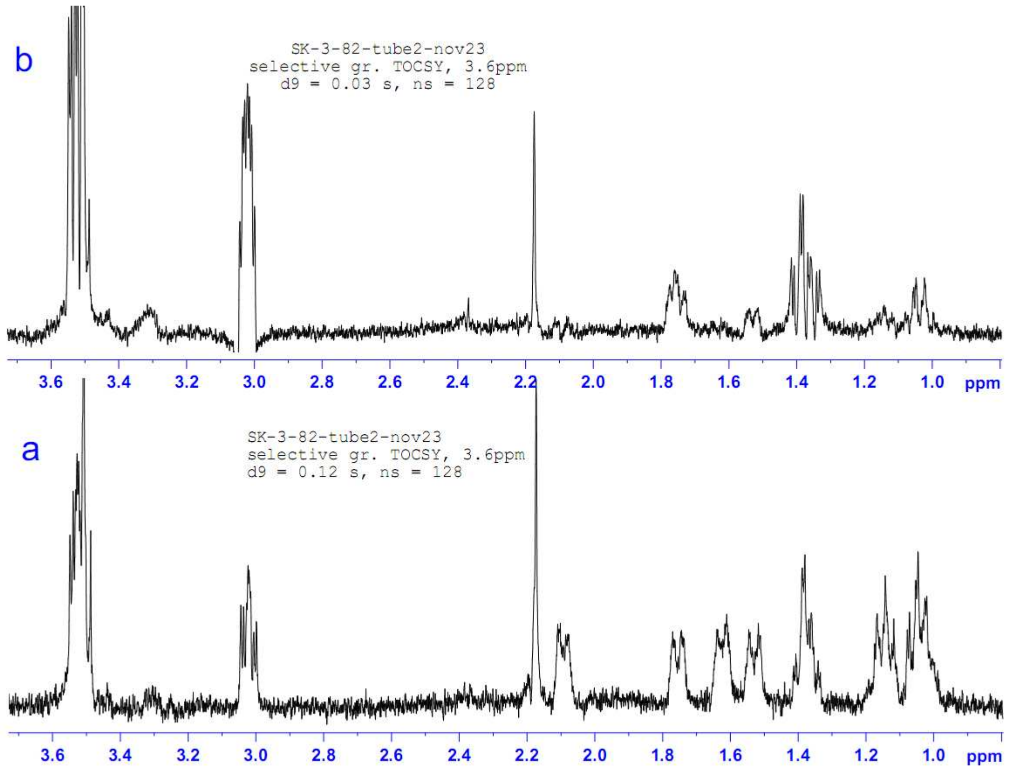

Figure 7.15. A TOCSY spectrum of a solution in Fig. 7.14b, obtained by irradiation of the peak at 3.6 ppm; (a) mixing time = 0.12 s, (b) mixing time = 0.03 s.

With the TOCSY spectrum in hand, the identification of this newly formed compound is drastically simplified. The spectrum of Fig. 7.15a was used as a projection for both axes of a COSY spectrum (Fig 7.16). The same trick can be applied to aid in the analysis of ^{1}H-^{13}C HSQC and HMBC spectra, as well as ^{1}H-^{29}Si HMBC spectra. The spectrum is consistent with structure **99**, the spectroscopic assignments for which are listed in Table 7.1.

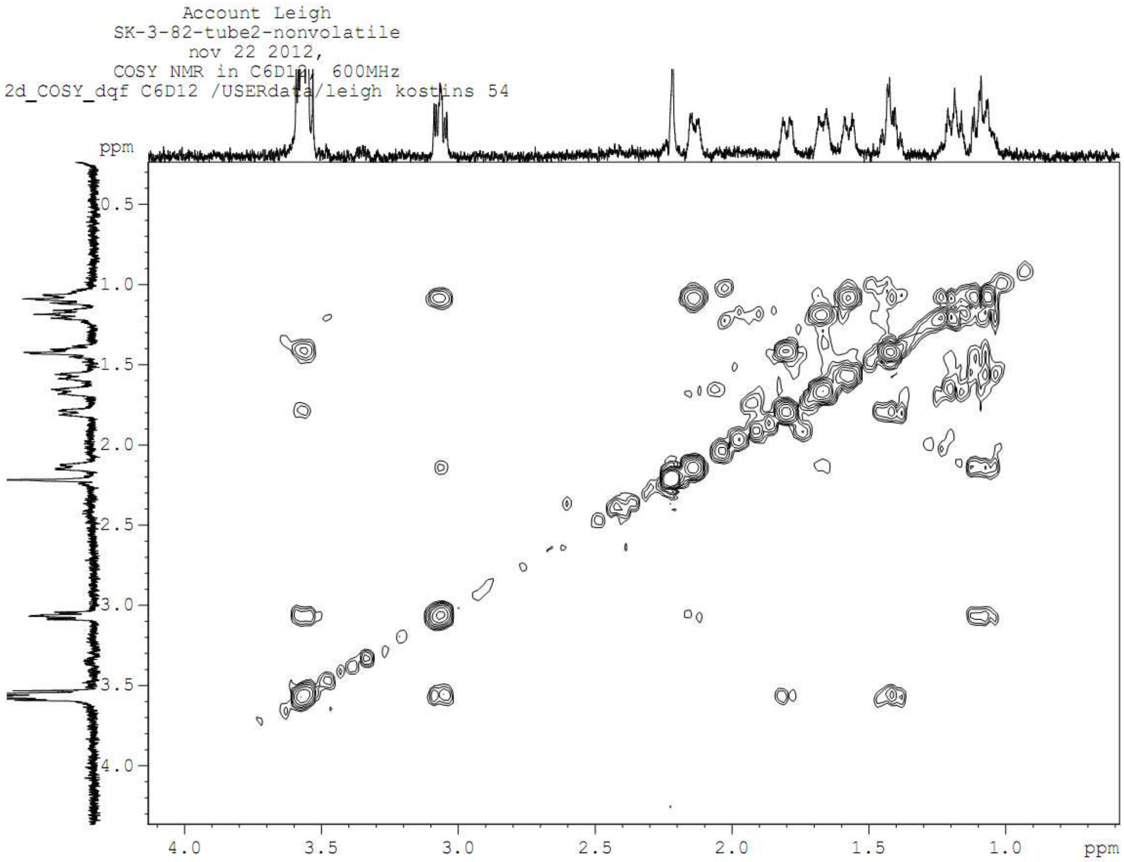

Figure 7.16. COSY spectrum of the solution of Fig 7.14b, with the TOCSY spectrum from Fig 7.15a used as a projection for both axes.

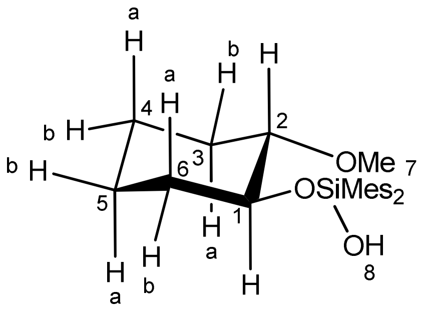

99

Table 7.1. The NMR assignments for compound **99**. The ^{13}C chemical shifts of the aromatic carbons could not be determined from the ^{1}H-^{13}C HMBC spectrum due to a low signal/noise ratio.

position	**^{1}H / ppm**	**^{13}C / ppm**	**^{29}Si / ppm**
1	3.522	74.3	(-24.9)
2	3.028	85.5	
3a	1.046	28.9	
3b	2.091		
4a	1.143	24.5	
4b	1.625		
5a	1.046	24.4	
5b	1.531		
6a	1.380	34.2	
6b	1.755		
7	3.293	55.9	
8	4.096	-	
Mes	2.155 (6), 2.373 (12), 6.65 (4)		

The two minor products were identified as $Mes_2Si(OMe)H$ (**100**) and $Mes_2Si(OMe)OH$ (**101**) based on the ^{1}H and ^{29}Si NMR spectra, the concentration vs time plots were linear in each case except that for CHO (Fig. 7.17). The yields of products were calculated with respect to the loss of **45** and are listed in eq. 7.9. The material balance is within the error margins of the experiment for each compound except CHO; evidence for oxirane polymerization is evident not only from significant broadening of the baseline but also from the curved plot of [CHO] vs time (Fig. 7.17a; slope obtained from the first 4 points).

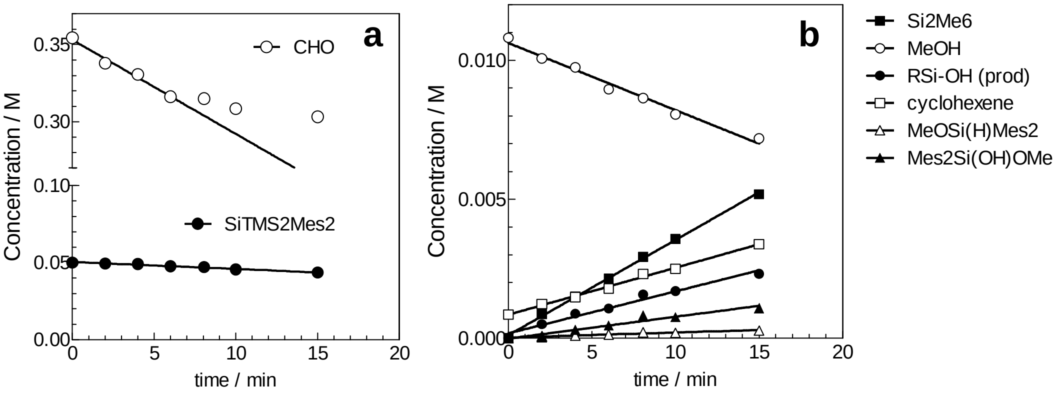

Figure 7.17. Concentration vs time plots for 254 nm irradiation of a deoxygenated solution of **45** (0.05 M) in C_6D_{12} containing CHO (0.35 M), MeOH (0.01 M) and TMS_2CH_2 (0.009 M). The solid lines are the least squares analysis of the data, the slopes of which are: (a) CHO (o) = -0.0061 ± 0.0006; **45** (●) = -0.00045 ± 0.00003; (b) MeOH (o) = -0.00024 ± 0.00001; Si_2Me_6 (■) = 0.000343 ± 0.000006; **99** (●) = 0.00015 ± 0.00001; **88** (□) = 0.000169 ± 0.000005; **100** (Δ) = 0.000018 ± 0.000002; **101** (▲) = 0.000079 ± 0.000009.

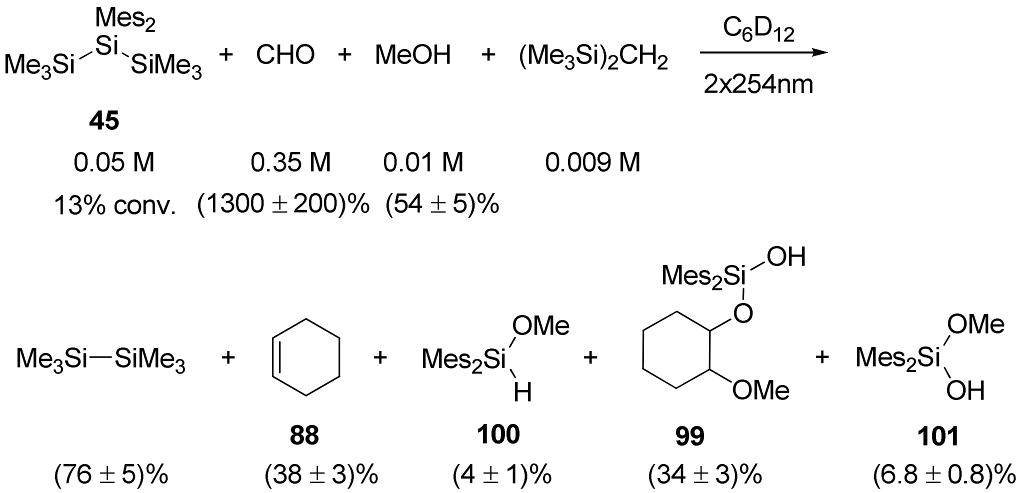

(7.9)

The identification of **100** was aided by conducting a control experiment involving 254 nm lamp photolysis of a C_6D_{12} solution containing **45** (0.05 M), MeOH (0.03 M) and TMS_2CH_2 (0.009 M). Under these conditions, the initially formed $SiMes_2$ reacts with MeOH to generate the O-H insertion product **100** in ca. 87% yield (eq. 7.10). Silylene quenching by MeOH is quantitative, because the yields of Si_2Me_6 and **100** are the same. An unidentified compound was also formed in this experiment in 12% yield; this compound contains a Si-H group and a methoxy group which were used to determine the yield. Although we were not able to derive the structure of this compound based on the available spectroscopic data (without isolation), a reasonable suspicion is that it results from the reaction of the photolysis by-product of **45** with MeOH, and contains two non-equivalent silicon environments, one of which is a TMS group. The spectral information is given below.

unknown: ^{29}Si (C_6D_{12}, δ in ppm): - 6.3, -20.6; ^{1}H (C_6D_{12}, δ in ppm): 5.499 (Si-H, 1H singlet), 3.379 (OMe, 3H singlet), 0.352 (6H singlet), 0.105 ($SiMe_3$, 9H singlet)

While the exact identity of this compound is important from the viewpoint of trisilane photochemistry, it is clear that $SiMes_2$ is not involved in its formation. The important result in this case is that the yield of this compound, in addition to the yield of **100**, provides for the material balance of consumed MeOH. Concentration vs time plots are shown in Fig. 7.18, while the ^{1}H NMR spectra collected prior to and 15 min after photolysis are shown in Fig. 7.19.

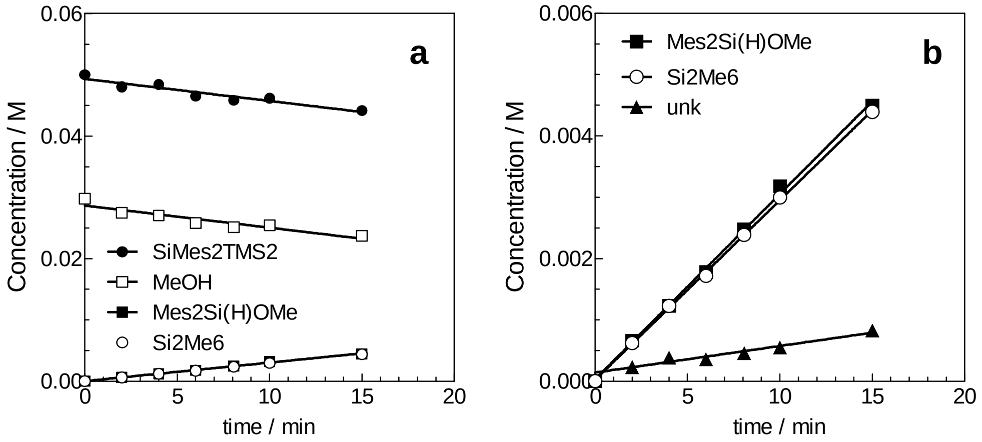

Figure 7.18. Concentration vs time plots for 254 nm irradiation of a deoxygenated solution of **45** (0.05 M) in C_6D_{12} containing MeOH (0.03 M) and TMS_2CH_2 (0.009 M). The solid lines are the least squares fits of the data, the slopes of which are: **45** (●) = -0.00036 ± 0.00005; (b) MeOH (□) = -0.00036 ± 0.00006; Si_2Me_6 (o) = 0.000293 ± 0.000003; **100** (■) = 0.000033 ± 0.000007; unknown (▲) = 0.000043 ± 0.000006.

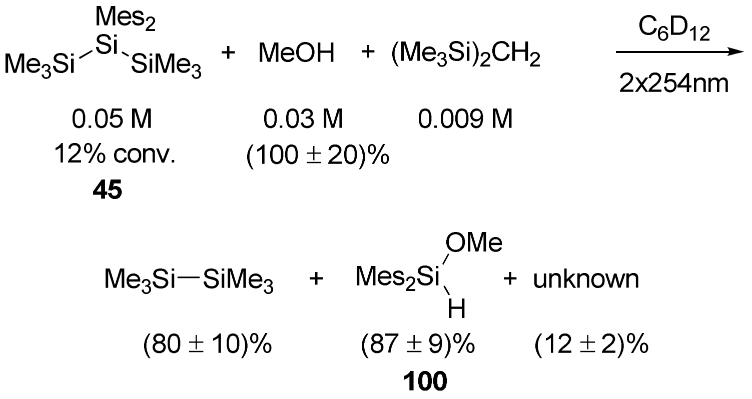

45

100

(7.10)

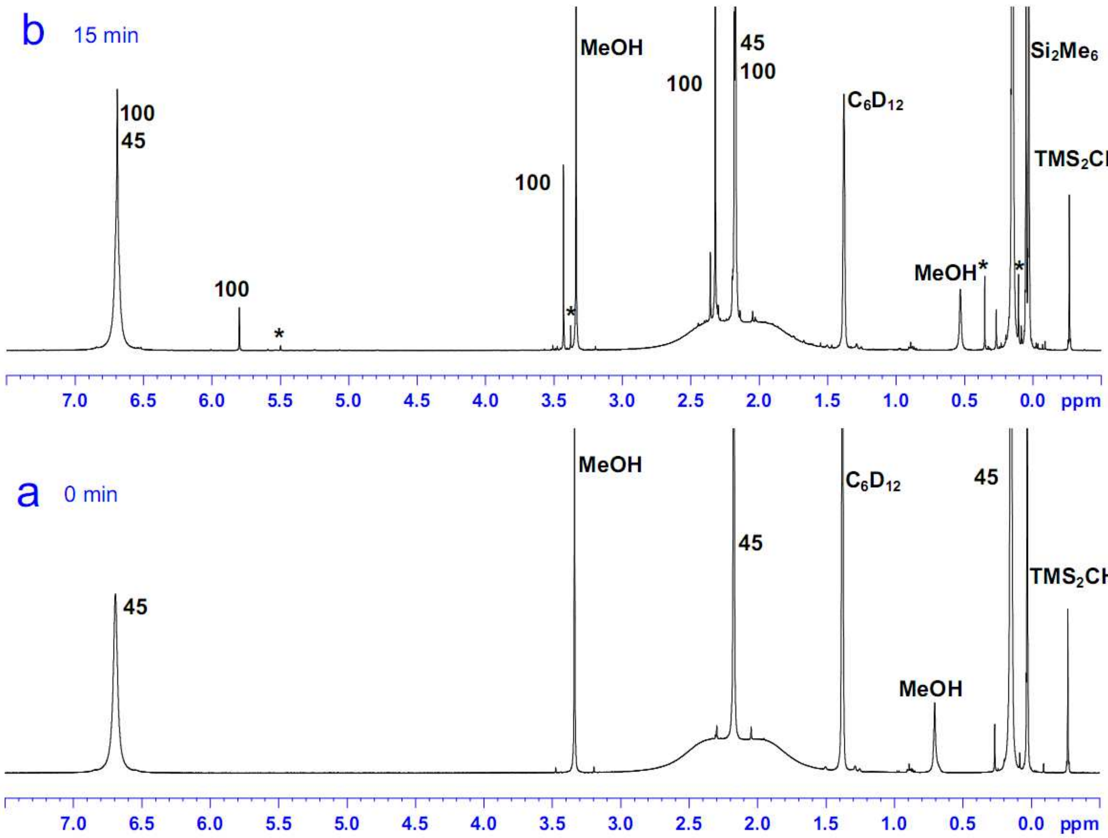

Figure 7.19. ^{1}H NMR spectra of a C_6D_{12} solution containing **45** (0.05 M), MeOH (0.03 M) and TMS_2CH_2 (0.009 M), recorded (a) after 15 min of irradiation, (b) before photolysis. The unidentified Si-containing product is indicated with *.

The proposed mechanism to account for the formation of compounds **99-101** in the reaction of $SiMes_2$ with CHO in the presence of MeOH is shown in Scheme 7.1. Methoxysilane **100** is likely formed from the side reaction of $SiMes_2$ with MeOH, while methoxysilane **101** is the anticipated trapping product of silanone with MeOH. More interesting is the formation of **99** as the major product. Since the Si=O double bond is highly polarized, the silanone is likely to engage in complexation with CHO to generate a silanone-oxirane complex. The oxirane ring in the complex can be expected to be more susceptible to nucleophilic attack by MeOH than is free CHO, and **99** would be formed as a result.

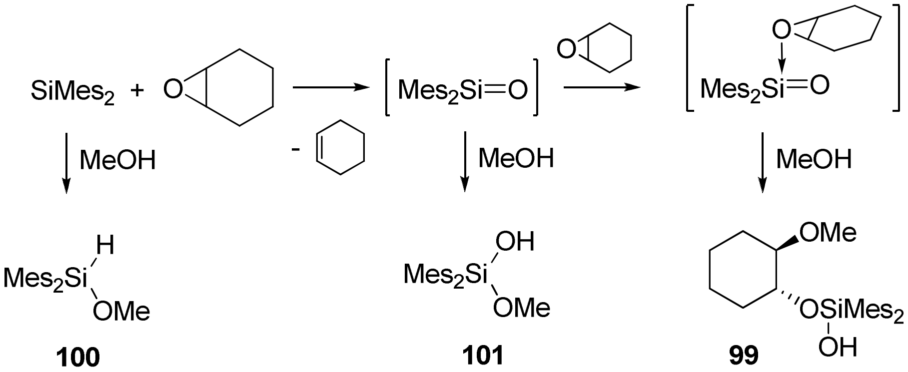

Scheme 7.1

The analogous reaction would also be expected to occur with PrO, and thus a solution of **45** (0.05 M), PrO (0.11 M), MeOH (0.008 M) and TMS_2CH_2 (0.009 M) in C_6D_{12} was irradiated to test this hypothesis. However, the resulting product mixture proved to be too difficult to analyze; at least 3 silicon-containing products were formed in small amounts, and none of them could be definitively assigned structurally. It should be noted that a lower concentration of PrO was used in this experiment compared to the amount of CHO employed in the experiment described above in order to reduce the amount of oxirane oligomerization.

7.2.2. Kinetic measurements

7.2.2.1. Reaction of $SiMe_2$ with oxiranes and thiiranes

Flash photolysis of a hexane solutions of **43** containing CHO (0.1 mM – 1.5 mM) showed shortened silylene lifetimes, suppression of the formation of Si_2Me_4, and a new transient absorption centered at λ_{max} = 310 nm, compared to experiments in the absence of substrate. The latter grew in on a similar timescale as the silylene decay at low CHO concentrations. The bimolecular rate constant for the reaction of $SiMe_2$ with CHO was determined from the slope of a plot of k_{decay} ($SiMe_2$) vs [CHO] according to eq. 7.11. The plot was linear and exhibited a slope of $k_1 = (1.9 \pm 0.2) \times 10^{10}$ M^{-1} s^{-1} (Fig. 7.20a). This value is quite similar to that for the reaction of $SiMe_2$ with THF under similar conditions (k_1 (THF) = $(1.7 \pm 0.2) \times 10^{10}$ M^{-1} s^{-1} in hexanes at 25 ^{o}C).[9]

$$k_{decay} = k_{-1} + k_1 [S] \qquad (7.11)$$

Figure 7.20b shows a series of transient absorption spectra recorded for **43** in hexanes containing 1 mM CHO, where the lifetime of $SiMe_2$ is reduced to $\tau \sim 60$ ns. The transient centered at λ_{max} = 310 nm decayed with clean first order kinetics, exhibiting a lifetime of $\tau \sim 230 \pm 12$ ns that was independent of CHO concentration up to 0.17 M (Fig. 7.21). The transient product is assigned to the Lewis acid-base complex of $SiMe_2$ with CHO on the basis of comparison of its spectrum to that of the $SiMe_2$-THF complex. [9, 18] No new UV/Vis absorptions were observed to be formed in the 270-550 nm spectral window as the species decayed, indicating that the products of decomposition of the complexes do not absorb significantly in this range.

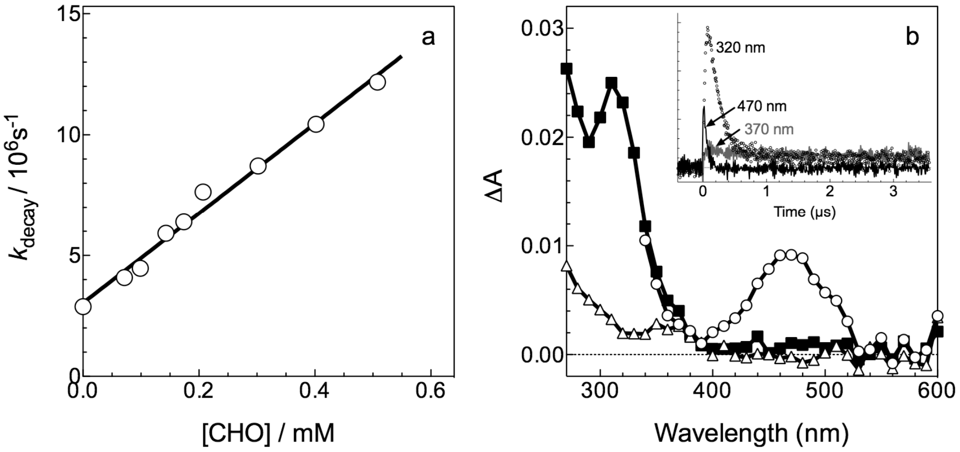

Figure 7.20. (a) Plot of the pseudo-first order decay coefficient (k_{decay}) of the $SiMe_2$ absorption at 470 nm vs. [CHO]. (b) Transient absorption spectra from laser flash photolysis of a hexanes solution of **43** containing 1 mM CHO, recorded 26-38 ns (○), 128-154 ns (■), and 1.49-1.51 µs (Δ) after the laser pulse (the portion of the 26-38 ns spectrum below 340 nm is distorted due to sample fluorescence and is not shown); the inset shows transient absorbance vs. time profiles recorded at 320, 370, and 470 nm.

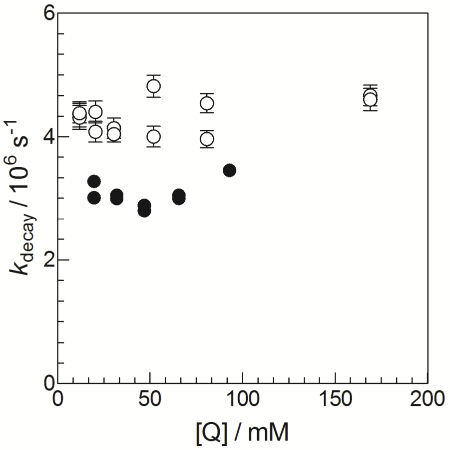

Figure 7.21. Plots of the first order rate coefficients for decay (k_{decay}) of the $SiMe_2$-CHO complex (O) and the $SiMe_2$-PrO complex (●) vs. CHO or PrO concentration (monitored at 310 nm).

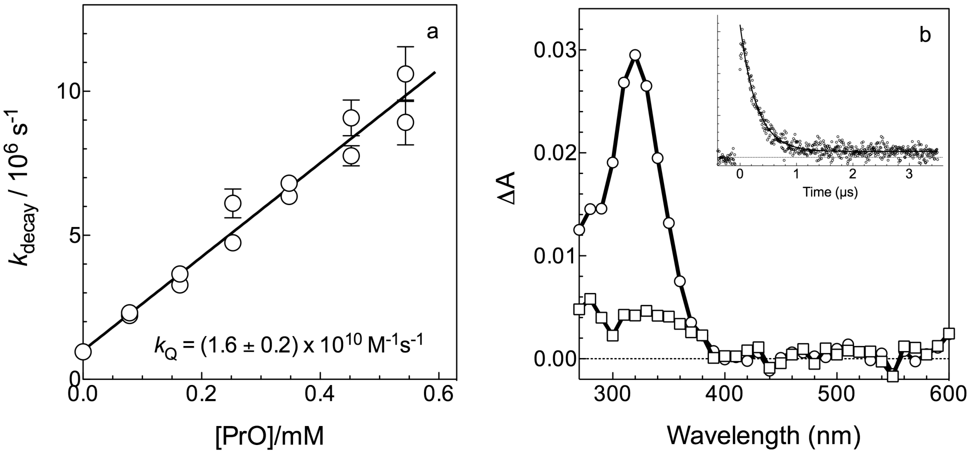

Figure 7.22. (a) Plot of the first order rate coefficients for decay (k_{decay}) of $SiMe_2$ (monitored at 470 nm) vs. [PrO]. (b) Transient absorption spectra from laser flash photolysis of a hexanes solution of **43** containing 10 mM PrO, recorded 83-109 ns (○) and 0.69-0.74 μs (□) after the laser pulse; the inset shows a transient absorbance-time profile recorded at 310 nm.

$SiMe_2$ reacted with PrO with similar rapidity; the plot of k_{decay} ($SiMe_2$) vs [PrO] also exhibited excellent linearity (Fig. 7.22a) and afforded a bimolecular rate constant for the reaction of $k_1 = (1.6 \pm 0.2) \times 10^{10}$ M^{-1} s^{-1}. Shortening of the silylene lifetime was accompanied by the formation of a new transient absorption centered at λ_{max} = 310 nm, which exhibited a first order lifetime of $\tau = 325 \pm 20$ ns and can be assigned to the $SiMe_2$-PrO complex (Fig. 7.22b). The lifetime of the complex was unresponsive to PrO concentrations up to 0.093 M (Fig. 7.21).

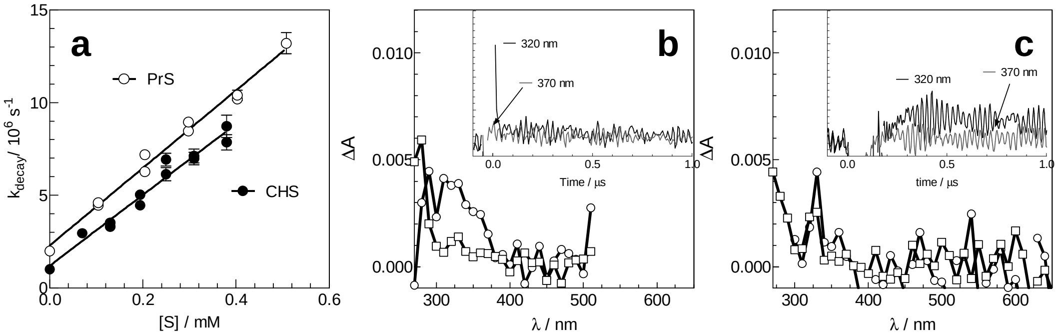

Figure 7.23. (a) Plot of the first order rate coefficients for decay (k_{decay}) of $SiMe_2$ vs. [PrS] (o) and [CHS] (●). (b) Transient absorption spectra recorded 19-32 ns (○) and 1.65-1.70 µs (□) after the laser pulse, by laser flash photolysis of deoxygenated hexanes solution of **43** containing 5.0 mM PrS. (c) Transient absorption spectra recorded 0.18-0.20 µs (○) and 1.65-1.70 µs (□) after the laser pulse, by laser flash photolysis of deoxygenated hexanes solution of **43** containing 5.0 mM CHS.

The response of the silylene lifetime to added PrS or CHS was nearly identical to that in the reaction with PrO; plots of k_{decay} ($SiMe_2$) vs [thiirane] were linear and afforded bimolecular rate constants of $k_{\text{PrS}} = (2.1 \pm 0.2) \times 10^{10}$ M^{-1} s^{-1} and $k_{\text{CHS}} = (1.9 \pm 0.2) \times 10^{10}$ M^{-1} s^{-1} (Fig. 7.23a). A transient absorption spectrum recorded in the presence of 5 mM PrS shows evidence of a new short-lived transient absorption centered at ~ 320 nm ($\tau \leq$ 25 ns, Fig. 7.23b). This new absorption was assigned to the Me_2Si-PrS complex since the $SiMe_2$-THT complex absorbs in the same region (see Chapter 3). In the experiments employing THT, however, the characteristic absorptions due to the disilene were prominent in the presence of up to 2 mM THT. In contrast, addition of submillimolar amounts of PrS resulted in complete suppression of the dimerization pathway, indicative of a rapid irreversible reaction being responsible for the decay of the $SiMe_2$-PrS complex.

Transient absorption spectra in the presence of 5 mM CHS is shown in Fig. 7.23c. Due to strong sample fluorescence no transient absorptions were detected that could be assigned to the $SiMe_2$-CHS complex.

7.2.2.2. Reaction of $SiPh_2$ with oxiranes and thiiranes

Addition of CHO, PrO, PrS or CHS to hexanes solutions of **44a** caused the decay of the silylene to accelerate, the transient decay profiles to follow clean first order kinetics and suppression of dimer formation. Plots of k_{decay} ($SiPh_2$) vs [substrate] were linear in each case and are shown in Fig. 7.24-7.26. In three cases (all except CHS), the decay of the silylene was accompanied by the growth of a new transient giving rise to strong characteristic absorption bands centered at $\lambda_{max} \approx 370$ nm and 290 nm. The transient decays with first order kinetics with lifetimes independent of substrate concentration in the range of 5 mM to 20 mM (Fig. 7.27).

Transient absorption spectra recorded with hexanes solutions of **44a** containing 17 mM CHO (Fig. 7.28) or 11 mM PrO (Fig. 7.29) are virtually indistinguishable, and both are nearly identical to those of the $SiPh_2$-THF complex recorded under similar conditions.[9] This allows for the assignment of these species to the corresponding $SiPh_2$-CHO and $SiPh_2$-PrO complexes, respectively. As found for the $SiMe_2$-oxirane complexes, the $SiPh_2$-PrO complex has a longer lifetime ($\tau = 295 \pm 15$ ns) than the $SiPh_2$-CHO complex ($\tau = 240 \pm 10$ ns). No products absorbing in the 270-650 nm spectral window accompanying the decay of the complexes were detected in either case.

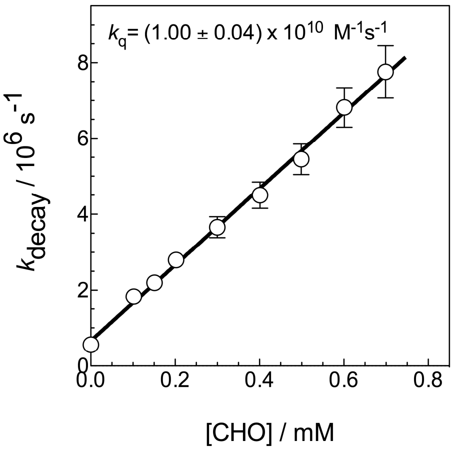

Figure 7.24. Plot of the first order rate coefficients for decay (k_{decay}) of $SiPh_2$ vs. [CHO].

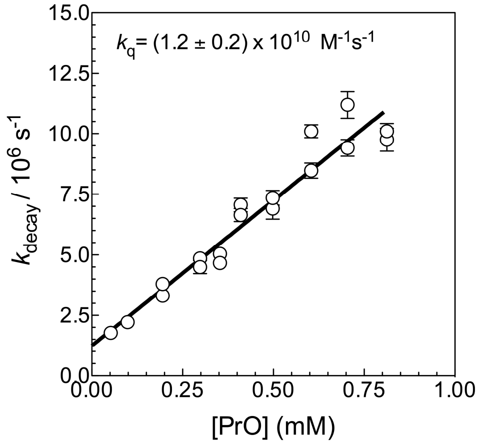

Figure 7.25. Plot of the first order rate coefficients for decay (k_{decay}) of $SiPh_2$ vs. [PrO].

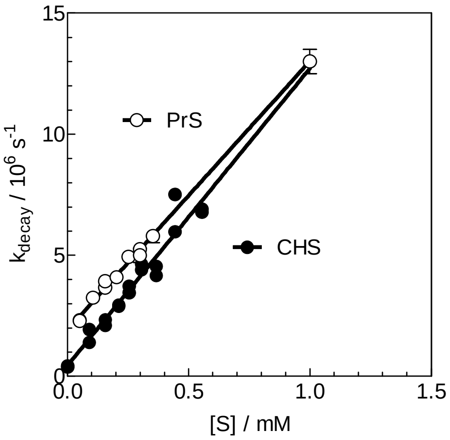

Figure 7.26. Plots of the first order rate coefficients for decay (k_{decay}) of $SiPh_2$ vs. [PrS] (o) and [CHS] (●).

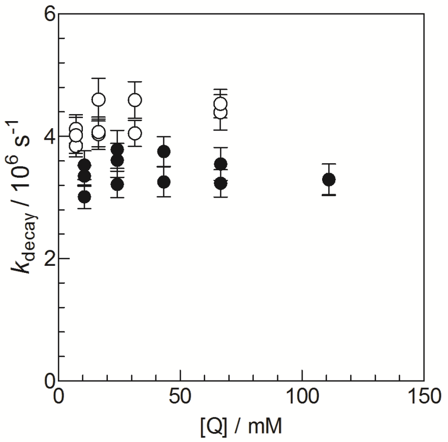

Figure 7.27. Plots of the first order rate coefficients for decay (k_{decay}) of the $SiPh_2$-CHO complex vs. [CHO] (○) and of the $SiPh_2$-PrO complex (●) vs. [PrO] (monitored at 370 nm).

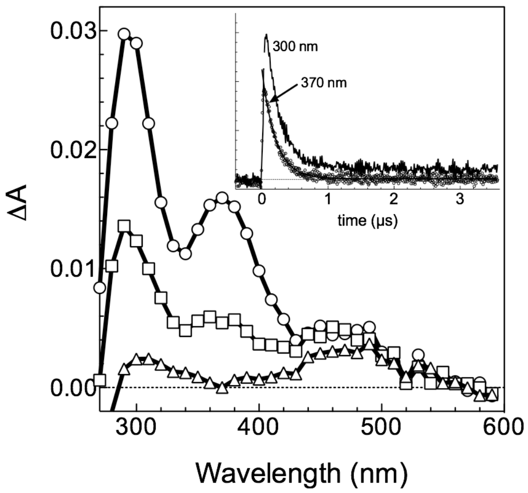

Figure 7.28. Transient absorption spectra recorded 65-77 ns (○), 0.27-0.29 μs (□), and 3.50-3.57 μs (Δ) after the laser pulse, by laser flash photolysis of a deoxygenated hexanes solution of **44a** containing 17.0 mM CHO; the inset shows transient decay/growth profiles recorded at 300 and 370 nm. The weak residual absorption centered at ca. 460 nm is due to the long-lived photolysis co-product (silene **68**).

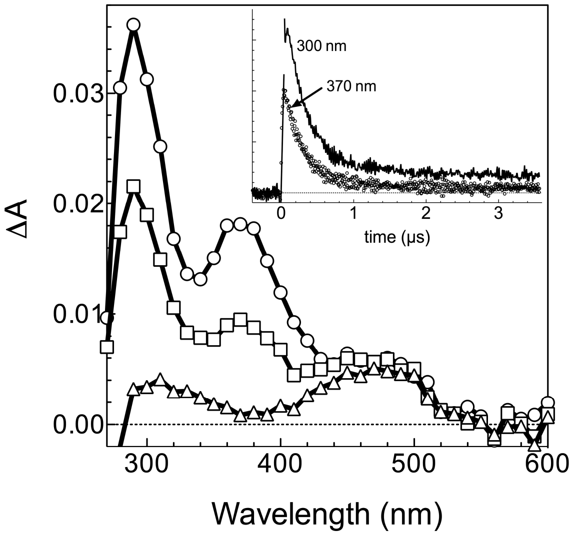

Figure 7.29. (a) Transient absorption spectra recorded 65-77 ns (○), 0.27-0.29 μs (□), and 3.50-3.57 μs (Δ) after the laser pulse, by laser flash photolysis of deoxygenated hexanes solution of **44a** containing 11.0 mM PrO; the inset shows transient decay/growth profiles recorded at 300 and 370 nm.

Transient absorption spectra of a hexanes solution of **44a** in the presence of 4.7 mM PrS are shown in Figure 7.30a. At this concentration of scavenger the lifetime of free diphenylsilylene has decreased to less than 25 ns (k_{decay} = (4 ± 1) × 10^7 s^{-1}) and a new species with weak absorptions centered at 370 nm appeared with k_{decay} = (2.1 ± 0.2) × 10^7 s^{-1} (τ = 48 ± 8 ns). The short-lived absorption band at 290 nm due to diphenylsilylene decayed to a residual level (Figure 7.30), which is indicative of an underlying absorption of a long-lived species. Similar long-lived species was detected in the experiments employing CHS, however strong sample fluorescence obscured any short-lived species (Fig. 7.30b). The band at 460 nm corresponds to the rearrangement by-product of the precursor (**68**) as discussed above; no disilene is formed due to efficient quenching of $SiPh_2$ by PrS. The band at 370 nm is assigned to the Ph_2Si-PrS complex based on the similarity of this spectrum to that of the $SiPh_2$-THT complex.[13]

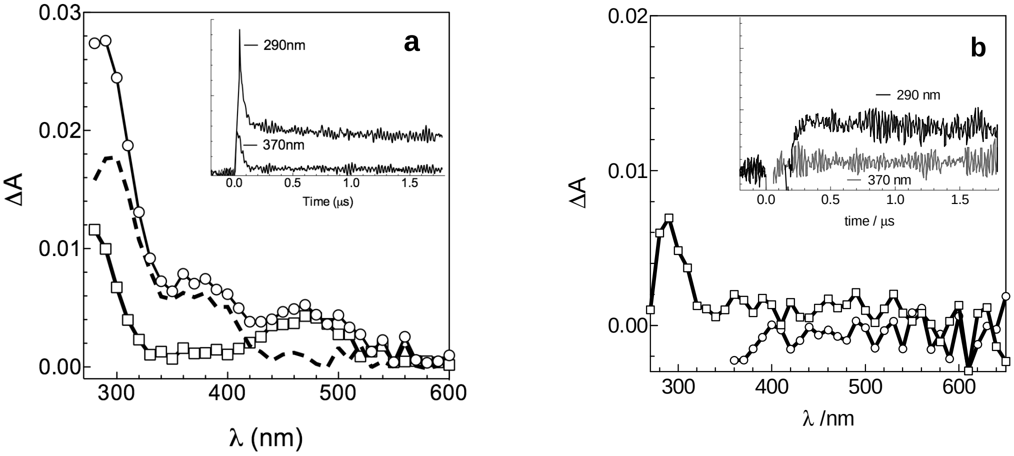

Figure 7.30. (a) Transient absorption spectra recorded 48-54 ns (○) and 0.70-0.72 μs (□) after the laser pulse, by laser flash photolysis of deoxygenated hexanes solution of **44a** containing 4.7 mM PrS; the dashed line shows the difference spectrum, constructed by subtracting the 0.70 μs spectrum from the 48 ns spectrum. (b) Transient absorption spectra recorded 0-16 ns (○) and 0.27-0.29 μs (□) after the laser pulse, by laser flash photolysis of deoxygenated hexanes solution of **44a** containing 11.4 mM CHS. The insets show transient decay/growth profiles recorded at 290 and 370 nm.

Longer timescale experiments indicated that the residual absorption at 290 nm in the presence of 4.7 mM PrS decays over ca. 200 μs with second order kinetics ($2k/\varepsilon = 1.5 \pm 0.4$). The decay coefficient did not vary upon increasing [PrS] over the 5-20 mM range. Laser photolysis of a deoxygenated 10 mM solution of PrS (alone) in hexanes gave rise to only very weak, non-decaying absorptions at this wavelength, ruling out the possibility that the species arises from photolysis of the substrate, which absorbs weakly at the excitation wavelength ($\varepsilon_{248} = 23\ M^{-1}\ cm^{-1}$). A second very weak band centered at $\lambda_{max} \approx$ 460 nm was also detected (Fig. 7.30a). A similar long-lived transient absorption was also present in the experiments employing 11 mM CHS (Fig. 7.30b).

7.2.2.2.1. The direct detection and kinetic characterization of $Ph_2Si{=}S$

The fact that the 290 nm species observed from **44a** in the presence of PrS decays with 2nd order kinetics is consistent with a tentative assignment of the species to diphenylsilanethione, as dimerization to the corresponding 1,3-disiladithietane is known to be the dominant fate of transient silanethiones in solution.[7, 19-21] Compounds of this type are also known to react with alcohols, affording the corresponding alkoxysilanethiols[7-8] or dialkoxysilanes,[19] and indeed such products were obtained upon steady-state irradiation of **44a** in the presence of PrS and MeOH (*vide supra*). We therefore examined the lifetime of the species, generated by laser flash photolysis of **44a** in hexanes containing 20 mM PrS, in the presence of 0.05 – 0.5 mM MeOH. Although MeOH reacts rapidly with $SiPh_2$ (k_{MeOH} = $(1.3 \pm 0.2) \times 10^{10}$ M^{-1} s^{-1}),[22] under these conditions the dominant mode of decay of the silylene is due to the reaction with PrS (k_{PrS} = $(1.32 \pm 0.03) \times 10^{10}$ M^{-1} s^{-1}) (Scheme 7.2).

Addition of the alcohol was indeed found to shorten the lifetime of the long-lived 290 nm absorption, and change its decay kinetics to pseudo first-order even in the presence of as little as 50 μM MeOH. Figure 7.31a shows the resulting plot of the pseudo first-order decay rate constant vs. [MeOH]; the plot is linear over the 0 – 0.5 mM concentration range and afforded a slope of k_{MeOH} = $(7 \pm 1) \times 10^8$ M^{-1} s^{-1}. Figure 7.31b shows a series of transient spectra and transient decay profiles recorded at the highest [MeOH] studied. A second determination of the rate constant afforded k_{MeOH} = $(1.0 \pm 0.2) \times 10^9$ M^{-1} s^{-1}.

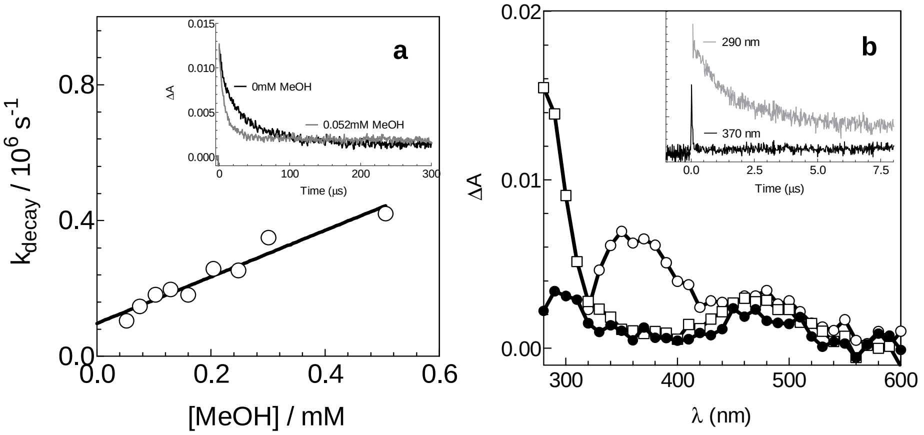

Figure 7.31. (a) plot of k_{decay} vs [MeOH]; the solid line is the linear least squared fit the data to eq. 10, which afforded a slope of $k_{\mathrm{MeOH}} = (7 \pm 1) \times 10^8$ M^{-1} s^{-1}. The inset shows decay traces recorded at 290 nm by flash photolysis of **44a** in hexanes containing 19.5 mM PrS and 0 mM MeOH (black) and 0.052 mM MeOH (gray). (b) Transient absorption spectra of a hexanes solution of **44a** in the presence of 19.5 mM PrS and 0.5 mM MeOH, recorded 0.016-0.080 μs (○), 0.128-0.192 μs (□), and 8.560-8.592 μs (●) after the laser pulse; the inset shows transient decay traces recorded at 290 nm and 370 nm.

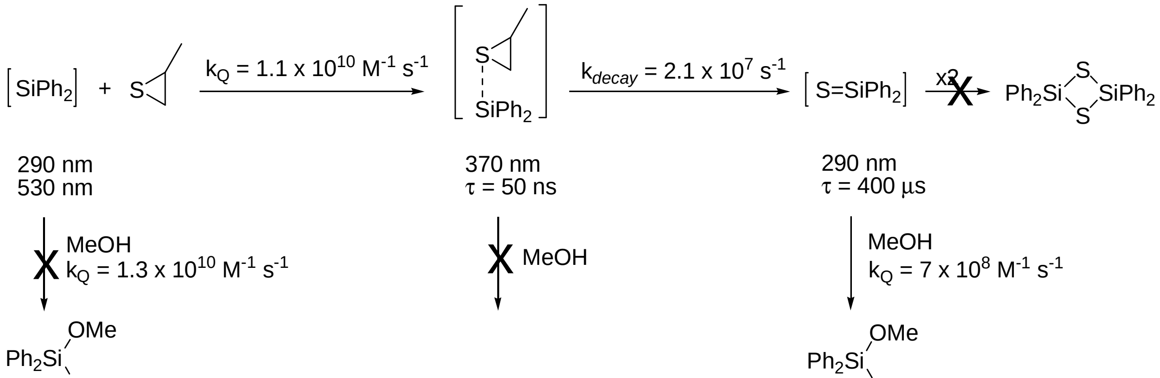

Scheme 7.2

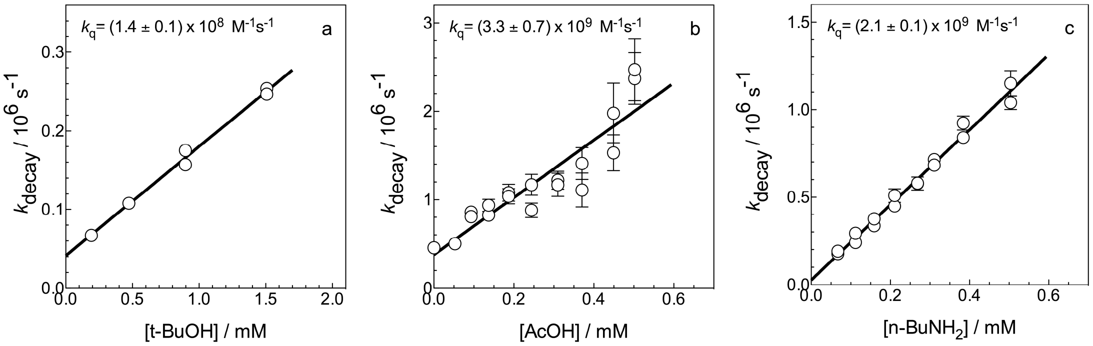

Figure 7.32. Plots of the first order rate coefficients for decay (k_{decay}) of the 290 nm absorption vs. (a) [t-BuOH] (b) [AcOH], and (c) [n-BuNH$_2$] from laser photolysis of a deoxygenated solution of **44a** containing 20 mM PrS.

Table 7.2. Absolute 2nd-order rate constants (k_1, in units of 10^9 $M^{-1}s^{-1}$) for quenching of the long-lived transient product of the reaction of SiPh$_2$ with PrS by MeOH, *t*-BuOH, AcOH, and *n*-BuNH$_2$ in hexanes at 25 ± 1 ˚C.[a]

Substrate	MeOH	*t*-BuOH	AcOH	*n*-BuNH$_2$
k_1 / 10^9 $M^{-1}s^{-1}$	0.85 ± 0.09 [a]	0.14 ± 0.01	3.2 ± 0.7	2.1 ± 0.1

[a] The average and standard deviation of two independent determinations.

Similar results were obtained upon addition of *tert*-butanol (t-BuOH; 0.2-1.5 mM), acetic acid (AcOH; 0.05-0.5 mM), or *n*-butyl amine (*n*-BuNH$_2$; 0.1-1.5 mM) to hexanes solutions of **44a**. Figure **7.32** shows the plots of k_{decay} (290 nm) vs [S] for each of these experiments, while the corresponding 2nd-order rate constants are listed in Table 7.2.

7.2.2.3. SiTmp$_2$ with oxiranes and thiiranes

For the kinetic measurements acyclic precursor **86** was used, while for the transient spectroscopy cyclic precursor **87** was used.[23] Laser flash photolysis of **86** in hexanes leads to the formation of SiTmp$_2$ exhibiting two absorption bands centered at λ_{max} = 320 and 520 nm. The long wavelength band overlaps with strong transient absorptions due to the silene **102** and Si$_2$Tmp$_4$ (λ_{max} = 460 nm). Nevertheless, the spectral overlap does not interfere in the determination of rate constants for reaction of the silylene with various substrates. Silene formation is largely suppressed from the cyclic precursor **87**, but since the synthesis of **87** is more elaborate than that of **86** this compound was used only to record transient absorption spectra.

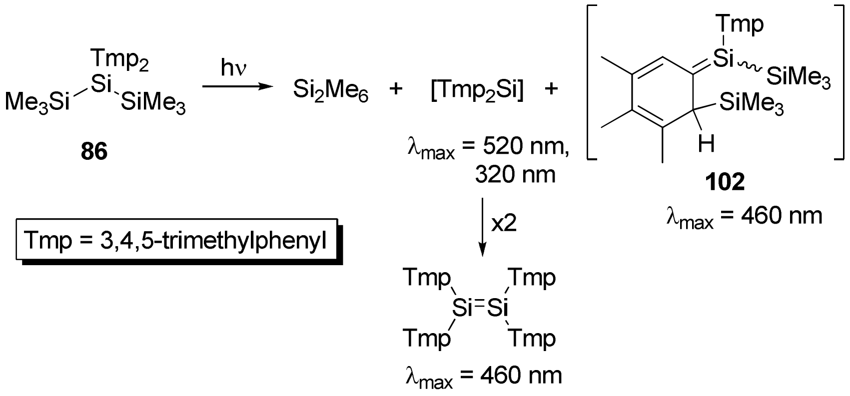

Scheme 7.3

Addition of either PrS or CHO to rapidly flowing hexanes solutions of **86** resulted in shortened silylene lifetimes and a change of the decay kinetics to first order, and the suppression of dimerization, similar to what was observed with SiMe$_2$ and SiPh$_2$. Plots of k_{decay} vs [PrS] and k_{decay} vs [CHO] were linear (Fig. 7.33), the slopes affording rate constant values of $k_1 = (9.7 \pm 0.8) \times 10^9$ M^{-1} s^{-1} and $k_1 = (6.3 \pm 0.9) \times 10^9$ M^{-1} s^{-1} for complexation with PrS and CHO, respectively.

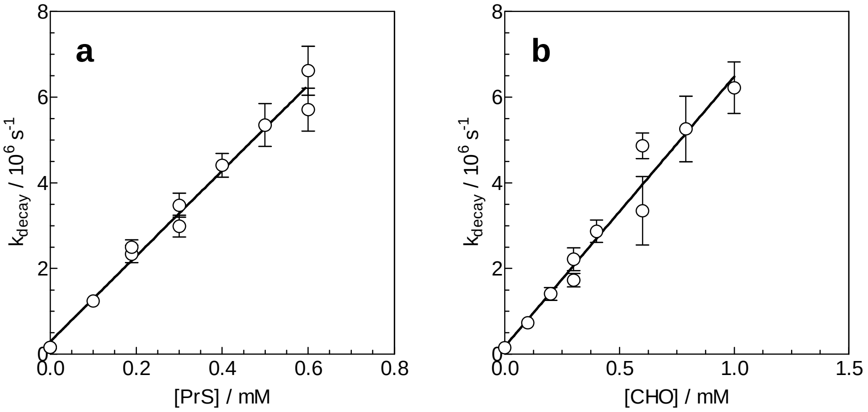

Figure 7.33. Plots of k_{decay} vs [S] for the reaction of $SiTmp_2$ with (a) PrS and (b) CHO. The solid lines are the linear least-squares fits of the data to eq. 7.11.

Transient absorption spectra recorded by laser flash photolysis of **87** in the presence of 5.4 mM PrS (Fig. 7.34a) show the presence of a new product absorption band centered at <280 nm which overlaps on a weaker band due to the silene.[23] The transient decays over ca. 200 μs with mixed order kinetics, similar to what was observed for $Ph_2Si{=}S$; the reactivity of the transient with silanethione scavengers was not investigated, however. Based on the similarity of the absorption spectra and the lifetime of the transient absorbing at < 280 nm to those of $Ph_2Si{=}S$, we tentatively assign it to $Tmp_2Si{=}S$. On the timescale of this experiment the $SiTmp_2$-PrS complex was not detected. On shorter timescales the complex also could not be detected, which suggests that either its lifetime is < 30ns, or its extinction coefficient is too low to be distinguishable from the background noise. We strongly favour the first possibility based on the analogy with the $SiPh_2$-PrS system.

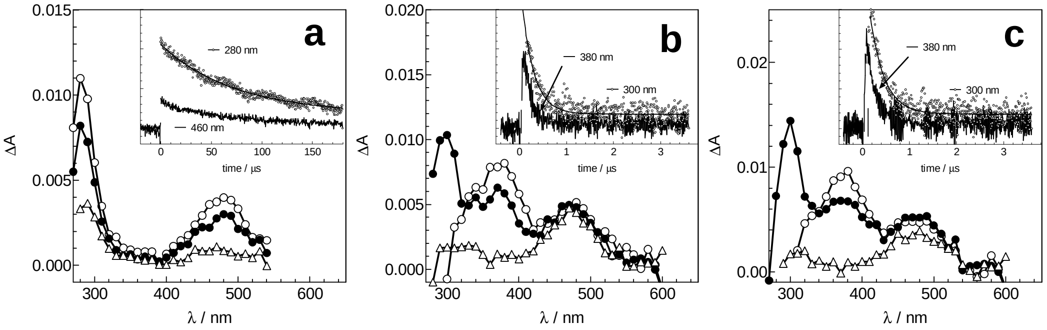

Figure 7.34. (a) Transient absorption spectra of a rapidly flowing hexanes solution of **87** in the presence of 5.4 mM PrS, 0-0.16 μs (o), 18.24-19.84 μs (●) and 139.84-141.44 μs (Δ) after the laser pulse. (b) Transient absorption spectra of a rapidly flowing hexanes solution of **87** in the presence of 10.4 mM CHO, 0.109-0.141 μs (o), 0.17-0.20 μs (●) and 1.52-1.55 μs (Δ) after the laser pulse. (c) Transient absorption spectra of a rapidly flowing hexane solution of **87** in the presence of 10.0 mM PrO, 0.096-0.128 μs (o), 0.17-0.20 μs (●) and 2.80-2.83 μs (Δ) after the laser pulse. The insets show transient decay traces recorded at representative wavelengths in the spectral windows.

A series of transient absorption spectra of **87** were collected in the presence of ca. 10 mM CHO and PrO and are shown in Fig. 7.34b and Fig. 7.34c, respectively. The spectra are indistinguishable from each other, and indicate the presence of a new species exhibiting two absorption bands centered at λ_{max} = 300 nm and λ_{max} = 380 nm. Both spectra are virtually identical to that of the $SiTmp_2$-THF complex, which allows their assignment to the $SiTmp_2$-oxirane complexes. The species decay with first order kinetics, and their lifetimes are similar to those of the $SiMe_2$-oxirane and $SiPh_2$-oxirane complexes (Table 7.3). No additional bands ascribable to the products of decomposition of the complexes can be observed in the 270-650 nm spectral window.

Table 7.3. First order decay rate coefficients for the decay of the silylene-oxirane complexes (/10^6 s^{-1}) in hexanes at 25° C.

	$SiMe_2$	$SiPh_2$	$SiTmp_2$
PrO	3.1 ± 0.2^a	3.4 ± 0.2^a	3.3 ± 0.2^b
CHO	4.3 ± 0.3^a	4.2 ± 0.3^a	3.9 ± 0.4^b

[a] average of 10-12 determinations in the 0.01-0.20 M concentration range of the substrate; [b] recorded in the presence of ca. 10 mM [oxirane]

7.2.2.4. $SiMes_2$ with oxiranes and thiiranes

Sections 7.2.2.1-7.2.2.3 describe the results of our studies of the reactions of $SiMe_2$, $SiPh_2$ and $SiTmp_2$ with oxiranes and thiiranes; in each case the results indicate that the initial complexation step is characterized by an equilibrium constant in excess of ca. 2.5×10^4 M^{-1}. With $SiMes_2$, however, it was shown that most complexation reactions occur with equilibrium constants in the small or medium regime (see Chapter 3).

$$\Delta A_0/\Delta A_{eq} = 1 + K_1 [S] \qquad (7.12)$$

$$K_1 = k_1/k_{-1} \qquad (7.13)$$

Indeed, addition of small amounts of PrO or CHO to a hexanes solution of the $SiMes_2$ precursor **45** resulted in a drop in the signal intensity *as well as* a decrease in the silylene lifetime, suggesting the same to be true in these cases as well. Dimesitylsilylene has been shown to react with THF and Et_2O with equilibrium constants of 2.4 and 0.9 M^{-1}, respectively. This result leads to the expectation that an oxirane should also react with this silylene with a low equilibrium constant, but it should be higher than 2.4 M^{-1}. Thus, only a drop in the silylene signal intensity might be expected. However, in the reactions with ethers the resulting silylene-ether complexes are long-lived, with the primary mode of decay leading to the disilene. The residual $SiMes_2$ present at equilibrium reacts by dimerization. Silylene-oxirane complexes, on the other hand, have been shown to undergo a rapid unimolecular decomposition to yield the abstraction products. In this case, the rate of the residual silylene decay will be dependent on the rate of the decomposition of the complex. The mechanism for the overall reaction is shown in eq. 7.14.

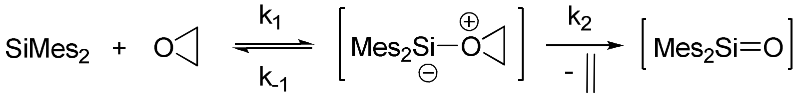

(7.14)

The kinetic expression that describes a situation involving an initial rapid equilibrium followed by a unimolecular irreversible step is shown in eq. 7.15, where k_{decay} is the observed rate coefficient, K_1 is the equilibrium constant for the complexation step, and S is the substrate.

$$k_{decay} = \frac{k_2 K_1 [S]}{1 + K_1 [S]} \qquad (7.15)$$

According to eq. 7.15, the dependence of k_{decay} on [S] should be non-linear; at low concentrations of S the relationship $K_1[S] << 1$ holds, which should result in a 1st order dependence of k_{decay} on [S] (eq. 7.16). At high [S], the relationship $K_1[S] >> 1$ holds, thus the value of the denominator approximately equals $K_1[S]$ and k_{decay} reaches a constant value of k_2 (eq. 7.17).

$$k_{decay} = k_2 K_1 [S], \text{ when } K_1[\mathrm{S}] << 1 \qquad (7.16)$$

$$k_{decay} = k_2, \text{ when } K_1[S] >> 1 \qquad (7.17)$$

For a fast pre-equilibrium, the observed lifetime of the silylene should equal the lifetime of the silylene-oxirane complex at each given concentration of [PrO] or [CHO], from which the value of k_{decay} in eq. 7.15 can be obtained using a pseudo first-order fit. If the approach to equilibrium is (at all concentrations of S) too fast to be resolved then the apparent initial intensity of the silylene signal should decrease with increasing scavenger concentration. To validate this expectation an optimal wavelength to monitor the decay of the complex needs to be identified, and thus a series of transient absorption spectra of **45** in the presence of PrO and CHO were obtained.

Transient absorption spectra of a hexanes solution of **45** in the presence of 9.5 mM CHO and 0.155 M CHO are shown in Fig. 7.35. The difference spectra show the peaks due to the $SiMes_2$-CHO complex after subtracting the contribution from the photolysis bi-product. The complex has two bands – a strong one at 290 nm, and a weak shoulder around 380 nm. Free $SiMes_2$ also has an absorption band at 290 nm which overlaps with that due to the complex, and therefore the weaker band at longer wavelength must be used to monitor the lifetime of the complex. A monitoring wavelength of 350 nm was selected as optimal, since at this wavelength the contributions to the absorptions from the silylene and from the long-lived product are minimized.

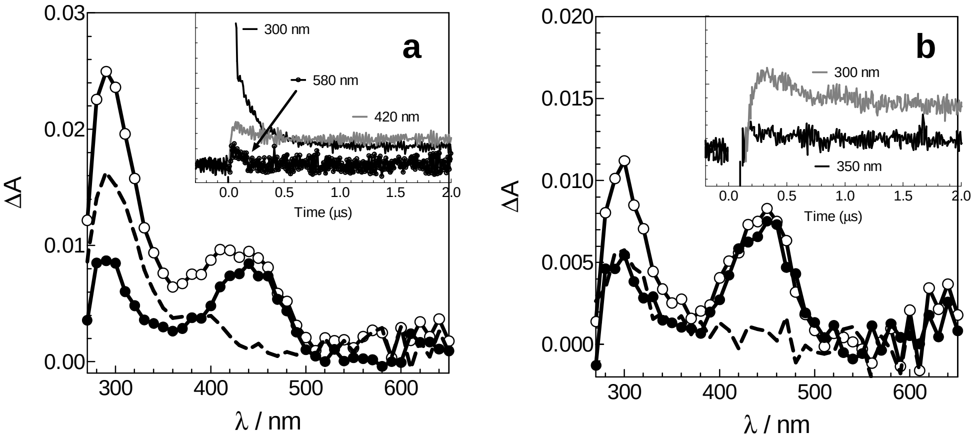

Figure 7.35. Transient absorption spectra of a rapidly flowing hexanes solution of **45** containing (a) 9.5 mM CHO, 0.08-0.10 μs (o) and 0.35-0.40 μs (●) after the laser pulse; and (b) 0.155 M CHO, 0.30-0.33 μs (o) and 3.44-3.47 μs (●) after the laser pulse. The insets show transient decay traces obtained at 300 nm, 350 nm, 420 nm or 580 nm.

Transient absorption spectra of a hexanes solution of **45** in the presence of 0.138 M PrO are shown in Fig. 7.36. The $SiMes_2$-PrO complex displayed an absorption spectrum quite similar to that of the $SiMes_2$-CHO complex, and so the 350 nm wavelength was again chosen to monitor the effect of substrate concentration on the lifetime of the complex. The spectra of both the $SiMes_2$-CHO and $SiMes_2$-PrO complexes are in good agreement with the reported spectra of other $SiMes_2$-ether complexes (see Chapter 3).

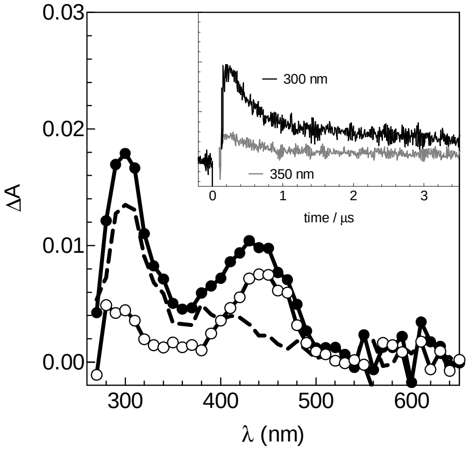

Figure 7.36. Transient absorption spectra of a rapidly flowing hexanes solution of **45** in the presence of 0.138 M PrO, obtained 0.205-0.237 μs (●) and 3.44-3.44 μs (o) after the laser pulse. The dotted line is the difference spectrum between (●) and (o). The inset shows transient decay traces at 300 nm and 350 nm.

The lifetime of the silylene signal at 580 nm was found to decrease with increasing PrO concentration, and the resulting plot of k_{decay} vs [PrO] is shown in Fig. 7.37a. As expected for the mechanism of eq. 7.14, the plot exhibits a downward curvature which can be analyzed with eq. 7.16. The apparent initial intensities of the signals were analysed as a function of [PrO] using eq. 7.12, the results of which are shown in Fig. 7.37b. The two treatments afforded the same equilibrium constant for complexation, $K_1 \approx 50$ M^{-1} (Table 7.4).

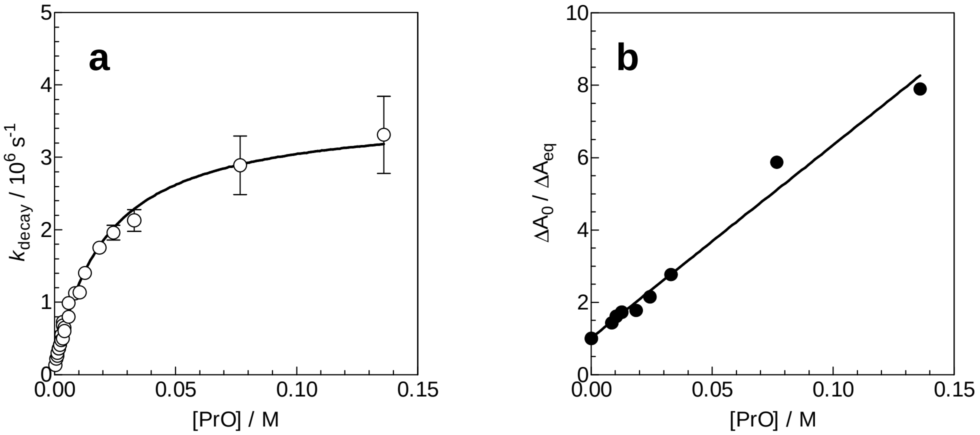

Figure 7.37. (a) Plot of k_{obs} (at 580 nm) vs [PrO] for the reaction of $SiMes_2$ with PrO. The line is the best fit to eq. 7.15. (b) Plot of ΔA_0 / ΔA_{eq} (at 580 nm) vs [PrO] for the reaction of $SiMes_2$ with PrO, the line is the best least-squares fit of the data to eq. 7.12.

The reaction of $SiMes_2$ with CHO was monitored at both 580 nm and 350 nm (in two separate experiments). The plots of k_{decay} vs [CHO] for both the silylene and the $SiMes_2$-CHO complex are in reasonable agreement with one another (Fig. 7.38a). The fits of the plots to eq. 7.15 yielded values of K_1 that are the same within experimental error (ca. 400 M^{-1}), which also coincides with the value obtained from analysis of the data according to eq. 7.12 (Fig 7.38b). The rate coefficient for decay of the complex from eq. 7.15 was ca. 6×10^6 s^{-1}, which is nearly two times higher than that for the decay of the $SiMes_2$-PrO complex.

A summary of K_1 and k_2 values obtained for the reactions of $SiMes_2$ with PrO and CHO are shown in Table 7.4.

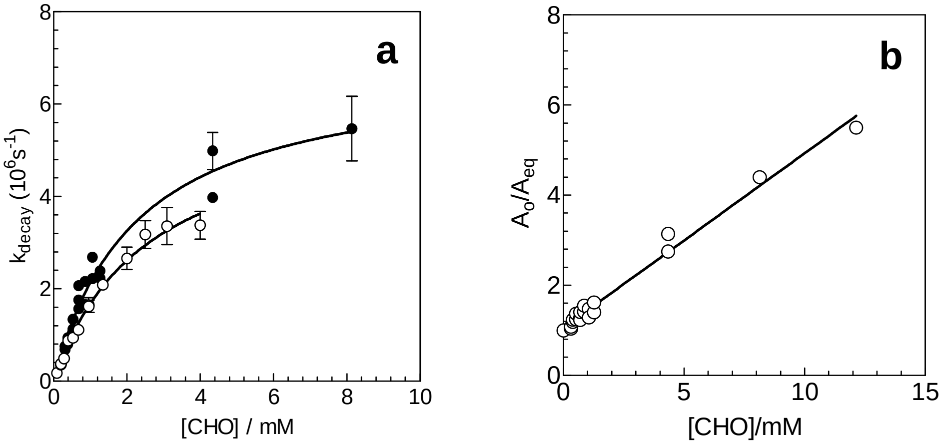

Figure 7.38. (a) Plot of k_{decay} (at 580 nm (●) and at 350 nm (o)) vs [CHO] for the reaction of $SiMes_2$ with CHO. The line is the best fit to eq. 7.15. (b) Plot of ΔA_0 / ΔA_{eq} (at 580 nm) vs [CHO] for the reaction of $SiMes_2$ with CHO, the line is the best least-squares fit of the data to eq. 7.12.

Table 7.4. Equilibrium constants for complexation of $SiMes_2$ with oxiranes (K_1 / M^{-1}) and first-order decay coefficients (k_2 / 10^6 s^{-1}) of the $SiMes_2$-oxirane complexes obtained by different methods. The errors are reported as twice the standard error from least squares analysis of the data in each case.

	PrO		CHO	
method	K_1 / M^{-1}	k_2 / 10^6 s^{-1}	K_1 / M^{-1}	k_2 / 10^6 s^{-1}
eq. 7.15 (580 nm)	51 ± 6	3.6 ± 0.2	400 ± 100	6.9 ± 0.8
eq. 7.15 (350 nm)	-	-	400 ± 100	5.9 ± 0.8
eq. 7.12 (580 nm)	53 ± 6	-	390 ± 20	-

Addition of sub-millimolar concentrations of PrS to a hexanes solution of **45** resulted in a systematic shortening of the silylene lifetime with no effect on the apparent initial intensity of the signal due to the silylene. The silylene decayed with pseudo first-order kinetics to a residual level indistinguishable from the baseline before the laser pulse,

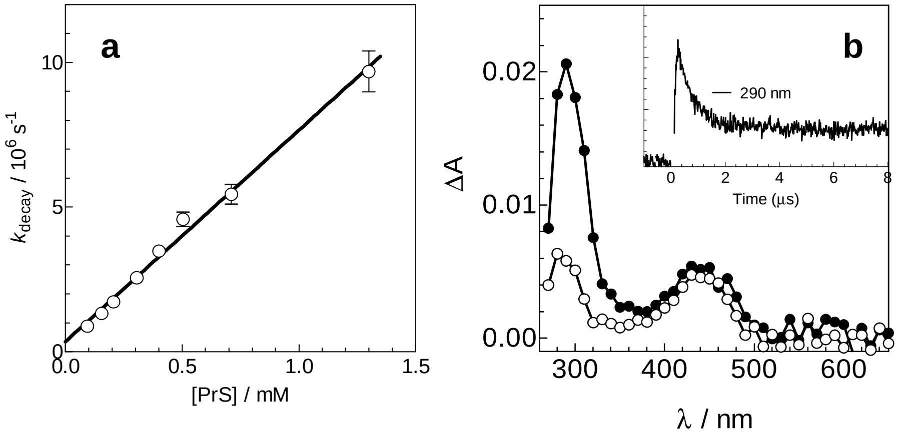

Figure 7.39. (a) Plot of k_{decay} vs [PrS] for the reaction of $SiMes_2$ with PrS. The solid line is the linear least-squares analysis of the data to eq. 7.11. (b) Transient absorption spectra of a rapidly flowing hexane solution of **45** in the presence of 20 mM PrS, obtained 0.256-0.320 μs (●) and 8.59-8.66 μs (o) after the laser pulse. The inset shows a transient decay trace recorded at 290 nm.

---

consistent with an equilibrium constant of > 25,000 M^{-1}. A plot of k_{decay} vs. [PrS] was linear with the slope yielding the second order rate constant of $k_1 = (7.3 \pm 0.5) \times 10^9$ M^{-1} s^{-1} (Fig. 7.39a). Transient absorption spectra recorded in the presence of 20 mM PrS show the prompt formation of a short-lived transient with λ_{max} = 290 nm. The transient decays with the first-order decay coefficient of $k_{decay} = (1.6 \pm 0.1) \times 10^6$ s^{-1} (τ = 620 ± 40 ns) to a weak residual absorption (Fig. 7.39b). Traces taken on a longer timescale reveal that the long-lived transient has an approximate lifetime of 0.5 ms, nearly the same as the lifetime of the signal at 440 nm due to the by-product of the photolysis of **45**. Addition of MeOH had no effect on the lifetimes of either the short or the long-lived transient at 290 nm, up to a maximum concentration of 0.5 mM MeOH.

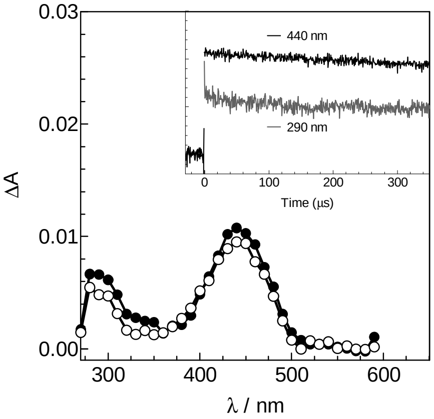

Figure 7.40. Transient absorption spectra of a rapidly flowing hexane solution of **45** in the presence of 20 mM PrS, obtained 0.0-2.6 μs (●) and 342.4-345.0 μs (o) after the laser pulse. The inset shows transient decay traces recorded at 290 nm and 440 nm.

A control experiment was performed to determine whether the long-lived residual absorption is due to the reaction of $SiMes_2$ with PrS or if it is in fact another band due to the photolysis by-product of **45**. Silylenes are known to react rapidly with AcOH and do not form any transients that absorb in the 270-650 nm range. The long-lived transient at 440 nm reacts with AcOH much slower than does the silylene, so a spectrum recorded in the presence of AcOH should be that due to the photolysis by-product of **45** alone. Transient absorption spectra of a rapidly flowing hexane solution of **45** in the presence of 5 mM AcOH are shown on Fig. 7.40. The spectra indicate the presence of two absorption bands due to the photolysis by-product, with the band at shorter wavelength of approximately half the intensity of the band at 440 nm.

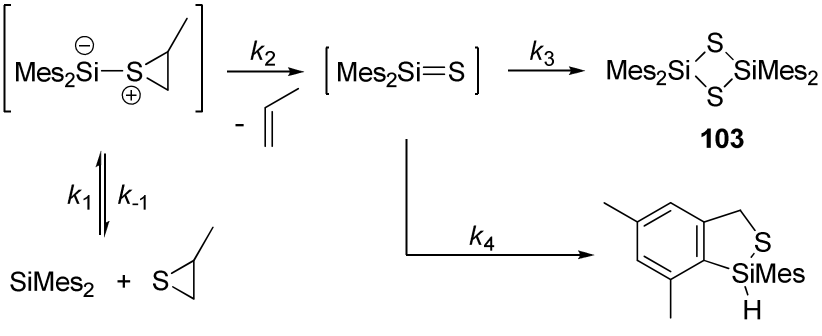

Scheme 7.4

Comparison of the spectra of **45** in the presence of AcOH to that in the presence of PrS suggests that there might be two overlapping bands at 290 nm with similar lifetimes in the millisecond range. Possible intermediates that could be formed in the reaction with the thiirane are shown in Scheme 7.4. The expected initial product of the reaction is the $SiMes_2$-PrS complex, which is expected to have a strong absorption band at ca. 300 nm and a shoulder at ca. 350 nm, analogous to the spectrum of the $SiMes_2$-THT complex (Chapter 3). Since the sulfur abstraction reaction proceeds with a lower activation barrier than oxygen abstraction in the cases of $SiMe_2$ and $SiPh_2$, the lifetime of the $SiMes_2$-PrS complex might be expected to be shorter than that of the $SiMes_2$-CHO complex ($\tau = 176 \pm 8$ ns). However, the spectral and temporal characteristics of the observed transients are not consistent with this assignment. The expected product of decomposition of the complex is dimesitylsilanethione ($Mes_2Si{=}S$), which could be expected to exhibit $\lambda < 300$ nm and should have a lifetime of $\tau > 100$ μs (based on our results with $Ph_2Si{=}S$) since its dimerization is expected to be slowed down due to the presence of the sterically bulky mesityl groups on silicon. Its decay characteristics in the absence of scavengers should be second order due to dimerization. The behaviour of the observed short-lived transient is inconsistent with this assignment. A possible reaction that would account for the shortening of the lifetime of $Mes_2Si{=}S$ would be addition of the ortho-methyl across the Si-S double bond to yield **104**. However, compound **104** should be easily identifiable by ^1H NMR spectroscopy by the presence of a singlet in the 5-6 ppm range due to the Si-H hydrogen. This peak was not observed in the preliminary product studies which employed 1,4-dioxane as the internal standard.

Another possible assignment of the long-lived transient is to a product of direct photolysis of PrS. It was shown that flash photolysis of a 20 mM hexanes solution containing PrS generates a long-lived transient at 290 nm with an initial signal intensity of 0.005. The sum of this weak absorption and the second band in the spectrum of the photolysis by-product of **45** could result in the two long-lived absorptions at 290 nm and 440 nm to have a similar intensity.

In order to determine if the new transient is also formed in the reaction of this silylene with a different thiirane, we employed cyclohexene sulfide (CHS) for comparison. The sample of CHS is available from Sigma-Aldrich in a maximum purity of only 85%, so the material was purified by distillation from anhydrous Na_2SO_4 prior to use.

Addition of CHS to a rapidly flowing hexanes solution of **45** resulted in shortening of the silylene lifetime in a similar fashion to what was observed for the reaction with PrS. A plot of k_{decay} vs [CHS] was linear, and afforded a bimolecular rate constant of $k_1 = (8 \pm 2) \times 10^9$ M^{-1} s^{-1} (Fig. 7.41a). The value is the same within error to those found for the

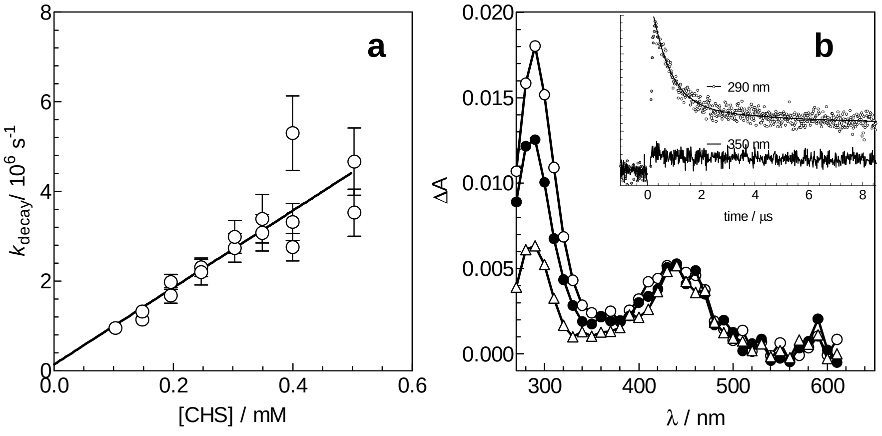

Figure 7.41. (a) Plot of k_{decay} vs [CHS] for the reaction of $SiMes_2$ with CHS. The solid line is the linear least-squares fit of the data to eq. 7.11, which yields a rate constant of (8 ± 2) × 10^9 M^{-1} s^{-1} (b) Transient absorption spectra of a rapidly flowing hexanes solution of **45** in the presence of 11 mM CHS, 0.27-0.35 µs (o), 0.91-0.99 µs (●) and 8.59-8.67 µs (Δ) after the laser pulse. The inset shows transient decay traces recorded at 290 nm and 350 nm.

---

reactions of $SiMes_2$ with PrS and THT (Table 7.5). Transient absorption spectra in the presence of 11 mM CHS also yields a short-lived transient with a lifetime of τ = (690 ± 10) ns (extracted from a two-phase fit) and $\lambda_{max} \approx 290$ nm, which decays to a residual absorbance of similar intensity and lifetime to that at 440 nm (Fig. 7.41b). The spectra of this transient are nearly identical to those shown in Fig. 7.39b, and thus it can be concluded that the new transient arises from the reaction of $SiMes_2$ with the thiirane. Its identity, however, cannot be assigned at this time, as its spectral characteristics and lifetime are not consistent with either the $SiMes_2$-thiirane complex or $Mes_2Si{=}S$.

Table 7.5. Forward rate constants (k_1) and equilibrium constants (K_1) for complexation of transient silylenes with sulfur donors in hexanes at 25 ^{o}C. The last column indicates the measured lifetime of the species at 290 nm formed in the sulfur abstraction reactions with thiiranes.

system	k_1 / 10^9 M^{-1} s^{-1}	K_1 / M^{-1}	τ (290 nm)
$SiMes_2$ + PrS	7.3 ± 0.5	>25,000	620 ± 40 ns
$SiMes_2$ + CHS	8 ± 2	>25,000	690 ± 10 ns
$SiMes_2$ + THT	7 ± 2	$1{,}500 \pm 100$	-
$SiMes_2$ + Et_2S	[a]	54 ± 3	-
$SiPh_2$ + PrS	11.2 ± 0.4	>25,000	~ 100 μs
$SiPh_2$ + CHS	12 ± 1	>25,000	~ 100 μs
$SiPh_2$ + THT	16 ± 2	>25,000	-
$SiTmp_2$ + PrS	9.7 ± 0.8	>25,000	~ 75 μs
$SiTmp_2$ + Et_2S	7.1 ± 0.6	> 25,000	-

[a] cannot be measured.

7.2.3. Kinetic simulations

Kinetic simulations were performed in an analogous fashion to those described in section 6.3. The same input equations were used as before (eq. 6.12-6.14) and they are listed again in eq. 7.18-7.20. The input mechanism has two consecutive steps – an initial reversible complexation to form SiD (eq. 7.19), which reacts unimolecularly to yield product P (eq. 7.20). The reaction of Si with D completes with dimerization of the silylene (eq. 7.18).

$$\mathrm{Si + Si \xrightarrow{k_{dim}} Si{=}Si} \qquad (7.18)$$

$$\mathrm{Si + D \underset{k_{-1}}{\overset{k_1}{\rightleftharpoons}} SiD} \qquad (7.19)$$

Table 7.6. Equilibrium constants for complexation of $SiMes_2$ with oxiranes (K_1 / M^{-1}) and first-order decay coefficients (k_2 / 10^6 s^{-1}) of the $SiMes_2$-oxirane complexes. The last row lists the input values used for kinetic simulations.

	PrO		CHO	
method	K_1 / M^{-1}	k_2 / 10^6 s^{-1}	K_1 / M^{-1}	k_2 / 10^6 s^{-1}
$SiMes_2$ (experiment)[a]	52 ± 4	3.6 ± 0.2	400 ± 50	5.9 ± 0.8[b]
sim. eq 7.15 (silylene)	53 ± 8	3.5 ± 0.2	290 ± 30	6.8 ± 0.2
sim. eq. 7.15 (complex)	54 ± 4	3.5 ± 0.1	310 ± 10	6.7 ± 0.1
sim. eq. 7.12 (silylene)	55.8 ± 0.2	-	520 ± 30	-
input values for simulation	50	3.6	400	6.4

[a] average of values determined by different methods as shown in Table 7.4; [b] the value obtained from the $SiMes_2$-CHO complex data.

$$\mathrm{SiD} \xrightarrow{k_2} \mathrm{P} \qquad (7.20)$$

The dimerization rate constant used in these simulations was 1×10^9 M^{-1} s^{-1}.[24] A rate constant for complexation of $SiMes_2$ with oxiranes could not be measured due to the small size of the equilibrium constants, so it was approximated as 7×10^9 M^{-1} s^{-1} for the simulation. This value is the reported value for the complexation of $SiMes_2$ with THT,[25] so it may be expected that the complexation rate constant with the oxirane will be of a similar value based on the trends established for the reactivity of $SiMe_2$ and $SiPh_2$ in Chapter 3. An appropriate value of k_{-1} was chosen to afford an equilibrium constant of either 50 M^{-1} (for PrO) or 400 M^{-1} (for CHO).

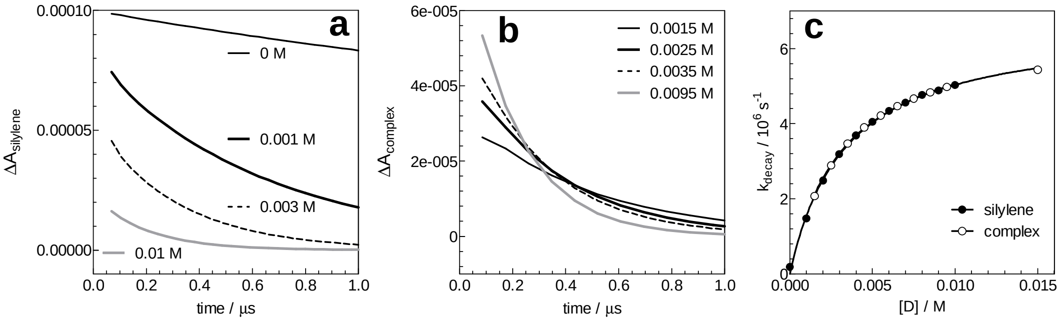

Figure 7.42. Simulated decay profiles of the signals due to a silylene (a) and the corresponding silylene-donor complex (b) at various substrate concentrations, for a situation involving an initial equilibrium followed by a unimolecular irreversible dissociation of the complex. The situation describes $SiMes_2$ reaction with CHO, for which the input values for the simulation are listed in Table 7.6. (c) Plot of k_{decay} vs [D], obtained from the simulated decay profiles for silylene (a) and the complex (b). The solid line is the fit of the data to eq. 7.15.

Analysis of the simulated data for the $SiMes_2$ with CHO reaction reveals that an increase in the substrate concentration does indeed result in the loss of the apparent intensity and reduction in the lifetime of the silylene (Si) signal (Fig. 7.42a). The intermediate SiD has an identical lifetime to that of the silylene at each concentration of D, while the intensity of the signal increases (Fig. 7.42b). The plots of k_{decay} vs [D] for silylene and SiD are identical (Fig. 7.42b) and both exhibit a downward curvature. Analysis of the two sets of data according to eq. 7.15 yields values of K_1 and k_2 that are the same as the input values. The loss in the intensity of the silylene signal was also analysed using eq. 7.12, which yields a linear plot of $\Delta A_0/\Delta A_{eq}$ vs [D] with a slope (of 520 M^{-1}) that is ca. 25% higher than the input value of 400 M^{-1}.

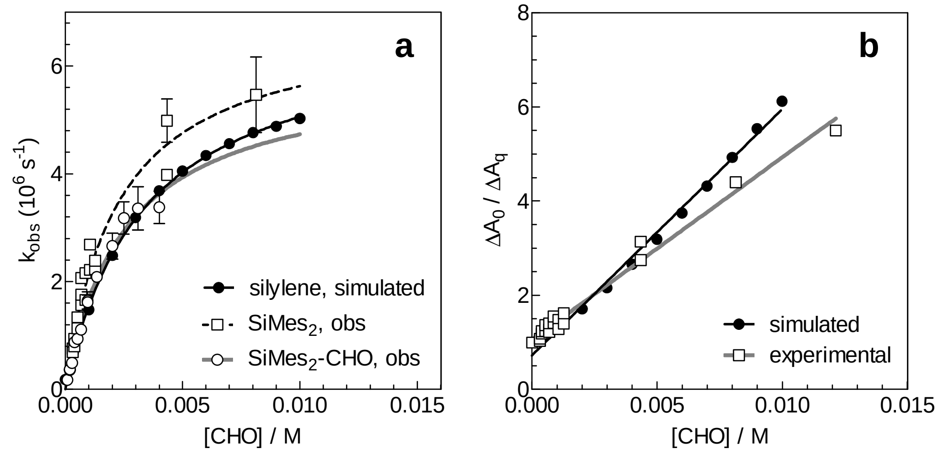

Figure 7.43. (a) Plot of experimental k_{decay} vs [CHO] data measured at 580 nm for SiMes$_2$ (□) and at 350 nm for the SiMes$_2$-CHO complex (o), and simulated k_{decay} vs [D] data for the silylene (●); the solid lines are the best fits of the data to eq. 7.15; (b) Plot of $\Delta A_0/\Delta A_{eq}$ vs [CHO] obtained from the analysis of the experimental data (□) and vs [D] fom the simulated data (●); the solid lines are the linear least squares analysis of the data to eq. 7.12.

The simulated data are shown plotted along with the experimental data for the SiMes$_2$-CHO system in Fig. 7.43. The agreement between the experimental data and the simulated results is excellent, considering the errors in the experimental values. The equilibrium constant obtained from the plot of ΔA_0 / ΔA_{eq} vs [D] was also in reasonable agreement with the experimental value, with the simulated value being slightly higher than the experimental (Table 7.6). Analogous kinetic simulations of the reaction of SiMes$_2$ with PrO also led to output values of K_1 and k_2 that agreed well with experimental results (Fig. 7.44). The values of K_1 and k_2 extracted from the fits of the experimental and simulated data to eq. 7.15 and eq. 7.12 are shown in Table 7.6.

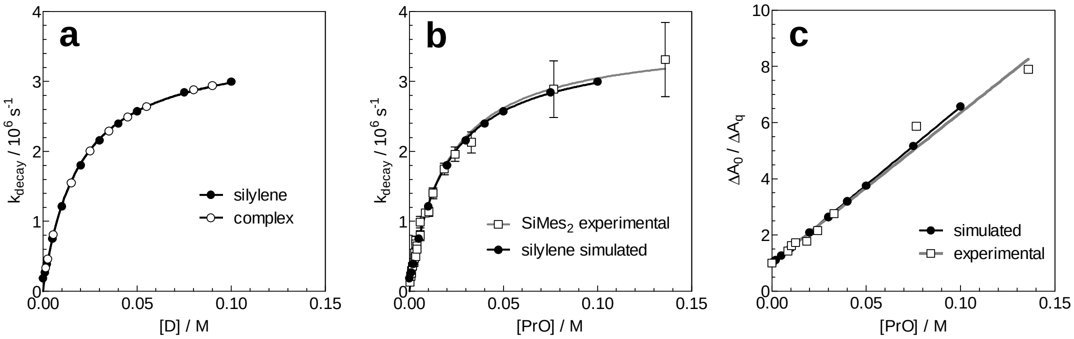

Figure 7.44. (a) Plot of k_{decay} vs [D], obtained from the simulated decay profiles for silylene and the complex, for the reaction of $SiMes_2$ with PrO. The solid line is the fit of the data to eq. 7.15. (b) A plot of experimental k_{decay} values vs. [PrO] of experimental values measured at 580 nm for $SiMes_2$ (□), and the corresponding simulated values for the silylene (●); the solid lines are the best fit of the data to eq. 7.15. (b) Plots of ΔA_0 / ΔA_{eq} vs [PrO] obtained from the analysis of experimental (□) and the simulated data (●); the solid lines are the linear least squares fits of the data to eq. 7.12.

7.3. Discussion

7.3.1. Product studies

The product studies indicate that $SiMe_2$ and $SiPh_2$ react with oxiranes in cyclohexane solution to afford the corresponding alkenes and products consistent with the formation of the corresponding silanones. The products of the reaction of $SiMe_2$ with CHO are consistent with those previously reported for the reaction of $SiMe_2$ with cyclooctene oxide.[2] Transient diphenylsilanone generated from the reaction of $SiPh_2$ with PrO was efficiently trapped by D_3, yielding propene and the product of trapping of $Ph_2Si{=}O$ by D_3 in a 1:1 ratio, indicative of ca. 100% trapping efficiency of the silanone by the oligosilane. $SiMes_2$ reacts with CHO to generate the corresponding alkene in a similar yield to those obtained with the $SiMe_2$ and $SiPh_2$ systems; however it is difficult to ascertain whether a transient silanone is involved in the absence of silanone trapping agents. Addition of MeOH as a silanone trap resulted in the formation of the novel product **99**, which is most likely formed by reaction of $Mes_2Si{=}O$ with one molecule each of CHO and MeOH. The relative yields of cyclohexene and the CHO/MeOH-trapping product are also 1:1 in this reaction, indicating quantitative trapping efficiency under the conditions of our experiments.

It is apparent that all three silylenes react with oxiranes with similar efficiencies, giving the corresponding alkenes and silanone-derived products in yields of 40-50% in each case (Table 7.7). These yields are significantly less than 100%, indicative of an alternate reaction pathway which we were unable to characterize fully. The amounts of consumed oxirane relative to the silylene precursors are considerably higher than 100% in

Table 7.7. The amounts of consumed oxirane and yield of alkene relative to consumed silylene precursor, determined from the plots of concentration vs. time from the reactions of $SiPh_2$ and $SiMes_2$ with oxiranes under various conditions. Photolysis conducted in cyclohexane solutions at 25°C unless noted otherwise, error margins are given in the text.

	Conditions	Amount of Consumed Oxirane	Yield of Alkene
1	**43** (0.5 M) + cyclooctene oxide (0.5 M)	-	62%[a]
2	**43** (0.05 M) + CHO (0.1 M)	-	49%[b]
3	**44a** (0.05 M) + PrO (0.15 M) + D_3 (0.2 M)	350%	45%
4	**44a** (0.05 M) + PrO (0.15 M)	210%	52%
5	**45** (0.05 M) + CHO (0.83 M)	1800%	40%
6	**45** (0.05 M) + CHO (0.14 M)	190%	43%
7	**45** (0.05 M) + CHO (0.35 M) + MeOH (0.01 M)	1300%	38%

[a] photolysis conducted at 40°C, ref. 2; [b] relative to consumed CHO.

all cases, as illustrated in Table 7.7. Oligomerization of the oxirane is evident from the broadening of the ^1H NMR spectra of the photolysis mixtures; however a complete characterization of the structure of the oligomers was not possible. Since the oxiranes do not absorb the incident light to an appreciable extent, photo-induced oligomerization of the oxirane can be ruled out. In fact, our results are consistent with either silylene or the silylene-oxirane complexes acting as an oxirane oligomerization catalyst. Photolysis of the mixtures in entries 4 and 6 in Table 7.7 results in similar consumption of the oxirane relative to that of the silylene precursor, indicating no significant change in the catalytic activity resulting from the Mes-for-Ph substitution on the silicon. Oligomerization pathways can also account for low yields of the alkenes in each case. It should be noted that the yield of cyclohexene in the photolysis of the mixture of entry 2 in Table 7.7 was determined relative to the consumed oxirane, while all the others were determined relative to the consumption of the silylene precursors.

The reactions of $SiMe_2$ and $SiPh_2$ with PrS have also been examined by steady-state photolysis methods. The results indicate that propene is formed in yields in the range of 33-65%, along with products consistent with the formation of the corresponding silanethione. Various reactions of $Me_2Si{=}S$ under thermolytic conditions have been reported,[4, 6, 20] and show that the silanethione either dimerizes in a head-to-tail fashion to generate tetramethyldisilthiane $(Me_2SiS)_2$ or can be trapped by D_3 to form **90**. Our results indicate that trapping of $Me_2Si{=}S$ by D_3 is only 50% efficient; in contrast, D_3 failed to trap the diphenyl analog $Ph_2Si{=}S$ at all. Interestingly, we were unable to find evidence for the formation of the silanethione dimer in the $SiMe_2$ system by ^1H NMR spectroscopy[6] or GC/MS, while tetraphenyldisilthiane (**94**) is the major product of the reaction of $SiPh_2$ with PrS in either the presence or absence of D_3. Analogous to the reactivity exhibited by stable silanethiones,[7-8] $Ph_2Si{=}S$ reacts with MeOH to generate the corresponding methoxysilanethiol **96** in an equimolar ratio to the formed alkene. As in the reactions with oxiranes, the yields of propene relative to consumed PrS are significantly less than 100% in each case, again suggesting the presence of alternate reaction pathways.

7.3.2. Kinetics and thermodynamics of the initial complexation of silylenes with our oxiranes and thiiranes

The laser flash photolysis results indicate that the reactions of transient silylenes with oxiranes and thiiranes proceed via multistep mechanisms involving the initial formation of a Lewis acid-base complex between the silylene and oxirane or thiirane, which reacts unimolecularly to form the corresponding silanone or silanethione. The complexes have been detected directly for all the silylene-oxirane systems, but only in some cases with the analogous thiirane systems (see section 7.3.3).

The rate constants for complexation fall in the range of 6.3×10^{9} M^{-1} s^{-1} to 21×10^{9} M^{-1} s^{-1}, and increase in the order $SiMes_2$ < $SiTmp_2$ < $SiPh_2$ < $SiMe_2$ (Table 7.8). The difference in the rate constants between $SiPh_2$ and $SiTmp_2$ reflect electronic effects introduced by the methyl groups, while the reduction in the rate constants for the $SiMes_2$ is caused by steric interactions. For a given silylene the rate constants do not vary significantly with the identity of the O- or S- donor, and all are within a factor of 3 of the diffusional rate in hexanes at 25 ^{o}C. Thus, the intrinsic free energy barrier for complexation is on the order of 4.0 kcal mol^{-1} or less for complexation with both oxiranes and thiiranes. Steric effects associated with the silylene substituents dominate the situation with the bulkier silylene, $SiMes_2$, resulting in destabilization of the resulting complexes with the oxiranes compared to those of $SiPh_2$. Equilibrium constants of 400 ± 50 M^{-1} ($\Delta G = -(1.7 \pm 0.1)$ kcal mol^{-1}) and 52 ± 4 M^{-1} ($\Delta G = -(0.45 \pm 0.05)$ kcal mol^{-1}) were measured for complexation with CHO and PrO, respectively, and reflect the trend expected based on the difference in the gas phase basicities of the two oxiranes.[26] The

Table 7.8. Forward rate (k_1) and equilibrium constants (K_1) for complexation of transient silylenes with oxiranes and thiiranes in hexanes at 25 ^{o}C.

substrate	k_1 / 10^9 M^{-1} s^{-1} [K_1 / M^{-1}]			
	$SiMe_2$	$SiPh_2$	$SiTmp_2$	$SiMes_2$
CHO	19 ± 2 [a]	10.0 ± 0.4 [a]	6.3 ± 0.9 [a]	[b] [400 ± 50]
PrO	16 ± 2 [a]	12 ± 2 [a]	[c]	[b] [52 ± 4]
CHS	19 ± 2	12 ± 1	[c]	8 ± 2 [a]
PrS	21 ± 2 [a]	11.2 ± 0.4 [a]	9.7 ± 0.8 [a]	7.3 ± 0.5 [a]

[a] K_1 > 25,000 M^{-1}; [b] the rate constant could not be measured due to a small equilibrium constant; [c] not determined.

equilibrium constants for complexation of this silylene with the thiiranes are above the measurement limit of our system ($K_1 \geq 25{,}000$ M^{-1}, $\Delta G \leq -4$ kcal mol^{-1}, reference state is the gas phase at 1 atm and 25 ^{o}C). The complexes with the O-donors are less stable than those with the S-donors in all cases, which can be attributed to a significantly shorter Si-O bond length in the $SiMe_2$-oxirane complex compared to that of a Si-S bond in the $SiMe_2$-thiirane complex, as indicated by calculations for these systems carried out at the B3LYP/6-311+G(d,p) level of theory.[13]

Table 7.9. UV-vis absorption maxima (nm) of the Lewis acid-base complexes of transient silylenes with oxygen and sulfur donors in hydrocarbon solvents at 25 °C.

	$SiMe_2$	$SiPh_2$	$SiTmp_2$	$SiMes_2$
PrO	310	290, 370	300, 380	300, 400 (sh)
CHO	310	290, 370	300, 370	300, 400 (sh)
Et_2O	305[18]	300, 375[25]	-	310[25]
THF	310[9]	295, 370[9]	375[23]	310, 380 (sh)[25]
PrS	320	290, 370	[a]	[a]
THT	325[13]	300, 370[13]	-	300, 400 (sh)[25]
Et_2S	320	300, 360	290, 350	300, ~400 (sh)

[a] could not be detected.

7.3.3. The substituent effect on the lifetime of the silylene-substrate complexes

The transient silylenes $SiMe_2$, $SiPh_2$ and $SiMes_2$ react with PrO and CHO to form the corresponding Lewis acid-base complexes in the initial stages of the reaction pathway, which have been detected and characterized in all cases. The complexes have been identified by comparison of their UV absorption spectra to those reported for the corresponding silylene-THF and –Et_2O complexes ($SiMe_2$ ref. [9, 18, 27], $SiPh_2$ ref. [9], $SiMes_2$ ref. [25], $SiTmp_2$ ref. [23]) (Table 7.9). Silylene-thiirane complexes have been detected for the $SiMe_2$-PrS and $SiPh_2$-PrS systems, but they absorb significantly more weakly than the corresponding oxirane complexes. Their transient absorption spectra are quite similar to those of the corresponding silylene-THT and silylene-Et_2S complexes (Table 7.9).

The complexes decay with first order decay kinetics in all cases. These complexes are significantly shorter-lived than the corresponding complexes with other ether and sulfide substrates such as THF and THT, respectively. This indicates that they possess low energy reaction channels that are absent in the “non-reactive” complexes. The THF

Table 7.10. First order decay rate coefficients for the decay of the silylene-oxirane and silylene-thiirane complexes (/10^6 s^{-1}).

	$SiMe_2$	$SiPh_2$	$SiTmp_2$	$SiMes_2$
PrO	3.1 ± 0.2	3.4 ± 0.2	3.3 ± 0.2	3.6 ± 0.2
CHO	4.3 ± 0.3	4.2 ± 0.3	3.9 ± 0.4	6 ± 1
PrS	≥ 40 ± 4	18 ± 3	[a]	[a]

[a] could not be detected

and THT complexes are long-lived, decay over several microseconds with second order kinetics to afford the corresponding disilenes. The silylene-PrO, -CHO, and –PrS complexes, on the other hand, do not generate the corresponding dimers. The rate of decay of the complexes is independent of the concentration of added substrate, indicating that a unimolecular process (C-X bond cleavage) is responsible for their decomposition. A summary of the first order decay rate coefficients of the complexes is provided in Table 7.10.

The data show that the k_2 values for the decomposition of the SiR_2-PrO complexes do not vary as a function of substituents on the silicon atom. In all cases but $SiMes_2$, the decomposition of the SiR_2-CHO complexes is more rapid by 15-40% than that of the SiR_2-PrO complexes. Steric considerations play a role in the CHO complexes, as is evident from the fact that the $SiMes_2$-CHO complex exhibits a significantly shorter lifetime than the corresponding -CHO complexes with the other three silylenes (Table 7.10). The rate constants correspond to free energies of activation in the 8.2-8.6 kcal mol^{-1} range for the reactions responsible for the decay of the complexes. These values are in good agreement with the calculated (B3LYP/6-311+G(d,p)//B3LYP/6-311+G(d,p))[13] free energy of activation for C-O bond cleavage in the $SiMe_2$-oxirane complex of E_a = 8.1 kcal mol^{-1} relative to the lower energy *anti* conformer.

Ab initio calculations by Apeloig and Sklenak[28] at the MP2 and QCISD levels of theory and DFT calculations by us[13] for the parent system (SiH_2-oxirane) indicate that the bond cleavage should proceed in a stepwise fashion, initially yielding a singlet biradical formed by cleavage of a C-O bond. DFT calculations for the $SiMe_2$-oxirane system are in agreement with those for the parent system, where the formation of a biradical is the lowest energy pathway for the decomposition of the complex. In both cases, the formation of the biradical is predicted to be exergonic, with the dimethyl system exhibiting greater exergonicity (ca. 18 kcal mol^{-1}) than the parent system (ca. 13 kcal mol^{-1}) at the UB3LYP/6-311+G(d,p) level.[13]

The experimental observation of a faster decay rate constant for the SiR_2-CHO complex compared to that for the corresponding SiR_2-PrO complex is consistent with a biradical mechanism for oxygen abstraction. Since the cleavage of either C-O bond in CHO would result in a secondary biradical, both C-O bonds are expected to be cleaved with equal probabilities. In PrO, however, the more substituted C-O bond would be expected to cleave preferentially. On the basis of statistical factors alone it is expected that the silylene-CHO complexes should cleave twice as fast as the PrO-complexes. The observed cleavage rate is less than twice as fast for the CHO systems, presumably reflecting a slightly higher enthalpic barrier for C-O bond cleavage for the disubstituted system.

Scheme 7.5 illustrates the pathways that could potentially be available for the decomposition of the biradical. Steady-state photolysis experiments (*vide infra*) indicate that the oxygen abstraction pathway accounts for *ca.* 50% of the material balance independent of substitution on silicon. Cyclization of the biradical could potentially lead to the formation of oxasilacyclobutane products; preliminary experiments by undergraduate students Alphonsus Ballesteros and Jordan Walwyn demonstrate that this process proceeds with *ca.* 30% efficiency in the $SiMe_2$-vinyloxirane and $SiPh_2$-vinyloxirane systems. With the CHO and PrO systems presented here, however, no evidence for this type of product was found. Another feasible reaction pathway for the biradical species is 1,3-H migration to form the corresponding silyl enol ether.[13] This structure should be stable under our photolysis conditions and would be easily identifiable by a characteristic Si-H peak in the NMR spectra, but we saw no evidence for its formation.

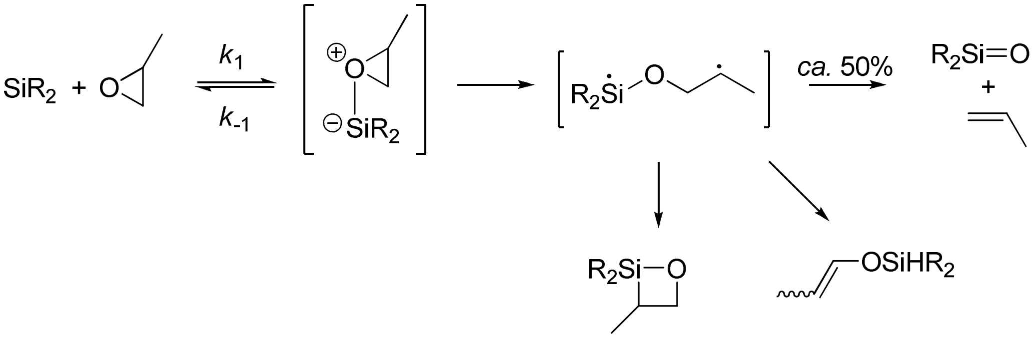

Scheme 7.5

Table 7.10 also demonstrates that the lifetimes of the $SiMe_2$-PrS and $SiPh_2$-PrS complexes are significantly shorter than those of the corresponding PrO-complexes. The lifetimes of the $SiTmp_2$-PrS and $SiMes_2$-PrS complexes are short, so much so that they cannot be detected on the timescales of our experiments. A lower limit of $k_2 \geq 4 \times 10^7$ s^{-1} was obtained for the dissociation of the SiMe$_2$-PrS complex ($\Delta G^\ddagger \leq 7.1$ kcal mol^{-1}). This value for the energy barrier is consistent with the calculated value of $\Delta G^\ddagger = 5.7$ kcal mol^{-1} for reaction of the SiMe$_2$-thiirane complex.[13] It is difficult to obtain a more accurate measure of the lifetime of the SiMe$_2$-PrS complex due to strong sample fluorescence in the region where the complex absorbs. In contrast to the oxirane systems, thiirane systems show a dependence on the substitution at silicon, such that the SiPh$_2$-PrS complex is longer lived than the SiMe$_2$-PrS complex. The decay rate constant of the SiPh$_2$-PrS complex of $k_2 = 2 \times 10^7$ s^{-1} corresponds to a free energy of activation of $\Delta G^\ddagger = 7.4$ kcal mol^{-1} for the further unimolecular reaction of the species, which is *ca*. 1 kcal mol^{-1} lower than that found for the SiPh$_2$-PrO complex.

The variation in the lifetimes of the SiMe$_2$-PrS and SiPh$_2$-PrS complexes suggests a different mechanism for their decomposition compared to the corresponding oxirane complexes. This is indeed indicated by calculations, as illustrated by the reaction coordinate diagram for the reaction of SiMe$_2$ with oxirane and thiirane of Fig. 7.45. In agreement with earlier calculations by Apeloig[28], DFT calculations predict a lower barrier for reaction of the SiMe$_2$-thiirane complex compared to the corresponding oxirane complex, and they predict the former to undergo concerted fragmentation to alkene and silanethione.

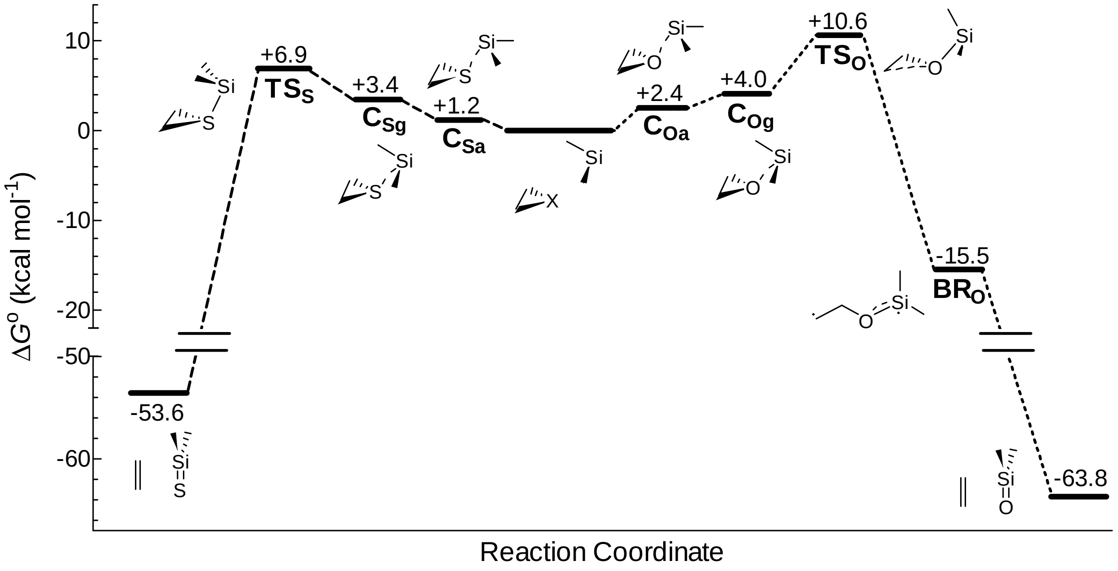

Figure 7.45. Reaction coordinate diagram for the reaction of $SiMe_2$ with oxirane and thiirane, calculated at the B3LYP/6-311+(G(d,p) level of theory.[13]

7.3.4. Diarylsilanethiones – spectra and reactivity

This study features the first spectroscopic detection of transient diphenylsilanethione ($Ph_2Si=S$), and consequently the first kinetic studies of some of the reactions of these species in solution. $Tmp_2Si=S$ was also tentatively identified based on the similarity of its spectra and lifetime to those of $Ph_2Si=S$ (Fig. 7.46a).

The spectroscopic properties of the transient silanethiones detected in this study are summarized in Table 7.11. Both transient diarylsilanethiones exhibit a strong absorption band centered at *ca*. 280 nm; in the case of $Ph_2Si=S$ a weak second band was also detected at longer wavelengths (460 nm). If this longer wavelength band is due to the n → π* absorption, it can be compared to that exhibited by the stable diarylsilanethione

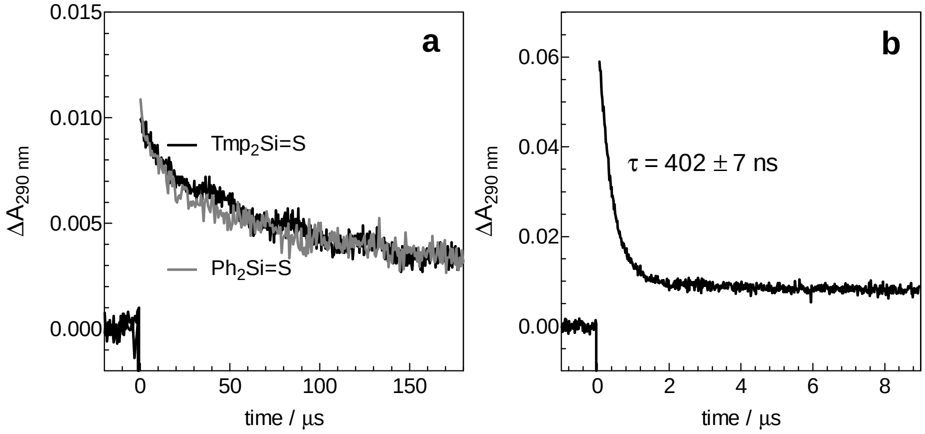

Figure 7.46. Transient decay traces recorded at 290 nm of a hexane solution containing (a) (—) **44a** and 20 mM PrS, (—) **87** and 5.4 mM PrS; (b) **45** and 10 mM PrS.

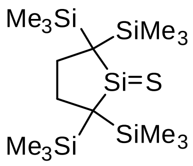

105

prepared by Tokitoh's group, Tbt(Tip)Si=S (396 nm, ε = 100).[29] Thus, phenyl substituents on the silicon induce a *ca*. 65 nm spectral shift relative to that reported for the bulkier analogue. The spectrum of Kira's diaryl silanethione (**105**) is blue-shifted relative to those of diaryl silanethiones (λ_{max} = 266, ε = 3000; λ_{max} = 336, ε = 17).[8] The base reaction that diphenylsilanethione undergoes is rapid head-to-tail dimerization with $2k/\varepsilon_{290\ nm} = (2.3 \pm 0.2) \times 10^{6}$ cm s^{-1} ($k_{dim} \approx 1 \times 10^{10}$ M^{-1} s^{-1} assuming $\varepsilon_{290\ nm} \approx 10{,}000$ dm mol^{-1} cm^{-1}); the dimer was detected as the major product in the steady-state experiments. A new transient was also detected in the SiMes$_2$-PrS system, however its spectral characteristics are inconsistent with those expected for either the SiMes$_2$-PrS complex or Mes$_2$Si=S; the absorbance-time profile is shown in Fig. 7.46b. The transient decays with *first* order kinetics and exhibits a lifetime of τ = (402 ± 7) ns, and thus is unlikely to be assignable to Mes$_2$Si=S.

Table 7.11. UV-vis absorption maxima of silanethiones in hydrocarbon solvents at 25 °C

silanethione	λ_{max} / nm
$Ph_2Si=S$	275 ($\pi \rightarrow \pi^*$), 460 ($n \rightarrow \pi^*$)
$Tmp_2Si=S$	≤ 280 ($\pi \rightarrow \pi^*$)
Tbt(Tip)Si=S[a]	396 ($n \rightarrow \pi^*$, $\varepsilon = 100$)

[a] Ref. 29, Tbt = 2,4,6-tris[bis(trimethylsilyl)methyl]phenyl, Tip = 2,4,6-triisopropylphenyl

Diphenylsilanethione was found to react rapidly with nucleophilic substrates such as aliphatic alcohols, acetic acid, and n-butyl amine (Table 7.12), all of which have been shown to react with other silanethione derivatives.[7-8, 19] The rate constants are in the range of 1.4×10^8 to 3.2×10^9 M^{-1} s^{-1} and are of the same magnitude as those reported for diphenylsilene ($Ph_2Si=CH_2$) with the same set of substrates. These rate constants correspond to free energies of activation in the 4.5 - 6.4 kcal mol^{-1} range. Fig. 7.47 illustrates the correlation between the free energy values of activation and gas phase basicities of the donors. No strong correlation is observed, only a general decrease in $\Delta G^\ddagger$ values with increasing basicity of the donor. The $\Delta G^\ddagger$ values obtained for the reaction of silene and silanethione with tBuOH are higher than those for all the other systems and may reflect steric effects on the complexation step. Figure 7.47 also shows that reaction of the silene generally proceeds with a lower activation barrier than the reaction of the silanethione with the same substrate, indicative of a lower degree of polarization of a Si=S bond compared to a Si=C bond.

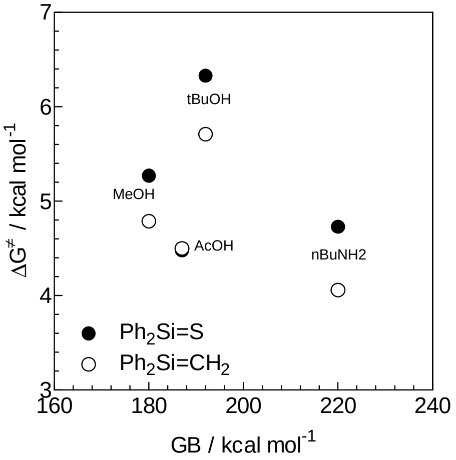

Figure 7.47. Plots of experimental free energy values of activation ($\Delta G^{\ddagger}$ / kcal mol^{-1}) of $Ph_2Si{=}S$ (●) and $Ph_2Si{=}CH_2$ (o) with various substrates vs gas basicity[26] of the donors.

Table 7.12. Absolute 2nd-order rate constants (k_1, in units of 10^9 $M^{-1}s^{-1}$) for quenching of the long-lived transient product of the reaction of $SiPh_2$ with PrS by MeOH, *t*-BuOH, AcOH, and *n*-$BuNH_2$ in hexanes.[a]

Substrate	$Ph_2Si{=}S$[a]	$Ph_2Si{=}CH_2$[b]	GB[c] / kcal mol^{-1}
MeOH	0.85 ± 0.09	1.9 ± 0.2[30]	180
t-BuOH	0.14 ± 0.01	0.40 ± 0.07[30]	192
AcOH	3.2 ± 0.7	3.1 ± 0.3[30]	187
n-$BuNH_2$	2.1 ± 0.1	6.5 ± 0.1[31]	220

[a] at 25 ± 1 ˚C, the average and standard deviation of two independent determinations; [b] at 23 ± 1 ˚C. [c] Ref. 26

The proposed mechanisms of the reactions of $Ph_2Si{=}S$ with the four substrates begin with nucleophilic attack at silicon followed by proton transfer, similar to the analogous reactions by transient silenes (Scheme 7.6).[31-32]

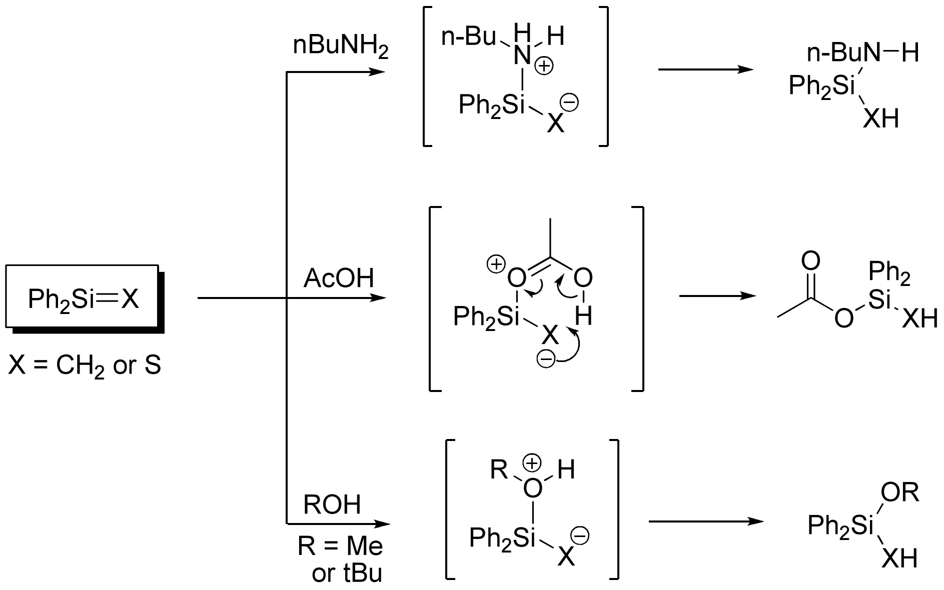

Scheme 7.6

7.4. Conclusions

The four silylenes studied in this work react rapidly with oxiranes and thiiranes to generate the corresponding Lewis acid-base complexes, which have been detected directly and characterized in all but two cases involving thiiranes. The complexes decay rapidly with first order kinetics to generate products consistent with chalcogen abstraction. End-product analysis indicates that chalcogen abstraction proceeds with *ca.* 50% efficiency to yield the corresponding alkenes along with products due to O- or S-abstraction. The experimental results are consistent with theoretical calculations that predict a stepwise process involving a biradical intermediate for decomposition of the silylene-oxirane complexes, and a concerted pathway for the thiirane systems.

Transient $Ph_2Si=S$ was detected for the first time in solution by laser flash photolysis, and characterized based on its reactivity towards MeOH, tBuOH, AcOH and $nBuNH_2$. These results compare reasonably well to the reported reactivity of diphenylsilene towards the same set of substrates. The UV-vis spectra exhibited by the silanethione have been compared to those reported for stable silanethiones, and are also in good agreement with spectra calculated at the TD-B3LYP/6-311G(d) level of theory. It is evident that further work will be necessary to establish the identity of the transients formed in the reaction of $SiMes_2$ with thiiranes, possibly involving synthesis of a silylene precursor with different substituents on the silicon.

7.5. References

1. Ishikawa, M.; Kumada, M., *J. Organomet. Chem.* **1972,** *42*, 325.

2. Goure, W. F.; Barton, T. J., *J. Organomet. Chem.* **1980,** *199*, 33.

3. Kovar, D.; Utvary, K.; Hengge, E., *Monatsh. Chem.* **1979,** *110* (6), 1295.

4. Soysa, H. S. D.; Weber, W. P., *J. Organomet. Chem.* **1979,** *165*, C1.

5. Teng, C. J.; Weber, W. P.; Cai, G., *Polymer* **2003,** *44*, 4149.

6. Sommer, L. H.; McLick, J., *J. Organomet. Chem.* **1975,** *101*, 171.

7. Suzuki, H.; Tokitoh, N.; Okazaki, R.; Nagase, S.; Goto, M., *J. Am. Chem. Soc.* **1998,** *120*, 11096.

8. Iwamoto, T.; Sato, K.; Ishida, S.; Kabuto, C.; Kira, M., *J. Am. Chem. Soc.* **2006,** *128*, 16914.

9. Moiseev, A. G.; Leigh, W. J., *Organometallics* **2007,** *26*, 6277.

10. Bothner-By, A. A.; Naar-Colin, C., *J. Am. Chem. Soc.* **1961,** *83* (1), 231.

11. Moiseev, A. G.; Leigh, W. J., *J. Am. Chem. Soc.* **2006,** *128*, 14442.

12. Lebedev, E. P.; Fridland, D. V.; Reikhsfel'd, V. O., *J. Gen. Chem. USSR* **1974,** *44*, 280.

13. Kostina, S. S.; Leigh, W. J., *J. Am. Chem. Soc.* **2011,** *133* (12), 4377.

14. Fink, M. J.; Kenneth, J. H.; West, R.; Michl, J., *J. Am. Chem. Soc.* **1984,** *106*, 822.

15. Fink, M. J.; DeYoung, D. J.; West, R.; Michl, J., *J. Am. Chem. Soc.* **1983,** *105* (4), 1070.

16. Sohn, H.; Tan, R. P.; Powell, D. R.; West, R., *Organometallics* **1994,** *13* (4), 1390.

17. Michalczyk, M. J.; Fink, M. J.; Haller, K. J.; West, R.; Michl, J., *Organometallics* **1986,** *5* (3), 531.

18. Levin, G.; Das, P. K.; Bilgrien, C.; Lee, C. L., *Organometallics* **1989,** *8*, 1206.

19. Arya, P.; Boyer, J.; Carre, F.; Corriu, R.; Lanneau, G.; Lapasset, J.; Perrot, M.; Priou, C., *Angew. Chem. Int. Ed. Engl.* **1989,** *28* (8), 1016.

20. Soysa, H. S. D.; Jung, I. N.; Weber, W. P., *J. Organomet. Chem.* **1979,** *171*, 177.

21. Haaf, M.; Schmiedl, A.; Schmedake, T. A.; Powell, D. R.; Millevolte, A. J.; Denk, M.; West, R., *J. Am. Chem. Soc.* **1998,** *120*, 12714.

22. Moiseev, A. G.; Leigh, W. J., *Organometallics* **2007,** *26*, 6268.

23. Bhattacharya, A., M.Sc. Thesis, McMaster University, Hamilton, ON, 2010.

24. Conlin, R. T.; Netto-Ferreira, J. C.; Zhang, S.; Scaiano, J. C., *Organometallics* **1990,** *9*, 1332.

25. Kostina, S. S.; Singh, T.; Leigh, W. J., *Organometallics* **2012,** *31* (9), 3755.

26. Hunter, E. P. L.; Lias, S. G., *J. Phys. Chem. Ref. Data* **1998,** *27* (3), 413.

27. Yamaji, M.; Hamanishi, K.; Takahashi, T.; Shizuka, H., *J. Photochem. Photobiol. A: Chem.* **1994,** *81*, 1.

28. Apeloig, Y.; Sklenak, S., *Can. J. Chem.* **2000,** *78*, 1496.

29. Suzuki, H.; Tokitoh, N.; Nagase, S.; Okazaki, R., *J. Am. Chem. Soc.* **1994,** *116*, 11578.

30. Leigh, W. J.; Bradaric, C. J.; Kerst, C.; Banisch, J.-A. H., *Organometallics* **1996,** *15* (9), 2246.

31. Leigh, W. J.; Li, X., *J. Phys. Chem. A* **2003,** *107*, 1517.

32. Bradaric, C. J.; Leigh, W. J., *Can. J. Chem.* **1997,** *75* (10), 1393.

8. Chapter 8 – O- and S- abstraction reactions by transient germylenes

8.1. Overview

The goals of this work were to investigate the kinetics and thermodynamics of the reactions of the transient germylenes $GeMe_2$ and $GePh_2$ with cyclohexene oxide (CHO) and propylene sulfide (PrS) in hexanes solution at 25 ^{o}C.

The reactions of $GeMe_2$ and $GePh_2$ with oxiranes and thiiranes were investigated using steady state and laser flash photolysis techniques. The results of the laser experiments are similar to those obtained in our studies of the reactions of germylenes with other O- and S- donors – germylene-heterocycle complexes are formed reversibly as long-lived, readily detectable transient species which decay with the concomitant formation of the corresponding digermenes. Product studies indicate that propene is formed in ca. 20% yield in the reaction of $GeMe_2$ with PrS, which is substantially lower than the yield obtained in the analogous reactions of $SiMe_2$ or $SiPh_2$ with PrS. The anticipated product of $Me_2Ge{=}S$ trimerization, $(Me_2GeS)_3$, could not be detected under the conditions of these experiments, and while several other Ge-containing products were detected by ^{1}H NMR and GC/MS spectroscopy, none of them could be identified.

8.2. Results

8.2.1. Product studies

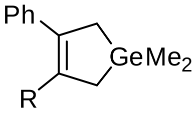

36. R = H
106. R = Me

Preliminary experiments were carried out using compound **106** as the source of $GeMe_2$ to investigate the nature of the products formed upon reaction of $GeMe_2$ with CHO or PrS. Photolyses were carried out on a 0.05 M solution of **106** in cyclohexane-d_{12} containing either CHO (0.2 M) or PrS (0.2 M) and employed Si_2Me_6 as an internal integration standard. In both experiments, however, the formation of oligomers interfered with the determination of product yields, as the apparent concentration of **106** was artificially enhanced due to significant overlap with product peaks. Nevertheless, a small amount of propene could be detected in the reaction employing PrS. In contrast, cyclohexene could not be detected as a product in the experiments with CHO as trapping agent, indicating that oxygen abstraction does not take place at room temperature in solution.

In order to measure the yield of propene formed in the reaction with PrS, **36** was employed as a source of the germylene because the vinylic hydrogen provides a good ^{1}H NMR handle for the accurate determination of the concentration of **36**. Thus, irradiation of a C_6D_{12} solution of **36** (0.047 M) containing PrS (0.07 M) and Si_2Me_6 (0.012 M) for 15 min (17% conversion of starting material) resulted in the formation of **77** (70%) and propene (20%) as the major products (eq. 8.1). The yields were determined from the relative slopes of concentration vs. time plots constructed for the reactants and products, as shown in Fig. 8.1. The plots reveal that despite roughly equal consumption of PrS and **36** in the photolysis, propene was formed in only 20% yield. This result suggests that PrS

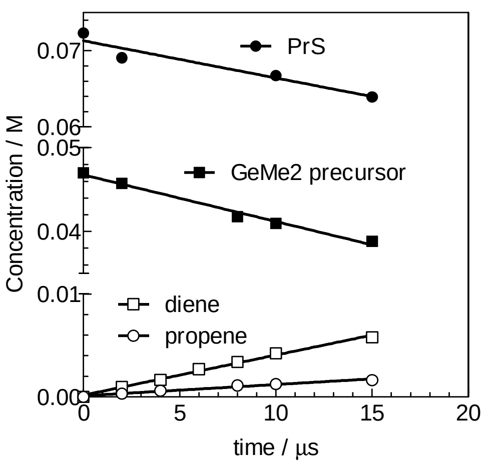

Figure 8.1. Concentration vs. time plots for 254 nm irradiation of a deoxygenated solution of **36** (0.047 M) in C_6D_{12} containing PrS (0.07 M) and Si_2Me_6 (0.012 M). The solid lines are the least squares fits of the data, the slopes of which are PrS (•), -0.0005 ± 0.0001; **36** (■), -0.00056 ± 0.00004; propene (o), 0.000109 ± 0.000009; **77** (□), 0.00039 ± 0.00001

---

either undergoes photochemical decomposition, or participates in other side reactions that do not produce propene as one of the products.

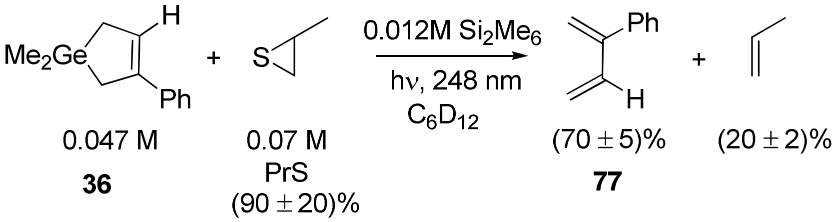

(8.1)

Analysis of the ^{1}H NMR spectra in the -0.2 – 1.2 region revealed several new products present in small quantities (Fig. 8.2). If the germanethione is the transient product of sulfur abstraction, its anticipated fate its trimerization to form **107**. In order to determine if any of the small peaks are due to **107**, an authentic sample was prepared in 60% yield by the reaction of Li_2S with Me_2GeCl_2 (see Chapter 10 for details). Spiking of the photolysis mixture with **107** showed that this compound was actually *not* formed in significant yield in the reaction (Fig. 8.3).

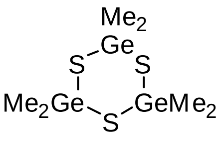

107

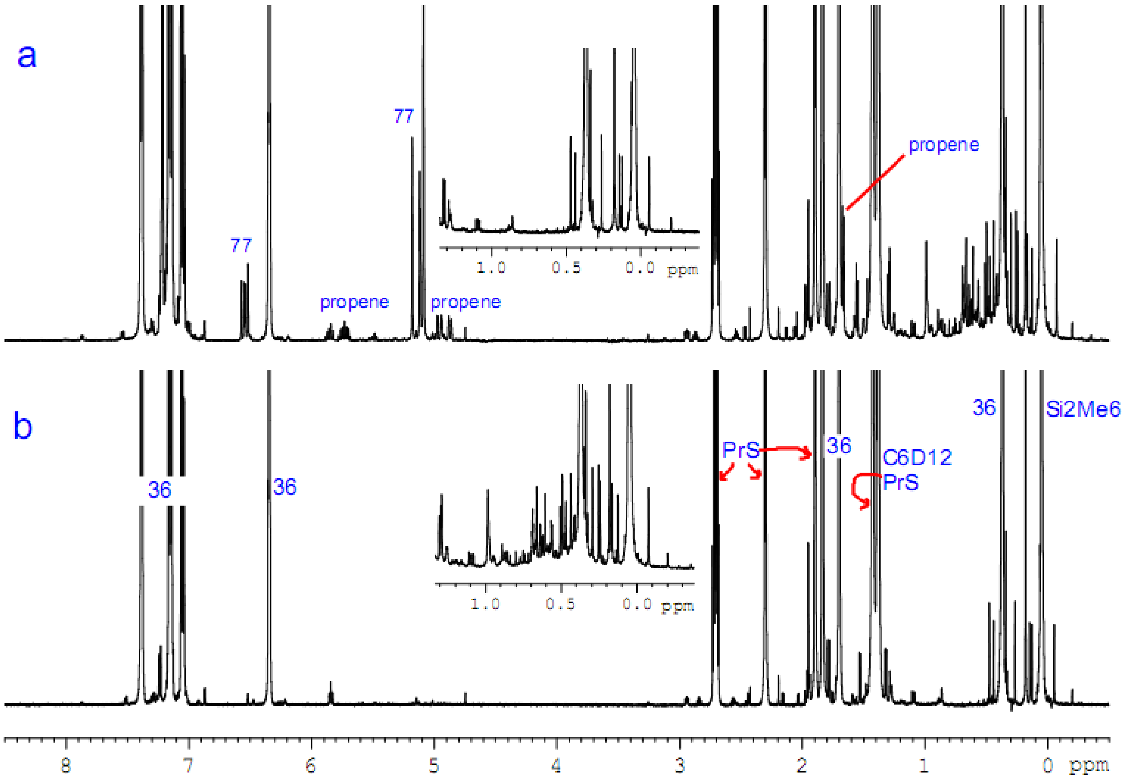

Figure 8.2. 600 MHz ^{1}H NMR spectra of the solution of Fig. 8.1 a) after 15 min of photolysis, b) before photolysis

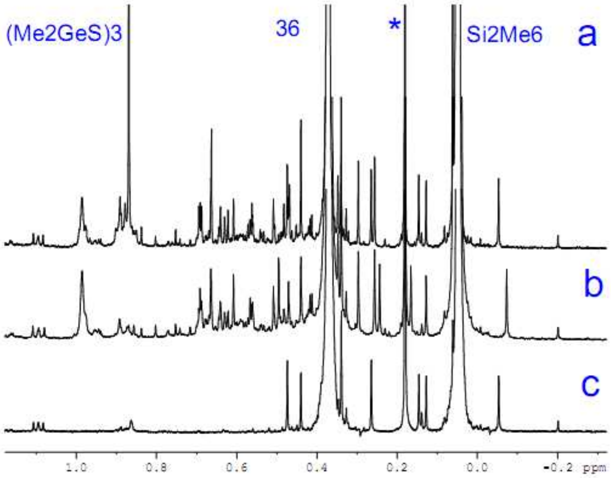

Figure 8.3. -0.2 – 1.2 ppm region of the 600MHz ^{1}H NMR spectra of the solution of Fig. 8.1 a) after 15 min of photolysis, spiked with **107**, b) after 15 min of photolysis, c) before photolysis. * - unreactive impurity.

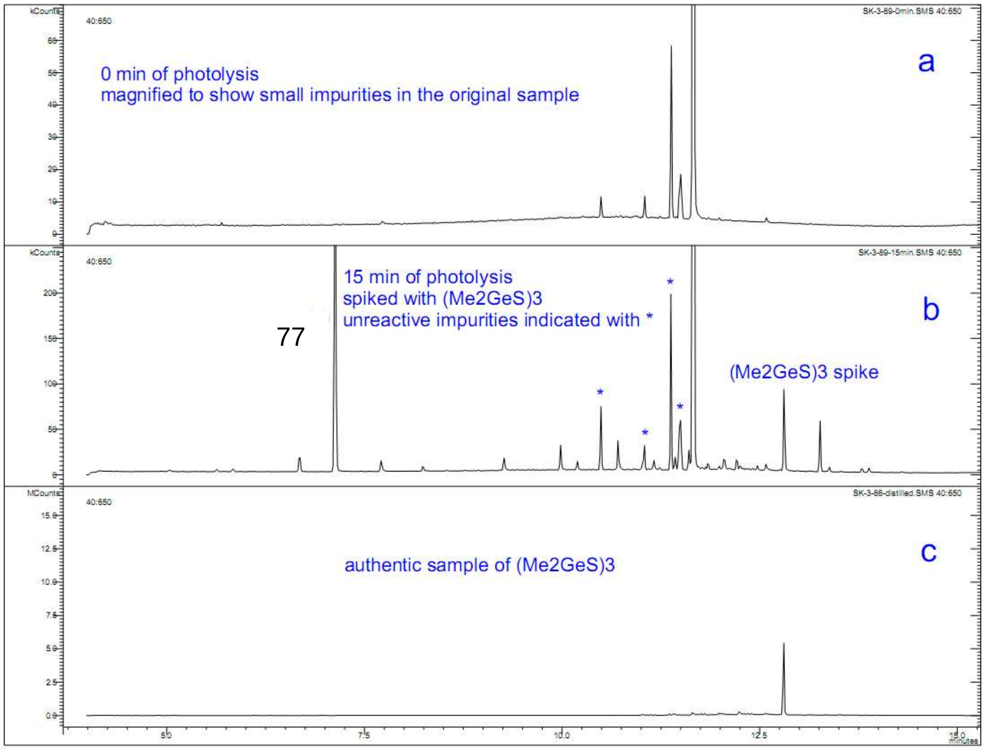

Figure 8.4. Gas chromatogram of the solution of Fig. 8.1, a) before photolysis and b) after 15 min of photolysis followed by spiking the mixture with authentic sample of **107**; c) GC of the authentic sample of **107**.

GC/MS analysis of the photolysate (Fig. 8.4 and 8.5) confirmed the formation of **77** as the major product and also showed at least 8 additional products, congruent with the results of the ^{1}H NMR analyses shown in Fig. 8.3. Unfortunately none of these compounds could be identified. Other potential products of Me_2GeS reactions could be **108** or **109**,[1] however no conclusive evidence for such structures was found in the spectroscopic data.

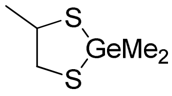

108

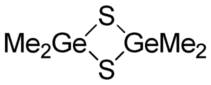

109

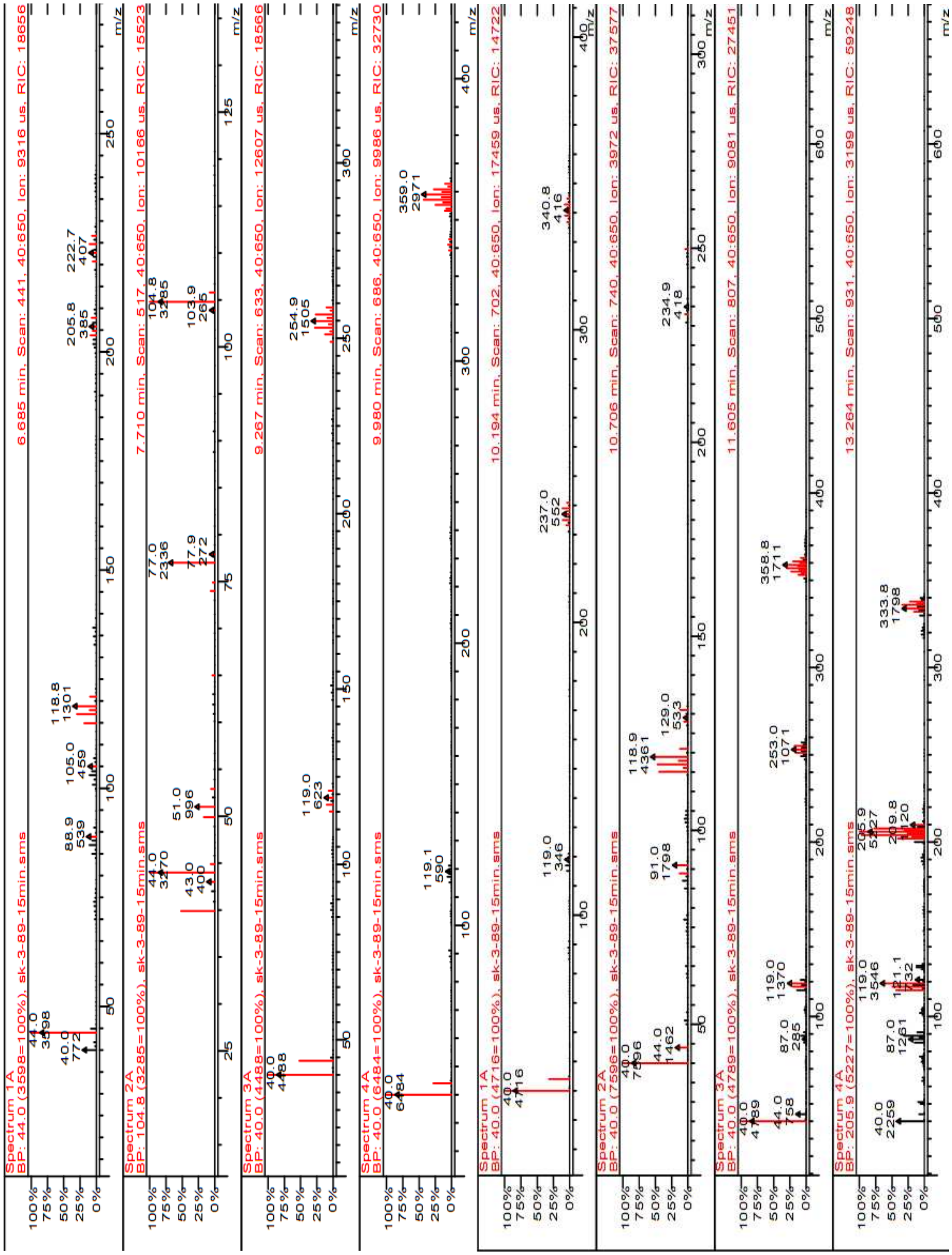

Figure 8.5. Mass spectra of the product mixture of Fig. 8.4b, elution times from the GC are indicated above each spectrum.

Based on the GC/MS spectral data, out of the eight compounds formed in this reaction all except one (2A in Fig. 8.5) contain germanium. The remaining seven all contain at least two germanium atoms and share the same fragment with m/z = 119, which is consistent with a $GeMe_3^+$ unit.

8.2.2. Kinetic and thermodynamic measurements

$GeMe_2$ (λ_{max} = 470 nm) and $GePh_2$ (λ_{max} = 500 nm) were generated by photolysis of germacyclopentene derivatives **36** and **37**.[2-4]

In the presence of submillimolar concentrations of CHO, transient decays recorded for $GeMe_2$ were bimodal, consisting of a rapid initial decay and a slowly-decaying residual absorbance. With increasing CHO concentration the initial fast decay became more rapid and the intensity of the residual absorbance was reduced. This behaviour is consistent with an equilibrium constant in the range of $1000^{-1} < K_1 < 25{,}000$ M^{-1} (see Ch. 2). The data were analysed according to the two phase decay kinetic expression of eq. 2.19 (see Ch. 2), and the faster of the two decay components were plotted against [CHO] to generate the plot shown in Fig. 8.6a. The linear least squares fit of the data according to eq. 8.2 gives a rate constant for complexation ($k_1 = (12 \pm 3) \times 10^9$ M^{-1} s^{-1}), while a plot of $\Delta A_0/\Delta A_{eq}$ vs. [CHO] gives $K_1 = 3{,}700 \pm 800$ M^{-1} from the slope of the linear regression (Fig. 8.6b).

$$k_{decay} = k_0 + k_1 [Q] \qquad (8.2)$$

$$\Delta A_0/\Delta A_{eq} = 1 + K_1[Q] \qquad (8.3)$$

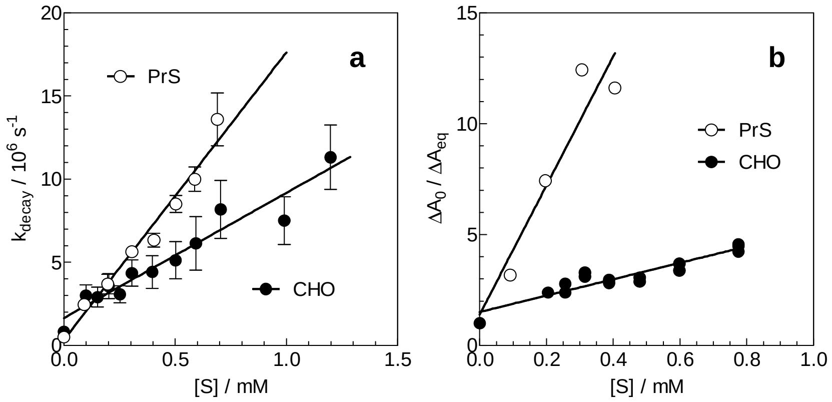

Figure 8.6. (a) Plots of k_{decay} vs [S] for the reactions of $GeMe_2$ with CHO (●) and PrS (o); the solid lines are the least squares analysis of the data to eq. 8.2. (b) Plots of $\Delta A_0/\Delta A_{eq}$ vs [S] for the reactions of $GeMe_2$ with CHO (●) and PrS (o); the solid lines are the least squares analysis of the data to eq. 8.3.

Addition of submillimolar concentrations of PrS also caused the germylene decay to become bimodal. Analysis of the data according to eq. 8.2 yielded a rate constant of k_1 = $(1.7 \pm 0.2) \times 10^{10}$ M^{-1} s^{-1}. The equilibrium constant in this case is substantially higher and is at the upper limit of our measurement (K_1 = 30,000 ± 10,000 M^{-1}). The plots used to extract the k_1 and K_1 values are shown in Fig 8.6.

Transient absorption spectra of a hexanes solution of **36** containing 50 mM CHO showed a new absorption band centered at 310 nm, which decays with second order kinetics with the concomitant formation of the digermene (Fig. 8.7a). Non-linear least squares analysis of the data according to eq. 8.4 gives $2k_{dim}/\varepsilon = (1.77 \pm 0.06) \times 10^5$ cm s^{-1} (Fig. 8.7b). The lifetime of this species was independent of CHO concentration over the 10-50 mM range. The decay characteristics and spectrum of the species is consistent with

Table 8.1. UV-vis absorption maxima and second order decay coefficients for the Lewis acid-base complexes of $GeMe_2$ and $GePh_2$ with CHO and PrS in hexanes solution at 25 ^oC.

	CHO		PrS	
	λ_{max} / nm	$2k/\varepsilon_{max}$ / 10^5 cm s^{-1}	λ_{max} / nm	$2k/\varepsilon_{max}$ / 10^5 cm s^{-1}
$GeMe_2$	320	1.77 ± 0.06[a]	310	1.49 ± 0.03
$GePh_2$	350	1.63 ± 0.02	350	3.70 ± 0.08[a]

[a] average and standard deviation of two independent determinations.

its assignment to the $GeMe_2$-CHO complex. A similar experiment with a hexanes solution of **36** containing 4.7 mM PrS afforded a transient spectrum quite similar to that recorded for **36** in the presence of 5 mM THT (see Fig. 8.8). In both cases, the second order decay of the new transient at 310 nm was accompanied by the formation of the corresponding digermene, and is consistent with an assignment to the $GeMe_2$-PrS complex. The value of $2k_{dim}/\varepsilon$ obtained from the analysis of the absorbance-time profile of the complex according to eq. 8.4 is listed in Table 8.1.

$$A = \frac{A_0}{1 + 2k_{\dim}\left(\frac{A_0}{\varepsilon l}\right)t} \qquad (8.4)$$

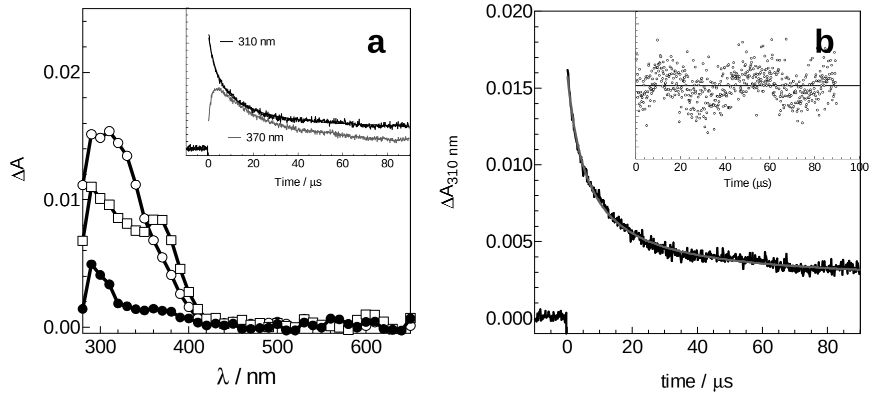

Figure 8.7. (a) Transient absorption spectra recorded 0.16-0.80 μs (○), 4.96-5.60 μs (□), and 85.76-86.40 μs (●) after the laser pulse, by laser flash photolysis of deoxygenated hexane solution of **36** with 50 mM CHO; the inset shows transient decay traces recorded at 310 nm and 370 nm. (b) decay trace from the spectrum in (a), the solid line is the non-linear least squares analysis of the data to eq. 8.4. The inset shows the residual plot from the non-linear least squares analysis.

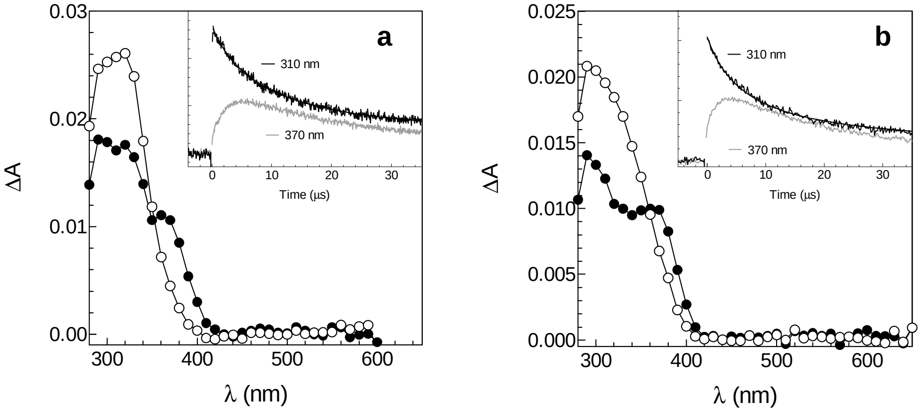

Figure 8.8. (a) Transient absorption spectra recorded 0.19-0.45 μs (○) and 5.25-5.50 μs (●) after the laser pulse, by laser flash photolysis of deoxygenated hexane solution of **36** with 5 mM THT; (b) Transient absorption spectra recorded 0.00-0.64 μs (○) and 5.60-6.24 μs (●) after the laser pulse, by laser flash photolysis of deoxygenated hexane solution of **36** with 4.7 mM PrS. The insets show transient decay traces recorded at 310 nm and 370 nm.

Table 8.2. The bimolecular rate constants, equilibrium constants and free energy values (reference state, gas phase, 1 atm, 25 ^{o}C) for complexation of $GeMe_2$ and $GePh_2$ with CHO and PrS in hexanes at 25 ^{o}C.

	k_1 / 10^9 M^{-1} s^{-1}	K_1 / M^{-1}	ΔG / kcal mol^{-1}
$GeMe_2$-CHO	12 ± 3	3700 ± 800	-3.0 ± 0.1
$GeMe_2$-PrS	17 ± 2	30000 ± 10000	-4.2 ± 0.2
$GePh_2$-CHO	8 ± 1	24000 ± 5000	-4.1 ± 0.1
$GePh_2$-PrS	8 ± 2	> 25,000	< -4.1

In the experiments with $GePh_2$ the rate coefficients for decay of the germylene data were determined using corrected absorbance-time data, recorded at 500 nm and corrected for the underlying contribution of the digermene absorption at this wavelength. [5-6]

Addition of submillimolar amounts of CHO to $GePh_2$ solution of **37** in hexanes caused the (corrected) germylene absorbance-time profiles to decay with bimodal kinetics consistent with a reversible germylene-substrate reaction. Analysis of the data according to eq. 8.2 and 8.3 afforded the rate and equilibrium constants listed in Table 8.2. When PrS was utilized in a similar fashion the germylene decayed with clean first order kinetics, consistent with an equilibrium constant above 25,000 M^{-1}. A plot of k_{decay} ($GePh_2$) vs [PrS] yielded a straight line with a slope of $(8 \pm 2) \times 10^9$ M^{-1} s^{-1} (Table 8.2). Transient absorption spectra recorded in the presence of 10 mM CHO show a new band centered at 360 nm which decays with second order kinetics with the concomitant formation of Ge_2Ph_4 (Fig. 8.9a). Another long-lived product exhibiting $\lambda_{max} \leq 280$ nm was also detected; its growth kinetics indicating that it is most likely associated with a reactive product of Ge_2Ph_4. A long-lived transient with similar characteristics was also evident in the transient spectrum of **37** in hexanes containing 5 mM PrS, although the signal was less intense (Fig. 8.9b).

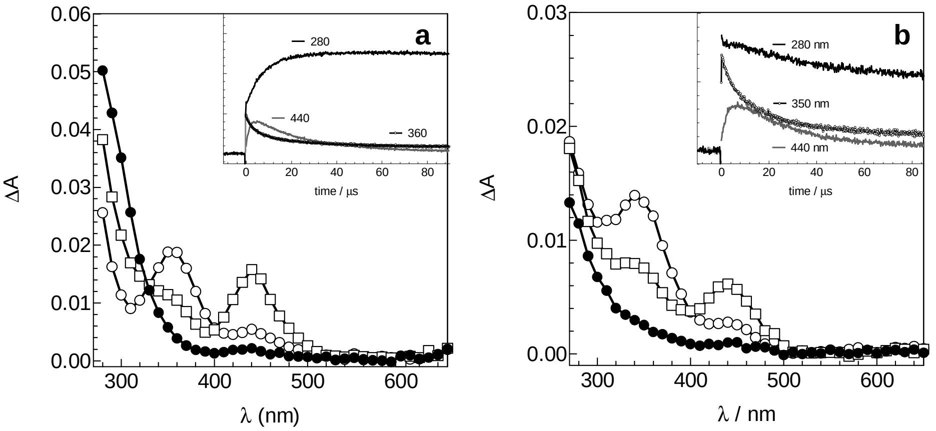

Figure 8.9. (a) Transient absorption spectra recorded 0.00-0.32 μs (○), 5.76-6.40 μs (□) and 69.60-70.24 μs (•) after the laser pulse, by laser flash photolysis of a deoxygenated hexanes solution of **37** containing 10 mM CHO. (b) Transient absorption spectra recorded 0.32-0.96 μs (○), 9.12-9.92 μs (□) and 69.92-70.72 μs (•) after the laser pulse, by laser flash photolysis of a deoxygenated hexanes solution of **37** containing 5.0 mM PrS. The insets show transient decay traces recorded at 280 nm, 350 nm and 440 nm.

There are at least two possible assignments for the long-lived transients observed at the blue edge of the spectral window in the two experiments. The first possibility is an oligomerization product of either the digermene or the germylene-donor complex, while the second (less likely) choice is the product of chalcogen abstraction by $GePh_2$. In order to test for the first possibility, the following control experiment was conducted.

The kinetics and thermodynamics of the reaction of transient germylenes with THF have been scrutinized in detail and are now well-known (Scheme 8.1, see Chapter 3 for discussion).[7-8] To investigate the behaviour of the transient at 290 nm in this reaction, the $GePh_2$-THF complex, tetraphenyldigermene and the long-lived transient were monitored at 350 nm, 440 nm and 290 nm, respectively, at THF concentrations spanning the range of 0.01 M to 0.20 M. It was found that the lifetime of the complex is independent of the substrate concentration (Fig 8.10b), while the intensity of the digermene signal decreased with increasing THF concentration (Fig 8.10c). As a result, the growth portion of the ΔA vs time plot recorded at 290 nm shortened and reached a lower maximum absorbance value (Fig 8.10a).

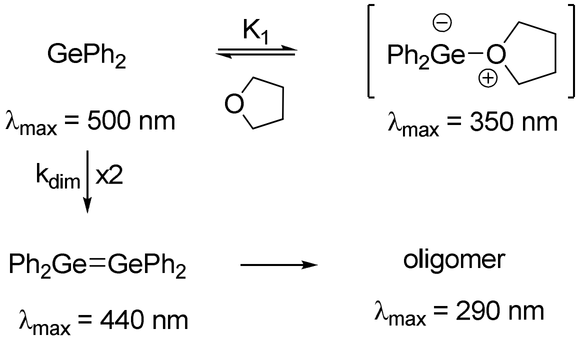

Scheme 8.1

The results of the experiment are consistent with the following mechanism – as the THF concentration is increased, there is an impurity in the THF that reacts with Ge_2Ph_4 and with the 290 nm species as well. Similar behaviour was seen in the reaction of $GePh_2$ with CHO, PrS and THT (Fig. 8.11). Therefore the species at <290 nm can only be attributed to $GePh_2$-oligomerization products, and not to the products of chalcogen abstraction.

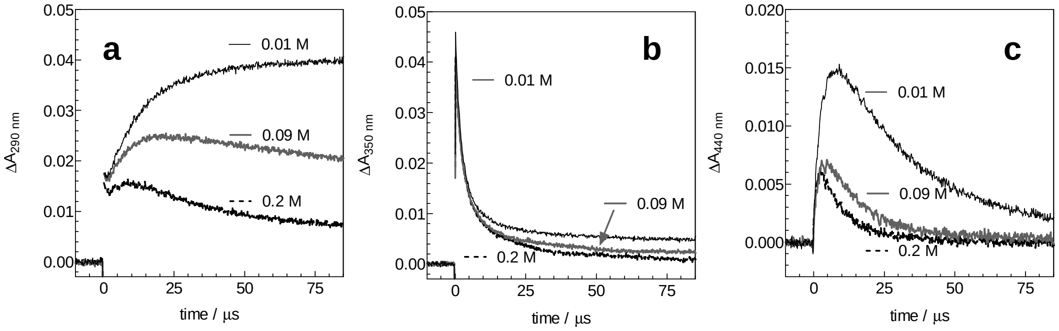

Figure 8.10. Transient decay traces recorded at (a) 290 nm, (b) 350 nm, and (c) 440 nm by laser flash photolysis of a hexanes solution of **37** in the presence of THF at various concentrations at 25 °C.

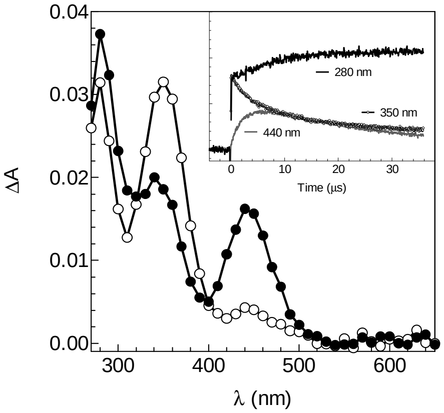

Figure 8.11. (a) Transient absorption spectra recorded 0.19-0.45 μs (○) and 6.34-6.46 μs (●) after the laser pulse, by laser flash photolysis of a deoxygenated hexane solution of **37** containing 5.5 mM THT. The inset shows transient decay traces recorded at 280 nm, 350 nm and 440 nm.

8.3. Discussion

The results of this study are consistent with oxiranes and thiiranes capturing transient germylenes in a reversible fashion to generate the GeR_2-CHO and GeR_2-PrS complexes; the complexes were detected in all four cases. The complexes decay by dimerization with the second order decay coefficients listed in Table 8.1. The spectra of the germylene-donor complexes show no systematic variation with O- to S- substitution on the substrate. The ΔG values for complexation span the range of -3.0 to -4.2 kcal mol^{-1} (Table 8.1). The formation of the GeR_2-CHO complex is 1.1 kcal mol^{-1} more favourable in the case of $GePh_2$ compared to $GeMe_2$, consistent with the higher Lewis acidity of $GePh_2$ compared to $GeMe_2$.[8] We also found that the reaction of $GeMe_2$ is more favourable with PrS by ca. 1 kcal mol^{-1} compared to that with CHO, consistent with the relative binding energies of $GeMe_2$ with non-reactive ethers and sulfides (Chapter 3).

The steady state photolysis experiments demonstrate that propene is formed in 20% yield upon the reaction of $GeMe_2$ with PrS. This implies that $GeMe_2$ abstracts sulfur from the thiirane with low efficiency. The expected product of the germanethione trimerization, $(Me_2GeS)_3$, could not be detected by either ^{1}H NMR spectroscopy or GC/MS. Instead, at least eight products were detected in small quantities, seven of which contain more than one germanium atom. In both cases no evidence could be found for the formation of either germoxetane (or germathietane), dioxagermacyclooctane (or dithiagermacyclooctane), or the products of $Me_2Ge{=}X$ insertion into the three-membered ring. Analogous products have been observed by Castel[9] and Barrau[1, 10-11] (see Section 1.4.3). No evidence of a reaction of $GePh_2$ with either CHO or PrS could be obtained.

Our results are consistent with the mechanism shown in Scheme 8.2, where the first step of the reaction of GeR_2 with oxirane or thiirane is reversible formation of an acceptor-donor complex. In contrast to the reaction with silylenes, germylenes do not abstract oxygen from CHO – this substrate reacts in an analogous fashion to THF. The ΔG values for complexation of the two germylenes with THF are 0.1-0.5 kcal mol^{-1} more favourable than those for complexation with CHO. This trend is opposite to that found in the analogous silylene-O-donor systems, although the differences are small (see Chapter 7). Sulfur abstraction, on the other hand, is a minor pathway of the decomposition of the $GeMe_2$-PrS complex, as evidenced by the steady-state photolysis results. Dimethylgermanethione was not detected as an intermediate by transient spectroscopy; its fate is also unclear from the end product analysis.

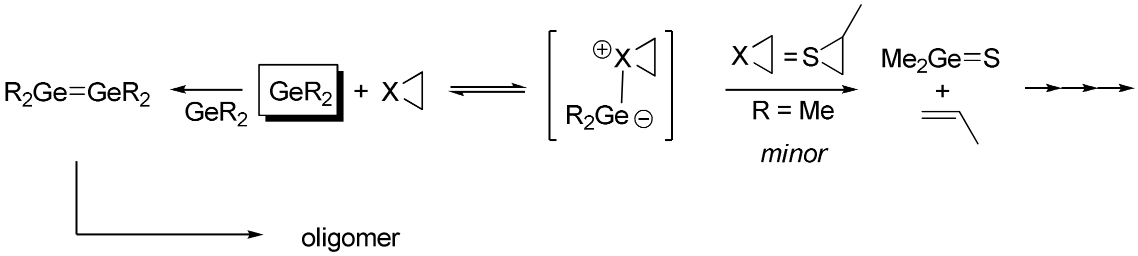

Scheme 8.2

8.4. Conclusions

The transient germylenes $GeMe_2$ and $GePh_2$ react with CHO and PrS reversibly to form the corresponding Lewis acid-base complexes, which were detected and characterized in all four cases by laser flash photolysis. Under the conditions of the kinetic experiments, the complexes decay over several microseconds with second order kinetics, to generate oligomerization products as the major mode of decay. O- and S-abstraction within the complexes is too slow to be detected by laser flash photolysis. Steady-state photolysis experiments indicate that it may occur in the case of $GeMe_2$ with PrS, albeit inefficiently.

8.5. References

1. Barrau, J.; Rima, G.; Lavayssiere, H.; Dousse, G.; Satge, J., *J. Organomet. Chem.* **1983,** *246*, 227.

2. Leigh, W. J.; Lollmahomed, F.; Harrington, C. R., *Organometallics* **2006,** *25*, 2055.

3. Leigh, W. J.; Lollmahomed, F.; Harrington, C. R.; McDonald, J. M., *Organometallics* **2006,** *25*, 5424.

4. Harrington, C. R.; Leigh, W. J.; Chan, B. K.; Gaspar, P. P.; Zhou, D., *Can. J. Chem.* **2005,** *83*, 1324.

5. Leigh, W. J.; Harrington, C. R.; Vargas-Baca, I., *J. Am. Chem. Soc.* **2004,** *126*, 16105.

6. Leigh, W. J.; Harrington, C. R., *J. Am. Chem. Soc.* **2005,** *127*, 5084.

7. Huck, L. A.; Leigh, W. J., *Organometallics* **2007,** *26*, 1339.

8. Kostina, S. S.; Singh, T.; Leigh, W. J., *Organometallics* **2012,** *31* (9), 3755.

9. Castel, A.; Riviere, P.; Satge, J.; Cazes, A., *C. R. Acad. Sci. Paris Ser. C* **1978,** *287* (Serie C), 205.

10. Barrau, J.; Bouchaut, M.; Lavayssiere, H.; Dousse, G.; Satge, J., *Helv. Chim. Acta* **1979,** *62* (1), 152.

11. Barrau, J.; Bouchaut, M.; Lavayssiere, H.; Dousse, G.; Satge, J., *J. Organomet. Chem.* **1983,** *243*, 281.

9. Chapter 9 – Summary and Contributions

In this thesis some fundamental reactions of transient silylenes ($SiMe_2$, $SiPh_2$, $SiTmp_2$ and $SiMes_2$) and germylenes ($GeMe_2$, $GePh_2$ and $GeMes_2$) have been investigated. The results demonstrate that *all* reactions presented here, whether sigma bond insertions or chalcogen abstractions, proceed via a two step mechanism beginning with a formation of a Lewis acid-base complex. Depending on the substrate, the second step could be either unimolecular (Si-O insertion and chalcogen abstraction reactions) or catalytic (O-H and N-H insertions).

When the barrier for the second step is too high for it to proceed under ambient experimental conditions the reaction stops at the complexation step. This is the case for the reactions of silylenes and germylenes with ethers, sulfides, tertiary amines and phosphines (Chapter 3), and acyclic oligosilanes (Chapter 6). One of the major contributions of this study is the classification of silylenes and germylenes as borderline soft Lewis acids, based on the correlation of calculated binding enthalpies (G4) of the MMe_2-donor complexes with Drago's E and C parameters.[1] Equilibrium constants measured for the six silylene-Et_2O and germylene-Et_2O systems (MMe_2, MPh_2 or $MMes_2$, where M = Si or Ge) led to the first experimentally-established trend in the Lewis acidities of the silylenes and germylenes, such that the Lewis acidities decrease in the order $SiPh_2 > SiMe_2 > GePh_2 > GeMe_2 > SiMes_2 > GeMes_2$. The free energies of complexation of $SiMes_2$ and $GeMes_2$ with a series of seven donors indicate that in all cases, the silylene forms the more stable complex with a given donor by ca. 1 kcal mol^{-1}.

The investigation of the reactions of $SiMe_2$ and $SiPh_2$ with alcohols (MeOL or t-BuOL, L = H or D) led to the direct detection and characterization of silylene-alcohol complexes in hexane solution.[2] The reactions were found to proceed via the initial formation of a complex, which undergoes a proton transfer to form the corresponding O-H insertion product. The complexes were detected directly in all cases as short-lived reactive intermediates, whose lifetimes are dependent on alcohol concentration. Isotopic substitution of the O-H groups in the alcohols allowed the measurement of kinetic isotope effects for both mechanistic steps. While D-for-H substitution had no effect on the rate constant for complexation, the second step was significantly slowed, consistent with a mechanism involving catalysis by a second molecule of alcohol to assist the H-migration process. These results can be compared to the analogous reaction involving germylenes, where both the $GePh_2$-MeOH and $GeMe_2$-MeOH complexes could be detected in neat methanol solutions[3] indicating that the barrier for the catalytic H-migration is significantly higher than in the silylene systems.

The N-H insertion reactions of transient silylenes with amines were also investigated.[4] The results indicate that the reaction proceeds in an analogous fashion to the O-H insertion reactions of silylenes with alcohols. The rate constants for complexation of $SiMe_2$ and $SiPh_2$ with amines (n-$BuNH_2$, Et_2NH and Et_3N) fall in the $10^9 – 2 \times 10^{10}$ M^{-1} s^{-1} range and decrease with increasing substitution on the amine. The catalytic rate constants are at least four orders of magnitude slower than those for the corresponding process in the silylene-alcohol systems.

Another contribution of this study stems from a detailed investigation of the reactions of silylenes with siloxanes and MeOTMS. The results indicate that the Si-O insertion reaction proceeds via initial complexation followed by unimolecular [1,2] silyl shift. Depending on the relative magnitude of the rate constants, the observed effect on the lifetimes of the silylenes and the silylene-donor complexes is different in each case. The experimental results are supplemented by kinetic simulations, which provide additional support for the two-step mechanism.

A significant body of work presented in this thesis focused on O- and S- abstraction reactions by silylenes and germylenes with oxiranes and thiiranes. In all cases, the reaction begins with complexation, followed by chalcogen abstraction within the complex. In the $SiMe_2$ and $SiPh_2$-oxirane and –thiirane systems, the chalcogen abstraction process proceeds in ca. 50% yield,[5] while the $GeMe_2$-PrS system yields propene in ca. 30% yield. Introduction of steric bulk on the silicon in the $SiMes_2$ destabilises the complexes with oxiranes, rendering the rate constants for complexation indeterminable due to unfavourable equilibrium. Attempts to trap the $Mes_2Si{=}O$ with MeOH in the reaction of $SiMes_2$ with CHO resulted instead in the formation of compound **99**, consistent with the trapping of the intermediary silanone-CHO complex with MeOH.

9.1. References

1. Kostina, S. S.; Singh, T.; Leigh, W. J., *Organometallics* **2012,** *31* (9), 3755.
2. Leigh, W. J.; Kostina, S. S.; Bhattacharya, A.; Moiseev, A. G., *Organometallics* **2010,** *29* (3), 662.
3. Lollmahomed, F.; Huck, L. A.; Harrington, C. R.; Chitnis, S. S.; Leigh, W. J., *Organometallics* **2009,** *28* (5), 1484.
4. Kostina, S. S.; Singh, T.; Leigh, W. J., *J. Phys. Org. Chem.* **2011,** *24*, 937.
5. Kostina, S. S.; Leigh, W. J., *J. Am. Chem. Soc.* **2011,** *133* (12), 4377.

10. Chapter 10 – Future Work

The knowledge of the reactions of tetrellylenes with oxiranes and thiiranes can be expanded quite substantially by exploring substituent effects either on the tetrel center or the substrate. One species of interest is bis(2,4-dimethylphenyl)silylene **111**, the proposed photochemical precursor of which is **110** (eq. 10.1). In the reactions of $SiMes_2$ with thiiranes, the identification of transient species formed along the reaction pathway was not possible; one hypothesis is that the ortho-methyl groups interact with the Si=S moiety. Therefore the effect of only one ortho-methyl group on the aryl ring is of interest, and may allow the identification of the new transient in the $SiMes_2$-PrS system.

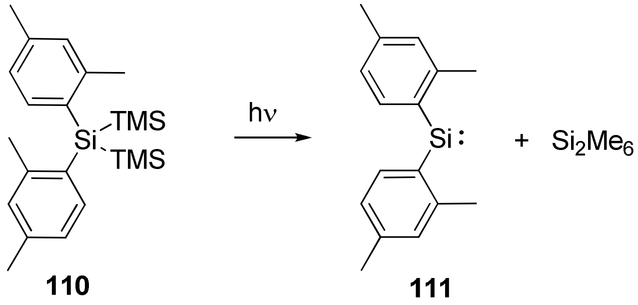

(10.1)

Our group has already started to examine the reactions of $SiMe_2$ and $SiPh_2$ with various oxiranes such as cis- and trans-2-butene oxide, 2-vinyloxirane, 2-methyl-2-vinyloxirane, 1,2-epoxy-5-hexene, and 2,2-dimethyloxirane, with the goals of obtaining experimental evidence for the biradical mechanism in the oxygen abstraction reaction. Determination of equilibrium constants for the two less-sterically hindered silylenes is not possible. However, $SiMes_2$ is expected to react with these series of oxiranes with small, measurable equilibrium constants (see Chapter 7), which will allow the substituent effect on the reaction thermodynamics to be explored.

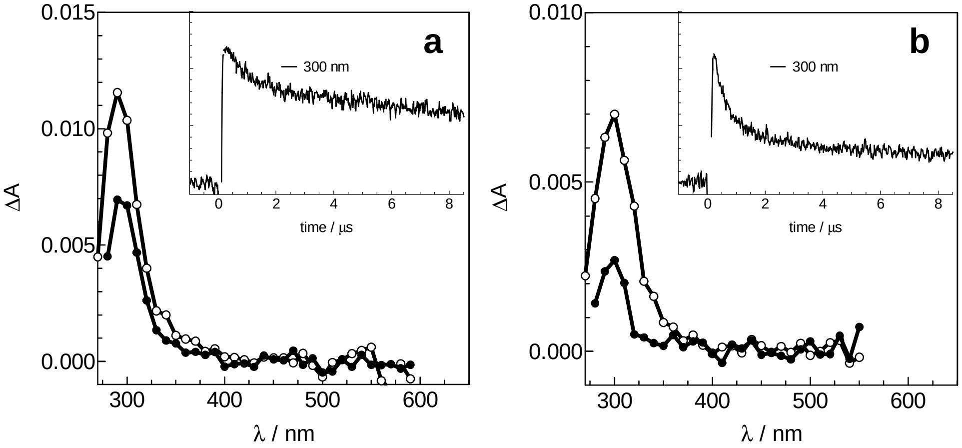

Figure 10.1. Transient absorption spectra from laser flash photolysis of a hexane solution of **36** containing (a) 2.0 mM 2-vinyloxirane, and (b) 4.9 mM 2-methyl-2-vinyloxirane, recorded 0.03-0.10 μs (o), and 6.99-7.07 μs (●) after the laser pulse; the insets show transient decay profiles recorded at 300 nm.

The transient germylenes $GeMe_2$ and $GePh_2$ were shown to be unreactive toward CHO under the conditions of our experiments (Chapter 8). Preliminary experiments employing $GeMe_2$ with 2-vinyloxirane and 2-methyl-2-vinyloxirane indicate that the vinyl group on the oxirane induces further reaction of the initially formed complexes. The transient absorption spectra shown in Fig. 10.1 demonstrate that the lifetimes of the $GeMe_2$-2-vinyloxirane and $GeMe_2$-2-methyl-2-vinyloxirane complexes are significantly shorter than the corresponding $GeMe_2$-PrO and $GeMe_2$-CHO complexes, and that the formation of Ge_2Me_4 is suppressed. A reasonable expectation based on the analogous silylene reactions is the formation of germaoxetane **112** (eq. 10.2), the activation barrier for the formation of which may be lowered by the vinyl group.

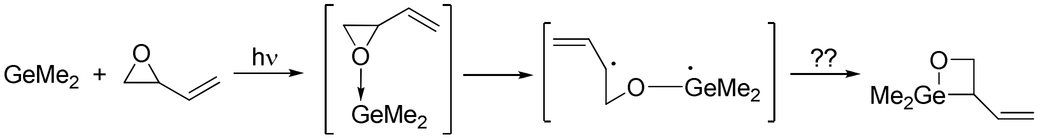

112

(10.2)

While dimethylsulfoxide (DMSO) was reported to be unreactive toward $SiMe_2$ at cryogenic temperatures,[1] it is readily reduced to dimethylsulfide (DMS) by $SiMe_2$ in solution at room temperature to afford products consistent with the formation of $Me_2Si=O$ as the primary product.[2-4] The authors suggested the O-transfer to occur via the silylene-sulfoxide Lewis acid-base complex (eq. 10.3).[3] Competition experiments with other dialkyl sulfoxides established a variation in relative rate constant spanning roughly a factor of 13, decreasing in the order tetrahydrothiophene oxide > Et_2SO > Me_2SO > i-Pr_2SO > t-Bu_2SO.[3]

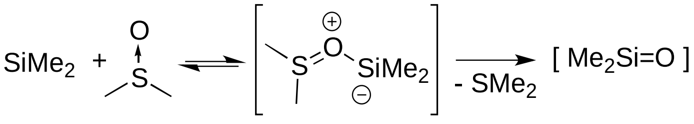

(10.3)

We attempted to detect the intermediates along the path of the reaction of $SiPh_2$ with dibutylsulfoxide (DBSF); the preliminary data are shown in Fig. 10.2. The rate constant for the reaction of $SiPh_2$ with DBSF was found to be $k_1 = (8.3 \pm 0.5) \times 10^9$ M^{-1} s^{-1} from the plot of Fig. 10.2a. Transient absorption spectra show the presence of a new short-lived transient, the spectral characteristics of which do not resemble those of typical $SiPh_2$-O-donor complexes. In order to gain mechanistic insight into the O-abstraction from sulfoxides, these studies need to be extended to those by $SiMe_2$ and $SiMes_2$. As a general interest of our group, analogous reactions by germylenes would be a desirable extension of this work.

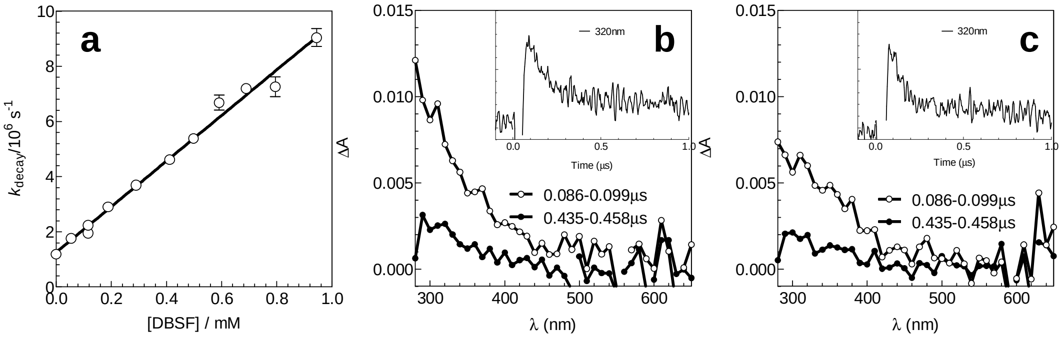

Figure 10.2. (a) A plot of k_{decay} vs [DBSF] for the reaction of $SiPh_2$ with DBSF; (b) Transient absorption spectra of a deoxygenated hexanes solution of **44a** containing 4.8 mM DBSF; (c) Transient absorption spectra of a deoxygenated hexanes solution of **44a** containing 10 mM DBSF. The insets show transient decay trances recorded at 320 nm.

A relatively unexplored sigma-bond insertion reaction by transient silylenes is that into the S-H bonds of thiols. In contrast to the potent reactivity of transient silylenes toward O-H insertions, photochemically generated $SiMe_2$ evidently fails to react with alkanethiols in diethyl ether[5] or hexane[6] solution. However, thiols can be expected to complex with silylenes at least as strongly as alcohols and are stronger Bronsted acids as well; theory predicts that (unimolecular) S-H insertion within the SiH_2-H_2S complex should be more facile than the corresponding process in the SiH_2-H_2O complex, with the overall activation barrier of only 5 kcal mol^{-1}.[7] On the other hand, $SiMe_2$ does react via S-H insertion with trialkoxysilanethiols at ambient temperatures in solution,[6] and Driess's stable N-heterocyclic silylene **112** reportedly reacts smoothly with H_2S to generate the isolable silathioformamide derivative **113** (eq. 10.4).[8] A long-term goal of our group would be to investigate the S-H insertion reactions by transient silylenes and answer the following questions: do simple alkanethiols react with transient silylenes in solution? How fast are these reactions? Can the intermediate complexes be detected and characterized? Does the insertion reaction occur in hydrocarbon solvents? How do these reactions compare to the analogous O-H and N-H insertion reactions by silylenes?

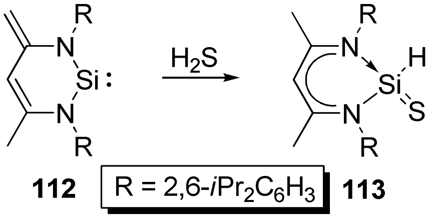

(10.4)

Trimethylsilyl substitution at silylene is a desirable future direction in our group. Initial studies focused on the reactivity of SiPh(TMS) in hexane solution[9] showed that the study of this silylene is difficult because the long-wavelength absorption band is too weak to be detected in solution, while the short-wavelength band overlaps with absorptions due to other transients. However, the more sterically bulky silylene SiMes(TMS), has been shown to exhibit absorption bands at 368 nm and 776 nm[10-11] in 3-methylpentane matrix at 77-78 K. While the band at 776 nm is too far to the blue to be detectable by our system, the band at 368 nm is in an advantageous spectral range to allow kinetic and thermodynamic studies to be performed.

10.1. References

1. Arrington, C. A.; West, R.; Michl, J., *J. Am. Chem. Soc.* **1983,** *105*, 6176.

2. Soysa, H. S. D.; Okinoshima, H.; Weber, W. P., *J. Organomet. Chem.* **1977,** *133*, C17.

3. Alnaimi, I. S.; Weber, W. P., *J. Organomet. Chem.* **1983,** *241*, 171.

4. Madesclaire, M., *Tetrahedron* **1988,** *44* (21), 6537.

5. Gu, T. Y.; Weber, W. P., *J. Organomet. Chem.* **1980,** *195* (1), 29.

6. Konieczny, S.; Wrzesień, K.; Wojnowski, W., *J. Organomet. Chem.* **1993,** *446* (1–2), 73.

7. Raghavachari, K.; Chandrasekhar, J.; Gordon, M. S.; Dykema, K., *J. Am. Chem. Soc.* **1984,** *106* (20), 5853.

8. Meltzer, A.; Inoue, S.; Präsang, C.; Driess, M., *J. Am. Chem. Soc.* **2010,** *132* (9), 3038.

9. Leigh, W. J.; Moiseev, A. G.; Coulais, E.; Lollmahomed, F.; Askari, M. S., *Can. J. Chem.* **2008,** *86* (12), 1105.

10. Michalczyk, M. J.; Fink, M. J.; De Young, D. J.; Carlson, C. W.; Welsh, K. M.; West, R., *Silicon, Germanium, Tin and Lead Compounds* **1986,** *9*, 75.

11. Bott, S. G.; Marshall, P.; Wagenseller, P. E.; Wang, Y.; Conlin, R. T., *J. Organomet. Chem.* **1995,** *499* (1–2), 11.

11. Chapter 11 – Experimental

11.1. General

^{1}H and ^{13}C NMR spectra were recorded on Bruker AV200, AV500 or AV600 spectrometers in deuterated chloroform or cyclohexane-d_{12} and were referenced to the residual solvent proton and ^{13}C signals, respectively, while ^{29}Si spectra were recorded on either the AV500 or AV600 using the HMBC pulse sequence and were referenced to an external solution of tetramethylsilane or (internal) bis(trimethylsilyl)methane (^{29}Si δ 0.16, ^{1}H δ -0.27 (s, 2H), 0.028 (s, 18H)). Gas chromatography/mass spectrometry (GC/MS) analyses were carried out on a Varian Saturn 2200 GC/MS/MS system equipped with a VF-5 ms capillary column (30 m × 0.25 mm; 0.25 μm; Varian, Inc.). High-resolution electron impact mass spectra and exact masses were determined on a Micromass TofSpec 2E mass spectrometer using electron impact ionization (25 eV).

Dodecamethylcyclohexasilane (**43**; Sigma-Aldrich) was dried under high vacuum before use. 1,1,3,3-Tetramethyl-2,2-diphenyl-1,2,3-trisilacyclohexane (**44a**) and 2,2-diphenyl-1,1,1,3,3,3-hexamethyltrisilane (**60**) were synthesized as reported previously.[1-2] They were purified by column chromatography on silica gel with hexanes as eluant, followed by recrystallization from methanol (m.p. = 50.4-50.8 ^{o}C (**44a**), m.p. ≈16 ^{o}C (**60**)) . The purities of the compounds were determined by GC/MS analysis and ^{1}H NMR spectroscopy and found to be >97% pure in each case.

Hexamethylcyclotrisiloxane (D_3) and octamethylcyclotetrasiloxane (D_4) were purchased from Sigma-Aldrich, D_3 was recrystallized from hexanes and dried under mild vacuum prior to use. D_4 was distilled by simple distillation. Propylene sulfide (PrS), cyclohexene sulfide (CHS, ~85%) and tetrahydrothiophene (THT, 99%) were obtained from Sigma-Aldrich and purified by bulb to bulb distillation from anhydrous sodium sulfate.[3] Cyclohexene oxide (CHO) and propylene oxide (PrO) were purchased from Sigma-Aldrich and purified by distillation from CaH_2. n-Butylamine ($nBuNH_2$), diethylamine (Et_2NH, ≥99.5%), and triethylamine (Et_3N, ≥ 99%) (Sigma-Aldrich) were refluxed over solid NaOH for 12 h and distilled under nitrogen. Triethylphosphine (Et_3P, 99% Sigma-Aldrich) was distilled under argon prior to use, while tricyclohexylphosphine (Cy_3P, ≥94% Sigma-Aldrich) was recrystallized from hexane; all manipulations of the phosphines were carried out in a glovebox under a dry argon atmosphere, purity was checked by ^{31}P NMR spectroscopy. Methanol (MeOH, Sigma-Aldrich) was refluxed over sodium and distilled. Bis(trimethylsilyl)methane (Sigma-Aldrich) was refluxed for 24 h over CaH_2 and distilled.

Dichlorodiphenylsilane (Gelest), 30% Lithium dispersion in mineral oil (Sigma-Aldrich), and elemental sulfur (Cerac) were used without further purification. Tetrahydrofuran (THF, Caledon Reagent) was refluxed over calcium hydride for two hours, distilled into a flask containing sodium and refluxed further for several days, and then finally distilled under nitrogen. Hexanes (EMD OmniSolv) and Et_2O (Caledon Reagent) were dried by passage through activated alumina under nitrogen using a Solv-Tek solvent purification system (Solv-Tek, Inc). Cyclohexane (Caledon Reagent) was refluxed over sodium for several days and distilled immediately prior to use.

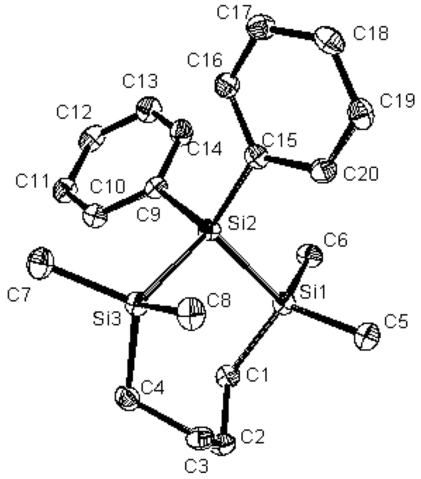

Figure 11.1. ORTEP drawing and labeling scheme of **65a.** Thermal ellipsoids are drawn at 30% probability level. Hydrogen atoms are omitted for clarity.

11.2. Crystallographic data for trisilanes

Single crystals of 2,2-diphenyl-1,1,3,3-tetramethyl-1,2,3-trisilacycloheptane (**65a**) suitable for crystallography were obtained by recrystallization from methanol at -22 °C for a period of one week. Compound **65a** crystallizes in the monoclinic space group $P2_1/c$; the ORTEP diagram is shown in Fig. 11.1. The branching $SiMe_2$ units are linked by a tetramethylene chain, resulting in a seven-membered carbosilane ring with a chair conformation. The two phenyl rings attached to Si2 exhibit a 56° twist relative to each other.

Single crystals of **44a** suitable for crystallography were obtained by slowly cooling a saturated methanol solution from room temperature to -78 °C (^{i}PrOH / solid CO_2). Compound **44a** crystallizes in the tetragonal space group $P4_2/n$ with the six-membered carbosilane ring adopting a chair conformation. The reduction in ring size compared to **65a** introduces greater ring strain which is evident by a reduced SiSiSi angle of 101°. As a result, the steric hindrance of the methyl substituents (C4-C7) on the phenyl rings is relieved. The crystal structure displays two phenyl rings twisted roughly orthogonal to

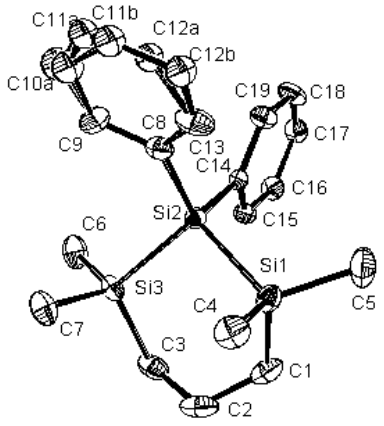

Figure 11.2. ORTEP drawing and labeling scheme of **44a.** Thermal ellipsoids are drawn at 30% probability level. Hydrogen atoms are omitted for clarity.

each other. The ring in the equatorial position shows disorder in the thermal motion as it is less sterically constrained than the ring in the axial position (Fig. 11.2).

Single crystals of **65a** suitable for X-ray crystallographic analysis were obtained by recrystallization from methanol at -22 °C over a period of two weeks. Figure 11.3 shows the ORTEP drawings (molecules 1 and 2) of the trisilane. Compound **65a** crystallizes in the triclinic space group $P\bar{1}$ with two unique molecules in the asymmetric unit. The shortest intermolecular distance is between two CH_3 groups (234 pm). Crystal data and structure refinement for the three trisilanes are summarized in Table 11.1.

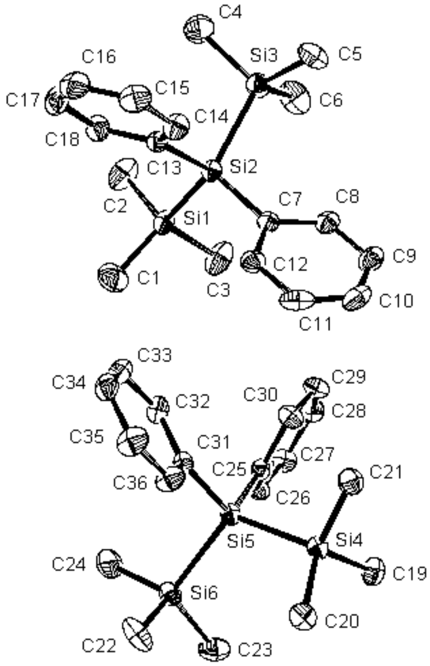

Figure 11.3. ORTEP drawing and labeling scheme for **65a** (molecule 1 – top, molecule 2 – bottom). Thermal ellipsoids are drawn at 30% probability level. Hydrogen atoms are omitted for clarity.

Table 11.1. Crystal data and structure refinement for trisilanes **44a**, **60** and **65a**

	65a	**44a**	**60**
Empirical formula	$C_{20}H_{30}Si_3$	$C_{19}H_{28}Si_3$	$C_{18}H_{28}Si_3$
FW, g/mol	354.71	340.68	328.67
Temp, K	173(2)	173(2)	173(2)
Wavelength, Å	0.71073	0.71073	0.71073
Cryst. syst.	Monoclinic	Tetragonal	Triclinic
Space group	$P2_1/c$	$P4_2/n$	$P\bar{1}$
Unit cell dimens.			
a (Å)	16.156(4)	19.263(3)	9.0570(10)
b (Å)	8.316(2)	19.263	9.8744(11)
c (Å)	17.347(5)	11.2057(18)	26.075(3)
α	90°	90°	91.233(2)°
β	115.522(5)°	90°	92.179(2)°
γ	90°	90°	114.698(2)°
Z	4	8	4
Volume, Å^3	2103.3(10)	4157.8(9)	2115.3(4)

Density (calc), Mg/m^3	1.120	1.088	1.032
Absorption coef., mm^{-1}	0.224	0.224	0.218
F(000)	768	1472	712
Crystal size, mm^3	0.40 × 0.20 ×0.03	0.50 × 0.35 × 0.03	0.42 × 0.22 × 0.04
θ range for data collection	2.52 to 28.30°.	1.50 to 28.49°.	2.27 to 25.00°.
Index ranges	$-21\le h\le 9$ $-10\le k\le 11$ $-21\le l\le 23$	$-25\le h\le 25$ $-25\le k\le 25$ $-8\le l\le 15$	$-10\le h\le 10$ $-11\le k\le 5$ $-30\le l\le 30$
Reflections collected	26179	54736	19542
Independent reflections	5194 [R(int) = 0.0981]	5240 [R(int) = 0.1168]	7297 [R(int) = 0.0549]
Completeness to θ = 28.30°	99.4 %	99.6 %	97.9 %
Absorption correction	None	None	None
Max. and min. transmission	0.9933 and 0.9157	0.9933 and 0.8961	0.9913 and 0.9139
Refinement method	Full-matrix least-squares on F^2	Full-matrix least-squares on F^2	Full-matrix least-squares on F^2
Data / restraints / param.	5194 / 0 / 328	5240 / 0 / 296	7297 / 0 / 603
Goodness-of-fit on F^2	0.983	1.016	0.987
Final R indices [$I>2\sigma(I)$]	R1 = 0.0538 wR2 = 0.1143	R1 = 0.0530 wR2 = 0.1117	R1 = 0.0483 wR2 = 0.0958
R indices (all data)	R1 = 0.1056 wR2 = 0.1361	R1 = 0.1136 wR2 = 0.1346	R1 = 0.0959 wR2 = 0.1160
Largest diff. peak and hole, e Å^{-3}	0.507 and -0.341	0.326 and -0.255	0.341 and -0.223

11.3. Laser flash photolysis

Laser flash photolysis experiments were carried out using a Lambda Physik Compex 120 excimer laser filled with a F_2/Kr/Ne mixture (excitation wavelength - 248 nm, 25 ns, 90-120 mJ/pulse) and a Luzchem Research mLFP-111 laser flash photolysis system. The solutions were prepared in deoxygenated anhydrous hexanes such that the absorbance at the excitation wavelength (248 nm) was between 0.7 and 0.9. The solutions were flowed rapidly through a 7 × 7 mm Suprasil flow cell connected to a calibrated 100 mL or 250 mL reservoir, which contained a glass frit to allow bubbling of argon gas through the solution for 40 min prior to and throughout the experiment. The flow cell was connected to a Masterflex^{TM} 77390 peristaltic pump fitted with Teflon tubing (Cole-Parmer Instrument Co.) which draws the solution through the cell at a constant rate of 2-2.5mL/min. Solutions of substrates of known concentrations were added directly to the reservoir using glass syringes. The Et_3P and Cy_3P stock solutions were prepared in a glovebox in volumetric flasks, transferred to a 25 mL Schlenk bomb, and attached to a Schlenk line under a dry Ar atmosphere. The stopcock on the bomb was replaced with a rubber septum, and the solution was then withdrawn using a 1 or 2.5 mL gastight syringe, which was inserted through the septum on the reservoir containing the precursor solution to allow the addition of the desired amounts of the substrate to the reservoir solution. The syringe was left attached to the reservoir until the end of the experiment to avoid contact with air and moisture.

Transient absorbance-time profiles were recorded by signal averaging of data obtained from 10-40 individual laser shots. Rate constants were calculated by linear least-squares analysis of decay rate constant-concentration data. Errors in the rate constants are quoted as twice the standard deviation from the linear least squares analyses (unless noted otherwise), which were carried out using the Prism 5.0 software package (GraphPad Software, Inc).

11.4. Steady-state photolysis

In a typical steady-state photolysis experiment, a solution of non-volatile reagents in 1 mL C_6D_{12} was placed in a quartz NMR tube, sealed with a rubber septum and degassed with dry argon for 5 min. Volatile reagents were then added as the neat liquids using a glass syringe. The solution was then photolyzed in a Rayonet photochemical reactor

(Southern New England Ultraviolet Co.) equipped with two RPP-2537 lamps and a merry-go-round apparatus, monitored periodically by ^{1}H NMR spectroscopy and GC/MS. The products were identified based on the following spectroscopic data:

$Ph_2Si(OMe)SH$ (96):

MS *m/z* M^+ 246.0527 (15), 213.0500 (100), 183.0495 (60), 181.0434 (8), 136.9829 (3), 105.0132 (2), 77.0351 (1)

^{13}C (δ in C_6D_{12}) (obtained from HSQC and HMBC data): 50, 134.8, 135, 131, 128.5

^{1}H (δ in C_6D_{12}): 7.25 (multiplet, 6H, m,p-Ph), 7.63 (dt, 4H, o-Ph), 3.59 (s, 3H, MeO), no SH

^{29}Si (δ in C_6D_{12}): -4.7

Diphenylsilanol (84),[4]

^{1}H NMR δ 7.57 (d, ^3J = 7.38 Hz, 4H), 5.47 (s, 1H), (the expected 6H multiplet at ca. 7.2 ppm is obscured by the resonances due to **2**).

Tetraphenyldisiloxane (85),[4-5]

^{1}H NMR, δ 7.47 (d, ^3J = 7.56 Hz, 8H), 7.20 (m, 12H), 5.58 (s, 2H)

^{29}Si NMR δ -19.2 ($^1J_{Si\text{-}H}$ = 219.6 Hz).

***N,N*-diethyl-1,1-diphenylsilanamine (83)**,[6]

^{1}H NMR, δ 7.53 (d, ^3J = 7.44 Hz, 4H), 7.25 (m, 6H), 5.30 (s, 1H), 2.94 (q, 4H, ^3J = 7.0), 0.67 (t, 6H, ^3J = 7.0),

^{29}Si NMR δ -14.0 ($^1J_{Si\text{-}H}$ = 205 Hz).

Methoxydiphenylsilane (71),[1]

^{1}H NMR, δ 7.54 (dd, ^3J = 1.38, ^2J = 7.86), 7.25 (m, 6H), 5.36 (s, 1H), 3.52 (s, 3H),

^{29}Si NMR δ -9.7 ($^1J_{Si\text{-}H}$ = 212 Hz).

11.5. Synthesis

11.5.1. $(Ph_2SiS)_3$ and $(Ph_2SiS)_2$

1,1,3,3-Tetraphenylcyclodisilthiane ($(Ph_2SiS)_2$, **94**) was prepared via a reported procedure[7] and purified by column chromatography on silica gel. The silica column was packed using dichloromethane as eluent, which was gradually changed to ethyl acetate (Rf = 0.7 in ethyl acetate) throughout the course of the purification, the solvent was removed under vacuum to afford a white powder (m.p. = 163-165 ^{o}C; lit[7]= 163-165 ^{o}C). The ^{1}H NMR (δ in $CDCl_3$, 7.79 (m, 4H), 7.48 (m, 2H), 7.43 (m, 4H)) and ^{29}Si NMR (δ in $CDCl_3$, -3.7) spectra were consistent with those previously reported. [7-8]

Compound $(Ph_2SiS)_3$ was prepared by a modification of the reported procedures.[8-9] Li_2S was prepared by treating lithium (0.94 g of a 30% dispersion in mineral oil; 60 mmol) with elemental sulfur (0.768 g, 30 mmol) in dry THF (10 mL) under N_2. Refluxing for 12 hrs yielded a black solution with a yellow layer on top. Dichlorodiphenylsilane (6.1 mL, 29 mmol) was added in THF (5 mL) through an addition funnel over 30 min at 0^{o}C. A tan suspension was formed after the addition was complete. THF was removed under vacuum and replaced with dry benzene, and the resulting precipitated lithium salts were filtered by gravity filtration to afford a brown filtrate. The solvent was removed under vacuum to afford a sticky brown solid, which was re-dissolved in 6:1 hexane:benzene to afford a yellow solution containing a brown solid suspension. The solution was filtered again to obtain a yellow filtrate, and hexane was then added dropwise until a crystalline precipitate appeared. The precipitate was collected by gravity filtration to yield the desired product as light yellow crystals (2 g, 9.7

mmol, 32%, m.p. = 182-183 °C, lit[9] = 183-184 °C). The ^{1}H NMR (δ in $CDCl_3$, 7.52 (m, 4H), 7.32 (m, 2H), 7.20 (m, 4H)) and ^{29}Si NMR (δ in $CDCl_3$, 4.3) spectra were consistent with those previously reported.[8]

11.5.2. $(Me_2GeS)_3$

Compound $(Me_2GeS)_3$ was prepared by a similar procedure to that described above for the preparation of $(Ph_2SiS)_3$. Tetrahydrofuran (THF) was distilled from $LiAlH_4$ immediately prior to use. To a dark brown solution of freshly prepared Li_2S (5.8 mmol, 0.267 g) in THF (ca. 3 mL) was added a solution of Me_2GeCl_2 (5.8 mmol, 1.01 g) in THF (2.5 mL) dropwise via a plastic syringe. The resulting mixture was dark brown with no visible change throughout 4 days of stirring at room temperature. The solvent was removed under high vacuum and 10 mL of benzene was added to yield a brown suspension which was filtered by gravity filtration. An additional 15-20 mL of hexane was added to the benzene solution, and the mixture was filtered. Evaporation of the solvent yielded the crude product as a green oil (0.50 g, 64 % yield). Further purification was carried out by vacuum distillation to a afford yellow oil (b.p. = 83-84 °C, 0.05 mmHg) which solidified at room temperature. The product was identified on the basic of its ^{1}H NMR (δ in $CDCl_3$, 0.98 (s)) and GC/MS spectra.[10] Although the ^{1}H NMR spectra of the product demonstrated some impurities in the sample, further purification by column chromatography was not carried out because TLC test of the distilled material showed decomposition of the product on the TLC plate.

11.6. References

1. Moiseev, A. G.; Leigh, W. J., *Organometallics* **2007,** *26*, 6268.

2. Kira, M.; Miyazawa, T.; Koshihara, S. Y.; Segawa, Y.; Sakurai, H., *Chem. Lett.* **1995**, 3.

3. Perrin, D. D.; Armarego, W. L. F.; Perrin, D. R., *Purification of laboratory chemicals*. Pergamon Press: Oxford, New York, 1980.

4. Gadek, A.; Szymanska-Buzar, T., *Polyhedron* **2006,** *25*, 1441.

5. Matarasso-Tchiroukhine, E., *Chem. Commun.* **1990**, 681.

6. Corriu, R. J. P.; Leclercq, D.; Mutin, P. H.; Planeix, J. M.; Vioux, A., *J. Organomet. Chem.* **1991,** *406*, C1.

7. Mayfield, D. L.; Flath, R. A.; Best, L. R., *J. Org. Chem.* **1964,** *29* (8), 2444.

8. Herzog, U.; Lange, H.; Borrmann, H.; Walfort, B.; Lang, H., *J. Organomet. Chem.* **2004,** *689*, 4909.

9. Bahr, S. R.; Boudjouk, P.; McCarthy, G. J., *Chem. Mater.* **1992,** *4*, 383.

10. Herzog, U.; Rheinwald, G., *J. Organomet. Chem.* **2001,** *627*, 23.